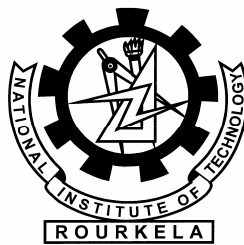


*Theoretical and Experimental Studies on  
Pulse Tube Refrigerator*

A Thesis Submitted for Award of the Degree of

Doctor of Philosophy

*Yamuna Prasad Banjare*



Department of Mechanical Engineering  
National Institute of Technology  
Rourkela, 769008

*Dedicated to*

*My  
Parents*

*And*

*My  
Teachers*



NATIONAL INSTITUTE OF TECHNOLOGY  
ROURKELA, INDIA

**Ranjit Kr Sahoo**  
**Professor**  
**Mechanical Engg. Department**  
**NIT Rourkela**

**Sunil Kr Sarangi**  
**Director**  
**NIT Rourkela**

**CERTIFICATE**

Date: January 11, 2009

This is to certify that the thesis entitled "**Theoretical and Experimental Studies on Pulse Tube Refrigerator**", being submitted by **Shri Yamuna Prasad Banjare** for the award of the degree of **Doctor of Philosophy** in Mechanical Engineering, is a record of bonafide research carried out by him under our guidance and supervision. Mr. Banjare has worked for more than three years on the above problem at the Department of Mechanical Engineering, National Institute of Technology, Rourkela and this has reached the standard fulfilling the requirements and the regulation relating to the degree. The work incorporated in this thesis has not been, to the best of our knowledge submitted to any other University or Institution for the award of any degree or diploma.

**ROURKELA**

(Ranjit Kr Sahoo)

(Sunil Kr Sarangi)

## *Curriculum Vitae*

---

---

### **Yamuna Prasad Banjare**

**E-mail** [yp\\_banjare@yahoo.co.in](mailto:yp_banjare@yahoo.co.in)

**Permanent Address** Village-Nangaradih  
P. O. - Piraiya  
Via - Bilha  
Dist. - Bilaspur  
Pin code - 495224  
Chhattisgarh, India

**Fields of interest** Thermal Engineering

#### **Education**

2009 Ph.D. Dissertation Submitted

1999 M. Tech.(Thermal, Energy and Environmental Engineering)  
IIT Kharagpur (W.B.)

1990 B.E. (Mechanical Engineering)  
Govt. Engg. College, Bilaspur  
Guru Gasi Das University, Bilaspur(C.G.)

#### **Personal information**

Date of birth 03-06-1967  
Nationality Indian

#### **Employment**

Duration	Designation	Organization
1994-1999	Lecturer (Mech. Engg.)	Govt. Engg. College Bilaspur,(C.G.)
1999-2004	Sr.Lecturer (Mech. Engg.)	Govt. Engg. College Bilaspur, (C.G.)
2004-Till date	Reader (Mech. Engg.)	Govt. Engg. College Bilaspur, (C.G.)

## Publications

1. Y.P. Banjare, R.K. Sahoo, S.K. Sarangi" Numerical Modeling of Pulse Tube Refrigerator". National Seminar on 'Technology for Sustainable Development Prespective and Strategies, IT GGDU Bilaspur, January 06-07, 2007.
2. Y.P. Banjare, R.K. Sahoo, S.K. Sarangi"Analysis of Single Stage Double Inlet Pulse Tube Refrigerator". National Seminar on "Achieving Technological Excellence in the New Millennium(ATENM)2007, Department of Mechanical Engineering Birla Institute of Technology Mesra Ranchi-835215, January 23-24,2007.
3. Y.P. Banjare, R.K. Sahoo, S.K. Sarangi,"CFD Simulation of Orifice Pulse Tube Refrigerators" International Conference on "Recent trends in Mechanical Engineering (IRCTME) 2007, Dept. of Mech. Engg. Ujjain Engineering College Ujjain October 4-6, 2007, Paper no. HT1, pp235-45.
4. Y.P. Banjare, R.K. Sahoo, S.K. Sarangi"CFD Simulation of Inertance Tube Pulse Tube Refrigerator. 19<sup>th</sup> National and 8<sup>th</sup> ISHMT-ASME Heat and Mass Transfer Conference JNTU College of Engineering Hyderabad, India January 3-5, 2008. Paper No. EXM-7, PP34.
5. Y.P. Banjare, R.K. Sahoo, S.K. Sarangi,"CFD simulation of GM type double inlet pulse tube refrigerator" 22<sup>nd</sup> National Symposium on Cryocoolers, Centre for Cryogenic Technology, IISC Bangalore,December4-6, 2008. Paper No. NSC22-405.
6. Y.P. Banjare, R. K. Sahoo, S. K. Sarangi,"CFD Simulation of a Gifford-McMahon type Pulse Tube Refrigerator"(Accepted for publication in International Journal of Thermal Science).
7. Y.P. Banjare, R.K. Sahoo, S.K. Sarangi,"3-D CFD Simulation and Experimental validation of a GM type double inlet pulse tube refrigerator" (Communicated to International Journal of Cryogenics).

## *Acknowledgements*

In every work there have so many heads behind the screen that I like to pay their credits forever. First, I would like to express my deep sense of gratitude and respect to my supervisors Prof. R. K. Sahoo and Prof. S. K. Sarangi for their excellent guidance, suggestions, endless effort and endless support and input which leads to my successful doctorate journey. I consider myself extremely lucky working under guidance of such a dynamic, hard working and genius personality. I will always remember their helping hands and moral support in my good and evil day during this period. I record my deepest gratitude to Madam Sahoo and Madam Sarangi for family support all the times during our stay at Rourkela.

I take this opportunity to express my deepest gratitude to the member of my doctoral scrutiny committee Prof. A.K. Satapathy, Chairman Prof. B.K. Nanda and also faculty members of the Mech. Engg. Department, for throughout advice, useful discussions, constant encouragement and support in pursuing the PhD work.

I would like to express my heartfelt gratitude to Dr. D.S. Bal Director, Technical Education, Govt. of Chhattisgarh, Raipur and his family for their help, encouragement and loving suggestions for my PhD study.

I am indebted to Prof. S. Kasthuriengan and his team, Centre for Cryogenic Technology, IISC Bangalore for sharing their vast experience on pulse tube refrigerator.

I also acknowledge the help extended by Prof. P. Rath, Prof. S.K. Mohapatra and my friends Dr. S.D. Patle, Dr. Anjan Sarkar, Prof. H.M. Jena, Mr. M.K. Singh, Mr. S.A. Alur and Mr. Harihar Barkey in academic and non-academic problems. I am thankful to my colleagues and faculty of my parent Institute Government Engineering College, Bilaspur (C.G.) for their help. I thank Dr. M.R. Meshram, Mr. I.P. Bhartiya, Mr. K.K. Ratrey and Mr. S.L. Mathur for their help and cooperation for my PhD study.

Thanks go to my uncles Sri L.P. Keshkar and Sri M. L. Kurrey and relatives Prof. G.R. Patle, Sri. D.R. Kurrey, Sri S.R. Shandilya and Sri G.P. Khunte for their loving support and encouragement for my PhD study. I thank my whole family for their loving support, especially my parents, my brothers Sri Kaushal, Sri Suresh and Dr. Rajkumar and my sister Sushila.

I am most grateful to my beloved wife Smt. Phuleshwari for her loving support, cooperation, encouragement and sacrifice, and to my son Bhavesh and daughter Garima for giving all that I need throughout my PhD work. You guys are the pure driving force of my life.

(January 11, 2009)

Yamuna Prasad Banjare

## *Abstract*

The pulse tube refrigerator (PTR) is a cryocooler which is capable of reaching temperature of a few tens of Kelvin in a single stage and a few Kelvin in two stages. Unlike ordinary refrigeration cycles which utilize the vapor compression cycle, a PTR implements the oscillatory compression and expansion of gas within a closed volume to achieve the desired refrigeration. Pulse tube refrigerator has the advantages of long-life operation, high reliability and low vibration over the conventional cryocoolers, such as G-M and Stirling coolers because of the absence of moving parts at their low temperature end. Due to its associated advantages, pulse tube refrigerators have several applications such as cooling of infrared sensors, night vision equipments, SQUID, cryopumping etc.

All pulse tube refrigerator units operate as closed systems where no mass is exchanged between the cryocooler and its environment. The only moving component is the piston (and the rotary valve) which oscillates back and forth to generate periodic pressure oscillation of the working fluid. Mostly helium is chosen as working fluid because it offers the lowest critical temperature compared to other available gases. It has also high thermal conductivity. Accurate modeling of the pulse tube cryocooler is essential to predict its performance and thereby arrive at optimum design. At the current stage of world wide research, such accurate models are not readily available in open literature. Further, the complexity of the periodic flow in the PTC makes analysis difficult. Although different models are available to simulate pulse tube cryocoolers, the models have its limitations and also range of applicability. In order to accurately predict and improve the performance of the PTC system a reasonably thorough understanding of the thermo fluid- process in the system is required. One way to understand the processes is by numerically solving the continuum governing equations based on fundamental principles, without making arbitrary simplified assumptions. The recent availability of powerful computational fluid dynamics (CFD) software that is capable of rigorously modeling of transient and multidimensional flow and heat transfer process in complex geometries provides a good opportunity for analysis of PTCs.

The experimental method to evaluate the optimum parameters of PTCs is difficult. On the other hand, developing a specialized computer code for its CFD analysis is equally complex. Thus numerical experimentation using CFD software is a suitable option. It should, however, be emphasized that CFD-type predictions, like other model-generated results, are reliable only when they are verified against experimental data. Therefore, importance of experimental

validation is to be emphasized. An issue of particular interest is the relevance of the predictions of one-dimensional models to assess the performance of pulse tube cryocoolers. This is important because the calculations for design procedure are usually based on one dimensional flow models. Thus the validity one-dimensional flow model to use for the multi-dimensional flow system is an important aspect of analysis. These issues are addressed in the dissertation.

In this study, multi-dimensional continuum governing equations are numerically solved to investigate the details of thermo-fluid process in Stirling type Orifice Pulse Tube Refrigerator (OPTR) and Inertance Tube Pulse Tube Refrigerator (ITPTR) and GM type Double Inlet Pulse Tube Refrigerator (DIPTR). The Stirling type system includes dual opposed piston compressor, regenerator, pulse tube, cold and hot heat exchangers, inertance tube/orifice and reservoir. In the GM type DIPTR the additional components are rotary and double inlet orifice valves. In this investigation the Commercial CFD package, FLUENT is utilized to study the flow phenomena and heat transfer characteristics in the pulse tube system. The simulation results are presented and compared with experimental data. The whole study is classified into three groups which are discussed below.

In the first part of study, Stirling type OPTR and ITPTR are considered for CFD simulation using Fluent software. Two-dimensional axis-symmetric geometry is considered for CFD simulations. The simulations represent a fully-coupled system operating in steady periodic mode, without any arbitrary assumptions other than ideal gas and no gravity effect. The sole external boundary conditions imposed on the model are a sinusoidal oscillating piston face velocity by user defined function (UDF) along with one of the thermal boundary conditions, adiabatic, isothermal or known heat flux at the cold end heat exchanger. The objective is to compare the performance of ITPTR and OPTR on the basis of CFD simulations. Where physical dimensions of components are kept same except that the inertance tube is replaced by an orifice valve. In order to observe the difference of refrigeration performance between an ITPTR and OPTR, pressure wave of same amplitude and frequency are applied.

For each system three separate simulations are analyzed. One simulation assumes an adiabatic cold-end heat exchanger (CHX); another assumes a known cooling heat load, and the last assumes a pre-specified CHX temperature. Each simulation started with an assumed uniform system temperature, and continued until steady periodic conditions are achieved. The transient CFD model successfully predicts pulse tube refrigerator performance through solving



the Navier–Stokes Equations for fluid momentum and heat transfer, along with an ideal gas equation. The result shows that the performance of the ITPTR is superior to that of OPTR. The use of the ITPTR configuration offers a better potential for higher performance and efficiency. The improvement can be explained in terms of mass flow rate inside the pulse tube and the favorable phase relation between the mass flow rate and pressure at the cold end section of the pulse tube.

In the second part of study, a single stage G-M type double inlet pulse tube refrigerators is considered for CFD simulation using Fluent software. The two-dimensional geometry is taken for simulation. In this simulation the physical dimensions of all the components are kept constant and pressure input is generated from the same UDF (User Defined Function) for different case of simulations. Initially the valve openings (orifice and double inlet valve) are optimized to achieve the lowest temperature at the adiabatic condition of cold end heat exchanger. This optimized valve openings are used for other boundary conditions i.e., known heat load and isothermal conditions. In the DIPTR system, five separate simulations are analyzed. For adiabatic cold end boundary conditions three cases are simulated to optimize the valve openings to achieve the lowest temperature at the cold end. Based on this optimized valve opening, simulations are performed on the known heat load boundary conditions and isothermal cold heat exchanger. Each simulation started with an assumed uniform system temperature, and continued until steady periodic conditions are achieved. The results showed that CFD simulations are capable of elucidating the complex periodic processes in DIPTR very well. This CFD simulation results are compared with the available experimental data. The comparisons show that there is an appreciable agreement between CFD simulation and experimental data.

In the third part of study the CFD simulation is extended to GM type DIPTR by taking three-dimensional geometry of the system to more accurately access the performance. In this DIPTR system five separate simulations are analyzed similar to 2D- GM cycle described earlier. For adiabatic cold end boundary conditions three cases are simulated to optimize the valve openings. Based on this optimized valve opening, simulations are performed on the known heat load and isothermal boundary conditions at the cold heat exchanger. The simulation results are validated with available experimental results. There is an excellent agreement of simulation result with the experimental data. These conclusions lead that numerical simulation by Fluent is capable of designing, predicting and optimizing the pulse tube cryocoolers.

# Contents

<i>Acknowledgements</i>	i
<i>Abstract</i>	ii
<i>List of Figures</i>	viii
<i>List of Tables</i>	xiv
<i>Nomenclature</i>	xv
<b>1. Introduction</b>	
1.1 General	1
1.2 Application of Cryocoolers	2
1.3 Comparisons between Stirling and GM type Cryocoolers	4
1.4 Pulse Tube Refrigerators	4
1.5 Classification of Pulse Tube Refrigerators	5
1.6 Types of Pulse Tube Refrigerators	6
1.7 Components of Pulse Tube Refrigerator	16
1.8 Aim of the Present Investigation	19
1.9 Organization of the Manuscript	21
<b>2. Literature Review</b>	
2.1 Introduction	22
2.2 Theoretical Investigations on PTRs	22
2.3 Experimental Investigations on PTRs	31
2.4 Review of CFD(Using Fluent Software) Simulations on PTRs	36
2.5 Efforts to Improve the Performance of Regenerator	38
2.6 Review of the Investigations of Thermoacoustic Machine	41
2.7 Development of the Volume Averaging Technique	42
<b>3. Pulse Tube Refrigerator Approximate Models: Review of Mathematical Analysis</b>	
3.1 Introduction	43
3.2 Pulse Tube Refrigerator Operation Principle	43

3.3	Pulse Tube Refrigerator Analysis Methods	45
3.4	First Order Analysis	45
3.4.1	Surface Heat Pumping Theory	45
3.4.2	Enthalpy Flow Analysis	46
3.4.3	Phasor Analysis	49
3.5	Second Order Analysis	57
3.5.1	Thermodynamic Non-Symmetry Effect	57
3.5.2	Approximate PTR Models: Adiabatic and Isothermal	61
<b>4.</b>	<b>Theory of Heat and Fluid Flow in Pulse Tube Refrigerator</b>	
4.1	Introduction	79
4.2	Porous Media	80
4.3	Volume Averaging Technique	80
4.4	Regenerator Materials	82
4.5	Porous Media Parameters for Regenerator Matrix	83
4.6	Permeability and Inertial Resistance Factors for Porous Media	87
4.7	Governing Equations for Pulse Tube Refrigerators	90
4.8	Computational Fluid Dynamics(CFD) Simulation Procedures	96
<b>5.</b>	<b>CFD Analysis of Stirling type Pulse Tube Refrigerators</b>	
5.1	Introduction	105
5.2	Inertance Tube Pulse Tube Refrigerator	106
5.3	Orifice Pulse Tube Refrigerator	110
5.4	Dynamic Meshing Function	114
5.5	User Defined Function	115
5.5.1	Compiling User Defined Function	116
5.5.2	Mesh Motion Preview	116
5.6	Results of CFD simulations of ITPTR	117
5.6.1	Case1: Adiabatic Boundary Condition	117
5.6.2	Case2: Known Heat Load Boundary Condition	121
5.6.3	Case3: Isothermal Boundary Condition	124
5.7	Results of CFD simulations of OPTR	126
5.7.1	Case1: Adiabatic Boundary Condition	126

5.7.2	Case2: Known Heat Load Boundary Condition	129
5.7.3	Case3: Isothermal Boundary Condition	131
5.8	Performance comparisons between ITPTR and OPTR	132
5.9	Discussions	136
<b>6.</b>	<b>CFD Analysis of G-M type Pulse Tube Refrigerators</b>	
6.1	Introduction	137
6.2	2-D Geometry of Double Inlet Pulse Tube Refrigerators	137
6.3	Results of 2-D Simulations	142
6.3.1	Case1: Adiabatic Boundary Condition	142
6.3.2	Case2: Known Heat Load Boundary Condition	148
6.3.3	Case3: Isothermal Boundary Condition	150
6.3.4	Comparison with Experimental Data	151
6.3.5	Discussions	154
6.4	3-D Geometry of Double Inlet Pulse Tube Refrigerators	154
6.5	Results of 3-D Simulations	157
6.5.1	Case1: Adiabatic Boundary Condition	158
6.5.2	Case2: Known Heat Load Boundary Condition	165
6.5.3	Case3: Isothermal Boundary Condition	166
6.5.4	Comparison with Experimental Data	169
6.5.5	Discussions	172
<b>7</b>	<b>Conclusions</b>	
7.1	Highlights of Stirling type PTR Models	173
7.2	Highlights of GM type Double inlet Pulse Tube Refrigerators	174
7.2.1	Highlights of DIPTR 2-D Simulations	174
7.2.2	Highlights of DIPTR 3-D Simulations	174
7.3	Scope of future work	175
	<b>References</b>	176
	<b>Curriculum Vitae</b>	

## *List of Figures*

<b>Figures</b>	<b>Title</b>	<b>Page</b>
Fig.1.1a	Stirling type basic pulse tube refrigerator	6
Fig.1.1b	G-M type basic pulse tube refrigerator	6
Fig.1.2	Schematic diagram of basic pulse tube refrigerator	7
Fig.1.3	Schematic diagram of orifice pulse tube refrigerator	8
Fig.1.4a	Schematic diagram of Stirling type double inlet pulse tube refrigerator	9
Fig.1.4b	Schematic diagram of G-M type double inlet pulse tube refrigerator	9
Fig.1.5	Schematic diagram of the inertance tube pulse tube refrigerator	10
Fig.1.6	Schematic diagram of pulse tube geometry (a) Linear (b) U-type (c) Coaxial	11
Fig.1.7	Schematic diagram of (a) Warm expander PTR, (b) Multiple-inlet PTR, (c) Four valve PTR	12
Fig.1.8	Schematic diagram of thermoacoustic PTR	13
Fig.1.9a	Two-stage G-M type double inlet pulse tube refrigerator	14
Fig.1.9b	Two-stage Stirling type double inlet pulse tube refrigerator.	14
Fig.1.10	Double inlet pulse tube refrigerator with minor orifice	15
Fig.1.11	Schematic diagram of active-buffer PTR	16
Fig.1.12	Typical pictures of (a) Regenerator (b) Pulse tube.	17
Fig.1.13	Schematic diagram of rotary valve	19
Fig.3.1	Schematic diagram of the simple vapor compression cycle	44
Fig.3.2	Schematic diagram of surface heat pumping theory for BPTR	46
Fig.3.3	Macroscopic energy balance for PTR	46
Fig.3.4	Energy balance of system components in an OPTR	47
Fig.3.5	Phase shift relation for gas temperature and mass flow rate	49
Fig.3.6	Schematic diagram of pulse tube refrigerator for phasor analysis	50
Fig.3.7	Energy balance for pulse tube section	50
Fig.3.8	Phasor representation of cold end mass flow rate and pressure for BPTR	52

Fig.3.9	Phasor representation of cold end mass flow rate and pressure for OPTR	53
Fig.3.10	Phasor representation of mass flow rate at and pressure for DIPTR	53
Fig.3.11	Phaser representation of mass flow rate and pressure for ITPTR.	54
Fig.3.12	Impedance for OPTR	54
Fig.3.13	Impedance for ITPTR	55
Fig.3.14	Phase lag representation of OPTR	56
Fig.3.15	Phasor diagram of the total system for OPTR	57
Fig.3.16	Schematic diagram of the idealized working processes of pulse tube refrigerators: (a) first half-cycle; (b) second half-cycle	59
Fig.3.17	Pressure versus time: (a) pressure in pulse tube; (b) Pressure externally applied the flow capacity of the regenerator	59
Fig.3.18	Temperature versus position of a gas element in the basic pulse tube (a) Adiabatic (b) with thermal contact	59
Fig.3.19	Temperature versus position of a gas element in the OPTR	60
Fig.3.20	Temperature versus position for gas elements in the DIPTR	60
Fig.3.21	Schematic diagram of the physical model for DIPTR	62
Fig.3.22	Schematic diagram of energy balance for compressor	64
Fig.3.23	Schematic diagram of the physical model for DIPTR	70
Fig.3.24	Control volume for isothermal model	71
Fig.3.25	Flow chart of the computer program for numerical simulation	78
Fig.4.1	The representative elementary volume to show the intermediate size relative to the sizes of the flow domain and the pores.	81
Fig.4.2	Temperature range for commonly used regenerator materials in cryogenic refrigerators	83
Fig.4.3	Woven wire mesh screens	84
Fig.4.4	Geometry of woven screen	85
Fig.5.1	Three-dimensional view of the inertance pulse tube refrigerator	106
Fig.5.2	Two-dimensional view of inertance pulse tube refrigerator	107
Fig.5.3	Two-dimensional axis-symmetric geometry of ITPTR	107
Fig.5.4	Two-dimensional axis-symmetric meshing of ITPTR	108

Fig.5.5	Three-dimensional view of the Stirling type OPTR	110
Fig.5.6	Two-dimensional view of OPTR	111
Fig.5.7	Two-dimensional axis-symmetric geometry of OPTR	111
Fig.5.8	Two-dimensional axis-symmetric mesh of OPTR	112
Fig.5.9	Mesh motion preview of dynamic meshing model (OPTR/ITPTR)	117
Fig.5.10	Pressure variations in compressor, pulse tube and reservoir for ITPTR	118
Fig.5.11	Cooling behaviour at the beginning of simulation	118
Fig.5.12	Cooling behaviour till cyclic steady state condition.	119
Fig.5.13	Cold end temperature variation at cyclic steady state condition.	119
Fig.5.14	Temperature distributions along axial direction for case1	120
Fig.5.15	Density distributions along axial direction for case1	120
Fig.5.16	Temperature contours for case1	120
Fig.5.17	Density contours for case1	121
Fig.5.18	Velocity vector in the pulse tube for case1	121
Fig.5.19	CHX wall temperature variation at cyclic steady state condition (case2)	122
Fig.5.20	Temperature distribution along axial direction for case2	122
Fig.5.21	Density distributions along axial direction for case2	122
Fig.5.22	Temperature contour along axial direction for case2	123
Fig.5.23	Density contour along axial direction for case2	123
Fig.5.24	Temperature distribution along axial direction for case3	124
Fig.5.25	Density distribution along axial direction for case3	125
Fig.5.26	Temperature contour for case 3.	125
Fig.5.27	Density contour for case3	125
Fig.5.28	Cooling behavior for orifice pulse tube refrigerator(Case1 and 2)	126
Fig.5.29	CHX wall temperature variation at cyclic steady state condition(Case1)	127
Fig.5.30	Temperature distributions along axial direction(Case1)	127
Fig.5.31	Density distributions along axial direction (Case1)	127
Fig.5.32	Temperature contour along axial direction (Case1)	128
Fig.5.33	Density contour along axial direction (Case1)	128
Fig.5.34	Velocity vector in the pulse tube	128

Fig.5.35	CHX wall temperature variation at cyclic steady state condition (case2)	129
Fig.5.36	Temperature distribution along axial direction (case2)	129
Fig.5.37	Density distributions along axial direction (case2)	130
Fig.5.38	Temperature contour along axial direction (case2)	130
Fig.5.39	Density contour along axial direction (case2)	130
Fig.5.40	Temperature distribution along axial direction for case 3	131
Fig.5.41	Density distributions along axial direction (case3)	131
Fig.5.42	Temperature contour along axial direction (case3)	132
Fig.5.43	Density contour along axial direction (case3)	132
Fig.5.44	Variation of cold wall temperature with frequency for ITPTR and OPTR	133
Fig.5.45	Phase relation between mass flow and pressure at CHX for ITPTR	134
Fig.5.46	Phase relation between mass flow and pressure at CHX for OPTR	134
Fig.5.47	Mass flow rates at cold end section for OPTR and ITPTR	135
Fig.5.48	Heat load comparisons for OPTR and ITPTR	135
Fig.6.1	Schematics of the physical model of G-M type DIPTR	139
Fig.6.2	Two-dimensional geometry with complete mesh for DIPTR	139
Fig.6.3	Cooling behavior of cold end temperature for DIPTR	143
Fig.6.4	Phase relation between pressure and mass flow rate for case1(a)	143
Fig.6.5	Temperature distribution along axial direction of pulse tube case1(a)	144
Fig.6.6	Temperature contour for case1(a)	144
Fig.6.7	Density contour for case1(a)	144
Fig.6.8	Phase relation between pressure and mass flow case1(b)	145
Fig.6.9	Temperature contour for case 1(b)	146
Fig.6.10	Density contour for case1(b)	146
Fig.6.11	Phase relation between pressure and mass flow rate case1(c)	147
Fig.6.12	Temperature contour for case1(c)	147
Fig.6.13	Density contour for case1(c)	147
Fig.6.14	Mass flow rates through pulse tube cross section	148
Fig.6.15	Cooling behavior of cold end temperature for case2	149
Fig.6.16	Phase relation between mass flow rate and pressure at cold end	149



Fig.6.17	Temperature contour for case2	149
Fig.6.18	Density contour for case2	150
Fig.6.19	Heat transfer rate over a cycle at CHX for case 3	150
Fig.6.20	Temperature contour for case 3	151
Fig.6.21	Density contours for case3	151
Fig.6.22	Comparison of pressure wave at the inlet of regenerator	152
Fig.6.23	Comparison of cool down behaviour.	152
Fig.6.24	Comparison of heat load	153
Fig.6.25	Comparison of temperature variation along the pulse	153
Fig.6.26	Different components of DIPTR for 3-D simulations	155
Fig.6.27	Three-dimensional mesh for G-M type DIPTR	155
Fig.6.28	Cool down behaviour at the beginning of simulation	159
Fig.6.29	Cool down behaviour till cyclic steady state condition for case1(a)	159
Fig.6.30	CHX Wall temperature variation at cyclic steady condition case1(a)	159
Fig.6.31	Temperature variation along pulse tube length for case1(a)	160
Fig.6.32	Phase relation between mass flow and pressure case1(a)	160
Fig.6.33	Temperature contour for case1(a)	160
Fig.6.34	Density contour for case1(a)	161
Fig.6.35	Velocity vector for the entire system case1(a).	161
Fig.6.36	Velocity vector near the cold end case1(a)	161
Fig.6.37	Wall temperature variation of the cold heat exchanger case1(b)	162
Fig.6.38	Phase relation between mass flow and pressure case1(b).	162
Fig.6.39	Temperature contour for case1(b)	163
Fig.6.40	Density contour for case1(b)	163
Fig.6.41	Wall temperature variation of the cold heat exchanger case1(c)	164
Fig.6.42	Phase relation between mass flow and pressure(c)	164
Fig.6.43	Temperature contour for case1(c)	164
Fig.6.44	Density contour for case1(c)	165
Fig.6.45	Wall temperature variation of cold heat exchanger for case2	165
Fig.6.46	Temperature contour for case2	166
Fig.6.47	Density contour for case2	166

Fig.6.48	Heat transfer rate over a cycle at CHX for case3	167
Fig.6.49	Wall temperature variation with time for case3	167
Fig.6.50	Temperature contour for case3.	167
Fig.6.51	Density contour for case3	168
Fig.6.52	Mass flow rates through pulse tube cross section	168
Fig.6.53	Comparison of pressure wave at the inlet of regenerator	170
Fig.6.54	Comparison of cool down behaviour.	171
Fig.6.55	Comparison of heat load.	171
Fig.6.56	Comparison of temperature variation along the pulse tube length	172

## *List of Tables*

<b>Table</b>	<b>Title</b>	<b>Page</b>
Table 3	Design data for adiabatic and isothermal models	77
Table 4.1	Friction factor correlations	89
Table 4.2	Operational parameters of the porous media	90
Table 4.3	Variables and respective convergence criteria used in the simulation	102
Table 5.1	Component dimensions of ITPTR	109
Table 5.2	Boundary and initial conditions for ITPTR	109
Table 5.3	Component dimensions of OPTR	113
Table 5.4	Boundary and initial conditions for OPTR	113
Table 5.5	Simulation result of ITPTR and OPTR	136
Table 6.1	Dimensions of DIPTR for 2-D simulations	140
Table 6.2	Boundary and initial conditions of DIPTR for 2-D simulations	140
Table 6.3	Percentage of valve opening	141
Table 6.4	Summery of result of 2-D simulation of DIPTR	154
Table 6.5	Dimensions of DIPTR for 3D simulations	156
Table 6.6	Boundary and initial conditions of DIPTR for 3D simulations	156
Table 6.7	Percentage of valve opening	156
Table 6.8	Summery of result of 3-D simulation of DIPTR	172

## *Nomenclature*

### *English symbols*

$a$	Sonic velocity, [m/s]
$a_0$	Transient advection coefficient
$a_k$	Combined advection and diffusion coefficient
$A_{di}$	Area of the double inlet orifice, [m <sup>2</sup> ]
$A_o$	Area of the orifice, [m <sup>2</sup> ]
$A_g$	Free flow cross sectional area of regenerator, [m <sup>2</sup> ]
$A_{rg}$	Cross sectional area of regenerator, [m <sup>2</sup> ]
$A_s$	Total surface area of connected voids, [m <sup>2</sup> ]
$A_t$	Cross sectional area of the pulse tube, [m <sup>2</sup> ]
$b$	Component of the linearized source term
$C_p$	Specific heat at constant pressure, [J/kg-K]
$C$	Inertial resistance factor, [m <sup>-1</sup> ]
$C_v$	Specific heat at constant volume, [J/kg-K]
$C_F$	Friction factor
$C_{fs}$	Skin friction factor
$C_{fd}$	Form drag correlation constant
$C_d, C_{di}, C_1$	Constants
$d$	Diameter, [m]
$d_o$	Outer diameter of screens, [m]
$d_h$	Hydraulic diameter of screen, [m]
$d_w$	Wire diameter of screen, [m]
$dt$	Differential time, [s]
$dT$	Differential temperature, [K]
$dX$	Differential piston displacement, [m]
$dV$	Differential volume, [m <sup>3</sup> ]
$D$	Viscous resistance factor, [m <sup>-2</sup> ]
$E$	Energy, [J]

$f$	Operating frequency, [Hz]
$g$	Gravity acceleration, [m/s <sup>2</sup> ]
$G$	Mass flow rate per unit of free flow area of screen, [kg/sm <sup>2</sup> ]
$h$	Local enthalpy, [W]
$H$	Enthalpy, [W]
$I$	Unit (Identity) tensor
$I_m$	Current
$k$	Thermal conductivity, [W/m-K]
$l$	Mesh distance, [m]
$L$	Length, [m]
$\dot{m}$	Mass flow rate, [kg/s]
$\dot{m}_c$	Mass flow rate at cold end section, [kg/s]
$\dot{m}_{cp}$	Mass flow rate at the outlet of the compressor, [kg/s]
$\dot{m}_{di}$	Mass flow rate through the double inlet valve, [kg/s]
$\dot{m}_h$	Mass flow rate at hot end section, [kg/s]
$\dot{m}_o$	Mass flow rate at through the orifice, [kg/s]
$\dot{m}_{rg}$	Mass flow rate through the regenerator, [kg/s]
$\dot{m}_p$	Mass flow rate due to pressurization of pulse tube, [kg/s]
$m$	Mesh size, [per inch]
$n$	Total number of screens used to pack the regenerator
$n'$	Number of packed screens per length
$P, p$	Pressure, [N/m <sup>2</sup> ]
$P_0$	Average pressure, [N/m <sup>2</sup> ]
$P_1$	Pressure amplitude
$P_t$	Pressure inside the pulse tube, [N/m <sup>2</sup> ]
$P_h$	High pressure, [N/m <sup>2</sup> ]
$P_l$	Low pressure, [N/m <sup>2</sup> ]
$P_m$	Mean pressure, [N/m <sup>2</sup> ]
$P_{cp}$	Pressure at compressor, [N/m <sup>2</sup> ]

$P_r$	Pressure at reservoir, [N/m <sup>2</sup> ]
$q$	Heat flux, [W/m <sup>2</sup> ]
$\dot{q}$	Heat flux rate, [W/m <sup>2</sup> /s]
$\dot{Q}$	Heat rate, [W]
$Q$	Heat transfer, [W]
$r$	Radial coordinate
$r_h$	Hydraulic radius of the screen matrix, [m]
$Re_l$	Reynolds number = $\dot{m}l / \beta A_r \mu$
$Re_h$	Reynolds number = $\dot{m}d_h / A_g \mu$
$R$	Ideal gas constant, [J/kg-K]
$s$	Pitch, [m]
$S_i$	Source term
$t$	Time, [sec]
$t_1, t_2$	Time interval, [sec]
$t_s$	Screen thickness, [m]
$T$	Temperature, [K]
$T_1, T_2, \dots, T_4$	Temperatures, [K]
$T_{ac}$	Gas temperature at after cooler, [K]
$T_c$	Gas temperature at cold end heat exchanger, [K]
$T_{cp}$	Gas temperature at the compressor, [K]
$T_h$	Gas temperature at hot end heat exchanger, [K]
$T_{mreg}$	Mean temperature of regenerator, [K]
$T_{rg}$	Gas temperature at the regenerator, [K]
$T_o$	Temperature of the ambient, [K]
$u$	Specific internal energy, [J/kg]
$U$	Internal energy, [J]
$v$	Physical velocity, [m/s]
$v_1$	Superficial velocity, [m/s]
$V$	Volume, [m <sup>3</sup> ]
$\dot{V}$	Volumetric velocity, [m <sup>3</sup> /s]

$V_{dac}$	Void volume of the aftercooler, [m <sup>3</sup> ]
$V_{cp}$	Compressor cylinder volume , [m <sup>3</sup> ]
$V_{dcx}$	Void volume of the cold end HX, [m <sup>3</sup> ]
$V_{drg}$	Void volume of the regenerator matrix, [m <sup>3</sup> ]
$V_{dhx}$	Void volume of the hot end HX, [m <sup>3</sup> ]
$V_o$	Compressor cylinder clearance volume , [m <sup>3</sup> ]
$V_s$	Compressor cylinder stroke volume , [m <sup>3</sup> ]
$V_t$	Pulse tube volume, [m <sup>3</sup> ]
$V_r$	Volume encompassing the wire, [m <sup>3</sup> ]
$W$	Mechanical work, [W]
$W_{cp}$	Work transfer, [W]
$\dot{W}$	Power, [W]
$W_p$	Weight of packed matrix material, [kg]
$x$	Axial coordinate
$x_t$	Transverse pitch, [m]
$x_l$	Lateral pitch, [m]
$X$	Piston displacement, [m]
$X_1, X_2$	Position along pulse tube length, [m]
$X_t$	Dimensionless cold volume

### *Greek symbols*

$\alpha$	Permeability, [m <sup>2</sup> ]
$\beta$	Opening area ratio of screen
$\gamma$	Ratio of specific heat
$\mu$	Fluid molecular viscosity, [kg/m-s]
$\rho$	Density, [kg/m <sup>3</sup> ]
$\lambda$	Index of polytrophic process
$\omega$	Angular frequency, [rad/s]
$\theta$	Phasor angle between $\dot{m}_c$ and P vector
$\vartheta$	Phasor angle between $\dot{m}_h$ and P vector

$\nu$	Specific volume, [m <sup>3</sup> /kg]
$\phi$	Porosity
$\varphi$	Generic variable
$\sigma$	Area density, [m <sup>-1</sup> ]
$\tau$	Stress tensor
$\zeta$	Period of the cycle, [sec]
$\psi$	Diffusion flux
$\xi$	Capacitance
$\partial$	Differential operator
$\nabla$	Gradient operator
$\nabla p$	Pressure drop
$\Gamma$	Exchange coefficient
E	Compliance
$\Omega$	Resistance
Z	Impedance
$\ell$	Inductance
$\Sigma$	Summation
$\rightarrow$	Vector Form
$\langle \rangle$	Cycle average quantity
$\oint$	Cyclic integral

### *Subscripts*

amp	Amplitude of piston displacement
ac	After cooler
avg	Average value
chx	Cold end heat exchanger
c	Cold end
coeff	Coefficient
cp	Compressor
d	Dead volume



di	Double inlet valve
eff	Effective
f	Fluid
h	Hot end
hhx	Hot end heat exchanger
In	incoming
j	Summation
loss	Losses
m	Mean value in one cycle
o	Orifice
out	Outgoing
p	Constant pressure
porous	Porous medium
pt	Pulse Tube
pv	PV work
r	Radial direction
rg	Regenerator
refrig	Refrigeration
reject	Rejection
s	Solid
t	Turbulence
$T_I$	Transfer line
x	Axial direction
t	Tube

### *Superscripts*

TP	Transpose
----	-----------

## *Abbreviations*

AFTC	After cooler
BC	Boundary condition
BPTR	Basic pulse tube refrigerator
CHX	Cold end heat exchanger
CV	Control volume
COMP	Compressor
COP	Coefficient of performance
DC	Direct flow
DIV	Double inlet valve
DIPTR	Double inlet pulse tube refrigerator
GM	Gifford Mc-Mahon
HHX	Hot end heat exchanger
HP	High pressure
ITPTR	Inertance tube pulse tube refrigerator
LP	Low pressure
MRI	Magnetic resonance imaging
NDE	Non-destructive evaluation
ORV	Orifice valve
OPTR	Orifice pulse tube refrigerator
PT	Pulse tube
PTR	Pulse tube refrigerator
REGEN	Regenerator
RESVR	Reservoir
SC	Superconducting magnet
SQUID	Superconducting quantum interference device
TAPTR	Thermo-acoustic pulse tube refrigerator
TAD	Thermo-acoustic driver

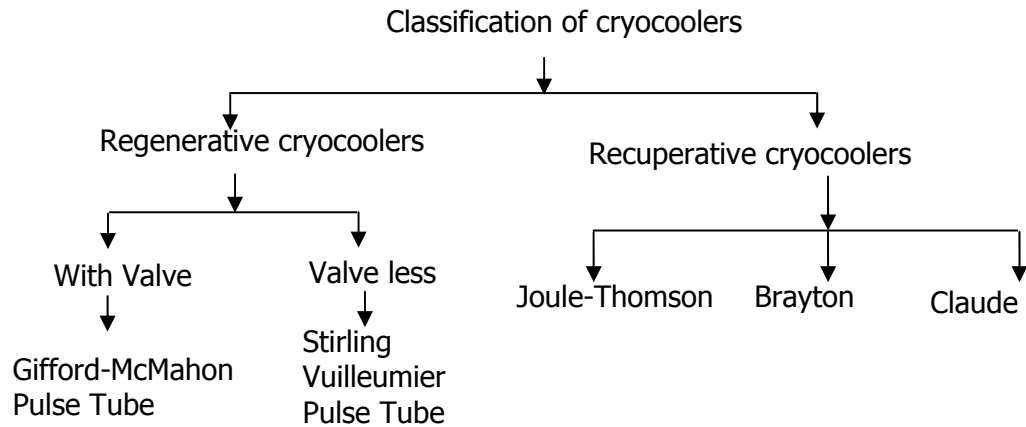
# *Chapter I*

## **Introduction**

### *1.1 General*

Cryogenics comes from the Greek word "kryos", which means very cold or freezing and "genes" means to produce. Cryogenics is the science and technology associated with the phenomena that occur at very low temperature, close to the lowest theoretically attainable temperature. In engineering, cryogenics can be best described as an application which operates in the temperature range from absolute zero to about 123K(-150°C). In particular, this includes refrigeration, liquefaction, storage and transport of cryogenic fluids, cryostat design and the study of phenomena that occur at these temperatures.

Cryocooler is a refrigeration machine with refrigeration temperature below 123K and with a small refrigeration capacity. According to the classification by Walker (1983) there are two types of cryocoolers: recuperative type and regenerative type. The former includes the Joules Thomson cryocooler and the Brayton cryocooler. The latter includes the Stirling type cryocooler and the Gifford-McMahon type cryocooler. These cryocoolers as enumerated by Radebaugh (1995), are mainly used for cooling of the infrareds sensors in the missile guided system and satellite based surveillance, as well as in the cooling of superconductors and semiconductors. The cryocoolers can also be used in other applications such as in cryopumps, liquefying natural gases, cooling of radiation shields, SQUID (super conducting quantum interference device), Magnetometers, SC Magnets, Semiconductor fabrication etc..



## 1.2 *Application of Cryocoolers*

The major applications of cryocoolers are summarized below [53].

### *A. Military*

- (i) Infrared sensors for missile guidance & night vision
- (ii) Infrared sensors for surveillance (satellite based)
- (iii) Gamma-ray sensors for monitoring nuclear activity
- (iv) Superconducting magnets for mine sweeping

### *B. Environmental*

- (i) Infrared sensors for atmospheric studies (satellite)
- (ii) Infrared sensors for pollution monitoring

### *C. Commercial*

- (i) Cryopumps for semiconductor fabrication
- (ii) Superconductors for cellular-phone base stations
- (iii) Superconductors for voltage standards
- (iv) Superconductors for high-speed communications
- (v) Semiconductors for high-speed computers
- (vi) Infrared sensors for NDE and process monitoring
- (vii) Industrial gas liquefaction

### *D. Medical*

- (i) Cooling superconducting magnets for MRI

- (ii) SQUID magnetometers for heart and brain studies
- (iii) Liquefaction of oxygen for hospital and home use
- (iv) Cryogenic catheters and cryosurgery

#### *E. Transportation*

- (i) LNG for fleet vehicles
- (ii) Superconducting magnets in maglev trains
- (iii) Infrared sensors for aircraft night vision

#### *F. Energy*

- (i) LNG for peak shaving
- (ii) Superconducting power applications (motors, transformers etc.)
- (iii) Infrared sensors for thermal loss measurements

#### *G. Police and security*

- (i) Infrared sensors for night-security and rescue

#### *H. Agriculture and Biology*

- (i) Storage of biological cells and specimens

Due to special application of the cryocooler as described above, the demands for high performance efficiency, reliability, low vibration, long life time, small size and weight become important aspects for the improvement of the cryocoolers. Since regenerative coolers have higher efficiency due to smaller heat transfer loss, Stirling coolers and Gifford-McMahon type coolers have been widely used in different application fields. In both the Stirling cryocoolers and Gifford-McMahon (G-M) cryocoolers there are expansion devices (i.e., moving parts) in the cold ends. The moving parts in the cold end are needed in order to adjust the phase angle and to recover the energy flow, which result in the decrease in reliability of the system and shorten the life times of the cryocoolers. The pulse tube refrigerator/cryocooler has the advantages over other cryocoolers due to simplicity in construction with no moving part at the cold end, and therefore is more reliable in operation. For this reason more attention has been paid to the investigation of pulse tube refrigerator/cryocoolers in recent years.

### 1.3 Comparisons between Stirling and G- M type Cryocoolers

In general there are two types of pulse tube refrigerator used in practice. The overall comparisons between these two systems are described below.

Stirling type cryocooler	G-M type cryocooler
Works at high frequency (20-120Hz)	Works at Low frequency (1-5Hz)
Compressor directly connected to expander	Compressor connected to expander through a valve
Use of dry compressor	Use of oil lubricated compressor
High COP	Low COP
Pressure ratios are low	Pressure ratios are high
Can attain 20K using two stages of cooler	Can attain below 2K using two stages of cooler
Compressors are small (capacity is in few hundred Watts)	Compressors are bulky(capacity is in kW )

### 1.4 Pulse Tube Refrigerators

Cooling effect at one end of a hollow tube with a pulsating pressure at the other end was first observed by Gifford and Longworth [1] in the early sixties. This marks the inception of one of the most promising cryogenics refrigerators know as 'basic pulse tube refrigerator' (BPTR). Due to the absence of the moving parts in the cold temperature region and the associated advantages of simplicity and enhanced reliability, the pulse tube system has become one of the most important topics in the field of cryogenics refrigeration. The main advantage of this new device, as compared to conventional Stirling and Gifford-McMahon systems, is its reliability and long life due to the absence of moving part at low temperature region.

- *Working Principle of the Pulse Tube Refrigerators*

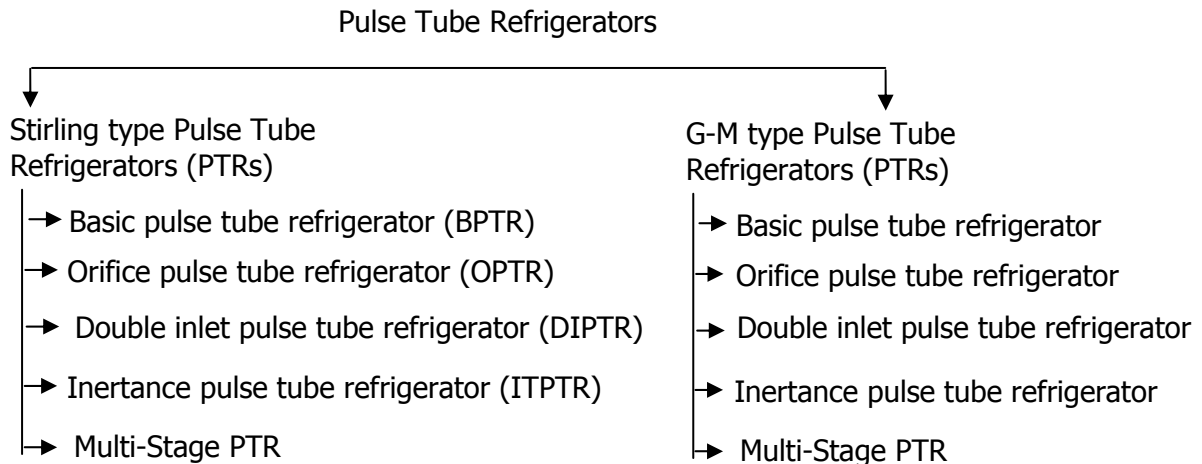
The pulse tube refrigerators (PTR) are capable of cooling to temperature below 123K. Unlike the ordinary refrigeration cycles which utilize the vapor compression cycle as described

in classical thermodynamics, a PTR implements the theory of oscillatory compression and expansion of the gas within a closed volume to achieve desired refrigeration. Being oscillatory, a PTR is a non steady system that requires time dependent solution. However like many other periodic systems, PTRs attain quasi-steady periodic state (steady-periodic mode). In a periodic steady state system, property of the system at any point in a cycle will reach the same state in the next cycle and so on. A Pulse tube refrigerator is a closed system that uses an oscillating pressure (usually produced by an oscillating piston) at one end to generate an oscillating gas flow in the rest of the system. The gas flow can carry heat away from a low temperature point (cold heat exchanger) to the hot end heat exchanger if the power factor for the phasor quantities is favorable. The amount of heat they can remove is limited by their size and power used to drive them.

### 1.5 Classification of Pulse Tube Refrigerators

There are many ways of classifications of pulse tube refrigerator.

- *Based on nature of pressure wave generator:*
  - (i) Stirling type PTR(valve less)
  - (ii) Gifford McMahon (GM) type PTR(with valve)



- *On the way of development:*
  - (i) Basic Pulse Tube Refrigerator(BPTR)
  - (ii) Orifice pulse tube refrigerator(OPTR)
  - (iii) Double inlet pulse tube refrigerator(DIPTR)

- (iv) Multiple inlet pulse tube refrigerator
  - (v) Inertance tube pulse tube refrigerator(ITPTR)
  - (vi) Single stage pulse tube refrigerator
  - (vii)Multi stage pulse tube refrigerator
  - (Viii)Thermoacoustic pulse tube refrigerator (TAPTR)
- *According to geometry or shape:*
    - (i) In-line type pulse tube refrigerator
    - (ii) U type pulse tube refrigerator
    - (iii) Coaxial type pulse tube refrigerator

## 1.6 Types of Pulse Tube Refrigerators

Pulse tube refrigeration systems can be classified as either a Stirling type or a GM type according to the method of pressurization and expansion as shown in Fig.1.1 (a) and (b). For a Stirling type pulse tube shown in Fig.1.1 (a) a piston cylinder apparatus is directly coupled to the hot end of the regenerator so that the pressure fluctuations are directly generated by the piston movement.

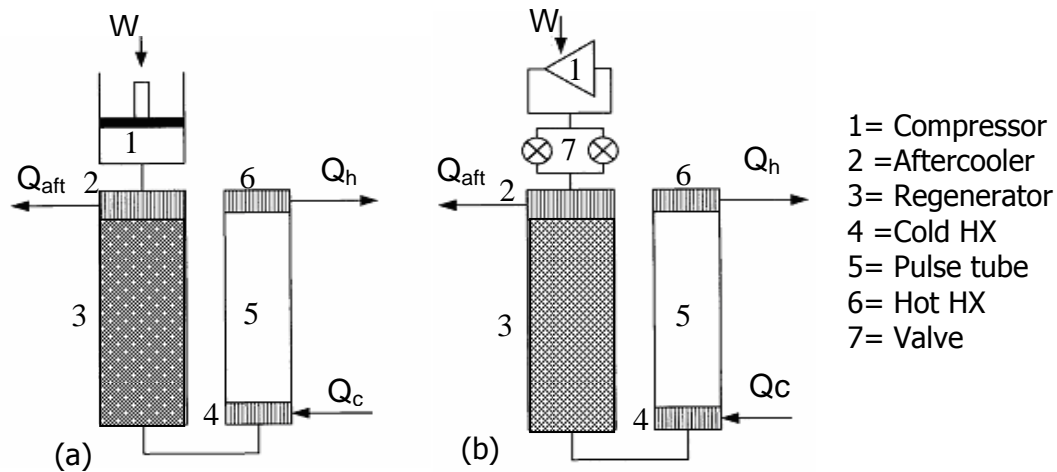


Fig.1.1 Schematics of basic pulse tube refrigerator (a) Stirling type (b) G-M type.

In Stirling type PTR, the frequency of the compressor is the same as that of the pulse tube. The heat of compression by the compressor must be removed to the environment by a heat exchanger between the compressor and the regenerator, commonly known as after cooler or precooler. These aspects are the same in Stirling type and G-M type refrigerators.



These are used for PTRs in the higher temperature ranges of about 50K. The typical operating frequency of Stirling type PTR is 10-120Hz, which is higher than that of a GM type pulse tube as shown in Fig.1.1 (b). Because of this high operating frequency and the absence of valve losses, Stirling type pulse tube systems generally produce higher cooling powers than GM type pulse tube. However the rapid flow oscillation of fluid heat exchange required in Stirling type pulse tube refrigerators limits their performance at low temperatures, such as at 10K and below. In this range, the longer time allowed for thermal diffusion by the slower frequency G-M type pulse tube refrigerators provides a higher efficiency option. The G-M type pulse tube refrigerator distributes high/low-pressure gas into the pulse tube and other components by use of a valve system. Generally a rotary valve or solenoid valve is used in G-M type cryocooler. The periodic opening/closing operation of the high/low pressure valves produces a pressure pulsation in the system. Because of the limitations associated with the valve operation a typical G-M type pulse tube operates at frequencies of a few hertz (1-5Hz). The valve system separating the compressor and the pulse tube system provides the possibility of eliminating vibration problems caused by the compressor and permits remote location of the compressor from the cold head.

Fig.1.2 shows the main components of Stirling type BPTR. It is composed of six components: compressor, after cooler, regenerator, cold heat exchanger, pulse tube and warm heat exchanger. In a BPTR, the oscillatory pressure waves impose a shuttling effect to the working fluid in the pulse tube. The shuttling effect creates an energy interaction between the pulse tube wall and the working fluid. This is known as surface heat pumping process [1]. Thus, the BPTR achieves refrigeration through the surface heat pumping process between the working fluid and the pulse tube walls. BPTRs have relatively low coefficients of performance and can typically reach a cold end temperature of the order of 124K.

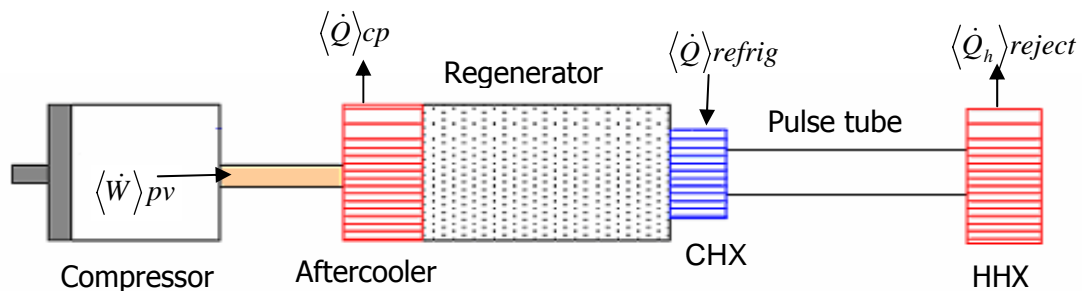


Fig.1.2 Schematic diagram of basic pulse tube refrigerator (BPTR).

The second type of the PTR is the Orifice Pulse Tube Refrigerator (OPTR), shown in Fig.1.3. OPTRs are significantly better than BPTRs, and are among most widely refrigerator until the mid 1990s in Stirling type PTR [97]. The schematic configuration of an OPTR can be viewed as a modification of the BPTR. This modification is made by including an orifice valve and a surge volume at the warm end of the BPTR, as depicted in Fig.1.3. Additional components create an advantage of in-phase relationship between the mass flow and the pressure within the pulse tube to enhance the heat transport mechanism. But the mass flow through the regenerator is increases leading to degradation of regenerator performance. This drawback is removed by adding a second orifice i.e. double inlet PTR.

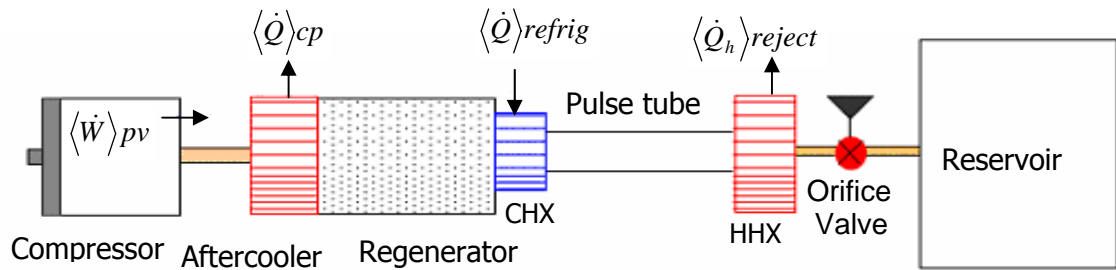


Fig.1.3 Schematic diagram of orifice pulse tube refrigerator (OPTR).

In the double-inlet pulse tube refrigerator (DIPTR)[35] the hot end of the pulse tube is connected with the entrance (hot end) of the regenerator by an orifice adjusted to an optimal value shown in Fig.1.4(a) and (b) for Stirling type and GM type DIPTR respectively. The double inlet is a bypass for the regenerator and hence reduces the cooling power. In addition, the valve is a dissipative device, which leads to a deterioration of the performance. However, both these disadvantages are overcome by the fact that the double inlet reduces the dissipation in the regenerator. As a result, the performance of the overall system is improved significantly.

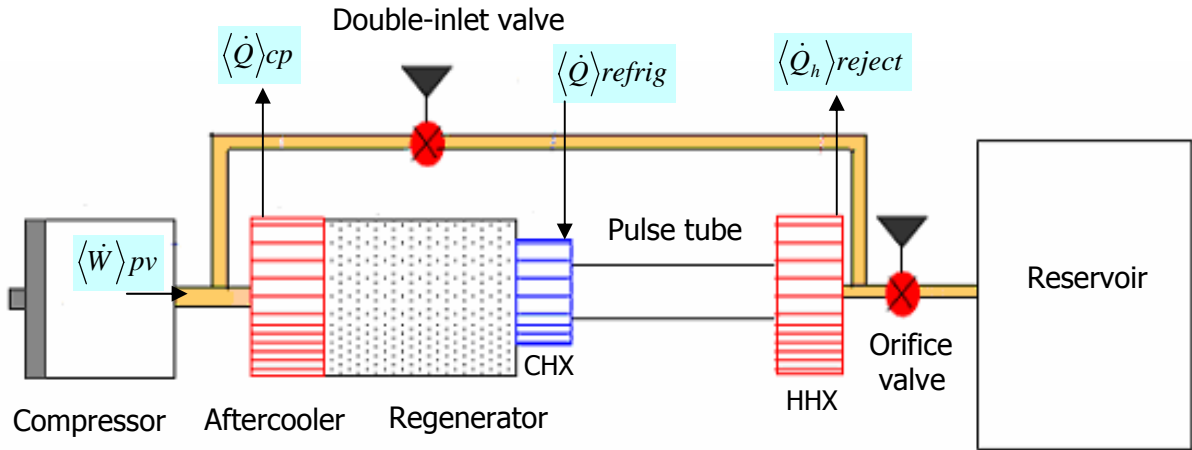


Fig.1.4 (a) Schematic diagram of Stirling type double inlet pulse tube refrigerator.

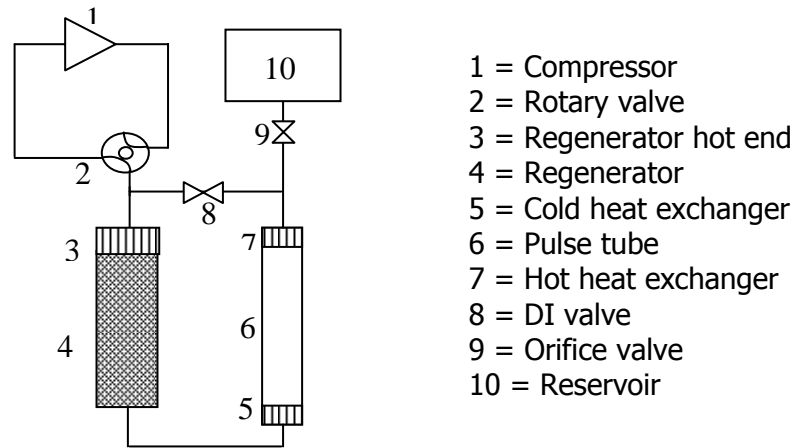


Fig.1.4 (b) Schematic diagram of G-M type double inlet pulse tube refrigerator.

The fourth and the most recently invented PTR is the inductance tube pulse tube refrigerator shown in Fig.1.5. In this type of PTR the orifice valve is replaced by a long inductance tube having very small internal diameter and adds reactive impedance to the system [58]. The implementation of this inductance generates an advantageous phase shift in pulse tube and produces an improved enthalpy flow. Studies show that use of the inductance tube is significantly beneficial for large-scale pulse tubes operating at higher frequencies.

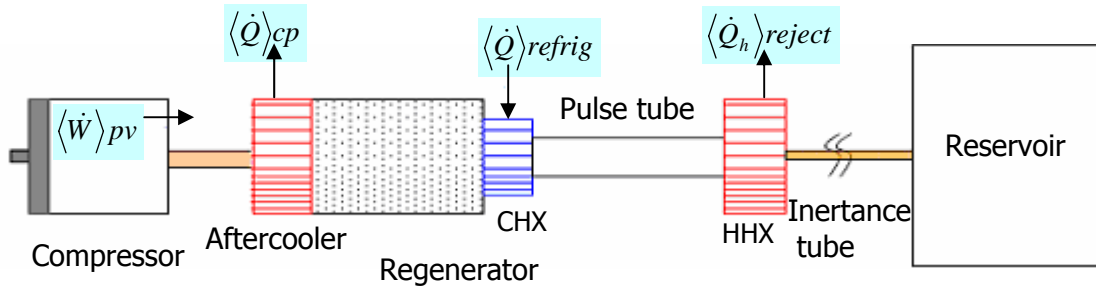


Fig.1.5 Schematic diagram of the inertance tube pulse tube refrigerator.

Pulse tube refrigerators are also classified according to their geometry or shape or the arrangement of components. These are linear type; U type and coaxial type, each of them are described below in brief.

- *Linear type PTR*

If the regenerator and the tube are in line as shown in Fig.1.6 it called a linear PTR. The best arrangement for mounting the PTR in the vacuum chamber is with the hot end of the tube, where heat is released to the environment, connecting to the vacuum chamber wall. However the cold end of the regenerator is inside the vacuum chamber.

- *U-shape type PTR*

The disadvantage of the linear PTR is that the cold region is in the middle of the cryocooler system. For many applications it is preferable that the cooling is produced at the end of the cooler. U shaped, PTRs shown in Fig.1.6(b) are made by bending the PTR at the cold end of the regenerator and the tube. Both hot ends can be mounted on the flange of the vacuum chamber at room temperature. This is the most common shape of PTRs.

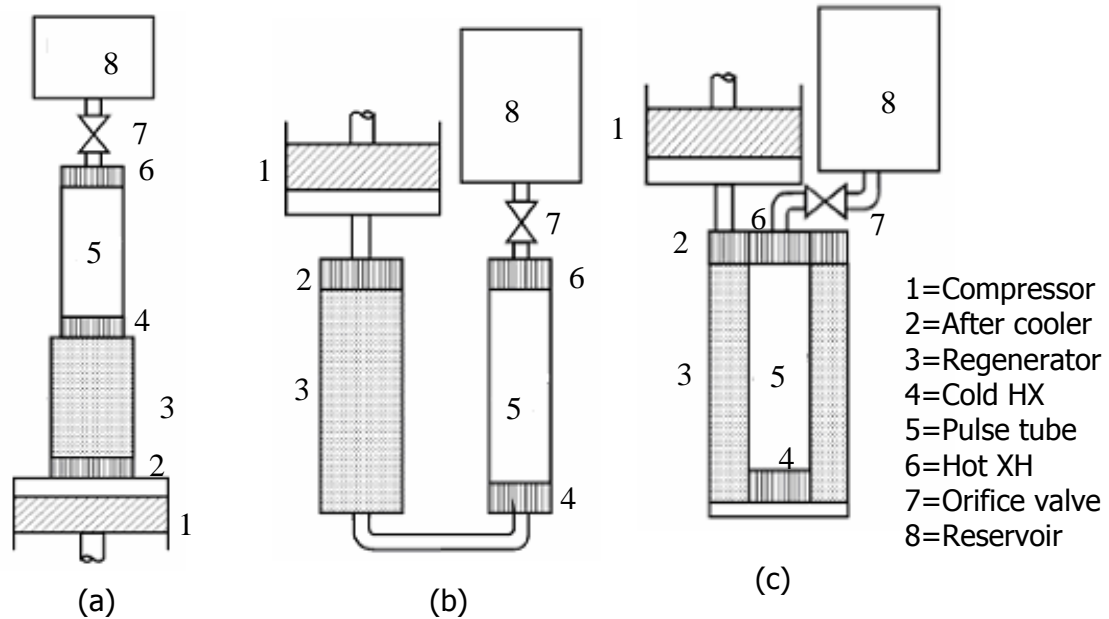


Fig.1.6 Schematic diagram of pulse tube geometry (a) Linear, (b) U-type, (c) Coaxial.

- *Coaxial type PTR*

For some applications it is preferable to have a cylindrical geometry. In that case the PTR can be constructed in a coaxial way so that the regenerator becomes a ring shape space surrounding the tube as shown in Fig.1.6(c). A disadvantage of this construction is that there is thermal contact between the tube and the regenerator. Generally the temperatures of the two components may differ. This leads to the degradation of regenerator performance.

- *Warm expander PTR*

In this system, instead of an orifice and buffer an expander is installed as shown in Fig.1.7 (a). Unlike the orifice in the single-orifice case there is no energy dissipation. The work that is recovered is used to improve the overall performance of the system. By actively controlling the amplitude and phase one can optimize the system. If the work is recovered, the COP of this type of PTR is higher than that of the PTR with passive elements at the hot end. This is important, especially for applications near room temperature where the difference between the COP of the ideal PTR and the Carnot COP is very high.

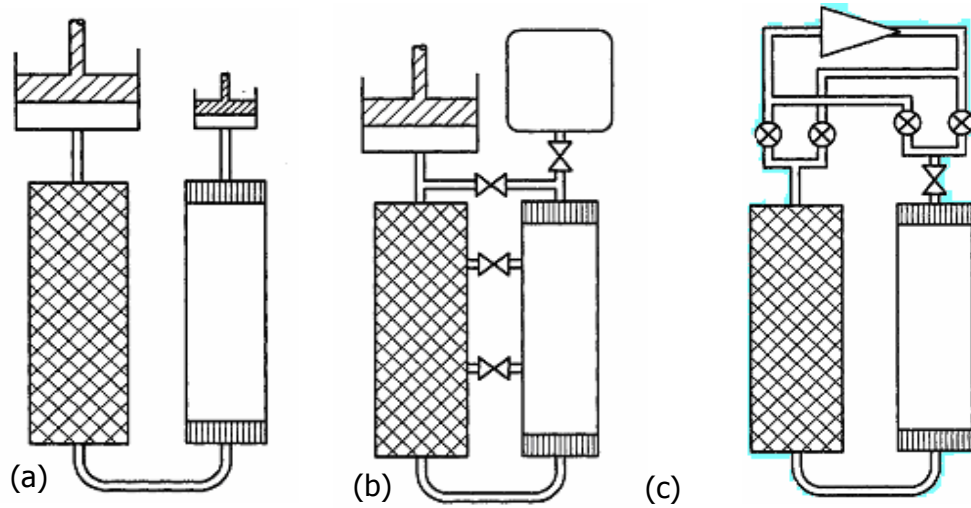


Fig.1.7 Schematic diagram of (a) Warm expander PTR (b) Multiple-inlet PTR (c) Four valve PTR.

- *Multiple-inlet type PTR*

In this type of PTR some points in the regenerator is connected to some points in the pulse tube via flow resistors. Fig.1.7(b) depicts schematic diagram of the multiple inlet system. The flow resistance of the connection must be of the same order as the flow resistance of the regenerator. This type of system improves the performance due to similar distribution of temperature along the length of both regenerator and pulse tube.

- *Four –valve type PTR*

The hot end of the tube is connected to the low-and high-pressure sides of the compressor by valves, which are opened and closed by a timing mechanism and are adjusted for optimum performance. Fig.1.7(c) shows the schematic diagram of the four –valve method. The opening and closing times of the orifice at the hot end of the tube are synchronized with the pressure wave in the tube and adjusted for optimum performance of the system. However, a small error in this timing can generate a big DC flow, which ruins the performance of the cooler. The advantages are that large and heavy buffer volume is omitted and that there is a large degree of freedom for optimization of the system.

- *Thermoacoustic PTR*

Thermoacoustic refrigerator is also known as resonant pulse tube. This works on the principle of thermo-acoustic pressure wave instead of a mechanical one. The thermoacoustic driver pulse tube refrigerator is shown in Fig.1.8. It was first demonstrated in 1990 in a joint effort of NIST and Los Alamos National Laboratories (1990) [9]. It reached a no-load temperature of 90K and is the first cryogenic refrigerator with no moving parts.

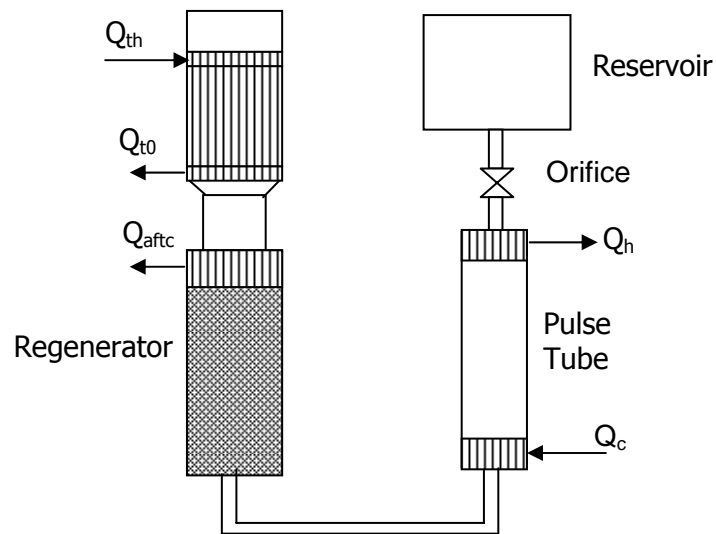


Fig.1.8 Schematic diagram of thermo-acoustic PTR.

- *Multistage arrangement type PTR*

It is really impossible to achieve very low temperature in a single stage of PTR. So one PTR can be used to pre-cool the other. For temperatures below 30K, it turns out to be advantageous to split the system in two i.e. double-stage PTR shown in Fig.1.9 (a) and (b). In this arrangement the hot end of the second tube is connected to the room temperature and not to the cold end of the first stage. In this way it is avoided that the heat released at the hot end of the second tube is a load on the first stage. Three-stage PTRs have also been introduced. With a three-stage PTR, 1.78K has been reached using  $^3\text{He}$  as the working fluid.

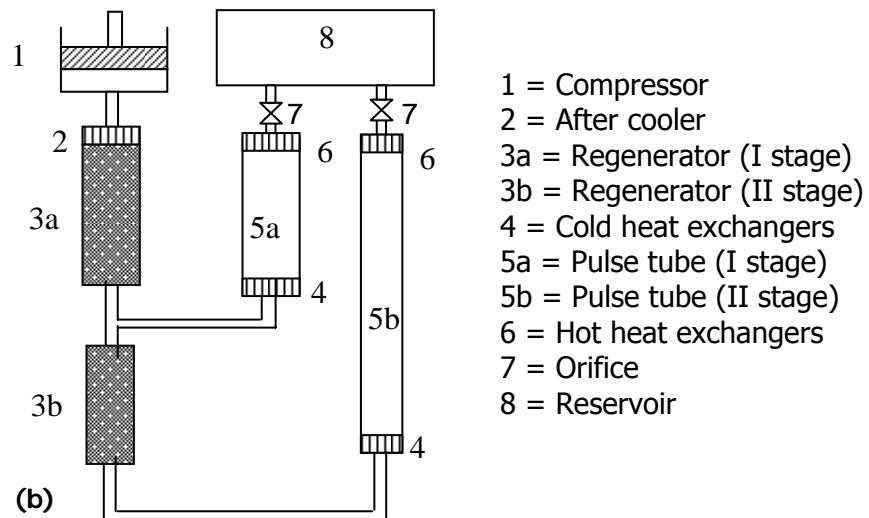
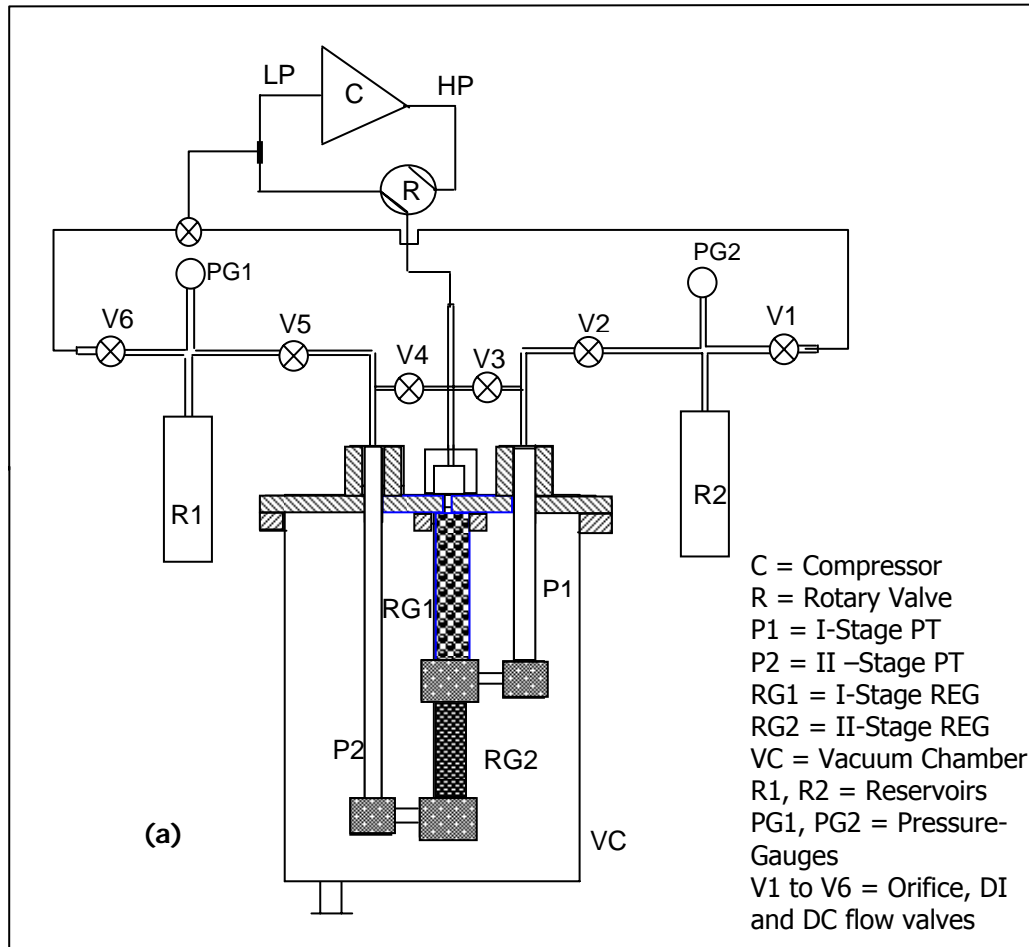


Fig.1.9 Two-stage double inlet pulse tube refrigerator (a) G-M type (b) Stirling type.



- *Minor orifice type PTR*

The presence of the second orifice (DI valve) inlet opens an internal circuit. If somewhere in this circuit there is an asymmetrical flow resistance, rectification of the flow takes place, which leads to an internal circulation through the loop of regenerator, pulse tube, and second inlet. In any case this circulation flows from the hot to the cold end, thus giving a heat load on the coldest parts of the cooler, which can lead to severe degradation of the performance. A way to overcome this internal circulation is by installing a minor orifice. Fig. 1.10 shows a GM-type double inlet PTR with minor orifice. The two valves in series with the minor orifice are used to connect the minor orifice to one of the two sides of the compressor.

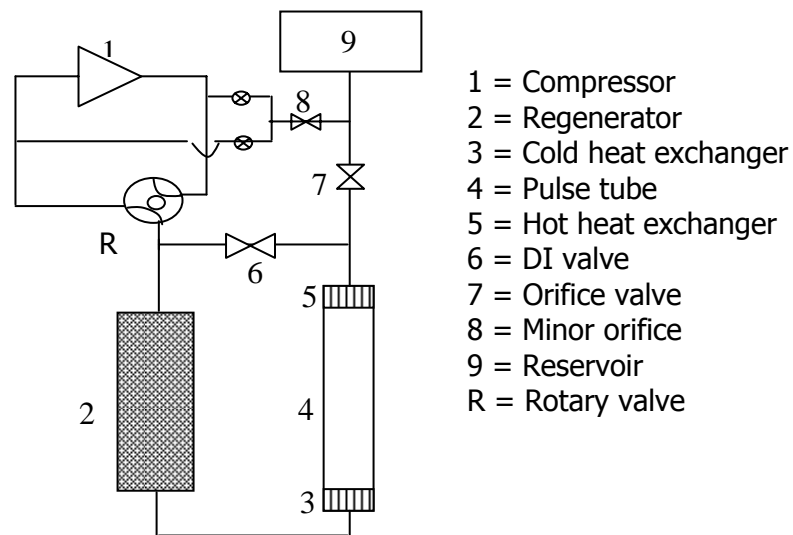


Fig.1.10. Double inlet pulse tube refrigerator with minor orifice.

This is an adjustable flow resistance in a flow line between the hot end of the tube and the high or low-pressure side of the compressor. By adjusting the minor orifice, direct current (DC) flow of gas can be superposed on the existing flow distribution. At the proper value of the minor orifice the unwanted DC flow can be suppressed. The experience with the minor orifice has shown that a small DC flow from the regenerator to the hot end of the tube is in fact beneficial for the operation of the PTR. It is postulated that the deliberately imposed DC flow reduces the heat flow from the hot end of the tube to the cold parts of the cooler.

- *Active buffer PTR*

Figure 1.11 gives the schematic diagram of the active buffer PTR. Two or more buffer volumes have placed instead of one buffer behind the orifice. The buffers are connected to

the warm end of the tube by valves, which are opened and closed by a timing mechanism; which is adjusted so that optimum performance is obtained.

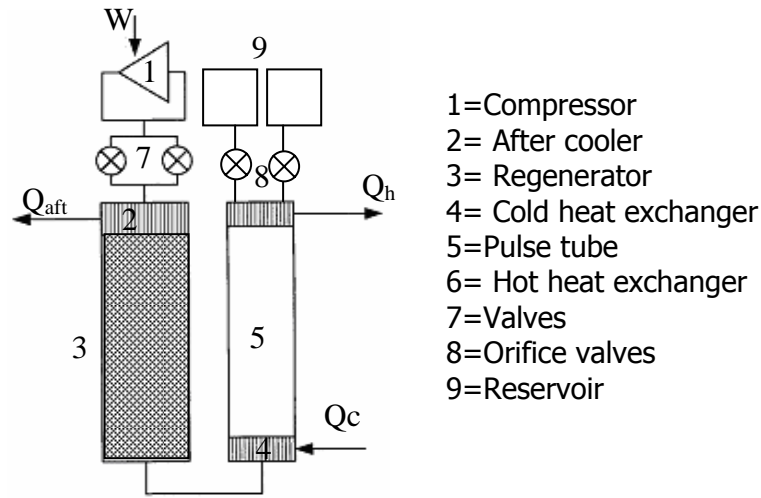


Fig.1.11 Schematics of the Active-buffer PTR.

### 1.7 Components of Pulse Tube Refrigerator

- *Compressor*

The main function of the compressor is to supply gas pressurization and depressurization in the closed chamber. Electrical power is applied to the compressor where this electrical work is converted into the mechanical energy associated with sinusoidal pressure waves, resulting in gas motion. In an ideal compressor, the electrical power provided to the compressor must be equal to  $f \oint PdV$ , where the integration is performed over an entire cycle, P is the compressor pressure, and f is the compressor frequency. In an actual system, however, the above-mentioned power (the PdV power) is always less than the actual measured electrical power due to the associated irreversibilities. Usually reciprocating nature of compressor is used in case of Stirling model; it may also be a dual opposed piston type.

- *After cooler*

The function of the ideal after cooler is to extract all the heat that is generated in the compressor volume during the gas compression and dispose to environment. This minimizes the warm end temperature so that the regenerator can work more efficiently and supply low

temperature working fluid to the system. Typically, these types of heat exchangers are assembled using copper wire mesh screens that are directly in contact with the housing wall.

- ***Regenerator***

The regenerator is the most important component in pulse tube refrigerator. Its function is to absorb the heat from the incoming gas during the forward stroke, and deliver that heat back to the gas during the return stroke. Ideally, PTC regenerators with no pressure drop and a heat exchanger effectiveness of 100% are desired, in order to achieve the maximum enthalpy flow in the pulse tube. The performances of the real regenerators are of course far from ideal. Stainless steel wire screens are usually selected as the regenerator packing material, since they offer higher heat transfer areas, low pressure drop, high heat capacity, and low thermal conductivity. A typical regenerator housing is shown in Fig.1.12 (a)

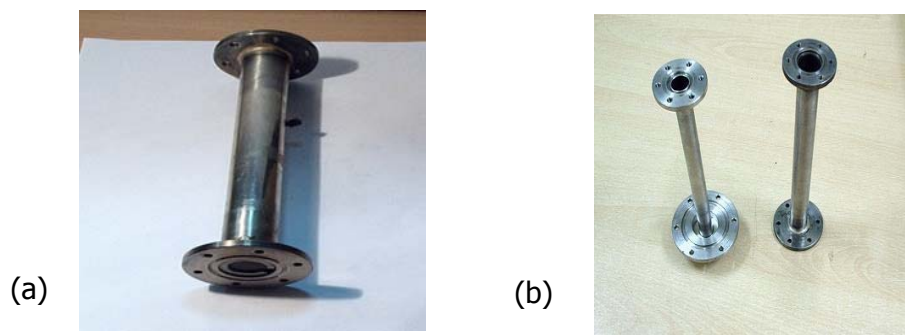


Fig.1.12 Typical pictures of (a) Regenerator (b) Pulse tube.

- ***Cold Heat Exchanger (CHX)***

CHX can be best viewed as the equivalent of the evaporator in the vapor compression refrigeration cycle. This is where the refrigeration load is absorbed by the system. This is the junction of the regenerator and pulse tube. Copper wire mesh screens are used to exchange heat with the housing wall, and thereby receive the applied heat load.

- ***Pulse Tube***

The pulse tube is the most critical component of the whole refrigerating system. The main objective of the pulse tube is to carry the heat from the cold end to the warm end by an enthalpy flow. By imposing a correct phase difference between pressure and mass flow in the pulse tube by phase shifting mechanisms, heat load is carried away from the CHX to the WHX.

Physically, the pulse tube is simply a hollow cylindrical tube made up of stainless steel with an optimum thickness to enhance the surface heat pumping. A typical picture of pulse tube is shown Fig.1.11 (b).

- *Hot Heat Exchanger (HHE)*

Hot end exchanger is where the gas rejects heat of compression in every periodic cycle of operation. Upon receiving the enthalpy flow from the pulse tube, the heat load at a higher temperature is rejected to the environment. Usually, air cooling or water cooling system is used to take away the heat from the hot end exchanger.

- *Orifice Valve, Inertance Tube and Surge Volume*

The role of either the inertance tube or the orifice valve is to appropriately adjust the phase difference between the mass flow rate and the pressure. By controlling the orifice diameter or the inertance tube diameter and length, the desired phase relationship can be obtained. In general, the orifice valve is a needle valve, and the inertance tube is an open cylindrical stainless tube. In comparison with the aforementioned pulse tube, the inertance tube is much longer, and its diameter is much smaller. The surge volume can be viewed as a closed buffer reservoir of sufficient volume to allow for small pressure variations resulting from the oscillating mass flow.

- *Rotary valve*

The rotary valve is one of the critical components of a GM type pulse tube refrigerator. The schematic of rotary valve is shown in Fig.1.13. It is used to switch high and low pressure from a helium compressor to the pulse tube system. The high and low pressure of helium compressor are connected to the rotary valve through the quick disconnect couplings. The rotary valve has a rulon part which is made to rotate with the help of a synchronous motor against an aluminium block with predefined passages connecting the high and low pressures from the helium compressor. The rotational frequency of the synchronous motor is controlled using an inverter drive. The rotary valve has been designed to produce pressure wave in the frequency range from 1Hz to 3Hz. A typical design of rotary valve is shown in Fig.1.13.

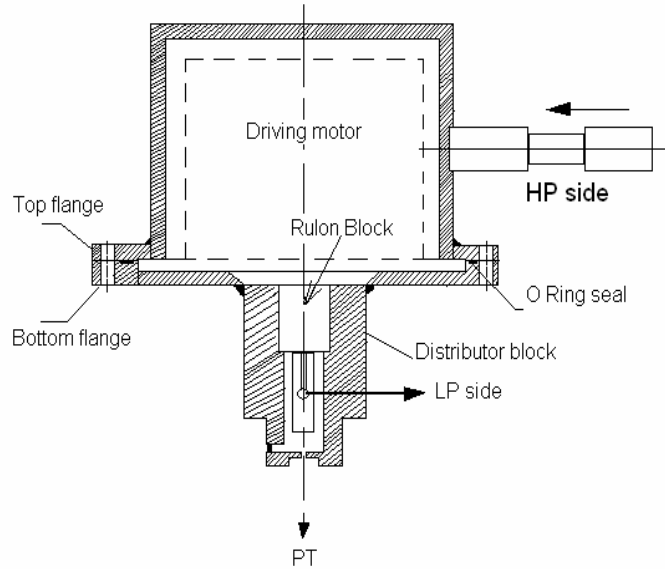


Fig.1.13 Schematic diagram of rotary valve.

### *1.8 Aim of the Present Investigation*

All pulse tube refrigerator units operate as closed systems where no mass is exchanged between the cryocooler and its environment. The only moving component is the piston (or the rotary valve) which oscillates back and forth to generate periodic pressure oscillation of the working fluid. Mostly helium is chosen as working fluid because it offers the lowest critical temperature compared to other available gases. It has also high thermal conductivity.

Accurate modeling of the pulse tube cryocooler is essential to predict its performance and thereby arrive at optimum design. At the current stage of world wide research, such accurate models are not readily available in open literature. Further, the complexity of the periodic flow in the PTC makes analysis difficult. Although different models are available to simulate pulse tube cryocoolers, the models have its limitations and also range of applicability.

In order to accurately predict and improve the performance of the PTC system a reasonably thorough understanding of the thermo fluid-process in the system is required. One way to understand the processes is by numerically solving the continuum governing equations based on fundamental principles, without making arbitrary simplifying assumptions.

The recent availability of powerful computational fluid dynamics (CFD) software [175] that is capable of rigorously modeling of transient and multidimensional flow and heat transfer

process in complex geometries provides a good opportunity for analysis of PTCs. A successful demonstration of the suitability of CFD type analysis for Stirling and Gifford-McMahon type PTCs is one of the main features of the investigation.

The experimental method to evaluate the optimum parameters of PTCs is difficult. On the other hand, developing a specialized computer code for its CFD analysis is equally complex. Thus numerical experimentation using CFD software is a suitable option. It should, however, be emphasized that CFD-type predictions, like other model-generated results, are reliable only when they are verified against experimental data. Therefore, importance of experimental validation is to be emphasized. An issue of particular interest is the relevance of the predictions of one-dimensional models to the performance of pulse tube cryocoolers. This is important because the calculations for design procedure are usually based on one dimensional flow models. Thus the validity one-dimensional flow model to use for the multi-dimensional flow model is an important aspect of analysis. These issues are addressed in the dissertation.

In this study, multi-dimensional continuum governing equations are numerically solved to investigate the details of thermo-fluid process in Stirling type Orifice Pulse Tube Refrigerator (OPTR) and Inertance Tube Pulse Tube Refrigerator (ITPTR), and GM type Double Inlet Pulse Tube Refrigerator (DIPTR). The system includes compressor, regenerator, pulse tube, cold and hot heat exchangers, inertance tube/orifice and by pass valves, and reservoir etc. In this investigation the Commercial CFD package, FLUENT is utilized[175]. The simulation results are presented and compared with experimental data.

Thus the present study aims to focus on the following points:

- Principle of low temperature generation in pulse tube cryocooler from phasor and one-dimensional model.
- Derivation of pressure drop characteristics of wire mesh matrix and other type of porous media regenerator.
- The simulation of PTC using a commercial CFD software, FLUENT to study the flow phenomena and heat transfer characteristics in the pulse tube system. Under this simulation the following models are analyzed.
  - (i) 2D -contour axis-symmetric problem of Stirling type orifice and inertance pulse tubes.
  - (ii) 2D –contour of GM type double inlet pulse tube.

- (iii) 3D-contour of GM type double inlet pulse tube.
- Comparison of experimental data with the models (ii) and (iii) as described above.

### *1.9 Organization of the Manuscript*

- The thesis contains seven chapters including the present chapter (Chapter I) on introduction. In this chapter, an introduction about cryocoolers, classification of cryocoolers, their working principles, general applications, comparisons and a brief description of the different types of pulse tube refrigerators along with their components are discussed.
- The second chapter deals with an overview of the subjects and review of the literatures on pulse tube refrigerators with related technologies.
- The third chapter describes the different methods of pulse tube refrigerator analysis. Surface heat pumping, enthalpy flow theory, phasor diagrams for different PTR models are presented. Also development of time dependent approximate theoretical models for pulse tube refrigerator is discussed.
- The fourth chapter describes the derivation of governing equations for fluid flow and heat transfer in pulse tube and regenerator. For regenerator which is modeled as porous medium, the methods are discussed to calculate porous media parameters with emphasis on wire mesh regenerators. Also the step by step procedures for CFD simulations are presented.
- Detailed CFD simulation, using commercial software, Fluent for Stirling type orifice pulse tube refrigerators (OPTR) and inertance tube pulse tube refrigerators (ITPTR) are presented in chapter V. Results and discussions of CFD simulations for these models are also presented in this chapter.
- For G-M type double inlet pulse tube refrigerator (DIPTR), details of geometry, meshing of the geometry, boundary conditions, CFD simulation results and discussions are presented in chapter VI.
- The final chapter reflects salient points and concluding remarks on the results and adopted methodology on previous chapters. Some recommendations have also been highlighted for further investigation.

## *Chapter II*

# Literature Review

### *2.1 Introduction*

This chapter represents a review of the literature. It can be broadly classified under three main categories. The first part of the survey deals with the theoretical investigations on pulse tube refrigerators, the second part deals with experimental investigations on pulse tube refrigerators and the third part deals with the efforts to improve the regenerator (porous-matrix) performance and also highlights some other useful literatures related to improve the overall performance of pulse tube refrigerator.

### *2.2 Theoretical Investigations on PTRs*

- *Basic Pulse Tube Refrigerator (BPTR):*

Gifford and Longworth from Syracuse University in 1963 pioneered the introduction of pulse tube refrigerator, a new method of achieving cryogenic temperature. Although the development of pulse tube models for research purpose started in 1963, their first paper was published on 1964 [1] giving a brief account of progress made. The phenomenon was described as “the pressurization and depressurization of any closed volume from a point on its periphery sets up temperature gradients in the volume”. Obviously the temperature gradients thus obtained depend upon the geometry of closed volume and the operating condition.

Their first design was based on a hollow cylindrical tube with one end open and the other end closed. The closed end is exposed to an ambient temperature heat exchanger, while the open end represents the cold end. As a result of the oscillatory flow field caused by piston, the open end was subjected to an oscillatory pressure from the regenerator, causing the open end to cool. This refrigerator is commonly known as Basic Pulse Tube Refrigerator (BPTR). In a second paper, published only months after the first, Gifford and Longworth [2] reported useful refrigeration in a pulse tube operating well below the critical pressure ratio. Later



Gifford and Longworth [3] developed a relation for the cold end temperature with zero heat pumping rate in terms of length ratio, hot end temperature and the ratio of specific heats of gas with the help of surface heat pumping mechanism. They stated that surface heat pumping is caused by an unusual interaction between fluid displacement along a surface, energy exchange in the fluid, and heat exchange with the surface, as a result of a periodic change of pressure of gas. In their fourth paper [4] they have reported the problem of reversible pulse tube and attempted to compare operation with that of a valved pulse tube.

de Boer [5] developed a thermodynamic model of BPTR with various improvements by taking into account the gas motion during the cooling and heating steps, that result in more accurate temperature profiles. In second paper [6] he has presented a thermodynamic analysis of the BPTR with a regenerator and heat exchangers at both ends. The performance of the regenerator and its adjacent heat exchangers has been investigated using control volume analysis to determine enthalpy flows and by control mass analysis to determine heat flows associated with individual gas elements. Soo et al.[7] studied the secondary flow in BPTR. The existence of large scale streaming and the effect of axial temperature gradient on secondary flow within the basic pulse tube configuration has been shown analytically. Efficiency of basic pulse tube was very poor, and, as a result, little work was done with the BPTR in the first twenty years after its discovery.

- *Orifice Pulse Tube Refrigerator (OPTR):*

Orifice pulse tube refrigerator was introduced in 1984 by Mikulin et al. The invention of the simple OPTR is regarded as the milestone of the developments of pulse tube cooler. Starch and Radebaugh [8] developed an analytical model for OPTR and made a simple expression for the gross refrigeration power, which agrees with experiments. Wu et al. [9] have done a numerical analysis for an OPTR with a valve less compressor and described the process occurring in the pulse tube. Richardson [10] reported that the valved pulse tube, otherwise known as the orifice pulse tube, is able to reach much lower temperatures. Tward et al. [11] studied the performance of pulse tube coolers in order to determine their suitability for development of long life space coolers. Lee et al. [12] showed the influence of gas velocity on surface heat pumping for the OPTR. Kasuya et al. [13] has discussed optimum phase angle between pressure and gas displacement in pulse tube refrigerator. Wang et al. [14] developed an improved numerical modeling technique for predicting the detailed performances and

characteristics of an orifice pulse tube refrigerator. They included some physical factors in order to improve the accuracy of the model such as flow friction, heat transfer in the heat exchanger and the regenerator, real material properties etc. In 1992, a research program began on pulse tube refrigerator at NASA –Ames Research Centre led by Kittel [15]. To improve the performance, this program mainly focused on the optimization of the pressure wave generator and thermal regenerator. Consequently, encouraging results have been obtained that added evidence to the advantages of pulse tube refrigerator as compared to Stirling refrigerator. David et al. [16] analyzed the mechanism of heat flow in the pulse tube and explained the refrigerating effect as the result of hysteresis of the gas elements entering and leaving the pulse tube.

Storch et al.[17] have described an analytical model of the orifice pulse tube refrigerator with the help of phasor analysis. Zhu et al. [18] introduced an isothermal model for an OPTR that is much simpler than nodal analysis. Wu et al. [19] developed a numerical model of OPTR by using the method of characteristics and made a preliminary comparison with experiment. Their suggestions are useful and convenient for understanding of the process and design of the device. Kittel et al. [20] performed a detailed study of the flow field in a pulse tube, and showed that flow circulation, commonly known as a secondary enthalpy streaming effect, creates a convective enthalpy flow from the hot end to the cold end that acts as a loss mechanism. Roach et al. [21] developed a simple modeling program for orifice pulse tube coolers and theoretical analysis of the behavior of a typical pulse tube and made a comparison with the earlier model. Rawlins et al. [22] developed a technique for the instantaneous measurements of mass flow rate and temperature in an OPTR during actual operation. Kittel et al. [23] described the qualitative behavior of pulse tube refrigerators on the basis of simple 1-D models. These models have been used to introduce and demonstrate the useful concepts of entropy flow and of Gibbs free energy flow.

Huang et al. [24] developed a linear flow network model for the analysis of an orifice pulse tube refrigerator. The flow network analysis has considered the pressure as the electric voltage and the mass as the electric current. Xu et al. [25] analyzed the behavior of the various gas elements, which enter the tube of a refrigerator from its cold end with the help of method of characteristics. Kuriyama et al.[26] discussed the relationships among the pressure, mass flow rate and temperature oscillations in an OPTR. de Waele [27] proposed a new definition of the efficiency of regenerator's that takes into account all forms of dissipation in

regenerators on an equivalent basis. In second paper [28] he reformulated the theory of pulse-tube operation from the ideal-gas situation to a real gas and found that the effect of non-ideal-gas properties has a profound effect on the energy balance in the regenerator and on the expression for the cooling power. Gerster et al. [29] described a new loss, called "hot end loss". This occurs due to the regenerative effect of the hot end heat exchanger. The hot end loss is described by means of the enthalpy flow model. Hagiwara et al. [30] have adopted measurement using Rayleigh scattering in order to measure the temperature profile in the pulse tube. de Boer [31] have presented optimization result for OPTR, for large orifice volume and zero regenerator volume. They found that all non-dimensional quantities of interest depend on frequency and ratio of orifice conductance to regenerator conductance. Roach [32] have developed a calculation model that evaluates all the components of an orifice pulse tube cooler. The results of the calculation are oscillating pressures, mass flows and enthalpy flows in the main components of the cooler. For OPTR phasor analysis has been presented for mass flow rate and pressure at cold end. Desai et al. [33] have calculated refrigeration power and COP. Smith [34] studied the system of partial differential equations on modeling of pulse tube refrigerators.

- *Double Inlet Pulse Tube Refrigerator (DIPTR):*

Zhu et al. [35] achieved a new constructional solution to increase the OPTR refrigeration efficiency. On the basis of theoretical analysis, a modified version called double inlet pulse tube refrigerator (DIPTR) was suggested, which had a second inlet at the hot end of the pulse tube connected to the pressure wave generator. Numerical analysis and experimental results conform that the double inlet pulse tube has improved performance over the OPTR. Ju et al.[36] developed an improved numerical model for simulating the oscillating fluid flow and detail dynamic performance of the OPTR and DIPTR. The simulation model is useful for understanding the physical process occurring in the pulse tube refrigerator, and also for predicting the effect of the orifice and double-inlet valve on the refrigeration power and efficiency of pulse tube refrigerator.

Wang et al. [37] developed a numerical model of a double inlet pulse tube refrigerator (DIPTR) and solved the equations of continuity, momentum and energy numerically. Predictions showed that DIPTR would result in higher refrigeration power with lower P-V work than does the conventional orifice version; the bypass valve in the DIPTR has

a significant effect on the phase and amplitude of the dynamic parameters. Harold et al.[38] developed an analytical model for the performance of a DIPTR employing a stepped piston compressor. Zhu et al. [39] documented the work loss in DIPTR. An analytical equation of the mass flow rate through the by pass of a DIPTR is obtained by an analysis of the pressure drop in the regenerator. Kirkconnell [40] developed a 1-dimensional model to simulate the thermo-fluid interactions in the pulse tube. Zhu et al.[41] described an integration formula of enthalpy flow rate along the pulse tube in pulse tube refrigerators on the assumption of sinusoidal mass flow rate and sinusoidal pressure fluctuation based on the Lagrange method. Thummes et al.[42] noticed that the use of double-inlet mode in the pulse tube cooler opens up a possibility of DC gas flow circulating around the regenerator and pulse tube. Numerical analysis shows that effects of DC flow in a single-stage pulse tube cooler are different in some aspects from that in a 4K pulse tube cooler. Liang et al.[43] idealized the pulse tube refrigeration process by simplifying the practical conditions without losing the main characteristics of pulse tube refrigeration. Based on this idealization, the thermodynamic non-symmetry effect of the gas element working at the cold end of the pulse tube has been described. The gas elements enter the cold end of the pulse tube at the wall temperature of the cold end heat exchanger but return to the cold end of the pulse tube at much lower temperatures. They termed it thermodynamic non-symmetry in entering and leaving the pulse tube during one cycle. This effect has been conveniently used to explain the refrigeration mechanism of the basic, orifice and double inlet pulse tubes.

In their second paper, Liang et al. [44] developed the compound pulse tube model based on the earlier analysis and incorporated the thermal and viscous influence of the pulse tube wall and proposed a thermal viscous layer in the pulse tube. Hofmann et al. [45] described different types of pulse tube refrigerators by phase diagrams. This provides a simple means for finding the optimum phase shift between pressure and flow rate for PTRs operating with different kinds of phase shifters. Yuan et al. [46] described a detailed thermodynamic analysis of the working process of an active valve pulse tube refrigerator, which is introduced to enhance the performance of a single stage pulse tube refrigerator. Xu et al. [47] have done theoretical analysis and shown that, using  $^3\text{He}$ , the temperature limit is below 2K, and the efficiency of a 4K pulse tube refrigerator can be improved significantly. de Boer [48] analyzed the performance of the double inlet pulse tube (DIPTR) as a linearized model that takes account of the void volume of the regenerator. The phasor analysis has been extended for

DIPTR [49]. They have mentioned that DIPTR improves the refrigeration power and COP. For approximate PTR, numerical model is developed for single stage DIPTR. This model explained isothermal and adiabatic gas behavior of compressor and pulse tube [50].

Atrey et al.[51] have done the cyclic analysis of Stirling type cryocooler. Details of cryocooler design theory and practice has been covered at a short term course [52]. Radebaugh [53] presented a review of the pulse tube refrigerator from its inception in the mid-1960s up to the present state. Various factors are discussed which brought it from a laboratory curiosity to the point where it is now the most efficient of all cryocoolers and reliable enough to be used on space missions.

Popescu et al. [54] have critically reviewed the design and theory of the regenerative pulse tube cryogenic system. A general outlook of the functional principle of the process occurring in this cryogenic system is presented. Zhang et al.[55] have analyzed the effects of the reservoir volume on the thermodynamic performance of various components in a simple orifice and a double-inlet pulse tube cooler by combining a linearized model. They have presented the expressions of entropy production for those components. The results show that the reservoir volume has a significant influence on the entropy production in the various components when the reservoir to pulse tube volume ratio is smaller than about 5. The ratio is important to determine the minimum reservoir volume for a pulse tube cooler.

Razani et al. [56] developed a thermodynamic model based on exergy flow through pulse tube refrigerators (PTRs).They has proposed an exergetic efficiency parameter representing the losses in the pulse tube itself. The effects of control parameters representing a general phase shifter and their effect on the system performance are discussed. Ju [57] discussed and explained the thermodynamic loss of the rotary valve and the COP of GM-type pulse tube refrigerator by using the first and second laws of thermodynamics.

- *Inertance Tube Pulse Tube Refrigerator (ITPTR):*

Gardner et al. [58] used inertance tube instead of orifice valve. They have calculated phase shift between oscillating pressure and velocity and found that use of inertance tube improves the cooling power. Roach et al. [59] studied the advantages to be gained by replacing the orifice of a pulse tube cooler with an inertance tube, a long thin tube that introduces the possibility of additional phase shift between pressure and mass flow rate in the pulse tube section. Comparisons between a laboratory cooler with an orifice and with two inertance tubes have been presented; the inertance tubes yielded dramatic improvements

over the use of the orifice. de Boer[60] found the rate of refrigeration of the inertance pulse tube refrigerator (IPTR) as a function of the relevant parameters in the simplified case of infinite volume of the reservoir and zero dead volume of the regenerator. It is found that the performance of the IPTR is superior to that of the orifice pulse tube refrigerator (OPTR) over a limited range of frequencies. Zhu et. al. [61] introduced a nodal analysis method for simulating inertance tube pulse tube refrigerators. Wei et al. [62] have done theoretical calculation for inertance tube without a reservoir and showed that this device provides a rather large phase-leading effect. Thus phasor diagram is used to analyze the relationship between phase-leading requirement and the pulse tube geometry. They noticed that a larger void volume of pulse tube would require a larger phase-leading effect.

- *Other Pulse Tube Refrigerator Models:*

Tward et al. [63] have reported the performance and flight qualification of miniature pulse tube cooler designed specifically for use on small satellites. They reported that the miniature pulse tube cooler is intended for greater than 10 year long-life space application and incorporates a non-wearing flexure bearing compressor vibrationally balanced by a motor-controlled balancer and a completely passive pulse tube cold head. de Waele [64] documented general relationships for the entropy production in the components of pulse tubes, which has a wide range of validity. Von et al. [65] described the cooling performance of a pulse tube extending to room temperature which is precooled by a single stage GM refrigerator. They found that this system is possible to reach liquid helium temperatures without using rare earth compounds as regenerator material. Neveu et al.[66] developed both ideal and dynamic models for better understand the energy and entropy flows occurring in the pulse tube coolers. Ideal modeling is sufficient to quantify the maximum performance, which could be reached, but dynamic modeling is required to perform a good design.

Chen et al.[67] introduced a modified Brayton cycle, predicting the thermodynamic performance of pulse tube refrigeration with a binary mixture refrigerant. They established theoretical expressions of cooling power, thermodynamic efficiency and required work of a refrigeration cycle. Baek et al. [68] obtained the time-averaged mass flux and the study component of the second order temperature with the help of two-dimensional analysis of the tapered pulse tube. The effects of the taper angle and frequency on the enthalpy flow loss due to the mass streaming are also shown. In the second paper [69], they reported the

effects of the taper angle and the frequency on the steady mass flux and the enthalpy flow loss associated with the steady mass streaming by two-dimensional analysis of the tapered pulse tube. de Waele , et al.[70] addressed the question of when and how multistage in pulse-tube refrigerators improves the performance. They derived analytical expressions for the position of the first stage connection to the regenerator in the case of maximum cooling power and in the case for the minimum temperature for two-stage PTR. Gao et al. [71] have used gas mixtures for comparison in order to improve the performance of a one-stage pulse tube cryocooler, which have been used in other cryocoolers. Guoqiang et al. [72] have discussed the flow characteristics of a metering valve in a pulse tube refrigerator.

de Waele et al.[73] studied the performance of pulse tube at very low temperatures. They found that the cooling power of pulse tube coolers is zero when the thermal expansion coefficient is zero. Pan et al. [74] developed a single stage pulse tube refrigerator driven by a 7kW scroll compressor that equipped with a set of solenoid valves such that two different operations could be realized, namely a 4-valve configuration and an active buffer configuration. Both systems are compared with respect to various operational parameters.

Brito et al.[75] numerically developed a novel cryocooler named "free warm expander pulse tube cooler "for long life applications. Park et al. [76] obtained unsteady components of the second order axial velocity and temperature within a tapered pulse tube by using a hybrid method of solution. Graziani et al. [77] discussed the characteristics and performance of a new class of  $^3\text{He}$  refrigerators. They introduced a  $^3\text{He}$  refrigerator, which allows a temperature of 296 mK to be reached with a starting point of 4.2K, without pumping on the main  $^4\text{He}$  bath.

Waldauf et al. [78] have observed temperature instabilities in a four-valve pulse tube refrigerator. Investigations have shown that the anomaly is caused by the dc-flow. They have presented an actively controlled dc-flow suppression device, which uses a temperature gradient in the regenerator as a control parameter. Masao , et al.[79] have studied secondary flow in an inclined orifice pulse tube refrigerator at typical inclination angles of 0–180° by using a smoke wire flow visualization technique. Ronald et al. [80] discussed the effect of angular orientation to the refrigeration performance of high frequency (10-40 Hz) Stirling-type pulse tube cryocoolers typical of those used in long-life space applications. Orientation effects on the performance of such cryocoolers have recently been observed during system-level testing of both linear and U-tube type pulse tubes. Will et al.[81] have described two types of

valves, which have balanced forces on the rotor. In the first valve the rotor and the stator make no mechanical contact. The second type is a contact valve, like the classical valves, but the forces on the rotor are balanced in a different way. Therefore, these valves are less liable to wear, and the torques needed to rotate the valves is small. Jiang et al. [82] has reported the performance of a two-stage pulse tube cooler using  $^3\text{He}$  as working fluid. He reached the world record in lowest temperature. Devlin et al.[83] present the design of a completely closed-cycle refrigeration system. The system consists of four stages; the first two, 40.5 and 2.7K are provided by a pulse tube cooler, the third and fourth stages by helium adsorption refrigerators. He et al. [84] have made numerical analyses for the PTR to reveal the variation of its cooling capacity with the phase angle shift between the velocity wave and pressure wave. Yang et al.[85] have reported on the design and test of a two-stage pulse tube cooler, which is driven by a linear compressor with nominal input power.

Dang et al.[86] have designed and tested a set of Stirling-type non-magnetic and non-metallic co-axial pulse tube cryocoolers, intended to achieve portable cryogen-free systems with very low interference for high- $T_c$  SQUIDs operation. Jeheon et al. [87] described simple analysis of the pulse tube expansion efficiency. Yong et al. [88] have examined individual loss associated with the regenerator and combined these effects to investigate size effects on the performance of Stirling cycle cryocoolers. For the fixed cycle parameters and given regenerator length scale, it was found that only for a specific range of the hydrodynamic diameter can produce net refrigeration and there is an optimum hydraulic diameter at which the maximum net refrigeration is achieved. Tanaeva et al. [89] developed a new three-stage pulse-tube refrigerator (PTR) by scaling down a working model PTR by 50%. With  $^3\text{He}$  as a working fluid a no-load temperature of 1.73K is reached and a cooling power of 124 mW at 4.2 K is realized. Qiu et al.[90] have designed and tested a novel 4K separate two-stage pulse tube cooler (PTC). They reported that the lowest refrigeration temperature obtained at the first stage pulse tube is 13.8K. This is a new record for single stage PTC. Will et al.[91] derived a complete set of relations for the operation of counter flow pulse-tube refrigerators. The input parameters depend on the working fluid, the geometries of the pulse tube and the counter flow heat exchanger, and the compressor characteristics. Koettig et al. [92] introduced a new kind of two-stage pulse tube refrigerators. The chosen entire coaxial configuration combines the advantages of the coaxial design with the two-stage pulse tube concept. Lead coated screens build the inhomogeneous regenerator matrix of the second



stage. Without any rare earth compounds the refrigerator reaches a no load temperature of 6.6 K at the second stage cold tip. Liang et al. [93] analyzed the first and second law of thermodynamics for orifice type and the double-inlet type of pulse tube refrigerator.

Razani et al.[94] developed a thermodynamic model based on exergy flow through pulse tube refrigerators (PTRs).They has proposed an exergetic efficiency parameter representing the losses in the pulse tube itself. Richardson [95] explained the influence of viscosity on the surface heat pumping mechanism. It had been shown that miniaturization of the pulse tube is quite feasible provided the effect of viscosity is appreciated.

### *2.3 Experimental Investigations on PTRs*

Longsworth [96] presented an experimental investigation of pulse tube refrigeration heat pumping rates. He has given an empirical relation for the heat-pumping rate to correlate the experimental data. He remarked that the heat pumping rate is directly proportional to tube length when other things being equal. Mikulin et al. [97] showed that the efficiency of the pulse tube refrigerator can be increased by fastening a buffer reservoir to the warm end of the pulse tube, through an orifice. In this construction, the reservoir is a buffer of quasiconstant pressure, and the orifice is a local gas dynamics resistance of adjustable section. By changing the flow area it is possible to obtain the optimal adjustment for the gas flow rate entering the reservoir, as well as the optimal phase shift between the incident and reflected pressure waves. Radebaugh et al. [98] discussed three types of PTRs. In their experiment they achieved a record low temperature of 60K using a single stage pulse tube. Narayankhedkar et al. [99] reported an experimental investigations and theoretical analysis of pulse tube refrigerator. Concepts of steps have been introduced for the deviation of cold end temperature with zero heat pumping rate. Richardson [100] had shown that transient radial heat transfer is the dominant effect in the pulse tube refrigerator. An analytical solution, which enables optimum pulse rate to be calculated, has been developed and the result is verified by experiment. The research had enabled a more comprehensive explanation of the heat pumping mechanism. The possible relevance of surface heat pumping to the non-ideal behavior in certain types of cryocooler has been highlighted.

Zhou et al. [101] made an experimental investigation to compare the performance of coiled pulse tubes with those of straight ones having similar cross sections, length and operating conditions. The performance degradation of coiled pulse tube has also been

reported when ratio of the axial radius to the radius of the cross-section is reduced. Liang et al. [102] developed a new type of orifice pulse tube refrigerator which could reach much lower temperature compared to that achieved by earlier designs. They have experimentally investigated the relation between the ratio of regenerator volume to the pulse tube volume and the minimum temperature of the orifice pulse tube and also the influence of the dimensions and the matrix materials of the regenerators on the performance of the orifice pulse tube refrigerator. They found that in the pulse tube refrigerator the amount of the gas that passes through the regenerator is quit large and the load on the regenerator is also large. Baks et al. [103] did an experimental verification of an analytical model for orifice pulse tube refrigerator. The cooling power of a pulse tube refrigerator has been expressed in terms of regenerator loss and average enthalpy flow through the pulse tube. Enthalpy flow through the pulse tube is dependent on the amplitudes of the pressure fluctuation in the pulse tube and the volume flow through the orifice. The interpretation of the experiment has been simplified by elimination of the influence of regenerator loss by keeping the cold end heat exchanger at ambient temperature. Kasuya et al. [104] studied on the role of heat exchange between the gases in the pulse tube and the tube wall in a pulse tube refrigerator. They experimentally investigated a system where the working fluid going through the pulse tube without heat exchange by mounting a piston on the hot end of the pulse tube. Refrigeration power was found to increase as the work flow reaching the hot-end piston increases. On the contrary, the heat flow released into a room temperature environment decreases as the workflow increases. This suggests that the work flow becomes more important as the refrigeration power increases. Cai et al. [105] described experimental results on the double-inlet pulse tube refrigerator. The effects of varying the amplitudes and the phase difference of the pressure wave and mass flow have been presented and discussed. The main contribution of the double-inlet pulse tube is to adjust the phase shift between the pressure wave and the mass flow rate in the pulse tube, and to increase their amplitudes. There is optimum matching between double-inlet resistance and the orifice resistance.

Wang et al.[106] suggested a modified refrigerator called a double inlet reversible pulse tube refrigerator (DRPTR). In a DRPTR an auxiliary piston is used instead of the orifice and reservoir as used for an OPTR. Experiments comparing the DRPTR and OPTR have verified that the former arrangement greatly improves the performance of a pulse tube refrigerator. Yuyama et al. [107] studied on experimental investigation on refrigeration losses

in pulse tube refrigerator. The heat input towards the cold end of a pulse tube refrigerator have been studied using combination of two regenerators and two pulse tube of different lengths. Changing the length alters the temperature gradient in the pulse tube or regenerator. Changing the regenerator length produces almost no effect on the minimum refrigeration temperature. In contrast, changing the pulse tube length appreciably affects the minimum refrigeration temperature. These results suggests that heat input due to shuttle gas motion in the pulse tube is the main origin of refrigeration loss. Huang et al. [108] carried out an experiment to investigate the system performance characteristics of pulse tube refrigerator. Both transient and steady state performance of pulse tube refrigerators involve transient heat transfer processes. Wang et al. [109] suggested a modified orifice pulse tube refrigerator (MOPTR) without a reservoir. In the modified arrangement, the crankcase of the compressor has been used instead of the reservoir to bring about the appropriate phase shift between the pressure and the flow velocity in the pulse tube. Numerical analysis and experiments had been verified that the MOPTR could operate as successfully as a conventional OPTR. Gao and Matsubara [110] studied experimental investigations to reach 4K using a pulse tube and the best multiple staging configurations for the pulse tube. Experiments are performed on several types of single stage pulse tube refrigerators coupled with a GM cryocooler. Cai et al. [111] described the structural characteristics and the mechanical performance of a co-axial pulse tube refrigerator with multi-bypass method with experimental analysis. It has been verified that the performance of a pulse tube refrigerator with a multi-bypass is better than that of a double-inlet pulse tube refrigerator. Wang et al. [112] performed an experimental investigation on a multi-bypass pulse tube refrigerator (MPTR) to study the effects of the middle bypass valve on the performance of the refrigerator and to determine the minimum regenerative temperature. The experimental results comparing the multi-bypass version with double inlet version showed that MPTR could reach lower temperature than DIPTR.

Liang et al. [113] studied an experimental verification on pulse tube refrigerator to validate their theoretical model. The influence of the important parameter, such as opening of the orifice and double inlet valves, frequency, average pressure, pressure oscillation amplitude in the pulse tube, diameter of the pulse tube on the refrigeration performance has also been intensively investigated. Xu et al. [114] reported experimental research on a miniature coaxial pulse tube refrigerator using nylon tube. The coaxial design has been used to decrease heat transfer between the pulse tube and the surrounding regenerator. Kirkconnell et al.[115]

experimentally studied the effect of the pulse tube aspect ratio (Length/Diameter ratio) on the overall performance of a PTC. They found that pulse tubes with different aspect ratios but identical volumes performed identically for the range of aspect ratios considered. Zhu et al. [116] has studied on the waiting time effect of a GM type orifice pulse tube refrigerator. The pressure differences across the high-pressure valve and the low-pressure valve are decreased by long waiting times. Thus, the cooling capacity and efficiency are increased, and the no-load temperature is decreased. The experimental results show that there is an optimum waiting time for cooling capacity, efficiency, and no-load temperature, respectively. Yang et al. [117] analyzed direct current flow due to double-inlet, and introduced a second orifice version pulse tube refrigerator experiment to diminish DC flow. Analysis based on some assumptions shows that DC flow through the double-inlet valve in the pulse tube refrigerator is not generally zero, and the DC flow direction may change when the pressure wave changes. Thus, different schemes should be developed for different DC flow directions. Yang et al. [118] proposed a mechanism of double-inlet to lower the temperature of pulse tube refrigerator by analyzing phase relation between pressure and the flow characteristics of double-inlet and multi-bypass, then another proposal is put forward to replace the low temperature multi-bypass valve, which is another double inlet valve at room temperature and a small tube prolonging to the low temperature part of pulse tube. Through experiment, this multi-double inlet version proved effective to lower the refrigeration temperature. Test acquired a lowest temperature of 77K with two double-inlet valves and 50K with one double-inlet valve. The concept of low temperature double-inlet is proposed for the first time. Luwei et al. [119] analyzed the mechanism of the symmetry nozzle instead of needle valve or orifice to improve the performance of pulse tube refrigerator in experiments. The flow coefficient of the symmetry nozzle is a positive feed back to flow rate while the orifice has little relation to flow rate. Charles I., et al. [120] have performed experiments on pulse tube coolers to demonstrate the effects of the permanent flow in the double inlet configuration. They found that this permanent flow affects the wall temperature profiles of the regenerator and the tube. They have tested the solutions to minimize the permanent flow and have led to a significant gain in performance. Von et al. [121] have presented a study on the experimental performance of a hybrid cooler. They considered two-stage unit consists of a commercial single-stage GM refrigerator to precool a pulse tube stage capable of reaching a minimum temperature of 2.2 K. The pressure waves for both stages are generated separately by independent rotary valves

using the same 6 kW helium compressor. The GM refrigerator operates at a fixed frequency of 2 Hz while the optimum frequency for the pulse tube stage is experimentally found to be lower. Neodymium is used as regenerator material in the coldest section. Gan et al. [122] have done experimental investigation on two-component multi-phase helium and nitrogen mixtures in a single-stage pulse tube refrigerator. The experimental results show that both coefficient of performance (COP) and cooling power can be improved to some extent at above 70K when the nitrogen fraction in the mixture is less than 25%.

Kasthuriangan et al. [123] have developed rotary valve for cryocooler applications. They found that the pressure wave form is in between the rectangular and sinusoidal shape. In his second paper [124] they developed single stage pulse tube of 6watt at 77K. In their technical report [125] detailed design parameters and experimental results have been presented for single stage G-M type DIPTR. Karunanithi et al. [126] have presented design and development of a single stage G-M type double inlet pulse tube refrigerator. They have used a rotary valve for pressure wave generation.

Huang et al. [127] carried out an experimental study on the design of a single stage orifice pulse tube refrigerator (OPTR). It was shown experimentally that there exists an optimum operating frequency, which increases with decreasing pulse tube volume. For a fixed pulse tube volume, increasing the pulse tube diameter will improve the performance. The experimental results are used to derive a correlation for the performance of OPTR, which correlates the net cooling capacity with the operating conditions and the dimensions of the OPTR. Some theoretical and experimental investigations on pulse tube refrigerator have been presented by Roy et al. [128]. Their numerical model could be used for approximate design of pulse tube refrigerators.

Ju et al. [129] measured the flow resistance and flow inductance of inertance tubes at high acoustic amplitudes for different inner diameters at various tube lengths at different frequencies. Lu et al.[130] carried out numerical and experimental study on a single -stage double-inlet G-M Pulse Tube Refrigerator, where the oscillating amplitude of physical quantities are large and oscillating frequencies are low in the system. They have measured the temperature distribution on the surface of the regenerator and the pulse tube, as well as the refrigeration capacities at different refrigeration temperatures under optimum operating conditions. A transient one-dimensional numerical simulator has been developed to verify experimental data and to study the nonlinear characteristics in the double inlet pulse tube

refrigerator. Masuyama et al. [131] has experimentally investigated a Stirling type pulse tube refrigerator with an active phase control. A phase shifter, which controls the phase angle between the mass flow and the pressure inside a pulse tube, plays a key role in the performance of pulse tube refrigerators. In this study, an electrically driven and mechanically damped linear compressor, which is directly connected at the warm end of the pulse tube using a connecting tube, is used as the active phase controller (APC). Wang et al. [132] have constructed single stage four-valve pulse tube refrigerator (FVPTR) with a 'L' type pulse tube structure and two orifice valves at the hot end of pulse tube in order to simplify the structure of the cold end of the pulse tube refrigerator (PTR) and have a better utilization of the cold energy of the system. Verification by experiments shows that a two-orifice valve structure gives different adjustments to the gas flow rate of the hot end of the pulse tube than that of the one-orifice valve structure. Koettig, S. Moldenhauer [133] have experientially investigated the direction and the quantity of transferred heat within a pulse tube refrigerator (PTR) in coaxial configuration. They located the pulse tube inside the regenerator matrix in axial direction. They found that an internal thermal contact between these two main components of the cold finger occurs. Results showed that intermediate cooling of the regenerator by the corresponding part of its own pulse tube can improve the cooling performance of a PTR. Therefore, a well-adapted geometrical arrangement between the pulse tube and the regenerator is essential.

#### *2.4 Review of CFD (using Fluent Software) Simulations on PTRs*

Barrett et al. [134] has used a commercial computational fluid dynamics (CFD) software package to model the oscillating flow inside a pulse tube cryocooler. Capabilities for modeling pulse tubes are demonstrated with preliminary case studies and the results presented. The 2D axis-symmetric simulations demonstrate the time varying temperature and velocity fields in the tube along with computation of the heat fluxes at the hot and cold heat exchangers. Yarbrough et al. [135] have done CFD modeling of pressure drop through wire mesh regenerator. They have presented three types of CFD regenerator models. They suggested that the use of computational fluid dynamics (CFD) to predict pressure drop through regenerator wire mesh screens would facilitate development of a cryocooler system model.

Anjun et al. [136] have performed combined experimental and numerical study to determine the heat transfer characteristics of cryogenic helium gas with temperature dependent thermo physical properties in a miniature tube. They found that the heat transfer characteristics of cryogenic gas with temperature-dependent thermo physical properties (TDTP) are different from those in the ambient condition with constant thermo physical properties. Cha et al. [137] modeled two inertance tube pulse tube refrigerator (ITPTR) systems operating under a variety of thermal boundary conditions using a computational fluid dynamics (CFD) code. They concluded that CFD simulations are capable of elucidating complex periodic processes in ITPTRs. They also showed that one-dimensional modeling is appropriate only when all the components in the system have large length-to-diameter (L/D) ratios. Gustafson, et al.[138]compared the result of three first-order models usually used to simulate the effect of inertance tube as a phase-shifter used in Pulse-Tube Refrigerators (PTRs) to the results of Computational Fluid Dynamics (CFD) simulation using a commercial CFD software package. The results of the CFD calculations are first validated by their comparison to experimental results for a compressor, inertance tube, and a reservoir system. Good agreement between experimental and numerical calculations is obtained. Zhang et al. [139] have performed a two-dimensional axis-symmetric computational fluid dynamic (CFD) simulation of a GM-type simple orifice pulse tube cryocooler. They have presented the detailed modeling process and the general results such as the phase difference between velocity and pressure at cold end, the temperature profiles along the wall as well as the temperature oscillations at cold end with different heat loads.

Xiao et al. [140] have performed computational fluid dynamic (CFD) simulation of an inter-phasing pulse tube cooler. Due to reduced turbulence this IPPTC provides improved performance compared with single OPTR. Banjare et al. have performed CFD simulations for OPTR [141] and ITPTR [142] respectively at different frequency by using dual opposed piston compressor. They have discussed that at higher frequency turbulence and recirculation of fluid is observed, which deteriorates the overall performance of the system. CFD simulation results showed that there is an optimum frequency for each PTR model at which it provides maximum refrigeration.

## *2.5 Efforts to Improve the Performance of Regenerator*

Extensive efforts have been focused on improvement in regenerator technology since the development of regenerative cryocoolers. These efforts have been categorized into areas of materials and geometry, modeling, and measurement. The problems with designing the optimum regenerator depend on the variation of thermal properties over the huge temperature range of the regenerator. Orders of magnitude decrease in thermal capacity of the material from 300 K to the cold temperature make different materials attractive in different areas of the regenerator. The basic problem focuses on increasing the heat transfer effectiveness between the gas and solid in the regenerator. The heat transfer effectiveness is a function of fluid properties, solid properties, and the flow geometry. Any change in these parameters will affect the regenerator performance. At temperatures below 20K, the solid properties appear to be a major contributor to the overall regenerator performance. This has led to a development of exotic materials and processes so that the regenerator has sufficient thermal capacity in the cold region. Several erbium alloys have been tested, but these magnetic alloys are brittle at cryogenic temperatures.

Roach et al. [143] carried out a theoretical analysis of the behavior of a typical pulse tube regenerator. Assuming simple sinusoidal oscillations, the static and oscillatory pressures, velocities and temperatures are determined for a model that includes a compressible gas and imperfect thermal contact between the gas and the regenerator matrix. For realistic material parameters, the analysis reveals that the pressure and velocity oscillations are largely independent of details of the thermal contact between the gas and the solid matrix. Only the temperature oscillations depend on this contact. de Waele [144] discussed the dynamic behavior of the temperature profiles in the regenerator and in the gas near the hot and cold ends of the tube. With some simplifying assumptions, the basic properties of the temperature profile in the regenerator and in the tube are understood. Liang et al. [145] established a theoretical model based on the analysis of the thermodynamic behavior of gas parcels in oscillating flow regenerators. They suggested that this can be used to study the influence of DC flow on the refrigeration performance. They developed a test bench, including a hot-wire anemometer to investigate the flow resistance characteristics of regenerators with oscillating flow. The results of measurement are correlated and served for practical design. Yonglin [146] has studied the behavior of working gas subjected to an oscillating flow in a confined passageway. They briefly summarize their previous works and presented some useful results,



including experimental measurements on the oscillating flow behaviors of regenerators filled with metallic wire screens and of cylindrical empty tubes, primarily DC-gas flow measurements, and a CFD model for thermal and fluid dynamic analyses of PTRs.

Kwanwoo et al. [147] developed an experimental apparatus to investigate detailed thermal and hydrodynamic characteristics of a regenerator at cryogenic temperature under oscillating flow and pulsating pressure conditions. They installed fine hot wire probes, at both ends of the regenerator, to measure the fast oscillating gas temperature and mass flow rate. In their studies, they characterized the thermal and hydrodynamic behaviors of the well-defined wire-screen regenerator. Firstly, pressure drop characteristics are discussed for different frequencies under room temperature. Secondly, ineffectiveness of the regenerator is obtained for different cold-end temperatures. Shaowei et al. [148] have introduced numerical method for regenerators. They showed that this method is not only suitable for the regenerators in cryocoolers and Stirling engines, but also suitable for the stacks in acoustic engines and the pulse tubes in pulse tube refrigerators. Sungryel et al. [149] developed a new oscillating flow model of the pressure drop in oscillating flow through regenerator under pulsating pressure. In this oscillating flow model, the amplitude and the phase angle with respect to the inlet mass flow rate represent pressure drop. It is found that the oscillating flow friction factor is a function of Reynolds number while the phase angle of pressure drop is a function of Valensi number and the gas domain length ratio. Chen et al. [150] found that computation with heat transfer, fluid flow and thermodynamics indicates that higher pulse tube refrigeration performance can be achieved with He-H<sub>2</sub> mixtures as working fluids than that with pure He in the cooling temperature region of 30K. In addition, it is found that Er<sub>3</sub>Ni, a regenerative material, is able to absorb H<sub>2</sub> and forms Er<sub>3</sub>NiH<sub>x</sub>. The calculation shows that the regenerative performance of Er<sub>3</sub>NiH<sub>3.5</sub> is better than that of Er<sub>3</sub>Ni due to its higher volume specific heat. Razani et al. [151] developed a first order model for a pulse tube refrigerator including the primary components and important parameters affecting the energy and exergy transport in the refrigerator. The model includes a recent empirical relation for pressure drop calculations in the regenerator, a simple model for the thermal analysis in the regenerator, and the important parameters for the compressor. Kwanwoo et al. [152] developed a new model for the oscillating flow combined with pulsating pressure in cryocooler regenerators to overcome inaccuracy of the conventional flow model based on steady flow friction factor. Empirical correlations of the parameters are obtained for screen regenerators.

Qiu et al. [153] have designed and tested a single-stage G-M type pulse tube cooler (PTC) to explore the lowest attainable refrigeration temperature and to further improve the cooling performance in the temperature range of 15–40K. The magnetic material Er<sub>3</sub>Ni is used as part of the regenerative material besides the phosphor bronze and the lead so as to improve the efficiency of the regenerator. Kwanwoo Nam et al.[154] presented the experimental results and correlations on the friction factor of screen regenerators, being focused on the effect of cryogenic temperature. In their second paper [155] they described development of novel regenerator geometry for cryocoolers.They developed a parallel wire type which is a wire bundle stacked in parallel with the flow in the housing, which is similar to a conventional parallel plate or tube. They performed hydrodynamic and thermal experiments to demonstrate the feasibility of the parallel wire regenerator. The pressure drop characteristic of the parallel wire regenerator is compared to that of the screen mesh regenerator. Cha et al. [156] have made measurements of the lateral or radial permeability and Forchheimer's inertial coefficient of widely used PTR regenerator filler. Using helium as the working fluid, steady-state pressure drops are measured over a wide range of flow rates in annular test sections that contained regenerator fillers. Wang et al. [157] have proposed a new type of copper foaming metal with high heat transfer area and low flow resistance in the heat exchanger instead of the copper screens. The heat transfer performances of the copper screens and the copper foaming metal are compared by theoretical calculation. Qiu et al. [158] have optimized a three-layer regenerator, which consists of woven wire screen, lead sphere and Er<sub>3</sub>Ni to enhance the cooling performance and explore the lowest attainable refrigeration temperature for a single-stage PTC. The efforts focus on the temperature range of 80–300 K, where woven wire screens are used. They have carried out theoretical and experimental studies to study the metal material and the mesh size effect of woven wire screens on the performance of the single-stage G-M type PTC. Chen et al.[159] have analyzed heat transfer characteristics of compressible oscillating flow in two kinds of simple regenerators filled with circular tubes or parallel plates under assumption of small perturbation. They have applied linear thermo acoustic theory for analysis. They have derived exact expressions of Nusselt number in complex notation based on the cross-sectional oscillating velocity and temperature distributions.

Bernd et al. [160] have presented an update on the evaluation of the different correlations for the flow friction factor and heat transfer of Stirling type regenerators.

Generally stainless steel woven wire mesh is used for cryogenic regenerative heat exchangers. The details of regenerator parameters are presented by Robbert [161].

## *2.6 Review of the Investigations of Thermoacoustic Machine*

The research on pulse tube cryogenerators have undertaken in the Los Alamos National Laboratory by Wheatley [162] who used a thermo-acoustic pressure wave generator instead of a mechanical one. Jin et al. [163] developed a single stage co-axial pulse tube refrigerator driven by a standing wave thermoacoustic prime mover and a minimum temperature of 117.6K is achieved. Qiu et al. [164] have proposed a simple and feasible calculation method to calculate temperature differences generated in thermo-driven thermo acoustic refrigerator (TAR). The network model is used to make numerical calculations under different conditions including heat-pump stack positions in TAR, different oscillating pressure ratios (PR), plate spacings and different stack geometries. Tang et al [165] have studied thermo acoustically driven pulse tube refrigerator. They found that after the modifications of jacket type water coolers and stacks, and the optimizations of the openings of orifice and double inlet valves, a refrigeration temperature as low as 115.4K has been achieved by a thermo acoustically driven pulse tube refrigerator. It provides the possibility of utilizing the low-grade heat energy. Sugita et al. [166] have studied thermally actuated pressure wave generators they used solid displacers instead of long and heavy resonance tubes as a resonator for compactness for less vibration and small loss. Tang et al. [167] simulated a standing wave thermo acoustic engine with linear thermo acoustics. Computed results show that an appropriate accretion of the resonance tube length may lead to a decrease of the working frequency and an increase of the pressure amplitude, which will improve the match between the thermo acoustic engine and the pulse tube refrigerator. Qiu et al. [168] has constructed a Stirling thermo acoustic heat engine. The pulse tube cooler (PTC) driven by a thermo acoustic engine can completely eliminate mechanical moving parts, and then achieves a simpler and more reliable device. Hu et al. [169] have reported that the lowest temperature of a thermo acoustically driven pulse tube cooler is generally limited by the pressure ratio provided by the thermo acoustic engine with helium as working gas. With the innovative configuration, the pulse tube cooler reached lowest temperature of 139K. On the other hand, without the membrane, the PTC only achieved a lowest temperature of 186 K when using nitrogen and 145 K with helium for both the PTC and the engine.

## *2.7 Development of the Volume Averaging Technique*

The volume averaging technique is an analytical tool for describing the flow and heat transfer in a porous media. The fluid in the porous media only occupies part of the whole space and is separated by a highly irregular solid surface. The hydrodynamic and thermodynamic quantities for fluid are continuous locally but discontinuous over the entire domain. However when averaged over a representative volume at a certain scale level the quantity associated with the fluid could be a continuous function spatially. Thus by using the volume averaging technique local conservation equations for a general fluid flow can be transformed into a set of global conservation equations.

This technique has found extensive uses in ground water and pollution transport science, petroleum reservoir modeling, catalytic reactors, and fluidized beds to mention a few. Hassanizadeh point out that there are at least three methodologies for describing the flow and heat transfer in multiphase systems, some of which rely mainly on intuition and empirical observations [170]. While these methodologies have led to some of the original models, such as the Darcy model, the volume averaging technique provides a formal framework for improving the science of porous media. All of the current regenerator models in the open literature, such as REGEN and Sage; rely on the intuitive and empirical knowledge of the flow in the regenerator without any application of the volume averaging technique. As a result, these models fall short of describing in an exact fashion the flow and heat transfer in the regenerator. Whitaker has been fundamental in the development of the volume averaging technique and its application to a variety of problems; diffusion and dispersion in a reactor, conduction in multi-phase systems and development of conditions for non-homogeneous porous media, local numerical studies and experimental validations to investigate the validity of volume averaging closure conditions [171]. Macroscopic approach using volume averaging technique has been excellently derived by Whitaker [172]. His studies have mainly focused on incompressible flow, but he has briefly described about the case of slightly compressible flow. Use of the volume averaging has been applied to a problem which is highly compressible due to mainly the large pressure oscillations and the large temperature gradient across the regenerator [173].

## *Chapter III*

# **Pulse Tube Refrigerator Approximate Models: Review of Mathematical Analysis**

### *3.1 Introduction*

Unlike the Stirling or Gifford Mc-Mahon Refrigerators, pulse tube refrigerator has no moving parts at the cold end region. The lack of cold moving parts has allowed it to solve some of the problem associated with the cryocooler in many different applications, such as vibration and reliability. With improved design and modification, it has now become the most efficient cryocooler for a given size. It is suitable for a wide variety of application from civilian to government to military and from ground equipment to space systems.

The moving displacer in the Stirling and Gifford Mc-Mahon refrigerator has several disadvantages. It is a source of vibration and has a short lifetime. It contributes to axial heat conduction as well as a shuttle heat loss. In the pulse tube refrigerator, the displacer is eliminated.

### *3.2 Pulse Tube Refrigerator Operation Principle*

The operation principles of PTRs are very similar as conventional refrigeration systems. The methods of removing heat from the cold environment to the warm environment are somewhat different. The vapor compression cycle shown in Figure 3.1 operates in a steady flow fashion where heat is transported from the evaporator to the condenser by a constant and steady mass flow rate. The PTR relies on an oscillatory pressure wave in the system for transporting heat from the cold end heat exchanger to hot end heat exchanger.

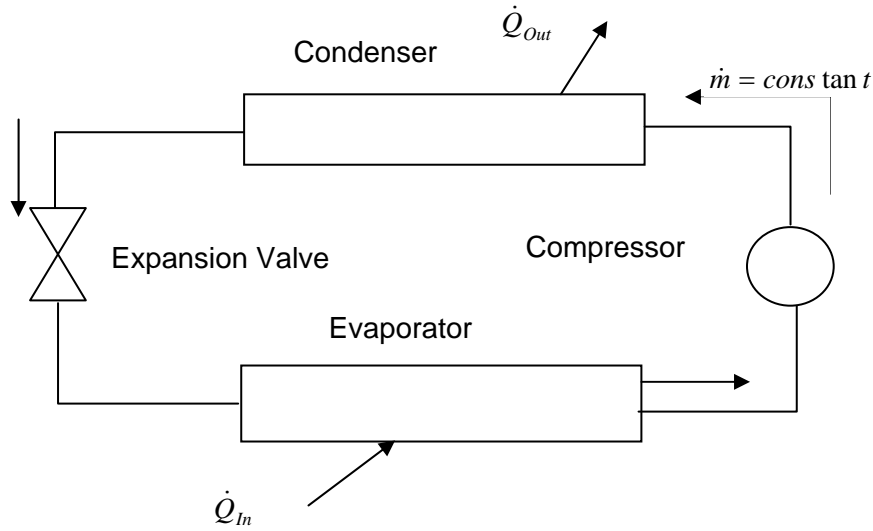


Figure 3.1 Schematic diagram of the simple vapor compression cycle.

In the pulse tube refrigerator the cooling actually occur in the oscillating pressure environment. The heat is absorbed and rejected at the two heat exchangers. It is a cyclic process. Because PTR operates in steady-periodic mode, the thermodynamic properties such as enthalpy flow,  $\langle \dot{H} \rangle$ , heat flow,  $\langle \dot{Q} \rangle$ , and power  $\langle \dot{W} \rangle$  are evaluated in the form of cyclic integrals. The appropriate instantaneous thermodynamic properties are integrated over the entire cycle and divided by the period of that cycle to obtain the cyclic averaged quantity of interest. For example, the compressor power is evaluated from the following integration.

$$\langle \dot{W} \rangle_{PV} = f \oint P \frac{dV}{dt} dt = \frac{1}{\zeta} \oint P(t) \dot{V}(t) dt \quad (3.1)$$

Where  $f$  is frequency,  $\zeta$  is period of the cycle,  $P$  and  $V$ , are instantaneous pressure and volume respectively. The average enthalpy flow over one cycle  $\langle \dot{H} \rangle$  and average heat flow rate,  $\langle \dot{Q} \rangle$ , are also calculated similarly.

### *3.3 Pulse Tube Refrigerator Analysis Methods*

Depending on the complexity of the problem and accuracy of the solution required for the pulse tube refrigerator there are three methods of analysis, which are given as [52]

#### *1. First Order Analysis*

- (i) Surface Heat Pumping
- (ii) Enthalpy flow Analysis
- (iii) Phasor Analysis

#### *2. Second Order Analysis*

- (i) Thermodynamic Non-symmetry effect
- (ii) Approximate Model (Adiabatic and Isothermal Models)

#### *3. Third Order Analysis*

- (i) Numerical Methods
- (ii) FCD Analysis

In this section the first and second order analysis methods are discussed in brief. The third order analysis method is discussed in detail in the subsequent chapters.

### *3.4 First Order Analysis*

#### *3.4.1 Surface Heat Pumping Theory*

Gifford and Longworth [1] proposed a surface heat pumping theory to explain the performance of the basic pulse tube refrigerator after they have constructed a prototype of BPTR as shown in Fig.3.2 (a). Consider a gas parcel in the pulse tube as shown in Fig.3.2 (b). Suppose that in the beginning of the cycle the gas parcel at position  $X_1$  has temperature  $T_1$ , and the temperature distribution of the wall is given as line 1-2. Consider the first half cycle where the pressure increases from the lowest to the highest. During this period, the gas parcel flows towards the closed end of the pulse tube to position  $X_2$  under going an adiabatic process, hence its temperature increases to  $T_3$ . Since  $T_3 > T_2$ , therefore heat is rejected to the wall by the gas parcel until temperature of the gas parcel equals to that of the wall,  $T_2$ . During the next half cycle, this gas parcel flows backward. This is an adiabatic expansion process where the temperature of the gas parcel decreases to  $T_4$ . Since  $T_4 < T_1$ , the gas parcel has refrigeration effect at the position  $X_1$ . This is so-called surface heat pumping theory. Based on

surface heat pumping theory, de Boer [21] also studied the performance of a basic pulse tube refrigerator using a thermodynamic analysis.

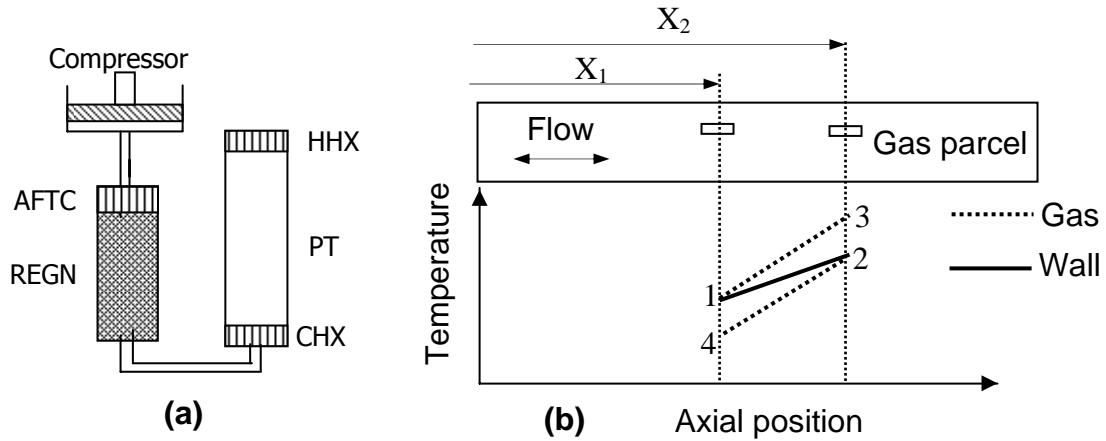


Fig.3.2 Schematic diagram of surface heat pumping theory for BPTR.

### 3.4.2 Enthalpy Flow Analysis

Figure 3.3 shows the schematic of a PTR along with energy flow at various components for enthalpy flow analysis [17]. This figure demonstrates that the PTR's heat absorption and rejection occur at the cold heat exchanger (CHX) and the two hot heat exchangers; (an after cooler (AFTC) and a hot end heat exchanger (HHX)).

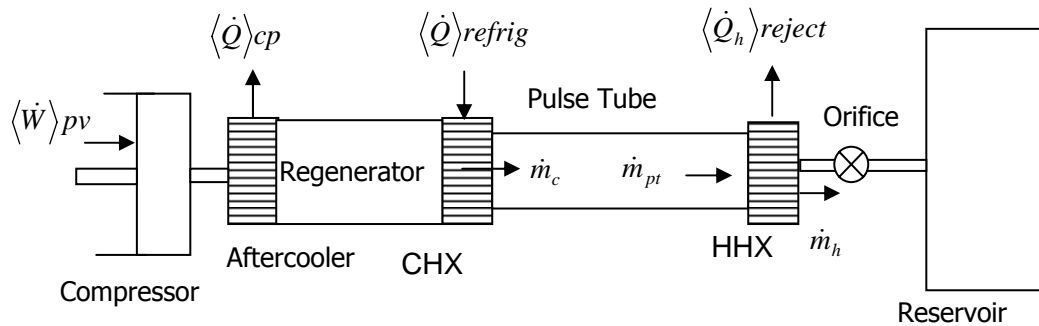


Fig.3.3: Macroscopic energy balance for PTR.

Clearly, HHX is equivalent to a condenser in a conventional vapor compression cycle, and CHX is equivalent to an evaporator. During the PTR operation, most of the heat generated due to compression is rejected through the after cooler. The rest of the energy that is not rejected through AFTC is carried through by the enthalpy flow  $\langle \dot{H} \rangle_{rg}$  in the regenerator. This



can be seen in the component energy balance schematics shown in Fig.3.4. The regenerator enthalpy flow  $\langle \dot{H} \rangle_{rg}$ , the additional refrigeration load  $\langle \dot{Q} \rangle_{refrig}$ , and the heat flow representing all the losses,  $\langle \dot{Q} \rangle_{loss}$  (such as gas conduction, solid matrix conduction, and dispersion), are all absorbed at the CHX, therefore,

$$\langle \dot{H} \rangle_{chx} = \langle \dot{Q} \rangle_{refrig} + \langle \dot{H} \rangle_{rg} + \langle \dot{Q} \rangle_{loss} \quad (3.2)$$

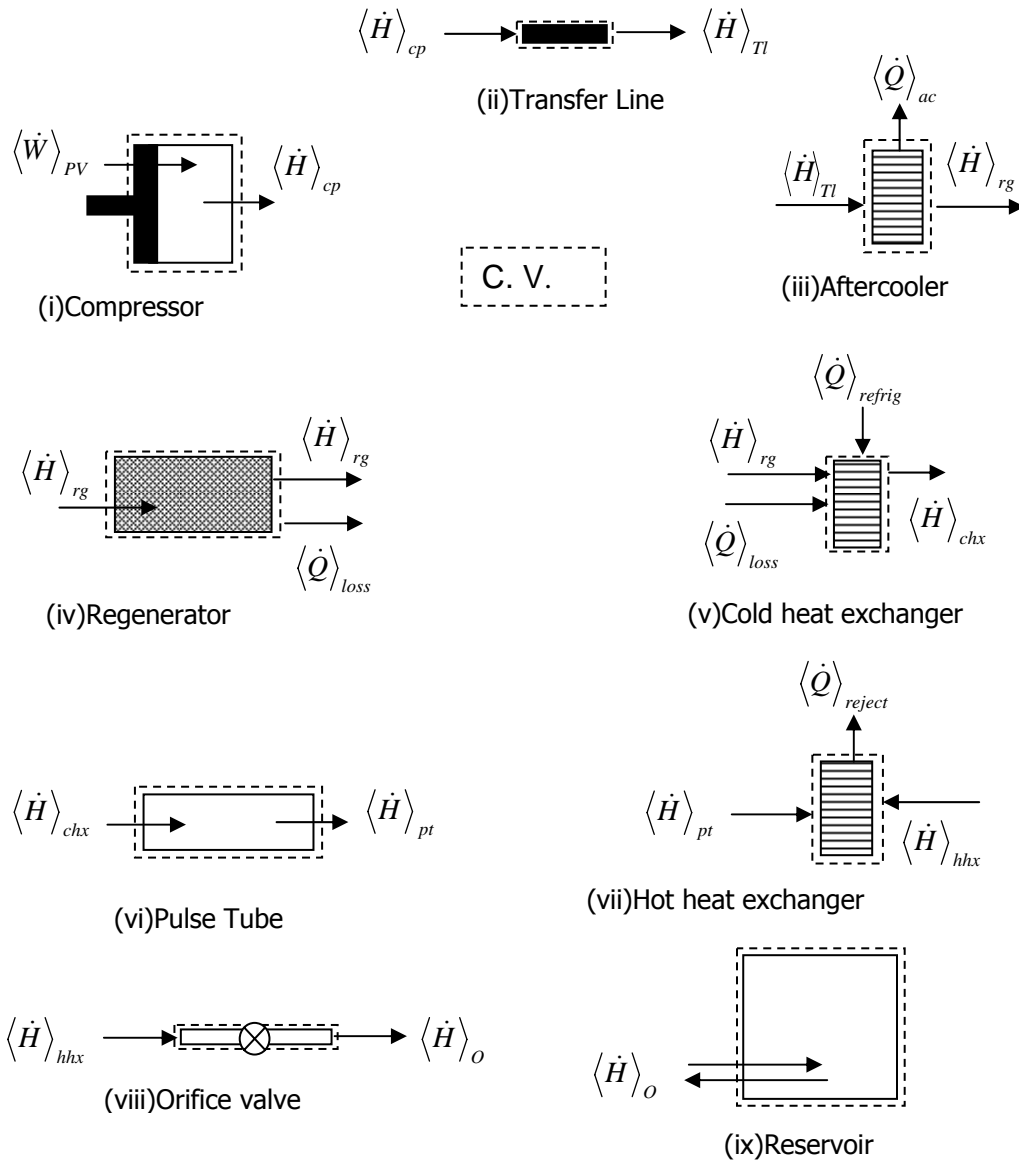


Fig.3.4 Energy balance of system components in an OPTR.

This enthalpy flow enters the pulse tube, and travels down the tube, reaches HHX and then part of this enthalpy is rejected to the environment. The remaining enthalpy which has not been rejected from HHX flows towards reservoir through orifice as shown in the energy balance figure.

The average enthalpy flow over a cycle by assuming ideal gas flow is given by

$$\langle \dot{H} \rangle_{chx} = \frac{C_p}{\zeta} \int_0^{\zeta} \vec{m} \cdot \vec{T} dt = \frac{C_p}{\zeta} \int_0^{\zeta} \dot{m} T \cos \theta dt \quad (3.3)$$

Where  $\zeta$  the period of the cycle,  $C_p$  is the heat capacity. The phasor quantities,  $\vec{m}$  and  $\vec{T}$  are mass flow rate and temperature respectively.

According to the equation (3.3), if an oscillating mass flow rate  $\dot{m}$  is in phase with the oscillating gas temperature  $T$  then a net enthalpy flow exists in the pulse tube flowing from the cold end to the warm end (i.e.,  $\langle \dot{H} \rangle_{chx} > 0$ ). (Note that  $\dot{m} > 0$  when flow is from left to right as shown in Fig.3.4. On the other hand, if an oscillating mass flow rate  $\dot{m}$  is out of phase with oscillating gas temperature  $T$ , then little or no enthalpy flow will exist in the pulse tube, which results in minimum cooling. Fig. 3.5 depicts two examples of phase shift between gas temperature and mass flux. The first example in Fig. 3.5a demonstrates a case where the mass flow rate and the temperature oscillations are about 90 degrees apart. In this circumstance, little or no enthalpy flow takes place. In fact, with temperature and the time mass flow rate being 90 degrees out of phase, one phasor quantity will always be zero when the other one is at its peak. Thus, out of phase relationships tend to produce poor refrigeration due to minimum enthalpy flow in the pulse tube. On the other hand, if the mass flow rate and the temperature oscillations are in phase as illustrated in the second example (Fig. 3.5b), good enthalpy flow can exist in the pulse tube. Thus in-phase and out -phase are the two extreme conditions. In actual pulse tube there exists same phase difference between the phasor quantities.

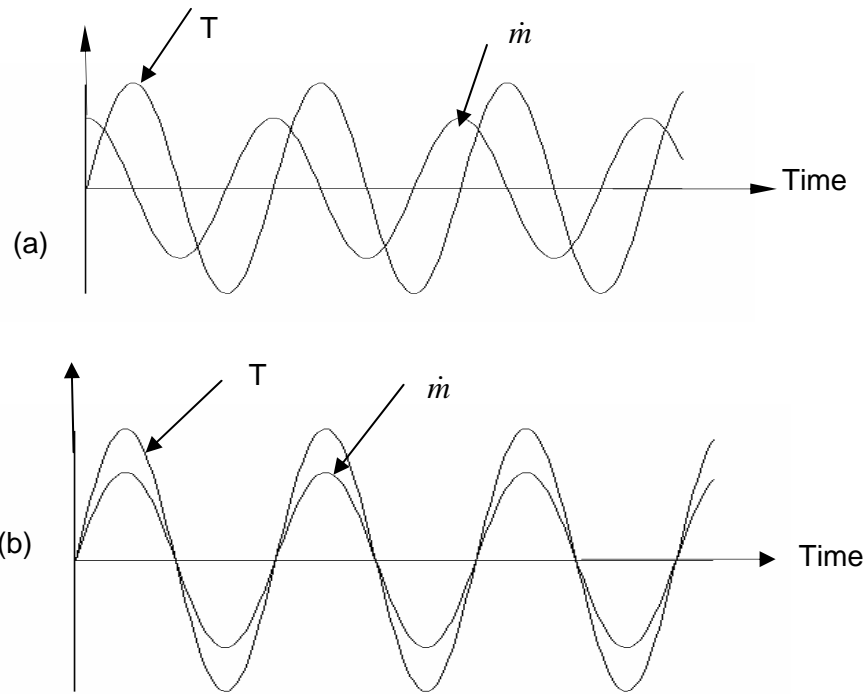


Fig. 3.5 Phase shift relation for gas temperature and mass flow rate.  
 (a) Out-of-phase by  $\pi/2$       (b) In -phase

For perfect regeneration without any loss,

$$\langle \dot{H}_{rg} \rangle = 0 \text{ and } \langle \dot{Q} \rangle_{loss} = 0$$

Refrigerating effect is obtained as

$$\dot{Q}_{refrig} = \langle \dot{H} \rangle_{chx} = \frac{1}{\zeta} \int_0^{\zeta} \dot{m}_c T dt \quad (3.4)$$

### 3.4.3 Phasor Analysis

Pulse tube refrigerators have shown dramatic improvements of performance in recent years. These improvements have paralleled advances in understanding the thermodynamics of pulse tube refrigerators. There have been several different approaches to model pulse tubes. Phasor analysis is one of such methods which has been proposed by Radebaugh [5].

The schematic of a simplified model of pulse tube refrigerator for phasor analysis as proposed by Radebaugh [5] is given in Fig. 3.6. This figure shows the mass flow rate at different part of the system and energy flow at cold end and hot end.

Phasor analysis is based on the following assumptions for phasor analysis.

- Adiabatic behavior of gas in the pulse tube
- Pressure is constant through out the pulse tube and amplitude of dynamic pressure is small compared to average pressure
- Sinusoidal variation of pressure and temperature with no phase difference between them.

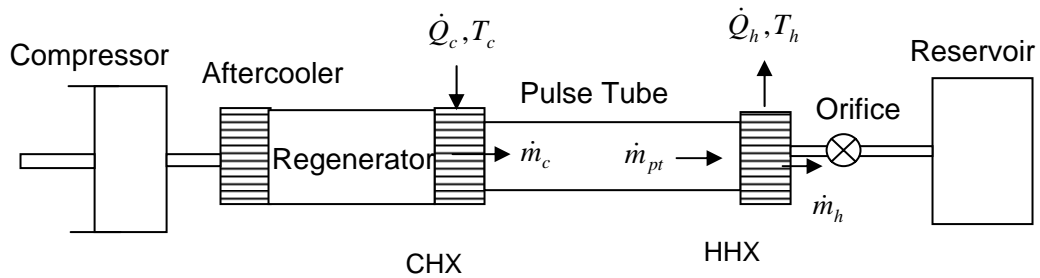


Fig. 3.6 Schematics diagram of pulse tube refrigerator for phasor analysis.

In the pulse tube the pressure and temperature variations are sinusoidal as

$$P = P_0 + P_1 \cos(\omega t) \quad (3.5)$$

$$T = T_0 + T_1 \cos(\omega t) \quad (3.6)$$

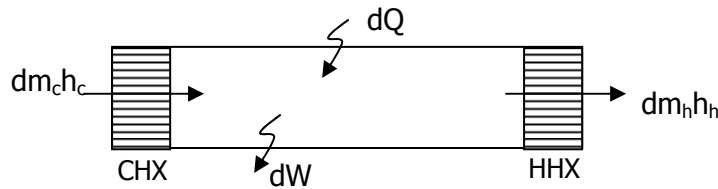


Fig.3.7 Energy balance for pulse tube section.

The mass flow rate is not same along the pulse tube. The mass accumulation takes place due to pressure variation. Applying the first law of thermodynamics to the control volume drawn around the pulse tube section as shown in Fig.3.7,

$$dm_c h_c + dQ = dm_h h_h + dW + (\Delta U)_\sigma \quad (3.7)$$

For adiabatic pulse tube  $dQ=0$ . On time rate Eq. (3.7) becomes

$$\begin{aligned}
\frac{dW}{dt} &= -\frac{(\Delta U)_\sigma}{dt} + \frac{dm_c}{dt} h_c - \frac{dm_h}{dt} h_h \\
p \frac{dV}{dt} &= -C_v \left( \frac{dm_c}{dt} T_c - \frac{dm_h}{dt} T_h \right) + C_p \left( \frac{dm_c}{dt} T_c - \frac{dm_h}{dt} T_h \right) \\
p \frac{dV}{dt} &= R \left( \frac{dm_c}{dt} T_c - \frac{dm_h}{dt} T_h \right) \\
p \frac{dV}{dt} &= R \left( T_h \frac{dm_h}{dt} - T_c \frac{dm_c}{dt} \right)
\end{aligned} \tag{3.8}$$

From an adiabatic system

$$pV_t^\gamma = \text{const}$$

On differentiating the above equation with time gives

$$\gamma p \frac{dV_t}{dt} + V_t \frac{dp}{dt} = 0 \tag{3.9}$$

Substituting  $\frac{dV_t}{dt}$  from equation (3.9) in equation (3.8) yields

$$\frac{dm_c}{dt} = \frac{V_t}{RT_c \gamma} \frac{dp}{dt} + \frac{T_h}{T_c} \frac{dm_h}{dt} \tag{3.10}$$

Equation (3.10) may be written as

$$\begin{aligned}
\dot{m}_c &= \frac{V_t}{RT_c \gamma} \frac{dp}{dt} + \frac{T_h}{T_c} \dot{m}_h \\
\dot{m}_c &= \frac{V_t \dot{P}}{RT_c \gamma} + \frac{T_h}{T_c} \dot{m}_h
\end{aligned} \tag{3.11}$$

Hence equation (3.11) can be represented in terms of rate of change of the mass stored in the pulse tube,  $\dot{m}_p$  as

$$\dot{m}_c = \dot{m}_p + \frac{T_h}{T_c} \dot{m}_h \tag{3.12}$$

Mass flow rate at the hot end is proportional to pressure change

$$\dot{m}_h \propto \Delta P \quad \text{where} \quad \Delta P = P_0 + P_1 \cos(\omega t) - P_0 = P_1 \cos(\omega t)$$

So hot end mass flow rate can be expressed as

$$\dot{m}_h = C_1 P_1 \cos(\omega t) \tag{3.13}$$

Substituting in equation (3.11) and expressing in phasor quantities gives,

$$\dot{m}_c = \frac{\omega V_t}{RT_c \gamma} P_1 \cos(\omega t + \pi/2) + \frac{T_h}{T_c} C_1 P_1 \cos \omega t \quad (3.14)$$

**Phasor diagram for BPTR:**

A vector representation of Equ. (3.12) is known as phasor diagram. The phasor diagram for basic pulse tube refrigerator is shown in Fig.3.8. The figure shows both the mass flow and the pressure phasors. For a BPTR there is no orifice valve and reservoir. The hot end of the pulse tube is closed, so hot end mass flow rate is zero ( $\dot{m}_h = 0$ ). The cold end mass flow rate  $\dot{m}_c$  is at right angle to pressure vector. Since pressure in the pulse tube is  $90^\circ$  from the mass flow there is no refrigeration (Ideally refrigerating effect for BPTR is zero). In practice, heat transfer between the gas and the pulse tube wall due to surface heat pumping causes a small phase shift. This is due to pressure drop for the associated gas flow which result small refrigeration. Under such condition, the compressor work is compensated by the regenerator loss.

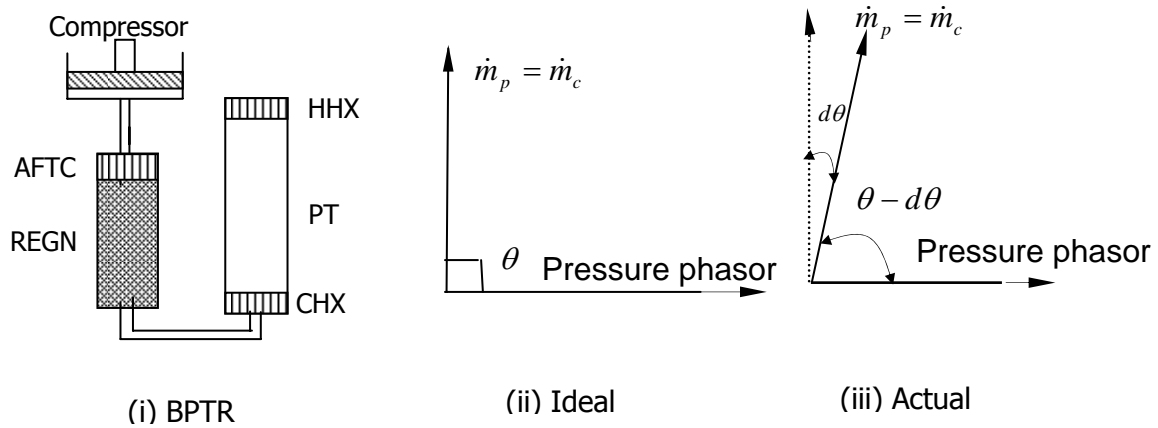


Fig. 3.8 Phasor representation of cold end mass flow rate and pressure for BPTR.

**Phasor diagram for OPTR:**

In the presence of mass flow rate at the hot end, the equation (3.14) can be applied. There is a mass flow rate at the hot end in case of an orifice pulse tube refrigerator. Fig.3.9 shows a phase representation of cold end mass flow rate. This figure shows that cold end mass flow rate makes an angle  $\theta$  with pressure vector. Since  $\dot{m}_c$  is no longer perpendicular

to the pulse tube pressure, there is refrigeration. The refrigeration power is proportional to  $\dot{m}_o P$ . Hot end mass flow rate  $\dot{m}_h$  is in phase with pressure vector.

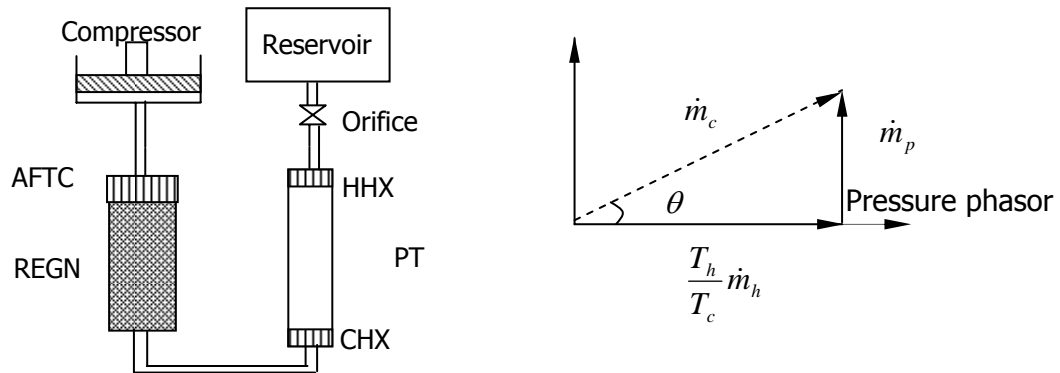


Fig. 3.9 Phasor representation of cold end mass flow rate and pressure for OPTR.

***Phasor Diagram of DIPTR:***

Similarly the Fig.3.10 represents the phasor diagram for double inlet pulse tube refrigerator (DIPTR). In this case the orifice mass flow rate is equal to the sum of hot end mass flow rate,  $\dot{m}_h$  and double inlet mass flow rate,  $\dot{m}_{di}$  ( $\dot{m}_o = \dot{m}_h + \dot{m}_{di}$ ). The orifice mass flow rate,  $\dot{m}_o$  is always in phase with pressure vector. Thus using equation (3.14), the phase difference between  $\dot{m}_c$  and pressure phasor can be drawn as shown in Fig.3.10. In the absence of double inlet valve mass flow rate through orifice and hot end mass flow rate are same. The angle  $\theta$  gets further reduced in compared to OPTR as shown in Fig.3.9. This improves the refrigeration performance of DIPTR compared with OPTR.

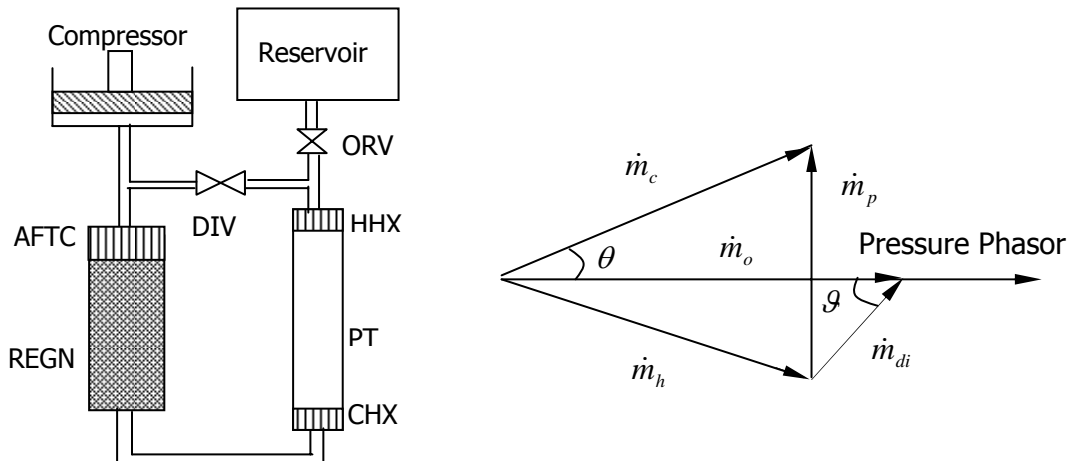


Fig. 3.10 Phasor diagram for double inlet pulse tube refrigerator.

### Phasor Diagram for ITPTR

The phasor diagram for ITPTR and also OPTR which is described earlier can be explained better by electrical analogy [58]. The word inertance is derived from two words Inertia and Inductance. In lumped electrical model oscillating pressure is considered as voltage and mass flow rate is equivalent to current. The reservoir is considered as a capacitor, the orifice (the flow resistance) is taken as a resistor and inertance tube is considered as the sum of a resistor and inductor in an equivalent electrical circuit.

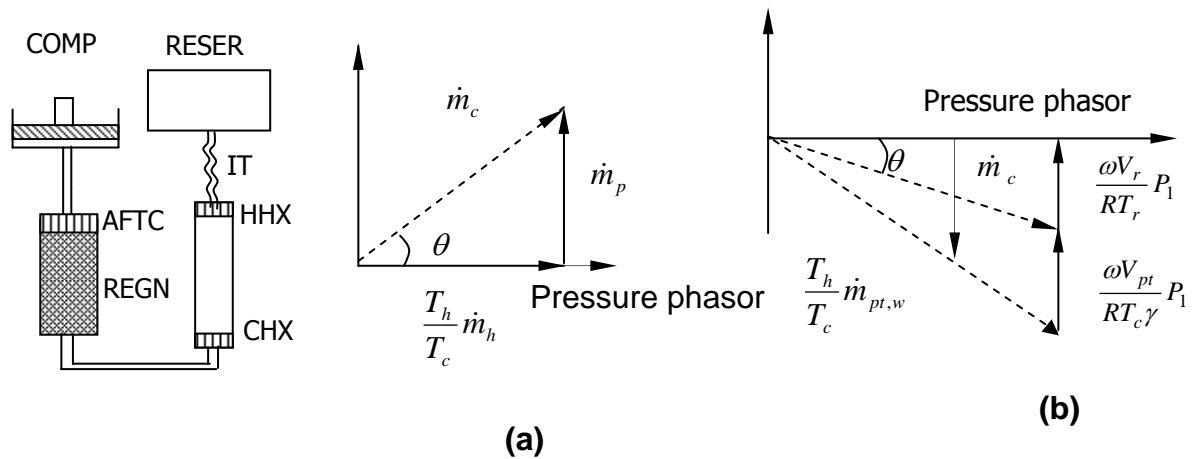


Fig. 3.11 Phasor representation of mass flow rate at the cold end for ITPTR.

Compliance of the reservoir,  $E = \frac{V_r}{\gamma P_m}$

Inductance of the Inertance tube  $\ell = \frac{\rho l}{A}$

The Fig. 3.12 and Fig. 3.13 shows the impedance of OPTR and ITPTR respectively.

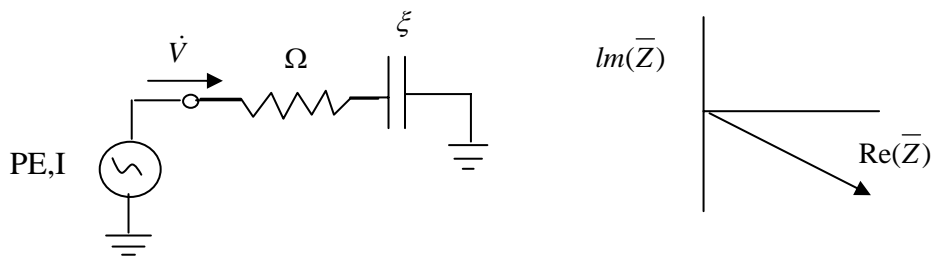


Fig. 3.12 Impedance for OPTR.



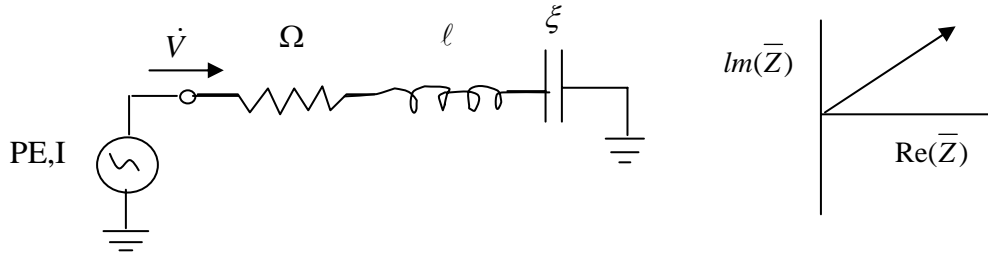


Fig. 3.13 Impedance for ITPTR.

OPTR is equivalent to  $\Omega - \xi$  circuit as shown in Fig.3.12. From equation (3.15) it is clear that the impedance  $Z$  is always negative for OPTR. In OPTR the impedance phasor lies in the fourth quadrant, hence the mass flow rate (electrical current) leads pressure (electrical voltage) as shown in Fig. 3.11(a). The wave form of the current and voltage is shown in Fig.3.14.

$$\text{Impedance} = Z = \Omega + \frac{1}{j\omega\xi} = \sqrt{\left[\Omega^2 + \left(\frac{1}{\omega\xi}\right)^2\right]} \quad (3.15)$$

ITPTR is equivalent to  $\Omega - \ell - \xi$  circuit as shown in figure 3.13. From equation (3.16) it is clear that the impedance  $Z$  could be, positive or negative. In case of ITPTR the impedance may lie in first or fourth quadrant depending upon the value of  $\ell$  and  $\xi$ . Those values depend on the dimension of the inertance tube and the reservoir. Mass flow rate will lead pressure if the impedance phase angle is negative and mass flow rate will lag if this phase angle is positive.

$$\text{Impedance} = Z = \Omega + j\left(\omega\ell - \frac{1}{\omega\xi}\right) = \sqrt{\left[\Omega^2 + \left(\omega\ell - \frac{1}{\omega\xi}\right)^2\right]} \quad (3.16)$$

The phasor diagram for leading mass flow rate and phasor diagram for lagging mass flow rate are shown in Fig.3.11 (a) and (b) respectively. Fig.3.14 shows the phase lag representation of OPTR. This depicts that Voltage  $Y_m$  lags current  $I_m$  by  $\theta$  in phase.

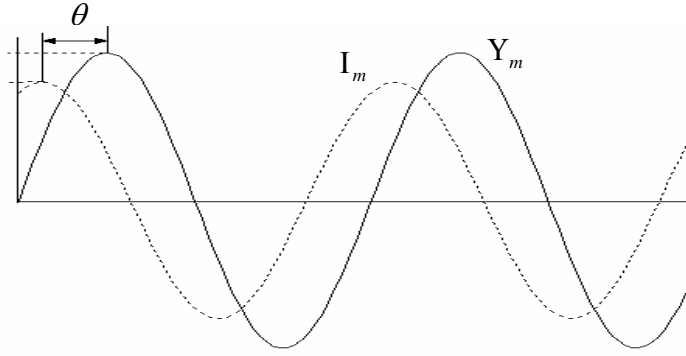


Fig.3.14 Phase lag representation of OPTR.

***Resultant Phasor Diagram of OPTR:***

The phasor quantities of OPTR consists of compressor, after cooler, regenerator, cold end HX, pulse tube , hot end HX and orifice. The pulse tube is under adiabatic condition, the compressor is under polytropic condition, and other units are under isothermal condition. In case of regenerator, the average temperature of hot and cold end is taken as the isothermal temperature. Thus the vector sum of all these quantities gives the resultant phasor as shown in figure 3.15. The mass flow rate through the compressor can be estimated as

$$\begin{aligned} \overrightarrow{(\dot{m}_{cp})} = & \overrightarrow{\left(\dot{m}_o \frac{T_h}{T_c}\right)} + \overrightarrow{\left(\frac{\omega P_1 V_{hx}}{R T_{hx}}\right)} + \overrightarrow{\left(\frac{\omega P_1 V_t}{\gamma R T_c}\right)} + \overrightarrow{\left(\frac{\omega P_1 V_{cx}}{R T_{cx}}\right)} + \\ & \overrightarrow{\left(\frac{\omega P_1 V_{rg}}{R T_{mrg}}\right)} + \overrightarrow{\left(\frac{\omega P_1 V_{ac}}{R T_{ac}}\right)} + \overrightarrow{\left(\frac{\omega P_1 V_{cp}}{nR T_{cp}}\right)} \end{aligned} \quad (3.17)$$

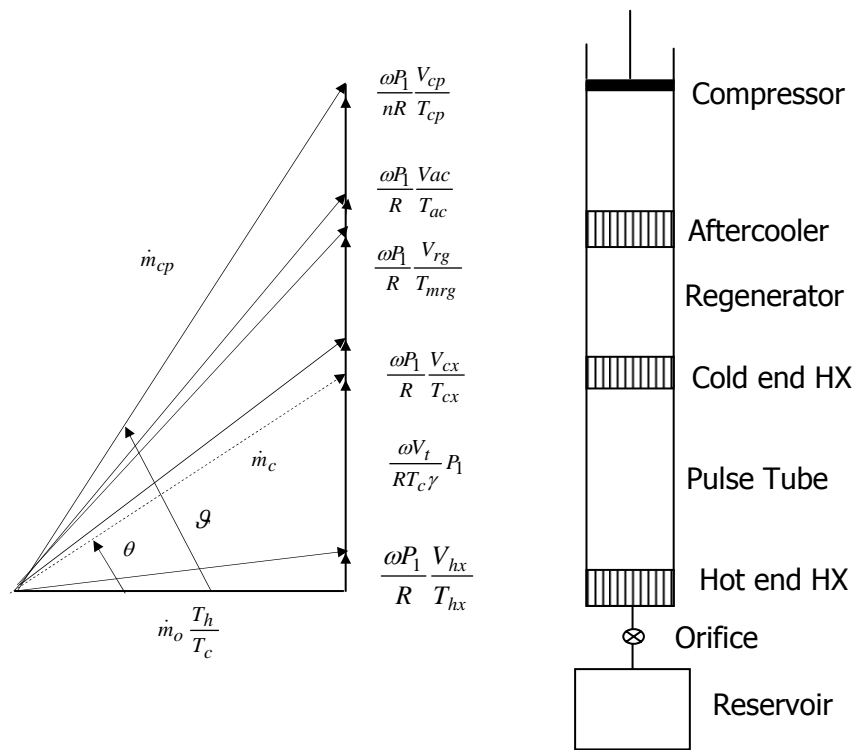


Fig. 3.15 Phasor diagram of the total system for OPTR.

### 3.5 Second Order Analysis

#### 3.5.1 Thermodynamic Non-Symmetry Effect

Important advances have been achieved during the last ten years or so in the art of pulse tube refrigeration. In order to meet the requirements for further development and practical applications, a systematic theoretical and experimental study on pulse tube refrigeration has been needed. The thermodynamic nonsymmetry effect, which is responsible for the production of refrigeration power is qualitatively described and demonstrated for the idealized case.

#### *Idealized pulse tube:*

Liang [28] proposed the so-called thermodynamic nonsymmetry effect in the orifice pulse tube. By tracing a thermodynamic cycle of the fluid parcel flowing from the cold end of the regenerator to the pulse tube and then flowing back to the regenerator, he found that the fluid gas parcel is undergoing a temperature decrease during this cycle, which he called the thermodynamic nonsymmetry effect. Based on this model, Liang [29] extended the theory of

surface heat pumping to all type of pulse tube refrigerators. He proposed that the surface heat pump theory prevailed only in the thermal boundary layer.

In order to explain non symmetry effect, the regenerator and the cold and hot end heat exchangers are assumed to be perfect. For simplicity, the working fluid is regarded as an ideal gas, and gas flow in the pulse tube is assumed to be adiabatic inviscid flow, with no length-wise mixing or heat conduction. The idealized working cycle is shown in Fig.3.16. The hot end of the regenerator and the upper side of the double-inlet valve (V2) are alternately connected to an infinitely large gas source at high pressure  $P_h$ , in the first half-cycle and then to an infinitely large gas volume at low pressure  $P_l$ , in the second half-cycle. Fig. 3.17 shows the pressure variation with time over one cycle. Each cycle consists of four processes:

- (i)  $0 - t_1$  :pressurization of gas element      (ii)  $t_1 - \zeta/2$  :displacement of gas element  
 (iii)  $\zeta/2 - t_2$  :depressurization of gas element      (iv)  $t_2 - \zeta$  :displacement of gas element

Since the flow capacity of the regenerator is constant, processes (i) and (iii) are assumed to endure for the same time period, i.e.  $t_1 = t_2 - \zeta/2$ .

The expression for mass flow rate at the cold end of pulse tube is as follows:

$$\dot{m}_c = \left( \frac{V_{pt}}{\gamma RT_c} + \frac{V_{dix}}{RT_c} \right) \frac{dp}{dt} \quad (3.18)$$

From this, one can see that the same mass of  $\dot{m}_c$  is leaving and entering the pulse tube at the cold end section.

(Rate of pressurization during 0 to  $t_1$ )= (Rate of depressurization during  $\zeta/2$  to  $t_2$ ). Thus

$$\left( \frac{dp}{dt} \right)_{0-t_1} = - \left( \frac{dp}{dt} \right)_{\zeta/2-t_2} \quad (3.19)$$

Pressure changes in these two processes are assumed to be linear for an idealized situation.

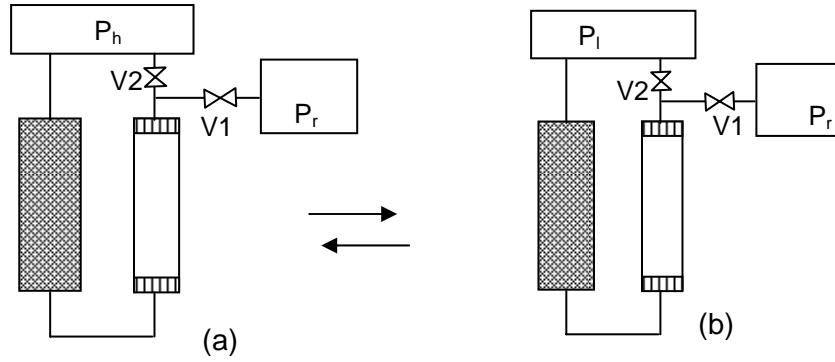


Fig.3.16. Schematic diagram of the idealized working processes of pulse tube refrigerators: (a) first half-cycle; (b) second half-cycle

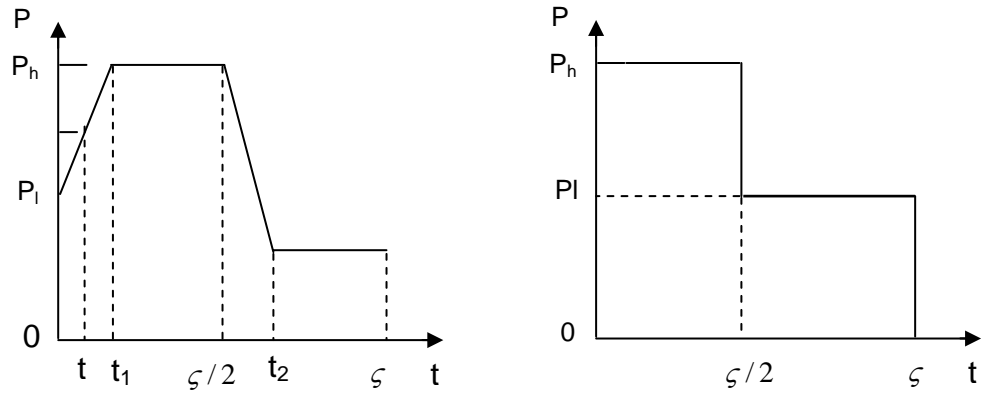


Fig.3.17 Pressure versus time: (a) Pressure in pulse tube; (b) Pressure externally applied.

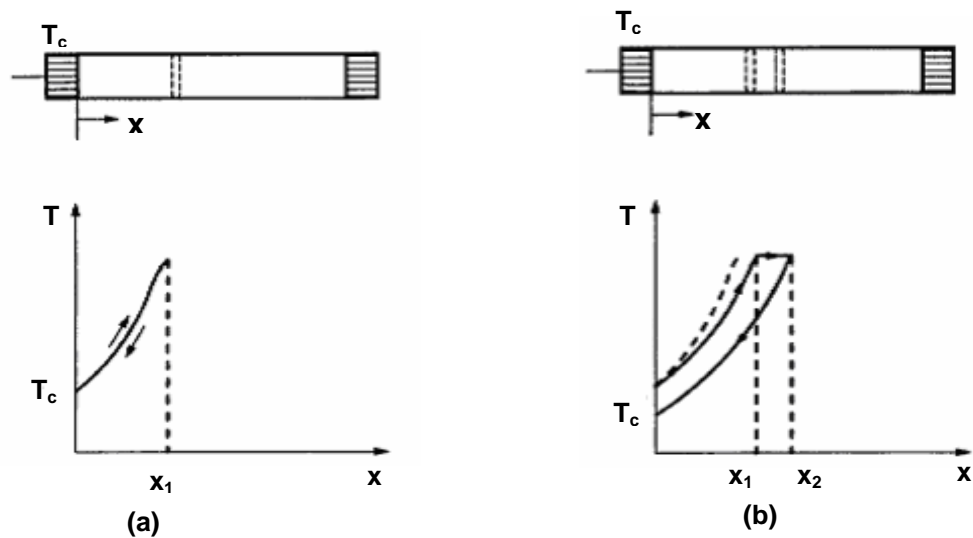


Fig. 3.18 Temperature versus position of a gas element in the basic pulse tube: (a) Adiabatic (b) with thermal contact

**Case I: Basic Pulse Tube Refrigeration:**

For a basic type pulse tube refrigerator [1], the orifice V1 and V2 are closed as shown in Fig.3.16. The gas element which enters the pulse tube at time  $t$  ( $0 < t < t_1$ ) undergoes a compression process from pressure  $P_l$  to  $P_h$ . From 0 to  $t_1$ , the gas element is adiabatically compressed from  $P_l$  to  $P_h$  and simultaneously moved to  $x_1$ . It stays there during process 2, in case of adiabatic hot end heat exchanger as shown in Fig3.18 (a). The gas element leaves the pulse tube at the same pressure as it enters in the third process. Consequently, the temperatures are also equal. In this case, the gas element is termed thermodynamically symmetric during the cycle and no refrigeration effect is obtained. For a non-adiabatic case i.e. with thermal contact, the gas element moves from  $x_1$  to  $x_2$  due to heat transfer of gas element with the wall. This is known as surface heat pumping. The gas element following in the process 3 and 4 is shown in Fig3.18 (b). Due to surface heat pumping for a non-adiabatic hot end, a small refrigeration effect is obtained by the decrease in temperature at the end of the process. The dotted path in Fig.3.18 (b) is same as the path in Fig.3.18 (a)

**Case II: Orifice Pulse Tube Refrigeration:**

In the case of the orifice pulse tube, the gas element will not be stationary during process 2, as shown in Fig.3.19. Instead, it moves toward the hot end due to the mass flow into the gas reservoir via the orifice. In process 3, it follows a path parallel to that of process 1 on the T-x diagram. Due to the increased displacement in process 2, it can be expanded more before it leaves the cold end of the pulse tube than it is compressed in the pulse tube during process 1. Therefore, it leaves the cold end of the pulse tube at a temperature lower than the temperature at which it enters the pulse tube. In this way, a refrigeration effect is produced and this effect is known as the thermodynamic nonsymmetry effect.

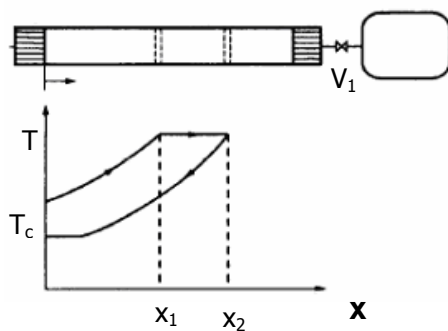


Fig. 3.19 Temperature versus position of a gas element in the OPTR.

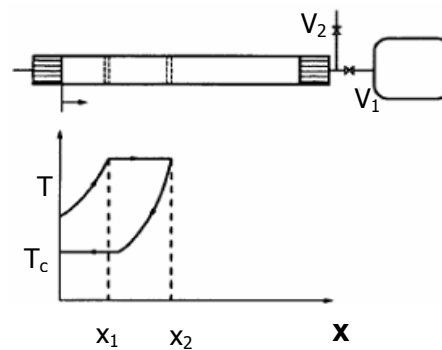


Fig. 3.20 Temperature versus position of gas elements in the DIPTR.

### *Case III: Double Inlet Pulse Tube Refrigeration:*

The double-inlet method enhances the nonsymmetry effect in the orifice pulse tube. Since gas enters and leaves the pulse tube in two directions, the gas elements that enter the pulse tube at the cold end are compressed to  $P_h$  within a shorter range of displacement due to the additional pressure through double inlet valve. It means a greater temperature increase per unit length of displacement. For the same reason, temperature decrease of gas elements per unit length of displacement in process 3 is also greater. Displacements of gas elements in processes 2 and 4 are not affected by the double inlet. All these effects permit the gas elements to expand to a greater extent, and more of them to expand to  $P_l$ , before leaving the pulse tube. As a result, more refrigeration power is produced. Fig.3.20 schematically shows the temperature of a gas element as a function of its position in a double-inlet pulse tube. The mechanism of the double inlet can be understood by comparing Fig.3.19 with Fig.3.20.

#### *3.5.2 Approximate PTR Models: Adiabatic and Isothermal:*

The working process of the pulse tube refrigeration system is very complex due to the unsteady, oscillating compressible gas flow, the porous media in regenerator, the presence of the orifice-reservoir, the double inlet valve etc. The cooling effect at cold end of the pulse tube occurs due to compression and expansion of the gas column lies somewhere between the adiabatic and isothermal processes, and may be assumed to be a polytropic process. To understand the basic phenomenon responsible for the production of cold effect at the pulse tube section, two limiting cases adiabatic and isothermal processes involving ideal gas have been considered. Both these models are approximate models which are dealt separately.

Liang et al. [43] tried to solve the working mechanism of the three common types of pulse tube refrigerator by analyzing the thermodynamic behavior of gas elements as adiabatic process in the pulse tube. They assumed the pressure variation inside pulse tube to be symmetric at the time of compression and expansion. For simplicity of calculation they took it as trapezoidal variation with time. In this model it has been assumed that the pressure variation is sinusoidal. Fig.3.21 shows the different components of DIPTR for adiabatic model. The following assumption has been made with adiabatic behavior of the gas.

- The regenerator, the cold end and hot end heat exchangers have been assumed to be perfect. That means that the regenerator will always maintain a constant temperature gradient between its hot and cold ends at steady operation. And heat addition at cold

end heat exchanger and heat rejection at hot end heat exchanger of pulse tube occur at constant temperature at steady conditions.

- The working fluid has been regarded as an ideal gas.
- The gas flow in pulse tube has been assumed to be adiabatic inviscid flow with no length-wise mixing or heat conduction.

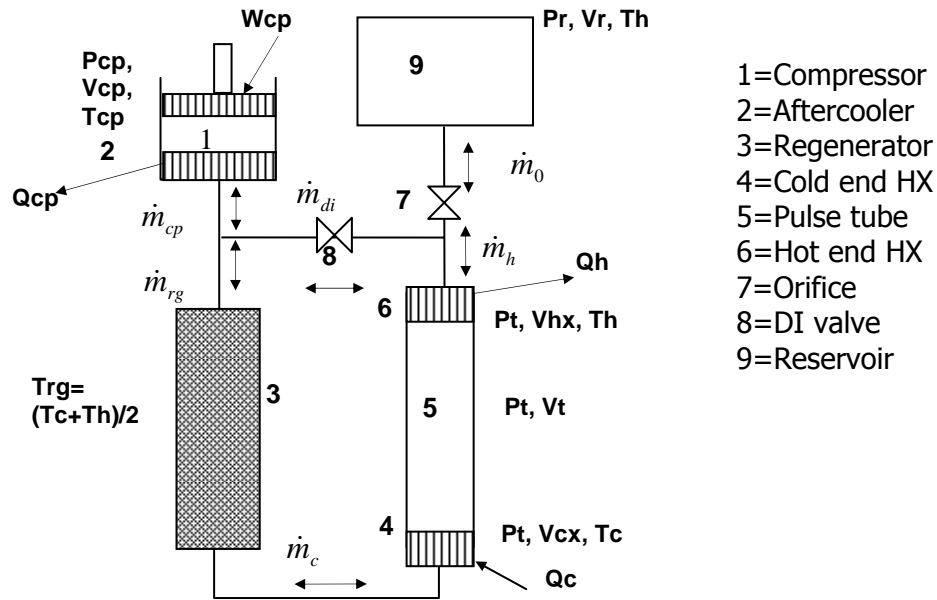


Fig.3.21 Schematic diagram of the physical model for DIPTR.

### Governing Equations:

The governing equations consist of continuity equation and energy equation.

The mass conservation on a control volume gives,

$$\left. \begin{aligned} \frac{\partial \rho}{\partial t} + \frac{\partial(\rho v)}{\partial x} &= 0 \\ \frac{\partial \rho}{\partial t} + \rho \frac{\partial(v)}{\partial x} + v \frac{\partial(\rho)}{\partial x} &= 0 \end{aligned} \right\} \quad (3.20)$$

The energy conservation equation from the first law of thermodynamics gives,

$$du = dq - dw \quad (3.21)$$

In an adiabatic case  $dq = 0$ , leads to

$$du = -dw = -pdv \quad (3.22)$$

For an ideal gas,



$$u = c_v T = \frac{R}{\gamma-1} T = \frac{p v}{\gamma-1} = \frac{(p/\rho)}{\gamma-1} \quad (3.23)$$

From equation (3.22) and (3.23)

$$\frac{1}{\gamma-1} d(p/\rho) + p dv = 0 \quad (3.24)$$

For a moving system, the time derivative is to be represented by substantial (or total) derivative as

$$\frac{1}{\gamma-1} \frac{D(p/\rho)}{Dt} + p \frac{Dv}{Dt} = 0 \quad (3.25)$$

Substituting  $v = \frac{1}{\rho}$  in equ. (3.25) gives

$$\left. \begin{aligned} \frac{1}{\gamma-1} \frac{D\left(\frac{p}{\rho}\right)}{Dt} + p \frac{D\left(\frac{1}{\rho}\right)}{Dt} &= 0 \\ \frac{1}{(\gamma-1)} \left[ \frac{1}{\rho} \frac{Dp}{Dt} + p \frac{D\left(\frac{1}{\rho}\right)}{Dt} \right] + p \frac{D\left(\frac{1}{\rho}\right)}{Dt} &= 0 \\ \frac{Dp}{Dt} - \frac{\gamma p}{\rho} \frac{D\rho}{Dt} &= 0 \\ \frac{\partial p}{\partial t} + v \frac{\partial p}{\partial x} - a^2 \left( \frac{\partial \rho}{\partial t} + v \frac{\partial \rho}{\partial x} \right) &= 0 \end{aligned} \right\} \quad (3.26)$$

Where  $a^2 = \frac{\gamma P}{\rho}$ ,  $v$  = the velocity of the gas along the tube.

### ***Adiabatic compressor modeling:***

In the Stirling type pulse tube refrigerator, the pressure wave in the pulse tube is provided with a compressor directly coupled to the hot end of the regenerator. This design is more compact and more efficient than the valved compressor with gas distributor design. The compressor cylinder has been assumed to be adiabatic in the analysis, since each of the compression and expansion processes occurs in such a short period of time that little heat

exchange between the gas and the cylinder wall can be affected. The gas adiabatically compressed in the cylinder is assumed to be cooled to room temperature by the adjacent after-cooler. The after-cooler has been assumed to be perfect, so that the temperature of the gas leaving it is always equal to its wall temperature.

***Change in compressor Volume:***

Sinusoidal variation has been taken for the compressor cylinder volume variation.

$$V_{cp}(t) = V_0 + \frac{V_s}{2} [1 + \sin(2\pi f t)] \tag{3.27}$$

Where  $V_0$  = clearance volume

$V_s$  = stroke volume and  $f$  = frequency

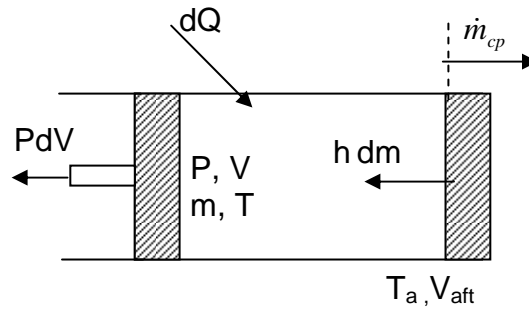


Fig. 3.22 Schematic diagram of energy balance for compressor.

Applying the first law of thermodynamics to the control volume drawn around the volume swept by the piston in the cylinder as shown in Fig.(3.22) gives

$$\frac{dU}{dt} = \frac{dW}{dt} + \frac{d(mh)}{dt} \tag{3.28}$$

$$\frac{d(mc_v T)}{dt} = -p \frac{dV}{dt} + c_p T \frac{dm}{dt}$$

$$c_v \left[ m \frac{dT}{dt} + T \frac{dm}{dt} \right] = -p \frac{dV}{dt} + c_p T \frac{dm}{dt}$$

$$mc_v \frac{dT}{dt} = -p \frac{dV}{dt} + RT \frac{dm}{dt} \tag{3.29}$$

In side a closed system  $Tp^{\frac{1-\gamma}{\gamma}} = C$ , taking log on both sides yields

$$\ln T + \frac{1-\gamma}{\gamma} \ln p = \ln C$$

On differentiating

$$\frac{dT}{T} + \frac{1-\gamma}{\gamma} \frac{dp}{p} = 0$$

$$p \frac{dT}{dt} + \frac{1-\gamma}{\gamma} T \frac{dp}{dt} = 0 \text{ or } \frac{dT}{dt} = \frac{\gamma-1}{\gamma} \frac{T}{p} \frac{dp}{dt} \quad (3.30)$$

Multiplying both sides by  $mc_v$  and using ideal gas equation  $PV=mRT$

$$mc_v \frac{dT}{dt} = mc_v \frac{\gamma-1}{\gamma} \frac{T}{p} \frac{dp}{dt} = \frac{R}{\gamma} \frac{mT}{p} \frac{dp}{dt} = \frac{V}{\gamma} \frac{dp}{dt} \quad (3.31)$$

Substituting Equ.(3.31) in Equ.(3.29) yields

$$\frac{V}{\gamma} \frac{dp}{dt} = -p \frac{dV}{dt} + RT \frac{dm}{dt} \quad (3.32)$$

Compressor pressure variation is expressed as

$$\frac{dp_{cp}}{dt} = \frac{\gamma}{V_{cp}} \left[ -\dot{m}_{cp} RT_{cp} - p_{cp} \frac{dV_{cp}}{dt} \right] \quad (3.33)$$

***Pressure variation at the pulse tube:***

Pulse tube pressure variation is a function of compressor pressure variation. So the pressure variation in the pulse tube can be derived in terms of compressor pressure variation along with various mass flow rate involved in the system. The cold end mass flow rate equation (3.11) derived earlier is

$$\dot{m}_c RT_c = \dot{m}_h RT_h + \frac{V_t}{\gamma} \frac{dp_t}{dt}$$

$$\dot{m}_c = \dot{m}_h \frac{T_h}{T_c} + \frac{V_t}{\gamma RT_c} \frac{dp_t}{dt} \quad (3.34)$$

Where  $T_c$  and  $T_h$  are the temperatures at cold end and hot end respectively and  $R$  is a gas constant.

In case of double inlet pulse tube refrigerator, the mass flow rate through the double inlet valve (DI) is due to the pressure difference between compressor and pulse tubes. If DI valve mass flow rate is  $\dot{m}_{di}$  and  $V_{d_{hx}}$  is the void volume of the hot end heat exchanger, then the cold end mass flow rate is given as

$$\dot{m}_c = (\dot{m}_0 - \dot{m}_{di}) \frac{T_h}{T_c} + \left( \frac{V_t}{\gamma} + V_{d_{hx}} \right) \frac{1}{RT_c} \frac{dp_t}{dt} \quad (3.35)$$

Gas flow in the regenerator of a pulse tube refrigerator is accompanied by significant pressure change. The pressurization and depressurization of the regenerator void volume, which is usually comparable with the pulse tube volume, consume a considerable part of the mass flow. This means that the mass flow rate is not the same along the length of regenerator at each point. The mass flow rate at the hot end of regenerator,  $\dot{m}_{rg}$ , may be calculated by the relation.

$$\dot{m}_{rg} = \dot{m}_c + \frac{V_{dcx}}{RT_c} \frac{dp_t}{dt} + \frac{V_{drg}}{RT_{rg}} \frac{dp_t}{dt} \quad (3.36)$$

Substituting Equ. (3.35) in Equ. (3.36) gives

$$\dot{m}_{rg} = (\dot{m}_0 - \dot{m}_{di}) \frac{T_h}{T_c} + \left( \frac{V_t}{\gamma} + V_{d_{hx}} \right) \frac{1}{RT_c} \frac{dp_t}{dt} + \frac{V_{dcx}}{RT_c} \frac{dp_t}{dt} + \frac{V_{drg}}{RT_{rg}} \frac{dp_t}{dt} \quad (3.37)$$

Where  $V_{dcx}$  is the dead volume of cold end heat exchanger and connecting tube and  $V_{drg}$  is the void volume of the regenerator.

Temperature distribution along the regenerator of a pulse tube refrigerator is usually found to be approximately linear. Therefore, the mean temperature of the regenerator is given as,

$$T_{rg} = \frac{T_h + T_c}{2} \quad (3.38)$$

Assuming that the temperature of the gas after the after cooler to be same as that in the hot end of the regenerator and pressure variation is similar to that of the compressor pressure, compressor out let mass flow rate is given as:

$$\dot{m}_{cp} = \dot{m}_{rg} + \dot{m}_{di} + \frac{V_{dac}}{RT_h} \frac{dp_{cp}}{dt} \quad (3.39)$$

Substituting equation (3.37) in equation (3.39) gives

$$\begin{aligned} \dot{m}_{cp} = & (\dot{m}_0 - \dot{m}_{di}) \frac{T_h}{T_c} + \left( \frac{V_t}{\gamma} + V_{d_{hx}} \right) \frac{1}{RT_c} \frac{dp_t}{dt} + \\ & \left( \frac{V_{dcx}}{T_c} + \frac{V_{drg}}{T_{rg}} \right) \frac{1}{R} \frac{dp_t}{dt} + \dot{m}_{di} + \frac{V_{dac}}{RT_h} \frac{dp_{cp}}{dt} \end{aligned} \quad (3.40)$$

Rearranging equation (3.40) one can get pressure variation equation for pulse tube as

$$\frac{dp_t}{dt} = \frac{R(\dot{m}_{cp} - \dot{m}_{di}) - R(\dot{m}_0 - \dot{m}_{di}) \frac{T_h}{T_c} - \frac{V_{dac}}{T_h} \frac{dp_{cp}}{dt}}{\left[ \frac{V_{drg}}{T_{rg}} + \frac{V_{dcx}}{T_c} + \frac{V_t}{\gamma T_c} + \frac{V_{dhx}}{T_c} \right]} \quad (3.41)$$

***Pressure variation at the reservoir:***

Pressure variation at the reservoir is due to the mass flow through the orifice and it is given as:

$$\frac{dp_r}{dt} = \frac{1}{V_r} (-\dot{m}_0 RT_h) \quad (3.42)$$

***Mass flow through regenerator:***

Mass flow in the regenerator has been evaluated through Ergun's equation,

$$\frac{dp}{dx} = \frac{G}{\rho d_h} \frac{(1-\phi)}{\phi^3} \left[ \frac{150(1-\phi)\mu}{d_h} + 17.5G \right] \quad (3.43)$$

Where  $G = \dot{m}_{rg} / A_{rg} =$  mass flow rate per unit area

For laminar flow

$$\frac{dp}{dx} = \frac{\dot{m}_{rg}}{A_{rg} \rho d_h} \frac{(1-\phi)}{\phi^3} \left[ \frac{150(1-\phi)\mu}{d_h} \right] \quad (3.44)$$

where  $\phi$  is the porosity of the porous medium,  $\rho$  is the density of the fluid,  $d_h$  the hydraulic diameter,  $\mu$  is the dynamic viscosity of the fluid and  $A_{rg}$  is the cross section area of the regenerator.

Assuming  $dx = L_{rg}$  (length of regenerator) and  $dp = \Delta p = (P_{cp} - P_t)$

The regenerator mass flow rate is expressed as

$$\dot{m}_{rg} = \frac{\rho \pi d_{rg}^2 d_h^2}{600 L_{rg} \mu} \frac{\phi^3}{(1-\phi)} (P_{cp} - P_t) \quad (3.45)$$

It may be noted that for wire mesh regenerator, the equation for pressure drop is different which has been derived in chapter (IV).

***Mass flow through orifice:***

Mass flow through the orifice has been assumed as a nozzle flow, calculated from well-known formula for a nozzle with a correction factor.

$$\dot{m}_0 = C_d A_0 \sqrt{2 \frac{\gamma}{\gamma-1} \frac{P_t}{\nu} \left[ \left( \frac{P_r}{P_t} \right)^{\frac{2}{\gamma}} - \left( \frac{P_r}{P_t} \right)^{\frac{\gamma+1}{\gamma}} \right]} \quad \text{Where } P_t > P_r \quad (3.46)$$

$$\dot{m}_0 = -C_d A_0 \sqrt{2 \frac{\gamma}{\gamma-1} \frac{P_t}{\nu} \left[ \left( \frac{P_t}{P_r} \right)^{\frac{2}{\gamma}} - \left( \frac{P_t}{P_r} \right)^{\frac{\gamma+1}{\gamma}} \right]} \quad \text{Where } P_t < P_r \quad (3.47)$$

Substituting  $\nu = RT / p$  for ideal gas

$$\dot{m}_0 = C_d A_0 \sqrt{2 \frac{\gamma}{\gamma-1} \frac{P_t^2}{RT_h} \left[ \left( \frac{P_r}{P_t} \right)^{\frac{2}{\gamma}} - \left( \frac{P_r}{P_t} \right)^{\frac{\gamma+1}{\gamma}} \right]} \quad \text{Where } P_t > P_r \quad (3.48)$$

$$\dot{m}_0 = -C_d A_0 \sqrt{2 \frac{\gamma}{\gamma-1} \frac{P_t^2}{RT_h} \left[ \left( \frac{P_t}{P_r} \right)^{\frac{2}{\gamma}} - \left( \frac{P_t}{P_r} \right)^{\frac{\gamma+1}{\gamma}} \right]} \quad \text{Where } P_t < P_r \quad (3.49)$$

***Mass flow rate through double inlet valve:***

Mass flow rate through double inlet valve has also been assumed as nozzle flow similar to that in the orifice. Here the mass flow occurs due to pressure differences between compressor and the pulse tube. Therefore, mass flow rate has been calculated as

$$\dot{m}_{di} = C_{di} A_{di} \sqrt{2 \frac{\gamma}{\gamma-1} \frac{P_{cp}^2}{RT_h} \left[ \left( \frac{P_t}{P_{cp}} \right)^{\frac{2}{\gamma}} - \left( \frac{P_t}{P_{cp}} \right)^{\frac{\gamma+1}{\gamma}} \right]} \quad \text{Where } P_{cp} > P_t \quad (3.50)$$

$$\dot{m}_0 = -C_{di} A_0 \sqrt{2 \frac{\gamma}{\gamma-1} \frac{P_t^2}{RT_h} \left[ \left( \frac{P_{cp}}{P_t} \right)^{\frac{2}{\gamma}} - \left( \frac{P_{cp}}{P_t} \right)^{\frac{\gamma+1}{\gamma}} \right]} \quad \text{Where } P_{cp} < P_t \quad (3.51)$$

***Analysis of Isothermal PTR Model:***

In this model, the compression and expansion processes are considered as isothermal. It shows higher efficiency than the adiabatic or any other model of the pulse tube. For the purpose of analysis, a pulse tube refrigerator system is divided into a few subsystems, which are coupled to each other. Different researchers have used different schemes for dividing the

full pulse tube refrigerator into subsystems. Zhu et al. [18], and Yuan and Pfothenauer [46] have proposed to divide the pulse tube section into three subsystems; the middle section of the tube is separating the cold and hot volumes. In their approach, the reversibility condition supposes that no heat exchange occurs in the middle-section, and that pressure variation induces temperature swing in the gas. In reality, wall and the gas can not be at the same temperature, heat transfer would generate entropy with consequent reduction in efficiency. Neveu and Babo [66] developed their isothermal model dividing the pulse tube section into two distinct volumes i.e. cold and hot volumes. They assumed that each volume is subjected to several complex processes. These are mainly heat exchange in the associated heat exchanger, surface heat pumping in the tube and the mixing of gas. They expressed this entire phenomenon through lumped parameters, considering isothermal heat exchange. They developed the model only for Stirling type orifice pulse tube refrigerator. In the present study, the isothermal model has been extended to double inlet pulse tube refrigerator. Its pressure, mass flow behavior and the cooling effect have been determined and compared with those of the earlier OPTR model.

The pulse tube device has been divided into six open subsystems. Three of them exchange work, heat and mass with the surroundings (compressor, cold and hot volumes), while the others exchange mass only (regenerator, double inlet valve and orifice-reservoir). It has been assumed that all heat exchanges are at constant temperature and that temperature of all subsystems exchanging heat is equal to those of the heat reservoirs. Another condition is that mechanical equilibrium is realized in each part of the device. These conditions lead to the model presented in Figure 3.23. The system described in the figure consists of six opened subsystems as,

- (i) Isothermal compressor at  $T_{cp}$ , exchanging mechanical work  $W_{cp}$  and heat  $q_{cp}$  with the surroundings at temperature  $T_h$  and mass,  $m_{cp}$  ( $= m_{rg} + m_{di}$ ); mass,  $m_{rg}$  with the regenerator and mass,  $m_{di}$  with the double inlet valve.
- (ii) Regenerator exchanging mass  $m_{rg}$  at  $T_{cp}$  with the compressor and  $m_c$  and at  $T_c$  with the pulse tube.
- (iii) Cold volume in the pulse tube at  $T_c$ , exchanging heat  $Q_c$  with the surrounding at temperature  $T_c$ , mass  $m_c$  with the regenerator, and mechanical work  $w_c$  with the hot volume.

- (iv) Hot volume in the pulse tube at  $T_h$ , exchanging mechanical work  $w_h$  with the cold volume, heat  $q_h$  with the surrounding at temperature  $T_{cp}$  and mass  $m_h = (m_o - m_{di})$  with the reservoir via orifice and with the DI valve.
- (v) Adiabatic orifice and reservoir exchanging mass  $m_o$  with hot volume.
- (vi) Double inlet valve exchanging mass  $m_{di}$  with compressor and hot volume.

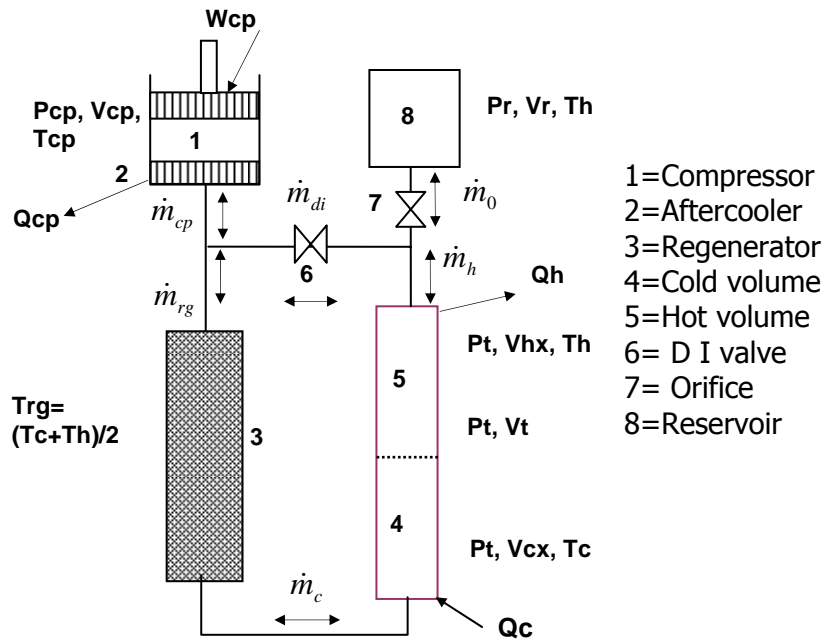


Fig. 3.23 Schematic diagram of the physical model for the DIPTR.

Each subsystem consists of two phases, gas and wall. Conservation of mass and energy have been applied to the six subsystems with the following assumptions:

- Ideal gas.
- Uniform temperature in each subsystem.
- Mechanical equilibrium in compressor and pulse tube, and ideal regenerator, i.e. front wave moving back and forth during a cycle.
- Piston flow in the pulse tube.
- Negligible gas volume in the regenerator compared to compressor, tube and reservoir.
- Negligible pressure losses due to pipe and bends.



This modeling consists of the application conservation of mass momentum and energy for these six subsystems. These have been illustrated separately as follows.

**Governing Equations:**

Figure 3.24 shows a control volume which represents an isothermal variable volume:

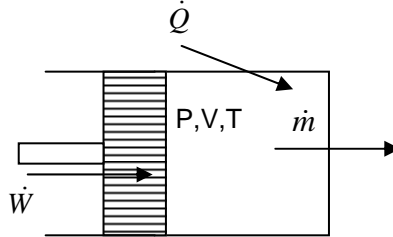


Fig. 3.24 Control volume for isothermal model.

From mass and energy conservation

$$\left. \begin{aligned} \frac{dm}{dt} &= \dot{m} \\ \frac{dU}{dt} &= \dot{W} + \dot{Q} + \dot{m}h \end{aligned} \right\} \quad (3.52)$$

Assuming gas in the pulse tube as an ideal gas

$$PV = mRT \quad (3.53)$$

Equation (3.53) can be written as

$$dm = m \left( \frac{dP}{P} + \frac{dV}{V} - \frac{dT}{T} \right) \quad (3.54)$$

Change of the internal energy of the gas in side the system volume can be written as

$$dU = mc_v dT + u dm \quad (3.55)$$

As the temperature has been assumed constant,  $dT=0$ , so the equations (3.54) and (3.55) can be simplified as,

$$\left. \begin{aligned} dm &= m \left( \frac{dP}{P} + \frac{dV}{V} \right) = \frac{1}{RT} (VdP + PdV) \\ \text{and} \\ dU &= u dm \end{aligned} \right\} \quad (3.56)$$

Substituting equations (3.52) in equation (3.56), and assuming mechanical equilibrium in the system,

$$\left.
\begin{aligned}
\frac{dP}{dt} &= \frac{1}{V} \left( \dot{m}RT - P \frac{dV}{dt} \right) \\
\dot{Q} &= P \frac{dV}{dt} - \dot{m}(Pv) = P \frac{dV}{dt} - \dot{m}RT \\
\text{Where, } \dot{W} &= -P \frac{dV}{dt}
\end{aligned}
\right\} \quad (3.57)$$

***For isothermal compressor:***

Applying the above sets of equations to the compressor, equation (3.57) becomes

$$\left.
\begin{aligned}
\frac{dP_{cp}}{dt} &= \frac{1}{V_{cp}} \left( -\dot{m}_{cp}RT_{cp} - P_{cp} \frac{dV_{cp}}{dt} \right) \\
\dot{Q}_{cp} &= P_{cp} \frac{dV_{cp}}{dt} + \dot{m}_{cp}RT_{cp} \\
\dot{W}_{cp} &= -P_{cp} \frac{dV_{cp}}{dt}
\end{aligned}
\right\} \quad (3.58)$$

***For pulse tube:***

Similarly to that in compressor, the pulse tube flow has been assumed to be a piston like flow. In other words, the displacer of the Stirling or the GM cryocooler has been converted into a gas piston. The pulse tube has been divided into two distinct volumes, one for cold volume  $V_c$ , and the other for the hot volume  $V_h$  at uniform temperature to ensure the reversibility of the model.

***For cold volume:***

$$\left.
\begin{aligned}
\frac{dP_t}{dt} &= \frac{1}{V_c} \left( \dot{m}_c RT_c - P_t \frac{dV_c}{dt} \right) \\
\dot{Q}_c &= P_t \frac{dV_c}{dt} - \dot{m}_c RT_c \\
\dot{W}_c &= -P_t \frac{dV_c}{dt}
\end{aligned}
\right\} \quad (3.59)$$

**For hot volume:**

$$\left. \begin{aligned} \frac{dP_t}{dt} &= \frac{1}{V_h} \left( -\dot{m}_h RT_h - P_t \frac{dV_h}{dt} \right) \\ \dot{Q}_h &= P_t \frac{dV_h}{dt} + \dot{m}_h RT_h \\ \dot{W}_h &= -P_t \frac{dV_h}{dt} = P_t \frac{dV_c}{dt} \end{aligned} \right\} \quad (3.60)$$

Mechanical equilibrium in the pulse tube states that when compression in the hot volume takes place the cold volume undergoes expansion and vice versa. Thus

$$\dot{W}_c + \dot{W}_h = 0 \quad (3.61)$$

Combining equations (3.59) to (3.60) leads to the following set of equations, for describing the pulse tube. The pressure variation in the pulse tube is the addition of two pressure variations in cold and hot volume.

$$\frac{dP_t}{dt} = \frac{1}{V_t} (\dot{m}_c RT_c - \dot{m}_h RT_h) \quad (3.62)$$

The fractional volume variation  $X_t = (V_c/V_t)$  can be expressed by equating first set equation in both the sets i.e., equ. (3.59) and equ. (3.60) as

$$\left. \begin{aligned} \frac{dX_t}{dt} &= \frac{1}{P_t V_t} (\dot{m}_c RT_c (1 - X_t) + \dot{m}_h RT_h X_t) \\ \dot{Q}_c &= P_t V_t \frac{dX_t}{dt} - \dot{m}_c RT_c \\ \dot{Q}_h &= -P_t V_t \frac{dX_t}{dt} + \dot{m}_h RT_h \end{aligned} \right\} \quad (3.63)$$

**Orifice and reservoir:**

For the reservoir, equations (3.57) become,

$$\left. \begin{aligned} \frac{dP_r}{dt} &= \frac{1}{V_r} (-\dot{m}_0 RT_h) \\ \dot{Q}_r &= \dot{m}_0 RT_h \\ \dot{W} &= 0 \end{aligned} \right\} \quad (3.64)$$

***Regenerator, orifice and double inlet mass flow rate:***

Mass flow rate through regenerator, orifice and double inlet valve depends on the pressure gradient. It has been assumed that gas volume in the regenerator is negligible. Thus equation (3.45) is used as the mass flow rate through the regenerator. The equations (3.46) to (3.51) are used to estimate the mass flow rate through orifice and double inlet valve. For isothermal model the change in compressor cylinder volume is assumed sinusoidal similar to adiabatic model as given earlier in Equ.(3.27).

***Solution Methodology***

The derivations of governing equations for adiabatic and isothermal models have been described earlier. The consolidated list of equations for the adiabatic model is:

$$\left. \begin{aligned} \dot{m}_{rg} &= \frac{\rho \pi d_{rg}^2 d_h^2}{600 L_{rg} \mu} \frac{\phi^3}{(1-\phi)} (P_{cp} - P_t) \text{ When } P_{cp} > P_t \\ \dot{m}_{rg} &= \frac{\rho \pi d_{rg}^2 d_h^2}{600 L_{rg} \mu} \frac{\phi^3}{(1-\phi)} (P_t - P_{cp}) \text{ When } P_{cp} < P_t \end{aligned} \right\} \quad (A1)$$

$$\left. \begin{aligned} \dot{m}_0 &= C_d A_0 \sqrt{2 \frac{\gamma}{\gamma-1} \frac{P_t^2}{RT_h} \left[ \left( \frac{P_r}{P_t} \right)^{\frac{2}{\gamma}} - \left( \frac{P_r}{P_t} \right)^{\frac{\gamma+1}{\gamma}} \right]} \text{ Where } P_t > P_r \\ \dot{m}_0 &= -C_d A_0 \sqrt{2 \frac{\gamma}{\gamma-1} \frac{P_t^2}{RT_h} \left[ \left( \frac{P_t}{P_r} \right)^{\frac{2}{\gamma}} - \left( \frac{P_t}{P_r} \right)^{\frac{\gamma+1}{\gamma}} \right]} \text{ Where } P_t < P_r \end{aligned} \right\} \quad (A2)$$

$$\left. \begin{aligned} \dot{m}_{di} &= C_{di} A_{di} \sqrt{2 \frac{\gamma}{\gamma-1} \frac{P_{cp}^2}{RT_h} \left[ \left( \frac{P_t}{P_{cp}} \right)^{\frac{2}{\gamma}} - \left( \frac{P_t}{P_{cp}} \right)^{\frac{\gamma+1}{\gamma}} \right]} \text{ Where } P_{cp} > P_t \\ \dot{m}_{di} &= -C_{di} A_{di} \sqrt{2 \frac{\gamma}{\gamma-1} \frac{P_t^2}{RT_h} \left[ \left( \frac{P_{cp}}{P_t} \right)^{\frac{2}{\gamma}} - \left( \frac{P_{cp}}{P_t} \right)^{\frac{\gamma+1}{\gamma}} \right]} \text{ Where } P_{cp} < P_t \end{aligned} \right\} \quad (A3)$$

$$V_{cp}(t) = V_0 + \frac{V_s}{2} [1 + \sin(2\pi f t)] \quad (A4)$$

From equation (A4) we can get compressor volume,  $V_{cp}$  at  $t=0$

$$V_{cp}(0) = V_0 + \frac{V_s}{2} \quad (A4a)$$

$$\frac{dV_{cp}}{dt} = V_s \pi f \cos(2\pi f t) \quad (\text{A4b})$$

$$\frac{dp_{cp}}{dt} = \frac{\gamma}{V_{cp}} \left[ -\dot{m}_{cp} RT_{cp} - p_{cp} \frac{dV_{cp}}{dt} \right] \quad (\text{A5})$$

$$\frac{dp_t}{dt} = \frac{R(\dot{m}_{cp} - \dot{m}_{di}) - R(\dot{m}_0 - \dot{m}_{di}) \frac{T_h}{T_c} - \frac{V_{ac}}{T_h} \frac{dp_{cp}}{dt}}{\left[ \frac{V_{drg}}{T_{rg}} + \frac{V_{dcx}}{T_c} + \frac{V_t}{\gamma T_c} + \frac{V_{dhx}}{T_c} \right]} \quad (\text{A6})$$

$$\frac{dp_r}{dt} = \frac{1}{V_r} (-\dot{m}_0 RT_h) \quad (\text{A7})$$

Similarly the consolidated list of equations for the Isothermal model is:

$$\left. \begin{aligned} \dot{m}_{rg} &= \frac{\rho \pi d_{rg}^2 d_h^2}{600 L_{rg} \mu} \frac{\phi^3}{(1-\phi)} (P_{cp} - P_t) \text{ When } P_{cp} > P_t \\ \dot{m}_{rg} &= \frac{\rho \pi d_{rg}^2 d_h^2}{600 L_{rg} \mu} \frac{\phi^3}{(1-\phi)} (P_t - P_{cp}) \text{ When } P_{cp} < P_t \end{aligned} \right\} \quad (\text{B1})$$

$$\left. \begin{aligned} \dot{m}_0 &= C_d A_0 \sqrt{2 \frac{\gamma}{\gamma-1} \frac{P_t^2}{RT_h} \left[ \left( \frac{P_r}{P_t} \right)^{\frac{2}{\gamma}} - \left( \frac{P_r}{P_t} \right)^{\frac{\gamma+1}{\gamma}} \right]} \text{ Where } P_t > P_r \\ \dot{m}_0 &= -C_d A_0 \sqrt{2 \frac{\gamma}{\gamma-1} \frac{P_t^2}{RT_h} \left[ \left( \frac{P_t}{P_r} \right)^{\frac{2}{\gamma}} - \left( \frac{P_t}{P_r} \right)^{\frac{\gamma+1}{\gamma}} \right]} \text{ Where } P_t < P_r \end{aligned} \right\} \quad (\text{B2})$$

$$\left. \begin{aligned} \dot{m}_{di} &= C_{di} A_{di} \sqrt{2 \frac{\gamma}{\gamma-1} \frac{P_{cp}^2}{RT_h} \left[ \left( \frac{P_t}{P_{cp}} \right)^{\frac{2}{\gamma}} - \left( \frac{P_t}{P_{cp}} \right)^{\frac{\gamma+1}{\gamma}} \right]} \text{ Where } P_{cp} > P_t \\ \dot{m}_{di} &= -C_{di} A_{di} \sqrt{2 \frac{\gamma}{\gamma-1} \frac{P_t^2}{RT_h} \left[ \left( \frac{P_{cp}}{P_t} \right)^{\frac{2}{\gamma}} - \left( \frac{P_{cp}}{P_t} \right)^{\frac{\gamma+1}{\gamma}} \right]} \text{ Where } P_{cp} < P_t \end{aligned} \right\} \quad (\text{B3})$$

$$V_{cp}(t) = V_0 + \frac{V_s}{2} [1 + \sin(2\pi f t)] \quad (\text{B4})$$

From equation (B4) we can get compressor volume,  $V_{cp}$  at  $t=0$

$$V_{cp}(0) = V_0 + \frac{V_s}{2} \quad (B4a)$$

$$\frac{dV_{cp}}{dt} = V_s \pi f \cos(2\pi f t) \quad (B4b)$$

$$\frac{dP_{cp}}{dt} = \frac{1}{V_{cp}} \left( \dot{m}_{cp} RT_{cp} - P_{cp} \frac{dV_{cp}}{dt} \right) \quad (B5)$$

$$\frac{dP_t}{dt} = \frac{1}{V_t} (\dot{m}_c RT_c - (\dot{m}_0 - \dot{m}_{di}) RT_h) \quad (B6)$$

$$\frac{dX_t}{dt} = \frac{1}{P_t V_t} (\dot{m}_c RT_c (1 - X_t) + (\dot{m}_0 - \dot{m}_{di}) RT_h X_t) \quad (B7)$$

$$\frac{dP_r}{dt} = \frac{1}{V_r} (-\dot{m}_0 RT_h) \quad (B8)$$

The energy exchange, equations (B9) for the case of isothermal model is calculated after solving equations (B1) to (B8).

$$\left. \begin{aligned} \dot{Q}_c &= P_t V_t \frac{dX_t}{dt} - \dot{m}_c RT_c \\ \dot{Q}_h &= -P_t V_t \frac{dX_t}{dt} + \dot{m}_h RT_h \\ \dot{W}_{cp} &= -P_{cp} \frac{dV_{cp}}{dt} \\ \dot{W}_h &= P_t \frac{dV_h}{dt} \end{aligned} \right\} \quad (B9)$$

The input parameters for both the models are shown in a tabular form in Table3.1. The numerical simulation is described in the flow chart as given in Fig.3.25. Initially, in the first cycle, the pressure is assumed to be constant. Using the initial value of  $V_{cp}$ , the pressure is recalculated using the mass flow rate in the different components. This pressure variation acts as a guess value for the next cycle. This process is repeated over every cycle till the convergence criteria are satisfied. The convergence criteria during the iterative process, is that the difference between two consecutive iterations of all quantities such as temperatures, pressures, velocities, densities etc. at all discretized point must be less than  $1e-5$ . The set of differential equations is converged when the system reaches the cyclic steady state.

Table 3 Design data for adiabatic and isothermal models

Components	Parameters
Compressor	Dead volume = $V_0 = 0.13 \times 10^{-3} \text{ m}^3$ Swept volume = $V_s = 0.5 \times 10^{-3} \text{ m}^3$
Regenerator	Length = $L_{rg} = 0.21\text{m}$ Diameter = $d_{rg} = 0.02\text{m}$ Porosity = 0.7 Hydraulic diameter = $d_h = 0.04\text{mm}$
Pulse tube	Length = $L_t = 0.25\text{m}$  Diameter = $d_t = 0.015\text{m}$
Cold end block	Dead volume = $V_{dcx} = 0.00002\text{m}^3$
Hot end block	Dead volume = $V_{dhx} = 0.00002\text{m}^3$
Orifice	Diameter = 1mm
DI valve	Diameter = 1mm
Reservoir	Volume = 0.5litre
Average pressure	16bar
Frequency	2Hz
Cold end temperature	100K
Hot end temperature	300K
Helium gas At 16bar and 300K temperature	Dynamic viscosity = $\mu = 15.21 \times 10^{-6} \text{ Ns/m}^2$ $\rho = 2.389 \text{ kg/m}^3$ $c_p = 5193.0\text{J/kg K}$ $R = 2074.6\text{J/kg-K}$ $\gamma = 1.67$

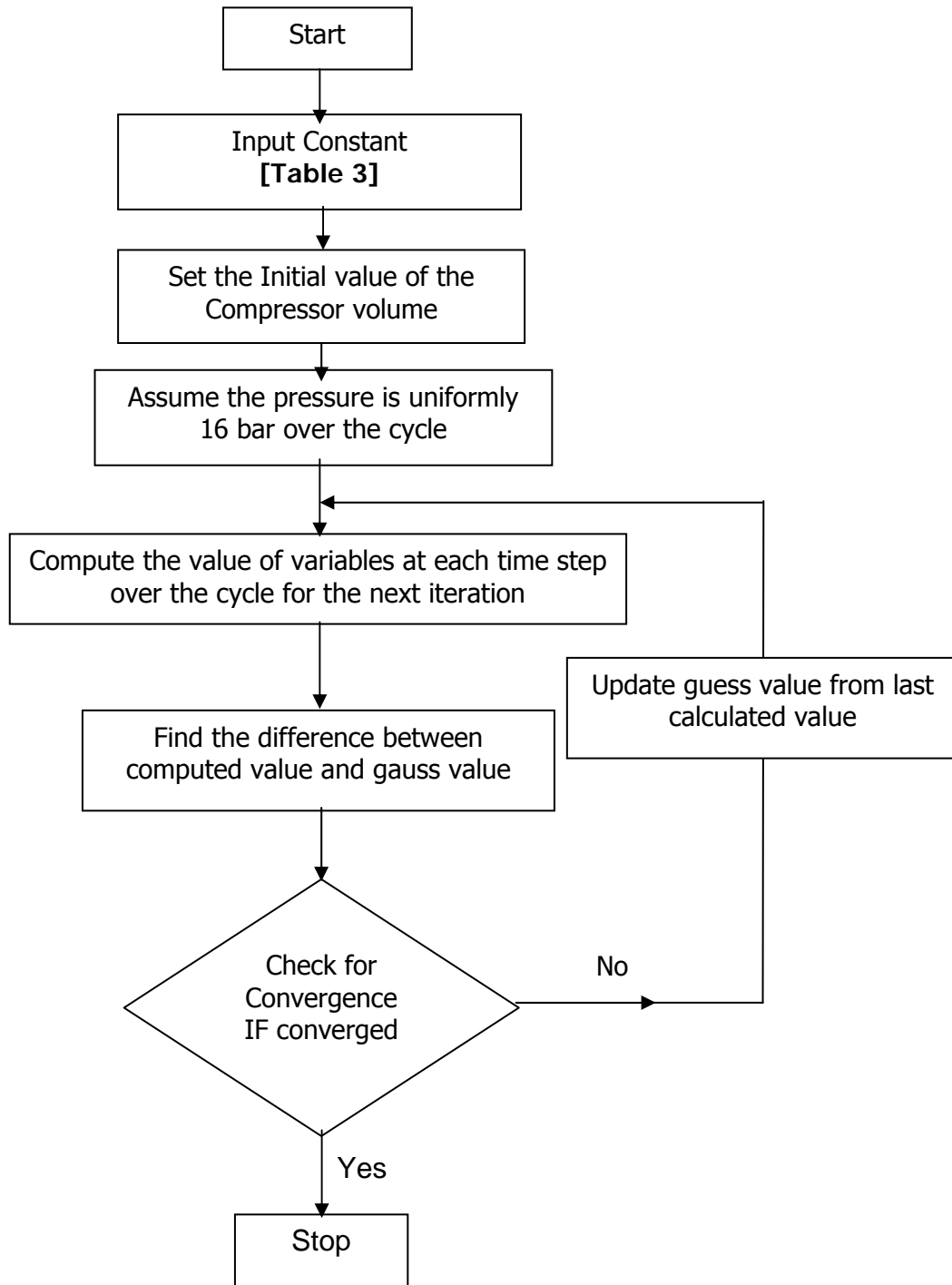


Fig.3.25 Flow chart of the computer program for numerical simulation.



## *Chapter IV*

# Theory of Heat and Fluid Flow in Pulse Tube Refrigerator

### *4.1 Introduction*

The pulse tube refrigerators are a class of rugged and high-endurance refrigeration systems that operate without a moving part at their low temperature end. Due to absence of moving component at low temperature end PTR has high reliability, low vibration, long life time, small size and weight. In general the pulse tube refrigerator consists of a pressure wave generator (compressor), an after cooler, a regenerator, a pulse tube, cold and hot heat exchangers, an inertance tube (or orifice valve or orifice valve and bypass valve), reservoir or buffer, vacuum chamber and coupling etc. The thermo-fluid processes in PTR are complicated, and the details of the mechanism underlying their performance are not well understood. Some components of PTRs like regenerator are presented as a porous medium, which consists of stainless steel woven wire mesh arranged in a proper way. Regenerator is very critical component of a pulse tube refrigerator. The performance of any cryocooler depends on the proper design of regenerator and selection of proper regenerator material for the given temperature range. Modeling the regenerator as a porous media requires some input parameters like porosity, inertial resistance and viscous resistance factors. Hence it is very essential to understand the thermodynamics of porous media.

This chapter is devoted to the derivation of heat and fluid flow through the porous media used for pulse tube refrigerator for the CFD analysis. Different analysis requires

different types of regenerator parameters. In this analysis the parameters used for CFD (particularly Fluent software) are derived from the basic principles. This caters the basic parameters of regenerator for the CFD simulation.

## *4.2 Porous Media*

In recent years heat transfer in porous media has been attracting the attention of an increasingly large number of investigators. The need for fundamental studies in porous media heat transfer stems from the fact that a better understanding of convective transport mechanism is required owing to the development of geothermal systems, thermal insulation, grain storage, solid matrix heat exchangers, oil extraction, cooling of nuclear fuel and many other areas. The accumulated impact of porous media studies is two folds: first to improve the performance of existing porous-media-related thermal systems and second to generate new ideas and explore new awareness with respect to the use of porous media in heat and fluid flow applications.

Porous media is defined as a material consisting of a solid matrix with interconnected voids (pores). The interconnected channels allow passage of one or more fluids. Examples of fluid flow and heat transfer in a porous media are: Underground water movement in soils, filtration and transport of gaseous reactance in a catalyst pore, cryocooler regenerators etc.

In a natural porous media, the distribution of pores with respect to shape and size is random and irregular. On microscopic scale, the transport process is also irregular if one tries to trace the path of a fluid element at a given location as it passes through the porous media. In practice, investigators are interested in properties/ quantities that are measured on a macroscopic scale by averaging over a representative elementary length/areas/volume containing large number of pores. This then provides the basis for deriving the transport laws governing the macroscopically averaged variables and thus removing the random components associated with the microscopic scale.

## *4.3 Volume Averaging Technique*

The volume averaging technique is an analytical tool for describing the flow and heat transfer in a porous media. The fluid in the porous media only occupies part of the whole space and is separated by a highly irregular solid surface. The hydrodynamic and

thermodynamic quantities for fluid are continuous locally but discontinues over the entire domain. However when it is averaged over a representative volume at a certain scale level the quantity associated with the fluid could be a spatially continuous function. Thus by using the volume averaging technique local conservation equations for a general fluid flow can be transformed into a set of global conservation equations.

The concept of continuum and field theory can be extended to a porous media. The procedure of analysis of transport phenomenon in a porous media is to obtain the macroscopic model from the microscopic one (continuum) by averaging over a representative elementary volume (r.e.v.) denoted as  $V_m$ . The selection, size and shape of a r.e.v. are arbitrary. They depend on the model objectives, resolutions requirements and the measurable characteristics of the porous media taken by the available instruments. It is assumed that the averaging results remain unaltered and are independent of the selection and the size of an r.e.v. Figure 4.1 illustrates a typical representative elementary volume (r.e.v.) in a flow domain, which requires that the characteristic length of an r.e.v. is much larger than the pore scale but considerably smaller than the scale of the phenomenon being studied. In this respect, an r.e.v. assumes the role of a point in a continuum. The macroscopic properties/quantities averaged over an r.e.v. are continuous over the porous domain and are differentiable functions of space coordinates. Based on the r.e.v. concept the governing equations for fluid flow and heat transfer through a regenerator in a PTR are presented in the forth coming sections.

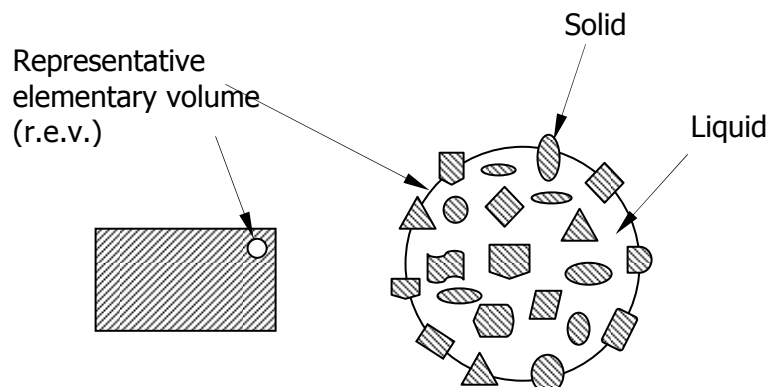


Fig.4.1 The representative elementary volume to show the intermediate size relative to the sizes of the flow domain and the pores.

## 4.4 *Regenerator Materials*

The regenerator is the most important component in pulse tube refrigerator. Its function is to absorb heat from the incoming gas during the forward stroke of the compressor, and deliver that heat back to the gas during the return stroke. Ideally, regenerator with no pressure drop and a heat exchanger effectiveness of unity are desirable, in order to achieve the maximum enthalpy flow in the pulse tube. The performances of real regenerators are of course far from the ideal. The regenerator materials and geometries generally fall into three groups, based on the temperature range over which they are most commonly used. The first groups are the oven screen materials-such as stainless steel, bronze, and copper which are easy to weave into the screen geometry. These materials are used over the temperature range from 30K to 300K, where they provide the following advantages:

- Low pressure drop
- High heat transfer area
- Low axial conductivity
- High heat capacity

At temperature below 30K screens lose their advantages and exhibit the following disadvantages:

- High void volume
- Low heat capacity

In the range between 10K and 30K lead and lead antimony spheres are used because of their higher heat capacity than any of the screen materials. In addition to the higher specific heat, spheres provide two advantages in this temperature range:

- Low void volume related to low porosity
- Low pressure drop reflecting the decrease in the fluid viscosity

A representation of regenerator materials used at different temperature range [161] are shown in Fig.4.2.

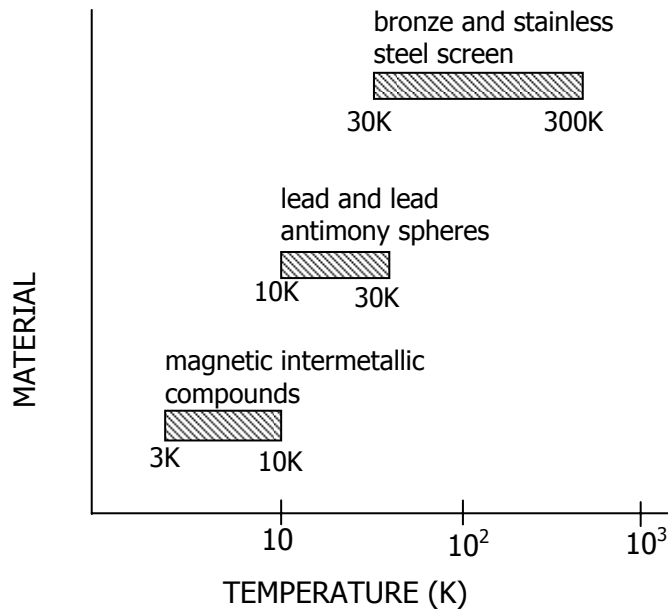


Fig.4.2 Temperature range for commonly used regenerator materials in cryogenic refrigerators.

#### *4.5 Porous Media Parameters for Regenerator Matrix*

The regenerator of a pulse tube refrigerator is a very critical component. The performance of any cryocooler greatly depends on regenerator material and its proper design. The regenerator is modeled as a porous media, for which some basic parameters like porosity, viscous resistance factor and inertial resistance factor are required as input parameters for CFD analysis. This section deals with the estimation of these basic parameters for regenerator porous matrix. The coefficients of porous media can be extracted from the experimental data in the form of pressure drop against velocity through the component. The oven wire mesh screen (Fig.4.3) is the most commonly used regenerator material. Its advantages are that it provides a high heat transfer area with minimum pressure drop and it is readily available in mesh sizes from 50mesh (50x50 opening per square inch) to over 250mesh. It is also available in many different materials. Woven bronze screen regenerators are widely used in the first stage of all commercial regenerative cryogenic refrigerators to provide cooling down to 30K. Below

30K, the loss in specific heat of the commercially available materials, such as bronze and stainless steel, limits the effectiveness of screen packing.

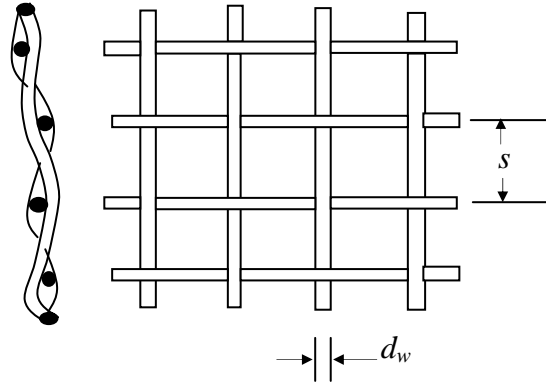


Fig.4.3 Woven wire mesh screens.

The geometrical parameters used in the description of screen regenerators are the porosity and area density. The porosity is defined as the ratio of the volume occupied by the fluid to the total volume. It could also be defined as the ratio of void volume to the total volume. It is expressed as

$$\text{Porosity} = \phi = \frac{\text{total volume of connected void space}}{\text{total volume of the matrix}} \quad (4.1)$$

The area density is defined as the ratio of void surface area to the total volume of the matrix. It is expressed as

$$\text{Area density} = \sigma = \frac{\text{total surface area of connected voids}}{\text{total volume of the matrix}} \quad (4.2)$$

From the porosity and area density, the important relationship for the hydraulic radius for a screen packing is given by

$$r_h = \frac{\phi}{\sigma} = \frac{\text{Fluid volume}}{\text{Heat transfer area}} = \frac{\text{Area}}{\text{Wetted perimeter}} \quad (4.3)$$

Experimentally, the porosity and area density can be found from the dimensions and weight of the screens. The porosity is found by weighing the packed regenerator and subtracting their tare weight of the regenerator canister.

$$\phi = 1 - \frac{W_p}{\rho_m V_r} \quad (4.4)$$

Where  $W_p$  is the weight of the packed matrix material,  $\rho_m$  is the density of the packing (matrix), and  $V_r$  is the regenerator volume. The area density for one screen as shown in Fig.4.4 is computed by calculating the circumferential heat transfer area of the wires and the total volume encompassed in one segment of screen mesh:

$$\sigma = \frac{A_s}{V_r} = \frac{1/2(\text{wire wetted perimeter})(\text{length of the opening})(4\text{sides})}{(\text{volume encompassing the wires})}$$

$$\sigma = \frac{\frac{1}{2}(\pi d_w)(1/m)(4)}{(1/m)^2 t_s} = \frac{2\pi m d_w}{t_s} \quad (4.5)$$

Where  $d_w$  is the wire diameter,  $t_s$  is the screen thickness, and  $m$  is the mesh size.

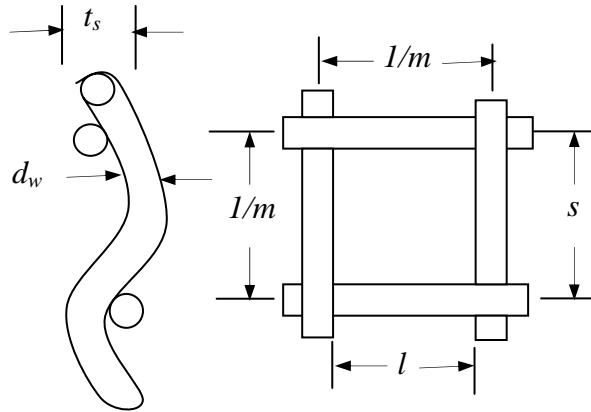


Fig.4.4 Geometry of woven screen.

From the area density, the total regenerator heat transfer area is given by

$$A = \sigma \times \text{Total volume of regenerator} = \left( \frac{2\pi m d_w}{t_s} \right) \left( \frac{\pi}{4} d_o^2 \right) (t_s n) \quad (4.6)$$

$$A = d_w \left( \frac{\pi}{4} d_o^2 \right) (nm) \quad (4.7)$$

Where  $d_o$  is the outer diameter of the screens and  $n$  is the total number of screens used to pack the regenerator.

Analytically the porosity and area density are calculated by considering a small segment of screen with a transverse pitch,  $x_t$  (designating the transverse spacing/ factor between wires) and a lateral pitch,  $x_l$  (designating the longitudinal spacing/ factor between wires). Referring to Fig.4.4 the pitches are related to the mesh size and screen thickness by

$$\frac{1}{m} = s = x_t d_w \quad \text{and} \quad t_s = 2x_l d_w \quad (4.8)$$

The Fig.4.4 is based on a perfect stacking of square mesh screens in which the weaving causes no inclination of the wires and the screen layers are not separated. These idealization lead to a matrix packing where the screen thickness,  $t_s$ , is equal to  $2d_w$ , and the porosity is given by

$$\phi = 1 - \frac{V_m}{V_r} \quad (4.9)$$

Where  $V_m$  is volume occupied by the screen material. Thus,

$$\phi = 1 - \frac{2[(\pi/4)d_w^2](x_t d_w)}{(x_t d_w)^2 (2d_w)} = 1 - \frac{\pi}{4x_t} \quad (4.10)$$

where

$$x_t = \frac{0.0254}{d_w m} \quad (4.11)$$

where  $m$  is mesh per inch;  $d_w$  is wire diameter of screen.

For a woven screen regenerator it is necessary to specify an additional analytical parameter, to define the ratio of the minimum free flow area to the frontal area. From the description of the screen geometry, shown in Fig.4.4

$$\beta = \frac{\text{open area}}{\text{total area}} = \frac{(x_t d_w - d_w)^2}{(x_t d_w)^2} = \frac{(x_t - 1)^2}{(x_t)^2} = \left(\frac{l}{s}\right)^2 \quad (4.12)$$



The area density is given by

$$\sigma = \frac{\pi}{x_i d_w} \quad (4.13)$$

From the porosity expression, equation (4.10) and area density equation (4.13), the hydraulic radius expression given by equation (4.3) can be expressed as

$$r_h = \frac{\phi d_w}{4.0(1 - \phi)} \quad (4.14)$$

For a woven screen regenerator if the wire diameter and mesh per inch is given, porosity, area density and hydraulic radius can be analytically obtained from Eq. (4.10), Eq. (4.13) and Eq. (4.14) respectively.

#### ***4.6 Permeability and Inertial Resistance Factors for Porous Media***

The porous media model can be used for a wide variety of problems, including flows through packed beds, filter papers, perforated plates, flow distributors, and tube banks. Heat transfer through these medium can be represented subject to the assumption of thermal equilibrium between the medium and the fluid flow. The porous media model incorporates an empirically determined flow resistance in a region of the model defined as "porous". In essence, the porous media model is nothing more than an added momentum source in the governing momentum equations of the Navier-stoke equation.

The source term is composed of two parts [175]: a viscous loss term (Darcy, the first term on the right-hand side of Eq. (4.15)), and an inertial term (the second term on the right-hand side of Eq. (4.15))

$$S_i = - \left( \sum_{j=1}^3 D_{ij} \mu v_j + \sum_{j=1}^3 C_{ij} \frac{1}{2} \rho v_{mag} v_j \right) \quad (4.15)$$

For a simple homogeneous porous media, the source term is

$$S_i = - \left( \frac{\mu}{\alpha} \bar{v} + C \frac{1}{2} \rho_f |\bar{v}| \bar{v} \right) \quad (4.16)$$

Where  $\alpha$  and  $C$  are the permeability and the inertial resistance factors, respectively. Thus, the mass, momentum and energy equations for the porous media can be expressed including porosity  $\phi$  of the porous media and the above source term. The source term is an additional pressure drop term due to porous matrix.

The following one-dimensional empirical equations are considered for the pressure gradient in the porous media

$$\frac{\partial p}{\partial x} = -f_F \frac{2\rho_f v^2}{d_h} \quad (4.17)$$

The Fanning friction factor  $f_F$  in Eq. (4.17) is determined from the steady flow experiment and its definition is as follows:

$$f_F = \frac{\Delta P d_h}{2\rho v^2 L_r} \quad (4.18)$$

$$\text{where } v = \frac{\dot{m}}{\rho A_g} \text{ and } d_h = \frac{\phi d_w}{1 - \phi} \quad (4.19)$$

Where the free flow cross sectional area  $A_g$  and regenerator cross sectional area  $A_r$  is related through porosity as  $A_g = \phi A_r$ .

The pressure drop in the matrix is caused by two physical factors: form drag and skin friction. Therefore their effect on the resulting equations for pressure drop and friction factor can be written as,

$$C_F = C_{fd} + \frac{C_{sf}}{R_{el}} \quad (4.20)$$

Where

$$C_F = \frac{\Delta P}{0.5\rho v^2 n}, R_{el} = \frac{\dot{m} l}{\beta A_r \mu}$$

In the above equation, the pressure drop is proportional to number of flow resisters,  $n$  of the matrix. In case of wire mesh screen,  $n=l/2d_w$ . These equations related to pressure drop is generally applicable to pressure drop data of regenerator matrices regardless of whether wire screens or metal felts are used.

In case of wire screen the two correlation constants for different investigators [152] are given in tabular form in Table 4.1.

Table 4.1 Friction factor correlations

Investigators[152]	$C_{fs}$	$C_{fd}$
Gedeon/Wood	68.556	0.5274
Tong/London	44.710	0.3243
Blass	47.245	0.4892
Miyabe	33.603	0.3370
Tanaka	40.7413	0.5315

Following Miyabe correlation

$$C_F = \frac{33.6}{R_{el}} + 0.337 \quad (4.21)$$

The pressure drop can be calculated as

$$\Delta P = \left( \frac{33.6}{2R_{el}} \rho v^2 n + \frac{0.337 \rho v^2 n}{2} \right) \quad (4.22)$$

Substituting Eq. (4.22) in Eq. (4.18) yields

$$f_F = \left( \frac{33.6 n d_h}{4L_r R_{el}} + \frac{0.337 n d_h}{4L_r} \right) \quad (4.23)$$

The two Reynolds number are expressed as

$$R_{el} = \frac{\dot{m} l}{\beta A_r \mu} \quad \text{and} \quad R_{eh} = \frac{\dot{m} d_h}{A_g \mu} \quad (4.24)$$

From above equation, eliminating mass flow rate gives

$$R_{el} = \frac{R_{eh} l}{d_h \beta} \phi \quad (4.25)$$

Substituting Eq. (4.25) in Eq. (4.23),

$$f_F = \frac{n \phi d_h^2}{4l \beta} \frac{33.6}{R_{eh} L_r} + 0.337 \frac{n \phi^2 d_h}{4 \beta^2 L_r} \quad (4.26)$$

If  $n'$  is number of packed screens per length ( $n' = n/L_r$ ), then the equation (4.26) can be expressed as

$$f_F = \frac{n' \phi d_h^2}{4l \beta} \frac{33.6}{R_{eh}} + 0.337 \frac{n' \phi^2 d_h}{4 \beta^2} \quad (4.27)$$

Substituting Eq. (4.27) in Eq. (4.17) the pressure drop term can be modified as

$$\frac{\partial p}{\partial x} = -\frac{33.6n'\phi v\mu}{2l\beta} - \frac{0.337n'\phi^2 \rho_f v^2}{2\beta^2} \quad (4.28)$$

Where  $l$  is the mesh distance,  $\beta$  is the opening area ratio of screen,  $d_h$  is the hydraulic diameter of screen,  $n'$  is the number of packed screens per unit length,  $\mu$  is the viscosity.

Comparing Eq. (4.16) with Eq. (4.28) leads to permeability and inertial resistance factors as

$$D = \frac{1}{\alpha} = \frac{33.6n'\phi}{2l\beta} \quad \text{and} \quad C = \frac{0.337n'\phi^2}{\beta^2} \quad (4.29)$$

So for a given screen wire mesh the value of permeability and inertial resistance factors can be obtained analytically using equation (4.29). Table 4.2 lists the important operational parameters of the porous media for the CFD simulation.

Table 4.2 Operational parameters of the porous media.

S No.	Material1	Material2	Material3
Material	304 SS	304SS	Copper
$n$	250	200	100
$n' (m^{-1})$	$1.2 \times 10^4$	$9.5 \times 10^3$	$1 \times 10^4$
$d_w(m)$	$4 \times 10^{-5}$	$5.2 \times 10^{-5}$	$1 \times 10^{-4}$
$l(m)$	$6.3 \times 10^{-5}$	$7.5 \times 10^{-5}$	$1.6 \times 10^{-4}$
$\beta$	0.373	0.349	0.377
$\phi$	0.694	0.679	0.697
$D$	$5.95 \times 10^9$	$4.15 \times 10^9$	$1.94 \times 10^9$
$C$	$1.299 \times 10^4$	$1.214 \times 10^4$	$1.15 \times 10^4$

#### 4.7 Governing Equations for Pulse Tube Refrigerator

The pulse tube refrigerator system for the present analysis consists of a dual opposed piston compressor, a transfer line, an after cooler, regenerator, cold end heat exchanger (CHX), pulse tube, hot end heat exchanger (HHX), inertance tube/orifice and a reservoir. Continuum-based conservation equations can be applied everywhere in the system. This is

appropriate since the mean free path of gas molecule is typically much smaller than the characteristic dimension of the system components. The regenerator and heat exchanger can in some circumstances be exceptions to the aforementioned statement. However, when the characteristic dimensions of their micro porous structure are comparable, or even smaller than the gas mean free path. For this reason, these components are modeled using porous media method as described later. Thus, continuum based conservation of mass, momentum, energy equations along with the equation of state of the working fluid are used for all components, except the regenerator and heat exchangers. The general governing equations used by the Fluent code [175] are as follows.

***Conservation of mass equation :***

$$\frac{\partial \rho}{\partial t} + \nabla \cdot (\rho \vec{v}) = S_m \quad (4.30)$$

Where

$\nabla$  = Gradient operator

$\rho$  = Density of the gas

$\vec{v}$  = Velocity in vector form

$S_m$  = Source term

t = Time

( $S_m = 0$  for this case)

***Conservation of momentum:***

$$\frac{\partial}{\partial t} (\rho \vec{v}) + \nabla \cdot (\rho \vec{v} \vec{v}) = -\nabla p + \nabla \cdot (\tau) + \rho \vec{g} + \vec{F} \quad (4.31)$$

Where:

p = Static pressure

$\tau$  = Stress Tensors

$\vec{g}$  = Gravity acceleration

$\vec{F}$  = External body forces or source terms e.g. terms associated with porous media.

Assuming that the working fluid is Newtonian, the constitutive relation for shear- stress strain rate is:

$$\tau = \mu \left[ (\nabla \vec{v} + \nabla \vec{v}^{TP}) - \frac{2}{3} \nabla \cdot \vec{v} I \right] \quad (4.32)$$

Where:

$\mu$  = Fluid molecular viscosity

I = Unit (Identity) tensor

TP = Transpose

**Conservation of energy:**

$$\frac{\partial}{\partial t}(\rho E) + \nabla \cdot (\vec{v}(\rho E + p)) = \nabla \cdot (k_{eff} \nabla T - \sum_j h_j \vec{\psi}_j + (\tau \cdot \vec{v})) + S \quad (4.33)$$

Where

$$E = h - \frac{p}{\rho} + \frac{v^2}{2} \quad (4.34)$$

$$h = \int_{T_1}^T C_p dT \quad (4.35)$$

$$k_{eff} = k + k_t \quad (4.36)$$

Where

k = Gas thermal conductivity

$k_t$  = Turbulence thermal conductivity

$C_p$  = Specific heat of gas

h = Local enthalpy

T = Temperature of the gas

v = Local velocity

$\psi_j$  = Diffusion flux of species

S = Source term which can be caused by chemical reactions or volumetric heat generation.

The diffusion flux is only important in multi component flows. Evidently  $\psi_j = 0$  for this case.

Equation of state assuming ideal gas behavior,

$$P = \rho RT \quad (4.37)$$

where R = Gas constant

The above equations can be simplified. First, given the axis-symmetric configuration of the modeled system and assuming a negligible asymmetry caused by gravity, the aforementioned equation can be cast in 2- dimensional cylindrical polar coordinate systems as:

**Continuity Equation:**

$$\frac{\partial \rho}{\partial t} + \frac{1}{r} \frac{\partial}{\partial r} (r \rho v_r) + \frac{\partial}{\partial x} (\rho v_x) = 0 \quad (4.38)$$

Where

r = Radial coordinate

x = Axial coordinate

v<sub>r</sub> = Velocity in radial coordinate

v<sub>x</sub> = Velocity in axial coordinate

**Momentum Equations in axial and radial directions:**

$$\begin{aligned} \frac{\partial}{\partial t} (\rho v_x) + \frac{1}{r} \frac{\partial}{\partial x} (r \rho v_x v_x) + \frac{1}{r} \frac{\partial}{\partial r} (r \rho v_r v_x) = - \frac{\partial p}{\partial x} \\ + \frac{1}{r} \frac{\partial}{\partial x} \left[ r \mu \left( 2 \frac{\partial v_x}{\partial x} - \frac{2}{3} (\nabla \cdot \vec{v}) \right) \right] + \frac{1}{r} \frac{\partial}{\partial r} \left[ r \mu \left( \frac{\partial v_x}{\partial r} + \frac{\partial v_r}{\partial x} \right) \right] \end{aligned} \quad (4.39)$$

$$\begin{aligned} \frac{\partial}{\partial t} (\rho v_r) + \frac{1}{r} \frac{\partial}{\partial x} (r \rho v_x v_r) + \frac{1}{r} \frac{\partial}{\partial r} (r \rho v_r v_r) = - \frac{\partial p}{\partial r} \\ + \frac{1}{r} \frac{\partial}{\partial r} \left[ r \mu \left( 2 \frac{\partial v_r}{\partial r} - \frac{2}{3} (\nabla \cdot \vec{v}) \right) \right] + \frac{1}{r} \frac{\partial}{\partial x} \left[ r \mu \left( \frac{\partial v_r}{\partial x} + \frac{\partial v_x}{\partial r} \right) \right] - 2 \mu \frac{v_r}{r^2} + \frac{2}{3} \frac{\mu}{r} (\nabla \cdot \vec{v}) \end{aligned} \quad (4.40)$$

Where v<sub>r</sub> and v<sub>x</sub> are the radial and axial components of the velocity vector respectively.

Where,

$$\nabla \cdot \vec{v} = \frac{\partial v_x}{\partial x} + \frac{\partial v_r}{\partial r} + \frac{v_r}{r} \quad (4.41)$$

Also note the body forces (gravity forces) and any other external forces have been neglected in the above equations.

**Energy Equation :**

$$\frac{\partial}{\partial t} (\rho E) + \nabla \cdot (\vec{v} (\rho E + p)) = \nabla \cdot (k_{eff} \nabla T + (\tau \cdot \vec{v})) \quad (4.42)$$

Equations (4.38) to Eq. (4.42) are to be numerically solved for the compressor, transfer line, pulse tube, inertance tube and the surge volume.

**Porous media equations for PTR:**

The regenerator, after cooler, cold end heat exchanger and hot end exchanger can be modeled using porous – media methods. The porous –media is modeled using the volume-averaged conservation equations for mass and momentum. The volume-averaged mass conservation equation is:

$$\frac{\partial}{\partial t}(\phi\rho) + \nabla \cdot (\phi\rho\vec{v}) = 0 \quad (4.43)$$

where  $\phi$  is the porosity of the porous medium.

The momentum equation for porous media are modeled by introducing two new terms to the volume –averaged momentum equation : the Darcy term ,which represents a pressure drops term directly proportional to the velocity , and an inertial term which is proportional to the velocity square. Assuming a homogeneous and isotropic solid matrix, the following force terms are included in the x and r volume – averaged momentum equations [175].

$$F_{porous\ x} = -\left(\frac{\mu}{\alpha}v_x + \frac{1}{2}C\rho|\vec{v}|v_x\right) \quad (4.44)$$

$$F_{porous\ r} = -\left(\frac{\mu}{\alpha}v_r + \frac{1}{2}C\rho|\vec{v}|v_r\right) \quad (4.45)$$

Where

$\mu$  = Fluid molecular viscosity

$\alpha$  = Permeability

C = Inertial resistance factor

v = Velocity

In the aforementioned equations, the first term represents the Darcy term. The second term is often referred to as the Forchheimer term and represents the fluid inertia. Fluent requires a user input inertial resistance factor C and the permeability parameter  $\alpha$  for the porous medium. The inertial resistance factor and the permeability must be specified on relevant correlations or experimental data. These factors for wire screen have been derived in equation (4.29). In summary, the porous –medium momentum equation, in generic vectorial form, can be represented as:

$$\frac{\partial}{\partial t}(\phi\rho\vec{v}) + \nabla \cdot (\phi\rho\vec{v}\vec{v}) = -\phi\nabla p + \nabla \cdot (\phi\tau) - \left(\frac{\mu}{\alpha}\vec{v} + \frac{1}{2}C\rho|\vec{v}|\vec{v}\right) \quad (4.46)$$

Where  $\vec{v}$  is the physical velocity and is related to superficial velocity  $\vec{v}_1$  according to

$$\vec{v}_1 = \phi\vec{v} \quad (4.47)$$

The axial and radial components of the above equation are:



***Porous –medium momentum equation in axial direction:***

$$\begin{aligned} \frac{\partial}{\partial t}(\phi \rho v_x) + \frac{1}{r} \frac{\partial}{\partial x}(\phi r \rho v_x v_x) + \frac{1}{r} \frac{\partial}{\partial r}(\phi r \rho v_r v_x) = -\frac{\partial(\phi p)}{\partial x} + \\ \frac{1}{r} \frac{\partial}{\partial x} \left[ r \mu \left( 2 \frac{\partial(\phi v_x)}{\partial x} - \frac{2}{3} (\nabla \cdot (\phi \vec{v})) \right) \right] + \frac{1}{r} \frac{\partial}{\partial r} \left[ r \mu \left( \frac{\partial(\phi v_x)}{\partial r} + \frac{\partial(\phi v_r)}{\partial x} \right) \right] + - \left( \frac{\mu}{\alpha} v_x + \frac{1}{2} C \rho |\vec{v}| v_x \right) \end{aligned} \quad (4.48)$$

***Porous –medium momentum equation in radial direction:***

$$\begin{aligned} \frac{\partial}{\partial t}(\phi \rho v_r) + \frac{1}{r} \frac{\partial}{\partial x}(\phi r \rho v_x v_r) + \frac{1}{r} \frac{\partial}{\partial r}(\phi r \rho v_r v_r) = -\frac{\partial(\phi p)}{\partial r} + \frac{1}{r} \frac{\partial}{\partial r} \left[ r \mu \left( 2 \frac{\partial(\phi v_r)}{\partial r} - \frac{2}{3} (\nabla \cdot (\phi \vec{v})) \right) \right] \\ + \frac{1}{r} \frac{\partial}{\partial x} \left[ r \mu \left( \frac{\partial v_r}{\partial x} + \frac{\partial v_x}{\partial r} \right) \right] - 2 \mu \frac{v_r}{r^2} + \frac{2}{3} \frac{\mu}{r} (\nabla \cdot \vec{v}) + - \left( \frac{\mu}{\alpha} v_r + \frac{1}{2} C \rho |\vec{v}| v_r \right) \end{aligned} \quad (4.49)$$

The porous medium energy equation must account for the fluid – porous structure interactions. When thermodynamic non-equilibrium between the fluid and the porous structure is accounted, separate energy conservation equation must be solved for the fluid and solid phases. The aforementioned thermodynamic non equilibrium is usually small. However and often a single energy equation representing both the solid and gas phase is used. Accordingly, in this study, local thermal equilibrium assumption is applied. The single energy equation is used as,

$$\frac{\partial}{\partial t}(\phi \rho_f E_f + (1 - \phi) \rho_s E_s) + \nabla \cdot (\vec{v}(\rho_f E_f + P)) = \nabla \cdot (k_{eff} \nabla T + \tau \cdot \vec{v}) \quad (4.50)$$

$$\text{Where } k_{eff} = \phi k_f + (1 - \phi) k_s \quad (4.51)$$

$\phi$  = porosity of medium

$k_s$  = Solid medium thermal conductivity

$k_f$  = Fluid thermal conductivity

$E_f$  = Total fluid energy

$E_s$  = Total solid energy

## *4.8 Computational Fluid Dynamics (CFD) Simulation Procedures*

The technology of computer CPU is growing in extremely fast rate. Consequently, standard computer processing time has decreased by many orders of magnitude compared to one at a decade ago, and high performance computers are now available. Engineers today have better tools for solving complex engineering problem in short time. The availability of fast computers equipped with very large memories also allow for remarkably precise numerical simulations. As a result computational fluid dynamics (CFD) tools, both for commercial and research purposes are now available. One of the most highly respected CFD code is Fluent [175]. Fluent is a state-of-the-art computer program for modeling fluid flow and heat transfer process in complex engineering problems. Fluent offers the flexibility of meshing any complex geometry and solving complicated 2-dimensional and 3-dimensional problems. Transient flow and transport phenomena in porous media, two phase flow, and volumetrically generating sources can all be modeled by Fluent. Fluent numerically solves the entire continuum fluid and energy balance equations with no arbitrary assumptions.

- *Finite Volume Formulation*

The Finite Volume Method (FVM) is one of the most versatile discrimination techniques used for solving governing equations for fluid flow and heat and mass transfer problems. The most compelling features of the FVM are that the resulting solution satisfies the conservation of quantities such as mass, momentum, energy and species. This is exactly satisfied for any control volume as well as for the whole computation domain. Even a coarse grid solution exhibits exact integral balances. Apart from this, it can be applied to any type of grids (structured or unstructured, Cartesian or body fitted), and especially complex geometries. Hence, it is the platform for most of the commercial packages like Fluent, Star-CD, and CFX etc. which are used to solve fluid flow and heat and mass transfer problems. In the finite volume method, the solution domain is subdivided into continuous cells or control volumes where the variable of interests is located at the centroid of the control volume forming a grid. The next step is to integrate the differential form of the governing equations over each control volume. Interpolation profiles are then assumed in order to describe the variation of the concerned variables between cell centroids. There are several schemes that can be used for interpolation, e.g. central differencing, upwind differencing, power-law differencing and quadratic upwind differencing schemes. The resulting equation is called the discretized or

discretization equation. In this manner the discretization equation expresses the conservation principle for the variable inside the control volume. These variables form a set of algebraic equations which are solved simultaneously using special algorithm.

- *CFD Modeling Procedure*

The computer simulation is performed using the CFD software package, Fluent (Version 6.1) to model the heat and mass transfer in pulse tube refrigeration systems. Details about the software can be found in the user's documentation for Fluent 6.1 [175]. Fluent is based on a finite volume computational scheme. The code solves the following general differential equations:

$$\frac{\partial(\rho\phi)}{\partial t} + \nabla \cdot (\rho v \phi) = \nabla \cdot (\Gamma \nabla \phi) + S_i \quad (4.52)$$

where the terms on the left represent accumulation rate and convection, while those on the right represent diffusion and creation / destruction of the generic variable  $\phi$ , that represent the variable solved (i.e.  $v_x, v_r, \rho_s, \rho_g$ ),  $\Gamma$  is the exchange coefficient.  $S_i$  represents the source term. The solution method involves integration of the governing differential equations over finite control volume and transforming them into a general algebraic form:

$$a_p \phi_p = \sum a_k \phi_k + a_o \phi_o + b \quad (4.53)$$

Where  $a_0$  is a coefficient due to transient advection,  $a_k$  represents the combined advection and diffusion coefficients and  $b$  is a component of the linearized source term.

In general the following steps are to be followed for CFD modeling of any system using Fluent software.

*(i) Geometry Creation*

To model heat and fluid flow in pulse tube refrigeration system using Fluent 6.1, first, a proper geometry is to be created using a separate model/ mesh generation package, or pre-processor. For the present study, Gambit [176] is used as a preprocessor for modeling the geometry and generating meshes. Once the dimensions of all components of pulse tube refrigerator are known, the geometry is entered into Gambit to create the faces or volumes of different components depending on the 2-D or 3-D simulations. For OPTR and ITPTR the 2-D model is used for face creation and for DIPTR, 2-D model is used for face creation and 3-D model is used for volume creation. Then all faces/volumes are united and then split zone

wise to enable to set boundary conditions at different zones. Since computational domain is axisymmetric for OPTR and ITPTR in the present case and hence only half of the domain is considered for analysis. For DIPTR the computational domain is not axi-symmetric, so complete geometry is drawn in 2-D and as well as 3-D. Once these faces/volumes are created, actual meshing process can be initiated.

### *(ii) Mesh Generation*

The reason for creating a mesh is that a partial differential equation generates an infinite dimensional problem and the solution must in general be sought in a finite dimensional space. By restricting the problem to a finite set of points or cells in which a finite dimensional representation of the solution is chosen, the problem becomes manageable for computer simulations. To mesh the given 2-D planar geometry or 3-D geometry the first step is to create nodes (points where the grid lines of the mesh connect) on the edges. This can be done either by specifying equidistance spacing between the nodes, which provides a uniform mesh, or a gradually increasing /decreasing spacing (boundary layer mesh), which provides a non uniform mesh with a finer resolution across a certain region in the domain, such as along the bottom and sides walls of the present geometry, to estimate the velocity and temperature gradients accurately near the walls. Once the nodes are created, one can then generate the actual mesh along the faces. Different options for mesh generation are available in Gambit [176]; to list a few are triangular elements, hexahedral elements and quadrihedral elements. If the computational domain under consideration does not contain any complex surface the structured quad element could be used for meshing.

### *(iii) Zone/Boundary setting*

After meshing, boundary zones are created on the geometry. These zones are used later by Fluent to specify the boundary conditions. In the present case, for OPTR and ITPTR all the top lines and side lines of the system are specified as "walls". A "wall" is defined as a surface that is assumed to be solid such that no fluid can flow through it. The bottom line is specified as centre line to enable it to be axis-symmetric geometry. The left wall of the system is specified as wall and linked with UDF (user defined functions) for piston head motion. Dynamic mesh option is used to model piston cylinder function. The list of details of boundary conditions specified at different zones for the complete system is shown in next chapter. In fluent, numbers of options are there for specifying boundary conditions at inlet, outlet and

walls etc. For example pressure inlet boundary conditions could be used when the inlet pressure is known but the flow rate and/or velocity is unknown. Inlet condition could also be specified by user defined function. It can be noted that zone types (wall, pressure inlet, etc.) can be changed with in fluent as well, as long as zones are defined. Once the mesh and zones are created, the mesh is then imported into Fluent. Gambit is the preprocessor and Fluent is known as solver.

#### *(iv) Fluent Setup*

The first step taken after importing the mesh geometry into Fluent involves checking the mesh/grid for errors. Checking the grid assures that all zones are present and all dimensions are correct. It is also important to check the volume and make sure that it is not negative. If the volume is shown as negative, there is a problem with the grid, since volume can never be negative. The grid can also be displayed to ensure that the mesh generation is qualitatively reasonable. When the grid is checked completely and free of errors, a scale and units can be assigned. Since gambit inputs the coordinates as non dimensional numbers, the grid can be scaled however if one chooses. For this study, the grid was created in mm, and then scaled to meter. The maximum and minimum values for the x and y directions in 2-D are given in the scaling window and in 3-D the minimum and maximum values are given for all the three coordinates. Since the left bottom corner of the system is set as the origin (0, 0) when drawn in Gambit, the minimum x value is 0 m and maximum 1.076m while for y minimum value is 0 m and the maximum value is 13mm respectively for ITPTR. Similarly one can specify the coordinates for OPTR and DIPTR.

#### *(v) Defining the Model*

The model properties are required to be specified. These properties include the type of Fluent solver, the species/material fluid and thermal properties apart from model operating conditions and grid boundary conditions. The following settings are used to create the model in Fluent.

#### *(a) Solver*

Fluent 6.1 have three different solver formulations, i.e. segregated, coupled implicit, and coupled explicit. The coupled and the segregated solvers differ in their approach to solving the equations governing the fluid flow and heat transfer. In the segregated solver

approach, the governing equations are solved sequentially (i.e. an equation for a certain variable is solved for all cells, and then the equation for the next variable is solved for all cells). The segregated solution method is the default method in most commercial finite volume codes. It is best suited for incompressible flows or compressible flows at low Mach number. The coupled solver solves the governing equations simultaneously (i.e. for a given cell equations for all variables are solved, and the process is repeated for all cells). This is a "modern" solver but consumes more memory. Compressible flows at high Mach number, especially when they involve shock waves, are best solved with the coupled solver. While implicit and explicit scheme define the way in which these coupled equations are linearized. In the present study segregated solver with implicit formulation has been used. The segregated solver is recommended for turbulent flow. For this study, the options chosen for Stirling type OPTR/ITPTR are as follows:

- Flow Model: 2D Axisymmetric, Unsteady, turbulent flow
- Solver: Segregated , Double Precision
- Unsteady Formulation: Second order Implicit
- Porous Formulation: Physical velocity

For G-M type DIPTR the options chosen are

- Flow Model: 2D and 3D, Unsteady, turbulent flow
- Solver: Segregated , Double Precision
- Unsteady Formulation: Second order Implicit
- Porous Formulation: Physical velocity

### *(b) Energy*

It enable energy equation in the solver for solving heat transfer problem. Accordingly, energy option is enabled.

### *(vi) Defining the Material Properties*

This section of the input contains the option for the materials chosen as the working fluid. For this case, the working fluid is the helium and the solid is copper and steel. Properties that can be specified in this section are density, specific heat, thermal conductivity, viscosity and diffusivity.

### *(vii) Defining the Operating Conditions*

The operating condition panel includes gravity and pressure. In horizontal axis-symmetric problem, the effect of gravity is not of much importance and hence it is neglected. In 2-D and 3-D models the effect of gravity is considered. Operating pressure is set to its default value of 1atm in this section to get the solution in terms of absolute value.

### *(viii) Defining the boundary conditions*

Proper specification of the boundary condition is an essential step to accurately capture the physics of physical model. In Fluent, boundary conditions must be specified at each surface defined in the mesh generation process as described in earlier section. Specifically, information about the pressure, temperature and density must be specified at each surface. For surfaces that have been defined as "walls", properties can be set to include density along a wall, as well as the thermal conditions by specifying temperature, heat flux, radiation or convection, or a combination. For left wall which is defined as piston input specification include velocity UDF for piston head motion for Stirling type PTR model and for DIPTR model pressure UDF is specified at inlet. For the modeling performed in this study, the boundary conditions are summarized in chapter 5 and chapter 6. Once all the models, operating conditions and boundary conditions are specified, the Fluent code can be executed.

### *(ix) Defining the Porous Zone*

The regenerator, after cooler, cold end heat exchanger and hot end exchanger of a pulse tube refrigerator is to be modeled using porous-media methods. A porous zone is modeled as a special type of fluid zone. To indicate that the fluid zone is a porous region, porous zone option in the fluid panel is enabled. The panel expands to show the porous media inputs. The user inputs for porous media model are:

- Define the porous zone.
- Identify the fluid material flowing through the porous media.
- Select the solid material contained in the porous media.
- Specify the porosity of the porous media.
- Set the viscous resistance coefficients and inertial resistance coefficients, and define the direction vectors for which they apply.

### *(x) Executing the Fluent CFD code*

The conservations equations given by Eqs. (4.38-4.43) and Eqs.(4.48-4.50) assuming two-dimensional axis-symmetric turbulent flow in cylindrical coordinates along with the

boundary conditions represent a set of non-linear , coupled differential equations, which are solved iteratively using the finite volume method. The combined convection diffusion coefficients are evaluated using (Patankar, 1980) upwind scheme. The PRESTO (Pressured Staggering Option) is used for obtaining the pressure values and PISO (Pressure Implicit with Splitting of Operators) is used to couple the interaction between pressure and velocity. A line-by line solver based on the TDMA (Tri-diagonal matrix algorithm) is used to iteratively solve the algebraic equations obtained after discretization. Details of the numerical method and solution procedures may be found in the work of (Versteeg and Malalasekera, 1995) and (Patankar, 1980). Proper under relaxation factors are used for the solution of the pressure correction equation, the two momentum equations and the energy equation respectively.

*(xi)Solution Initialization*

Each case must be initialized before the fluent code begins iterating towards a converged solution. Initializing the case essentially provides an initial guess for the first iteration of the solution. In the initialization process, the user must specify which zone is be provided with initial condition. Different model properties viz. continuity, x-velocity, y-velocity, energy,  $k$  and  $\varepsilon$  were monitored by Fluent’s solver and checked for convergence. This criterion requires that the scaled residuals decrease to  $10^{-3}$  for all equations except the energy equation, where the criterion is  $10^{-6}$ . At the end of each solver iteration, the residual sum for each of the conserved variables is computed and stored. Thus it records the convergence history. Table4.3 shows the list of variables at their respective convergence criteria used in the present model.

Table4.3 Variables and respective convergence Criteria used in the simulation

Variable	Convergence Criterion
Continuity	0.001
X-velocity	0.001
Y-velocity	0.001
Z-velocity	0.001
Energy	1e-06
$k$	0.001
$\varepsilon$	0.001



Once all the above mentioned steps are over, iteration can be initiated with the time step of 0.001 second with total number of iterations equal to 500000 and number of iterations per time step to be 20. The typical CPU time taken for running a model in Pentium 4 processor machine with 1 GB RAMS is nearly two weeks for 2-D simulations and two months for 3-D simulations.

### *(xii) Post- processing*

The results obtained from the above steps are then checked to see if the solution is physically reasonable. Also, information about the parameters is obtained and presented in a visual forms i.e., graph, contours, XY plots etc. This step is also referred to as post – processing stage of the CFD analysis. These are the basic steps to be followed for the simulation of different pulse tube refrigerator such as OPTR, ITPTR and DIPTR which are discussed in chapter -V.

### *(xiii) Simulation in Fluent and Grid Independent Test*

After setting all the required parameters in Stirling type and G-M type DIPTR models such as boundary conditions, material properties, viscous model, convergence tolerance, discretization scheme, under relaxation factors UDFs etc. one writes case and data file by giving suitable file name. This becomes the original file ready for simulation. Now the last step is to start the simulation. For this, one clicks Solve → Iterate...then the iterate panel opens. In this panel one needs to give time step size, number of iterations and maximum iterations per time step then clicking iterate will start the simulation. The simulation will continue till the desired level of convergence is achieved or the number of iterations given is completed, whichever is achieved earlier. This is unsteady state (transient) problem and generally the time step size is in the range of milli second. So to get cyclic steady state solution, it usually takes a week or a month depending on the problem and type of simulation (2 or 3-dimensional). Periodic steady conditions are assumed when all system parameters are repeated from one cycle to the next with an acceptable predefined tolerance. After getting periodic steady conditions the final “case and data” file could be written. This file is used for post processing purpose. The details of post processing results will be presented in the next chapter.

- *Convergence and Grid Independence:*

The periodic nature of the flow and boundary conditions in the aforementioned simulations renders the issue of convergence and the conditions necessary to reach steady-periodic conditions. There are many ways to verify the convergence of the entire system. One way is when the system reaches a cyclic steady state, cycle averaged parameters (such as fluid and solid temperature, pressures, velocities, densities) would not change any more with time. Hence the difference between two consecutive iterations of cyclic averaged quantity is less than pre-specified tolerance value, to reach a cyclic steady state condition. For grid independence solution one should start with coarse grid then refine the grid to get grid independent solution.

## *Chapter V*

# CFD Analysis of Stirling Type Pulse Tube Refrigerators

### *5.1 Introduction*

Computational fluid dynamics or CFD is the analysis of systems involving fluid flow, heat transfer and associated phenomenon such as chemical reactions by means of numerical simulations. The technique is very powerful and spans a wide range of industrial and non industrial application areas. The availability of fast computers equipped with very large memories allow for remarkably precise numerical simulations. The main CFD tools are PHONICS, FLUENT, FLOW3D and STAR-CD etc. The fluent is one of the most highly respected CFD codes [175]. Fluent is a state-of-the-art computer program for modeling fluid flow and heat transfer process in complex engineering problems. With the help of this one can generate code and set boundary condition by User Defined Functions (UDF). Fluent has also a dynamic meshing function. This function allows the user to create deforming mesh volumes such that applications involving volume compression and expansion can be modeled. Thus in view of Fluent's versatility, its capability for solving the compression and expansion volume, allowing UDF boundary conditions and modeling capability for porous media, it is selected for the simulation of the Stirling type OPTR and ITPTR.

This chapter presents the details of geometry and boundary conditions for CFD simulations of Stirling type OPTR and ITPTR by using commercial software, Fluent6.1. For CFD simulation of any model the basic required parameters are their dimensions and boundary conditions. Therefore the geometrical dimensions of each component of pulse tube refrigerator model is created in gambit software and complete meshing of the geometry and also the boundary conditions for each model are presented in this chapter. As first part of the

investigation Stirling type ITPTR simulation is performed then the same process of simulation is extended for OPTR and performance comparisons is done for both models.

## 5.2 Inertance Tube Pulse Tube Refrigerator

The pressure waves in a Stirling-type pulse tube refrigerator are generated directly by a valve less compressor. Thus, a Stirling-type pulse tube refrigerator usually works at high frequencies (10Hz-50Hz). The dimensions of the Stirling type inertance tube pulse tube refrigerator (ITPTR) are taken from literature [137], except the compressor is replaced by a dual opposed piston model in the present simulation. Figure 5.1 shows the three-dimensional view of the inertance tube pulse tube refrigerator systems of interest in the present simulations. Similarly Fig. 5.2 illustrates the 2-dimensional physical geometry of the ITPTR. Figure 5.1 shows that every component of the ITPTR system is in fact cylindrical in shape and all the components are aligned in series to form an axis-symmetric system. The ITPTR is therefore modeled in a 2-dimensional axis-symmetric co-ordinate system. Figure 5.3 shows the geometry of ITPTR created in gambit software. First, an actual physical drawing of the system is created in the 2-dimensional axis-symmetric co-ordinate system using gambit software. Initially the whole geometry is created as single components then it is split in different zones. The function of splitting is to divide the geometry as different components so as to enable to set different boundary conditions at different zones as needed. The figure 5.4 shows the enlarged view of the axis-symmetric geometry of the different components of the ITPTR with complete meshing. It can be seen from above figures that the regions deemed more sensitive, such as the vicinity of component to component junctions are presented by finer mesh than others. Once the model are created and exported to fluent, the model boundaries have to be defined.

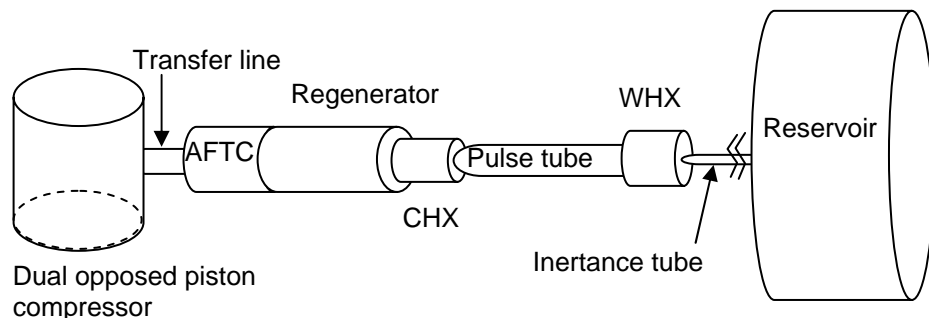


Fig.5.1 Three-dimensional view of the inertance pulse tube refrigerator.

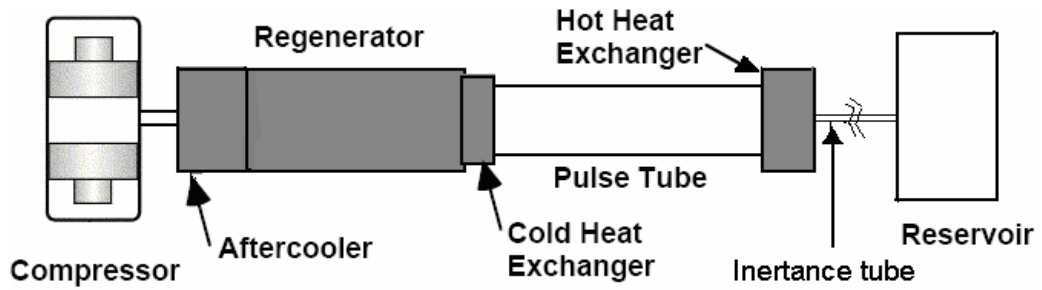


Fig.5.2 Two-dimensional view of inertia tube pulse tube refrigerator.

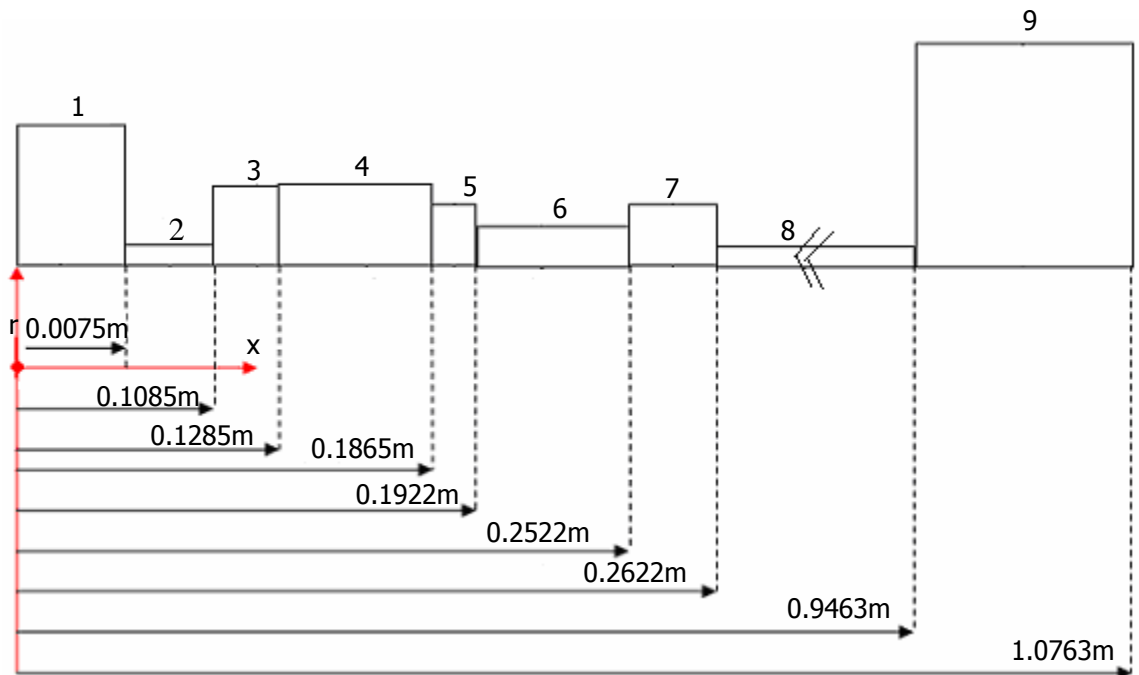


Fig.5.3 Two-dimensional axis-symmetric geometry of ITPTR

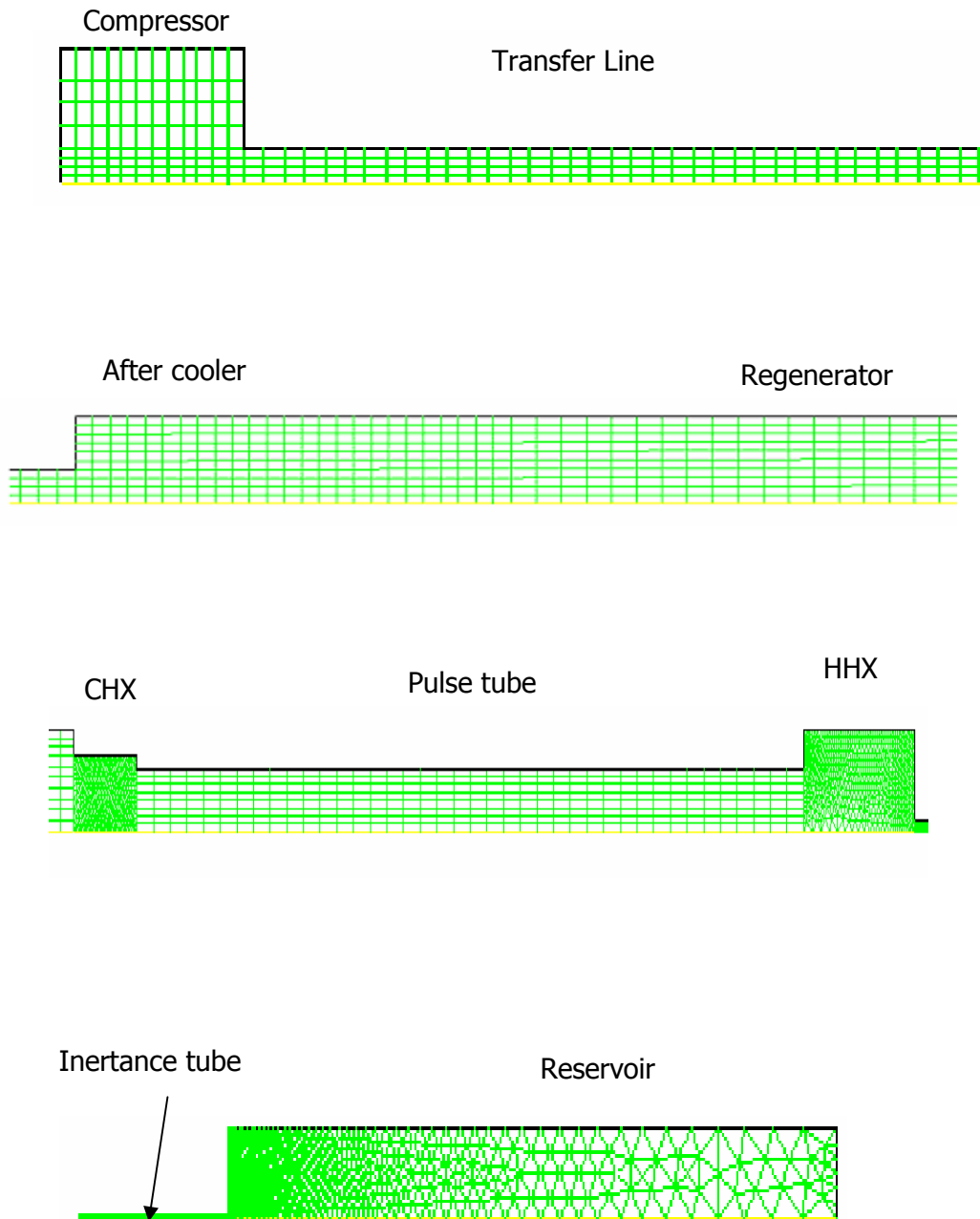


Fig. 5.4 Two-dimensional axis-symmetric mesh of ITPTR.

Table 5.1 Component dimensions of ITPTR

SNo.	Components	Radius (m)	Length (m)
1	Compressor	9.54E-03	7.50E-03
2	Transfer line	1.55E-03	1.01E-01
3	After cooler	4.00E-03	2.00E-02
4	Regenerator	4.00E-03	5.8E-02
5	Cold heat exchanger	3.00E-03	5.7E-03
6	Pulse tube	2.5E-03	6.0E-02
7	Hot heat exchanger	4.00E-03	1.0E-02
8	Inertance tube	4.25E-04	6.84E-01
9	Surge volume	1.30E-02	1.3E-01

Table 5.2 Boundary and initial conditions for ITPTR

Study Case	Case 1	Case 2	Case 3
Compressor wall	Adiabatic	Adiabatic	Adiabatic
Transfer line wall	Adiabatic	Adiabatic	Adiabatic
After cooler wall	293K	293K	293K
Regenerator wall	Adiabatic	Adiabatic	Adiabatic
Cold end wall	Adiabatic	Heat flux 5W	150K
Pulse tube wall	Adiabatic	Adiabatic	Adiabatic
Hot end wall	293K	293K	293K
Inertance tube wall	Adiabatic	Adiabatic	Adiabatic
Surge volume wall	Adiabatic	Adiabatic	Adiabatic
Viscous-resistance ( $m^{-2}$ )	9.44e+9	9.44e+9	9.44e+9
Inertial-resistance( $m^{-1}$ )	76090	76090	76090
Initial conditions	300K	300K	300K
Cold end load	0	5W	5.23W*
Cold end temp	87.4K*	147.5K*	150

\*Output result obtained from Fluent Analysis

### 5.3 Orifice Pulse Tube Refrigerator

The geometry of orifice pulse tube refrigerator (OPTR) is same as ITPTR except the long narrow tube of ITPTR is replaced by a short tube with orifice valve. The three-dimensional view of the OPTR system is shown in Fig.5.5. The system consists of a compressor (dual opposed piston model), a transfer line, an after cooler, a regenerator, cold end heat exchanger, pulse tube, hot end heat exchanger, connecting tube, a needle valve and a reservoir. Figure5.6 illustrates the two-dimensional physical geometry of the OPTR. Figure 5.5 shows that every component of the OPTR system is in fact cylindrical in shape and all the components are aligned in series and form an axis-symmetric system. The OPTR is therefore modeled in a 2-dimensional axis-symmetric co-ordinate system similar to ITPTR. The potential asymmetry caused by gravity is thus neglected. This gravity term however will be important if the order of magnitude of the acceleration become comparable with the other terms (such as temporal acceleration, convective acceleration etc.) in the momentum equation. Figure5.7 shows the two-dimensional geometry of the OPTR which is created in Gambit software. The face mode option of gambit is used to create the geometry.

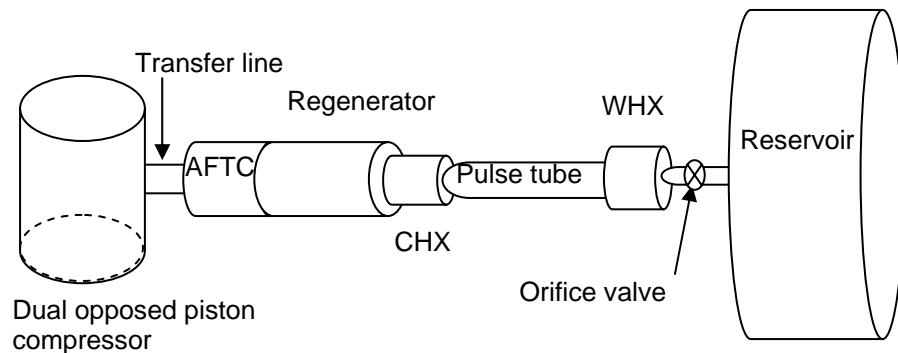


Fig.5.5 Three-dimensional view of the Stirling type OPTR.



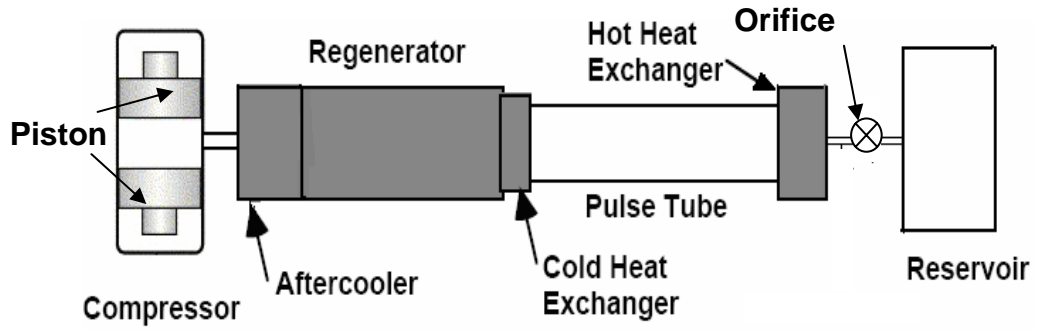


Fig.5.6 Two-Dimensional view of orifice pulse tube refrigerator.

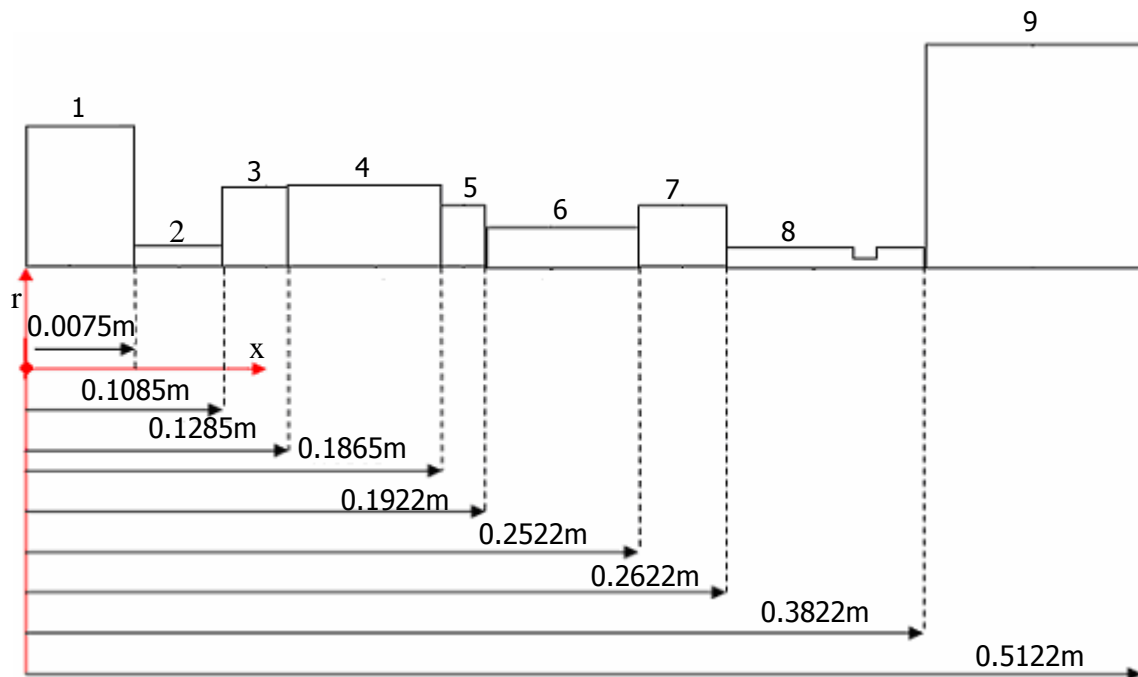


Fig.5.7 Two-dimensional axis-symmetric geometry of OPTR.

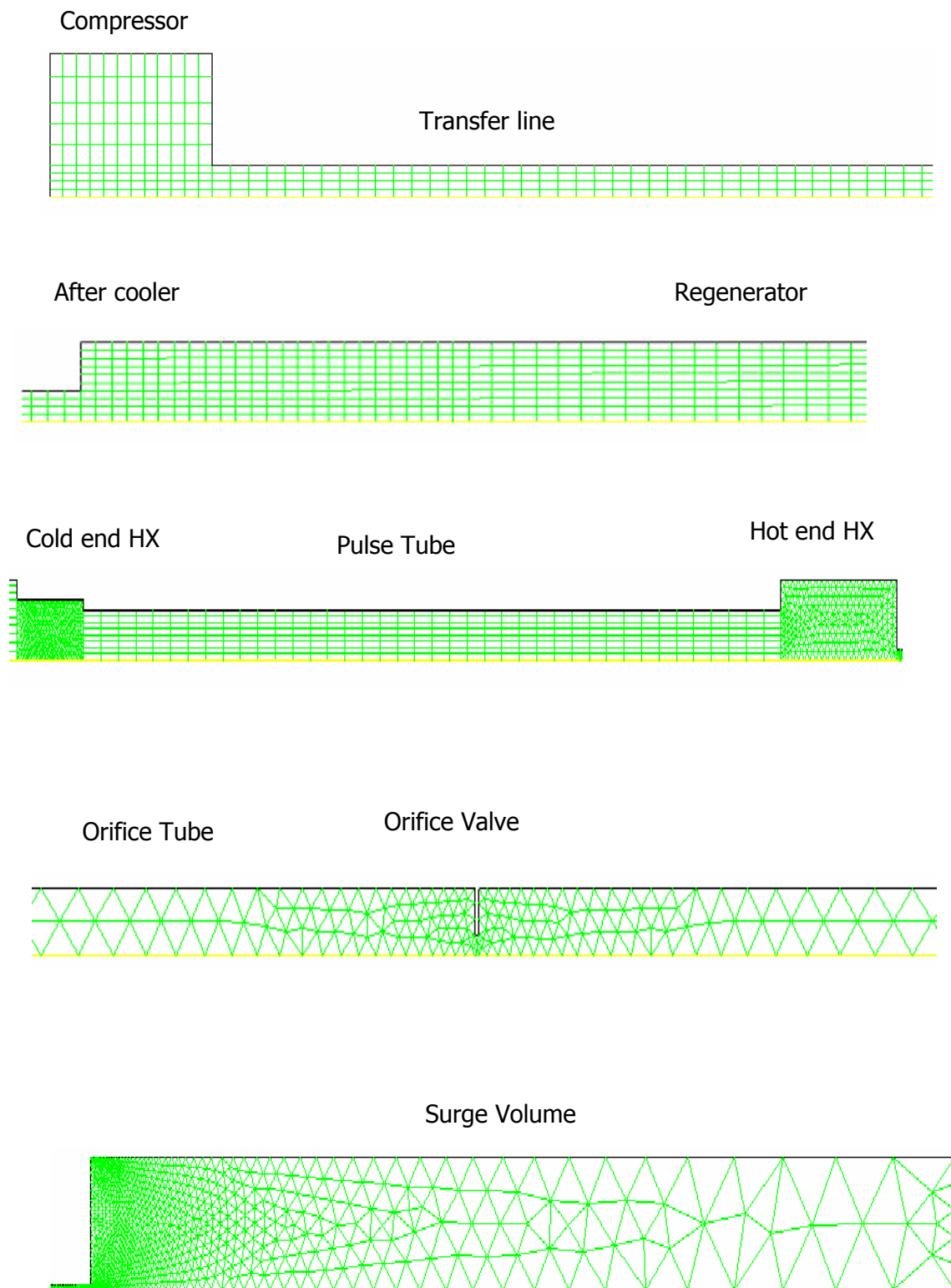


Fig.5.8 Two-dimensional axis-symmetric mesh of OPTR.

Table 5.3 Component dimensions of OPTR

SNo.	Components	Radius (m)	Length (m)
1	Compressor	9.54E-03	7.50E-03
2	Transfer line	1.55E-03	1.01E-01
3	After cooler	4.00E-03	2.00E-02
4	Regenerator	4.00E-03	5.8E-02
5	Cold end heat exchanger	3.00E-03	5.7E-03
6	Pulse tube	2.5E-03	6.0E-02
7	Hot end heat exchanger	4.00E-03	1.0E-02
8	Orifice tube	1.00E-03	1.2E-01
9	Surge volume	1.30E-02	1.3E-01

Table 5.4 Boundary and initial conditions for OPTR

Study Case	Case 1	Case 2	Case 3
Compressor wall	Adiabatic	Adiabatic	Adiabatic
Transfer line wall	Adiabatic	Adiabatic	Adiabatic
Aftercooler wall	293K	293K	293K
Regenerator wall	Adiabatic	Adiabatic	Adiabatic
Cold end wall	Adiabatic	Heat flux 5W	150K
Pulse tube wall	Adiabatic	Adiabatic	Adiabatic
Hot end wall	293K	293K	293K
Surge volume wall	Adiabatic	Adiabatic	Adiabatic
Viscous-resistance(m <sup>-2</sup> )	9.44e+9	9.44e+9	9.44e+9
Inertial-resistance(m <sup>-1</sup> )	76090	76090	76090
Initial conditions	300K	300K	300K
Cold end load	0	5W	3.72*
Cold end temp	109.7K*	181*	150

\*Output result obtained from Fluent analysis

## 5.4 Dynamic Meshing Function

Fluent 6.1 has a dynamic meshing function. The dynamic mesh model in Fluent can be used to model flows where the shape of the domain is changing with time due to motion on the domain boundaries like in reciprocating compressor when piston moves the domain of fluid will change with time in case of compression and expansion of fluid. This type of model could be handled in fluent by using dynamic meshing function. The motion can be a prescribed motion or an un prescribed motion where the subsequent motion is determined based on the solution at the current time. The update of the volume mesh is handled automatically by fluent at each time step based on the new positions of the boundaries. To use the dynamic mesh model, it is needed to provide a starting volume mesh and the description of the motion of any moving zones in the model. Fluent allows describing the motion using either boundary profiles or user-defined functions (UDFs) [177]. Thus in view of Fluent's versatility, its capability for solving the compression and expansion of volumes, compressor has been modeled using dynamic meshing in Stirling type pulse tube refrigerators. In Fluent different methods are available for mesh update like smoothing, layering and remeshing for dynamic meshing. The compressor is modeled as a solid wall (piston) that sinusoidally oscillates in and out along a fixed stroke length. The piston and cylinder walls are nominally specified as adiabatic boundaries. Work input at the piston in cylinder of a compressor provides the oscillating pressure that drives the cycle.

In order to model the piston and cylinder, Fluent dynamic meshing function must be used. A user defined function (UDF) is developed in C programming language to simulate the piston cylinder effect [177]. The compressor used in this simulation is a reciprocating dual opposed-piston design. The piston head motion is accordingly found from the following equations

Piston displacement is expressed as

$$X = X_{amp} \times \sin(\omega t) \quad (5.1)$$

Differentiating equation (5.1) with respect to time gives the piston head velocity as

$$V = \frac{dX}{dt} = \omega \times X_{amp} \times \cos(\omega t) \quad (5.2)$$

Where  $\omega = 2\pi f$  [rad/s],  $X_{amp}$  is amplitude of piston[m] and t is time. The value of t varies from zero to time period of the cycle. The time increment of 0.7milli second is assumed for the piston movement. For all the case the operating pressure is 35bar and frequency is 20Hz.

The working fluid is research grade helium, modeled as an ideal gas and having constant viscosity, heat capacitance and thermal conductivity. Nodalization of pulse tube refrigerator is done by the Gambit software. First, an actual physical drawing of the problem is created in the 2-dimensional axis-symmetric co-ordinate system using gambit software. Table 5.3 shows the model boundary conditions. In porous regions the momentum transport equations include a source term with inertial and viscous resistance coefficient which has been specified. After the boundaries are defined, the solver and flow characteristics are detailed in Fluent. A segregated solver is used for all models. This solver solves the flow and energy equation separately and implicitly.

### *5.5 User Defined Function (UDF)*

The dynamic mesh options of the fluent are used to model the compressor of Stirling type ITPTR and OPTR. For this the velocity user defined function (UDF) could be written in C programming language with the help of Fluent UDF manual [177]. This UDF is saved by giving suitable name like “**velocity.c**”. This is stored in the same folder where mesh files are saved. In Fluent this UDF needs to be compiled and then linked with piston which makes the reciprocating motion possible on the piston. Using Fluents user defined function manual [177] the velocity UDF for piston head motion is as follows

```
#include "udf.h"
DEFINE_CG_MOTION (vel_comp, dt, vel, omega, time, dtime)
{
real freq = 20.0;
real w = 2.0 * M_PI * freq;
real Xcomp = 0.004511;
NV_S(vel, = ,0.0);
NV_S(omega, = ,0.0);
vel[1] = w * Xcomp * cos (w * time);
}
```

### *5.5.1 Compiling User Defined Function (UDF)*

For compiling UDF in fluent the first step is to click Define → User-Defined → Functions → Compile..... By this command the compiled UDFs panel will open. In this window one select proper path and select the source code "**velocity.c**", and click 'ok'. By clicking load will load the UDF library just compiled. The second step is to activate dynamic mesh motion by clicking the option Define → Dynamic Mesh → Parameters...Under this smoothing and layering option is chosen. The third step is Define → Dynamic mesh → Zones. In this option one specifies the piston as rigid body and side walls as deforming body. Then clicking create will link the UDF with piston. One can see the piston head motion by mesh motion preview option as discussed below before starting the simulation.

### *5.5.2 Mesh Motion Preview*

After compiling UDF and defining dynamic mesh zones it is necessary to check the motion of mesh whether it is moving properly or not. For mesh motion preview one select only the compressor portion of the geometry. Mesh motion preview of Stirling type pulse tube refrigerator after compiling user defined function (UDF) is shown in figure 5.9(a) and (b). At initial condition, piston is at rest. When the piston moves, the compression and expansion of the gas system inside the cylinder takes place.

The mesh motion preview gives an information regarding motion of the mesh in either direction from its initial position with respect to time. This shows the compression and expansion process of compressor. From initial condition mesh moves in upward direction reaches TDC and then returns down till BDC. First set of Figure5.9 (a) shows the axis-symmetric geometry and the second set (b) shows the mirror view of the axis-symmetry geometry. If there is not proper matching between grid size spacing and time increment the mesh won't move. In this case fluent will show an error message for negative volume. So before starting the simulation it is necessary to check the motion of the mesh for the selected grid size. If it shows error then the grid size for compressor or time step size is changed and the process is repeated.

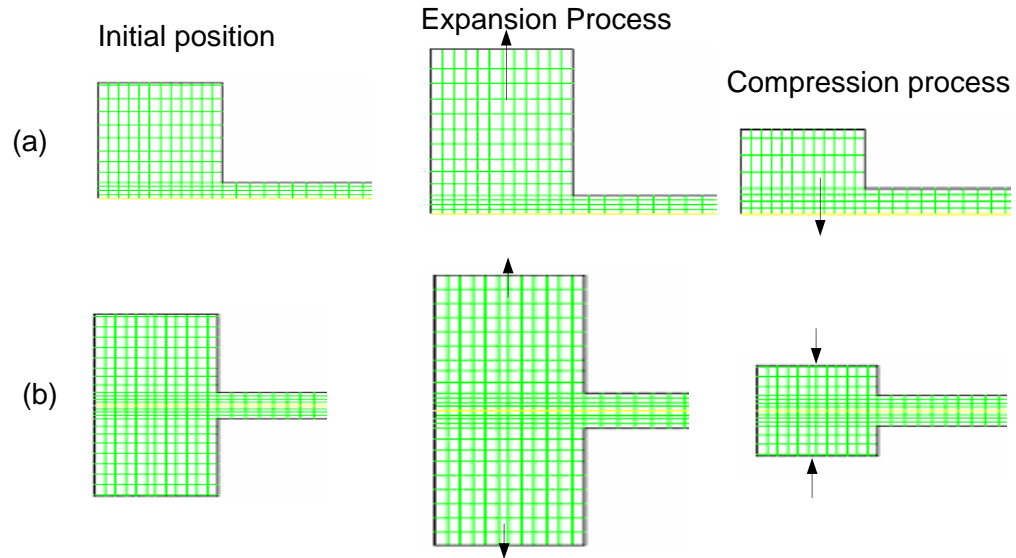


Fig. 5.9 Mesh motion preview of dynamic meshing model (ITPTR/OPTR).

## 5.6 Results of CFD Simulations of ITPTR

Computational fluid dynamic simulations are performed for single stage Stirling type inertance tube pulse tube refrigerator (ITPTR) and orifice pulse tube refrigerator (OPTR) by using a commercial CFD software Fluent6.1 as first part of the investigation. On the basis of CFD simulations the performance of these two models are compared. Mainly in each model three different boundary conditions at cold end heat exchanger are used: adiabatic, known heat load and isothermal. The other boundary conditions for different components do not change for different pulse tube. For ITPTR the dimension of component and its different boundary conditions are given in Table 5.1 and 5.2 respectively. For inertance tube pulse tube refrigerator steady periodic CFD simulation results will be discussed in this section for different boundary conditions at cold end heat exchanger.

### 5.6.1 Case 1: Adiabatic Boundary Condition

This corresponds to an adiabatic wall boundary condition at the cold end which is equivalent to no refrigeration load applied to the overall system. This analysis leads to the minimum temperature achievable in pulse tube refrigeration. The simulation is started from an assumed initial temperature of 300K and continued until steady periodic conditions are reached.

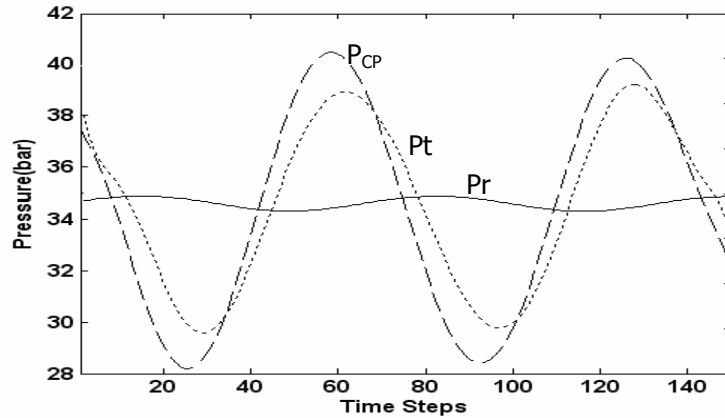


Fig.5.10 Pressure variations in compressor, pulse tube and reservoir for ITPTR.

Pressure variation in compressor, pulse tube as well as reservoir has been depicted in Fig. 5.10. From the above figure it is obvious that the reservoir pressure is almost constant. This is required for the best performance of the system. Fig.5.11 shows the variation of the cold tip temperature as a function of time at the beginning of simulation. It shows that the cold end heat exchanger wall temperature gradually decreases with time till cyclic steady state condition is reached. The Fig.5.12 shows the gradual decrease of the cyclic steady state cool down behaviour for case1 and case2. The ultimate cold end temperature of 87.4 K is obtained after a simulation of 150 seconds for case1. In the depicted simulation, to verify that the system has reached steady periodic simulation, Fluent examines the cold end to see if the temperature of the cold end is identically repeated from one cycle to the next cycle which is shown in Fig.5.13 and confirms the cyclic steady state condition. However, it should be emphasized that in the actual systems the cooling time will be higher than what is predicted in the result since the thermal mass has not been implemented in the system.

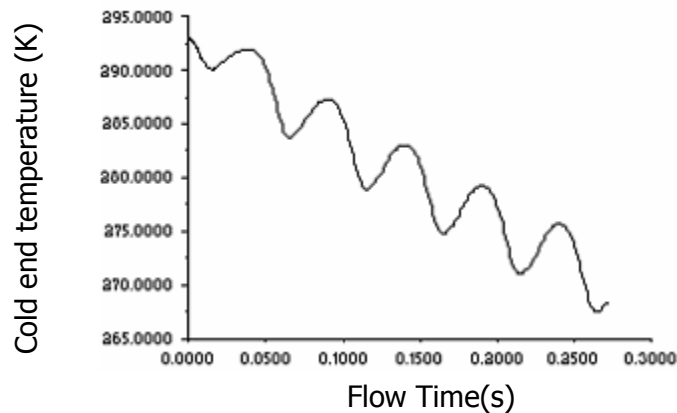


Fig.5.11 Cooling behaviour at the beginning of simulation.



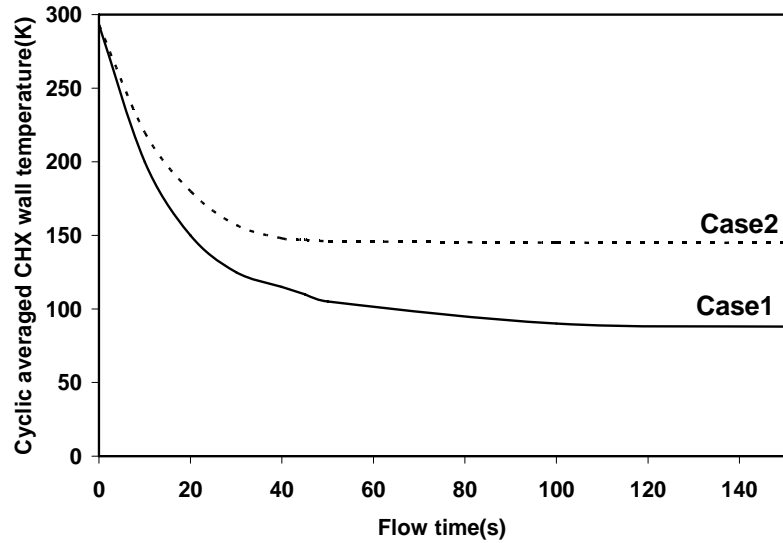


Fig.5.12 Cooling behaviour till cyclic steady state condition.

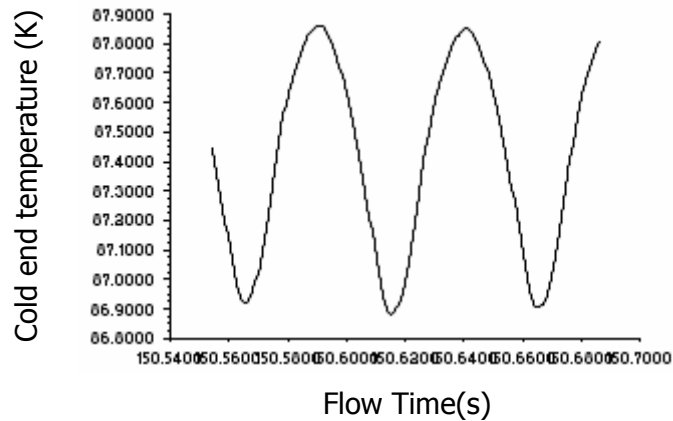


Fig.5.13 CHX wall temperature variation after cyclic steady state condition (case1)

Figures 5.14 and 5.15 display the temperature and density distributions respectively, along the length of entire simulated system. The cyclic average temperature and density profiles depict a local instantaneous snapshot of the system. The density distribution trends are consistent with the ideal gas equation of state. Figures 5.16 and 5.17 depicts the temperature and density contours respectively under steady periodic conditions. The contours are of course consistent with Figures 5.14 and 5.15. The Fig. 5.18 shows the velocity vector in the pulse tube, which depicts the smooth flow without swirl in the pulse tube section.

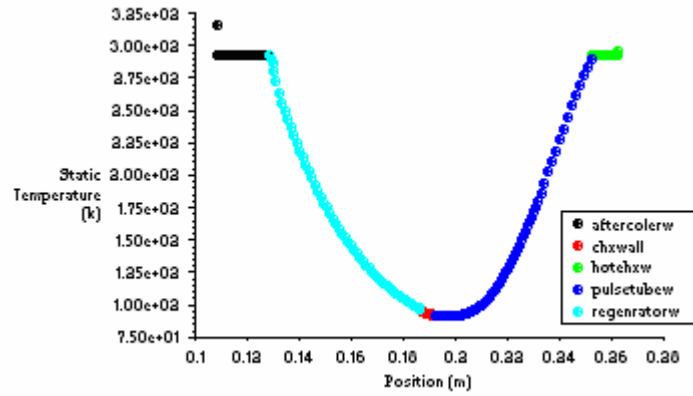


Fig.5.14 Temperature distributions along axial direction for case1.

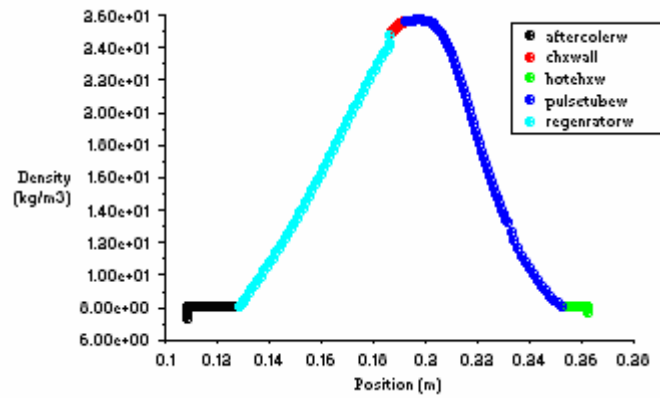


Fig.5.15 Density distributions along axial direction for case1.

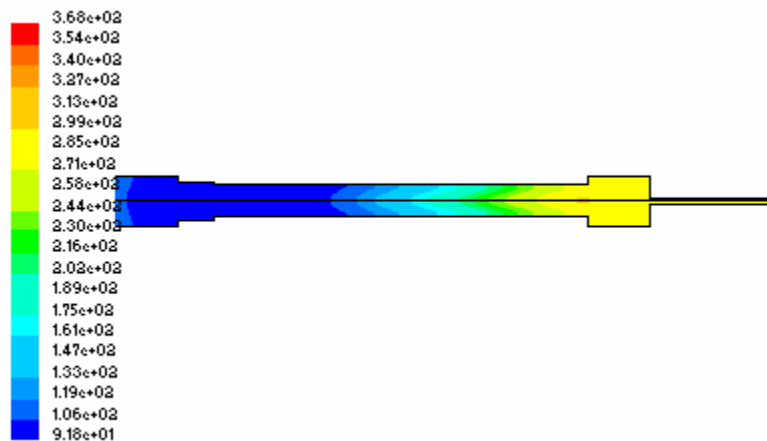


Fig.5.16 Temperature contours for case1.

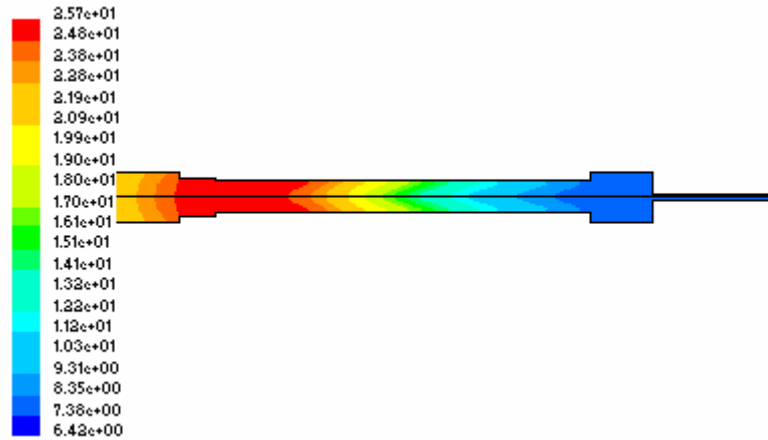


Fig. 5.17 Density contours for case1.

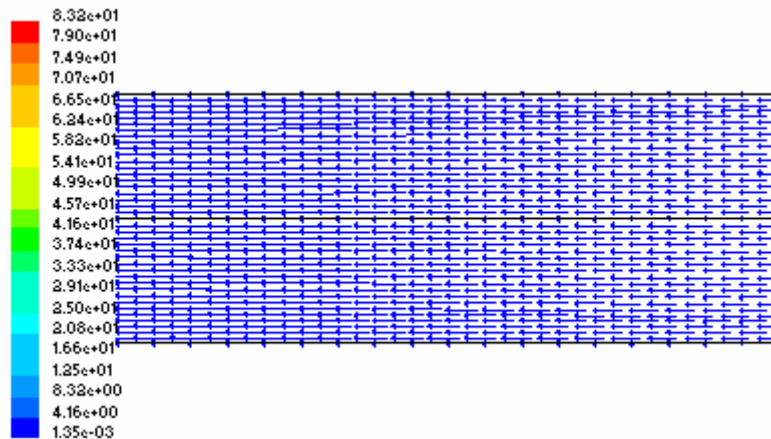


Fig.5.18 Velocity vector in the pulse tube for case1.

### 5.6.2 Case 2: Known Heat Load Boundary Condition

This case represents the simulation of inertance type pulse tube with constant heat load of 5W at cold end heat exchanger. This is equivalent to the system undergoing a refrigeration load of 5W. The simulation is started from an assumed initial temperature of 300K and continued until steady periodic conditions are reached. Figure 5.12 displays the variation of temperature of the cold end surface with respect to time. As noted from the graph, the simulation predicts a cold end temperature of 147.5K which is also shown in Fig.5.19 and confirms the cyclic steady state condition.

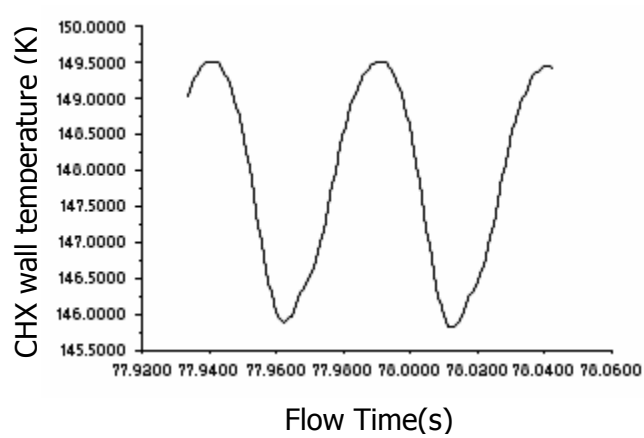


Fig.5.19 CHX wall temperature variation at cyclic steady state condition (case2).

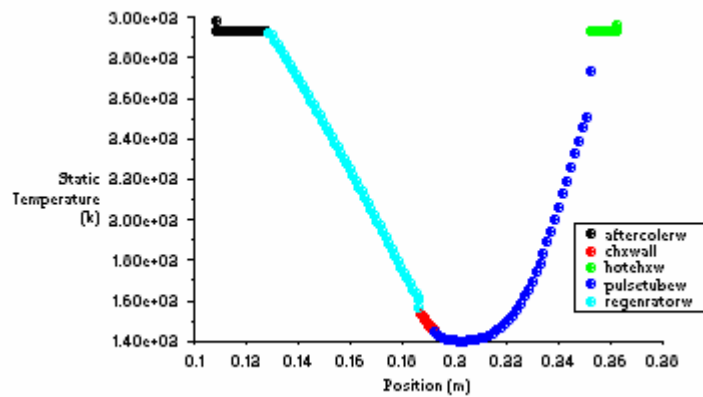


Fig.5.20 Temperature distribution along axial direction for case2

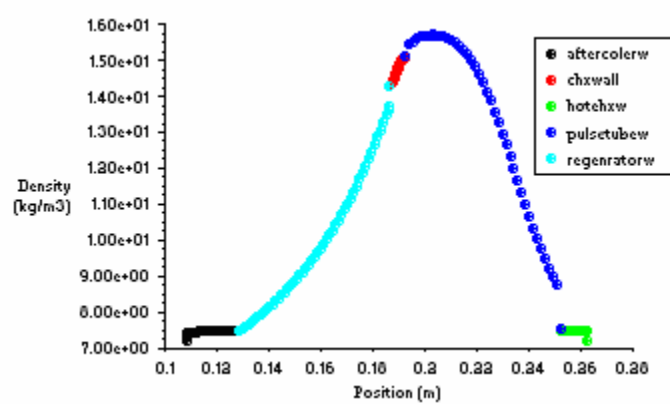


Fig.5.21 Density distributions along axial direction for case2

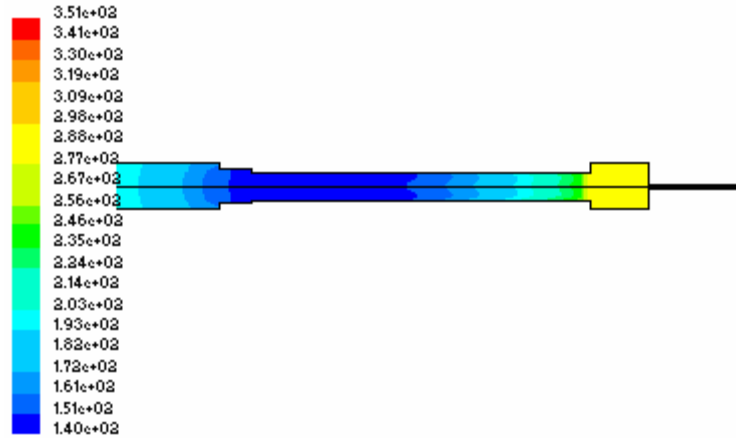


Fig.5.22 Temperature contour along axial direction for case2

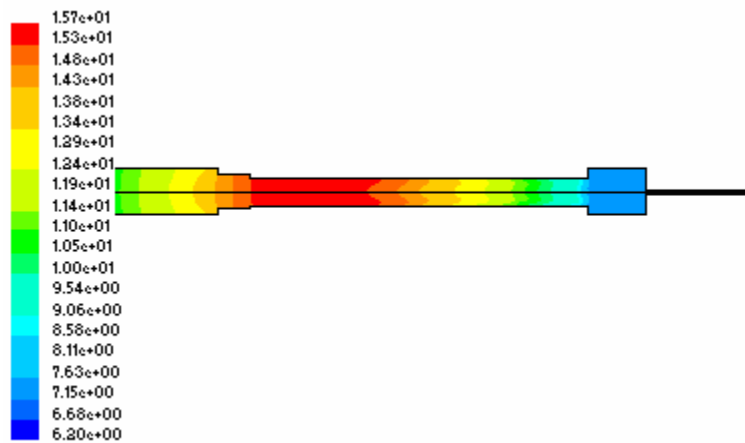


Fig.5.23 Density contour along axial direction for case2

In comparison with case1, which represents the same physical system and boundary conditions but with zero cooling load, the cold end stabilizes at a significantly higher temperature. This is of course expected because when a heat load is applied to the system, the operating cold tip temperature should increase. Figure5.20 and 5.21 display the temperature and density distributions along the entire simulated system, respectively. The contours of temperature and density are shown in Fig.5.22 and Fig.5.23 respectively. These contours are qualitatively similar to the contours depicted in Figures 5.16 and 5.17.

### 5.6.3 Case 3: Isothermal Boundary Condition

In this case also the physical system and boundary conditions are same as case1 and case2, with exception of the boundary condition at cold end heat exchanger. For the isothermal boundary condition, a constant surface temperature of 150K has been imposed at the cold end heat exchanger. At this imposed cold end isothermal wall boundary condition, the heat load rate coming into the cold end is calculated. Accordingly steady- periodic condition should in principle be assumed when the cold end wall heat flux is identically repeated from one cycle to the next. For this simulation quasi steady periodic condition implies time-invariant properties when these properties are averaged over several cycles. According to the simulation results, steady periodic state has reached with a cooling load of 5.35W. This heat load over a period is calculated from the summation of heat fluxes over a small time interval from the Fluent Software under the name wall heat flux. That means the system is disposing 5.35W of refrigeration load at an operating cold end temperature of 150K. Figures 5.24 and 5.25 show the temperature and density distribution along axial direction. Similarly Figures 5.26 and 5.27 show the contour of temperature and density respectively. These contours are qualitatively similar to the contours depicted in Figures 5.16 and 5.17.

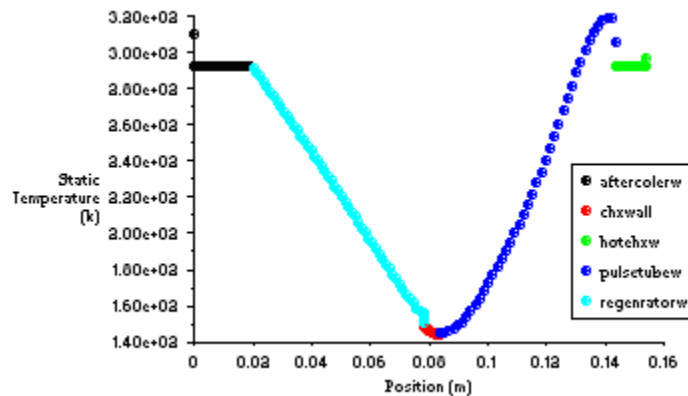


Fig.5.24 Temperature distribution along axial direction for case 3

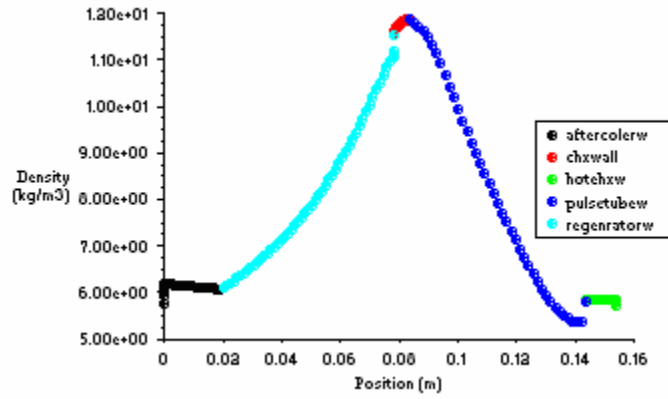


Fig.5.25 Density distribution along axial direction for case3

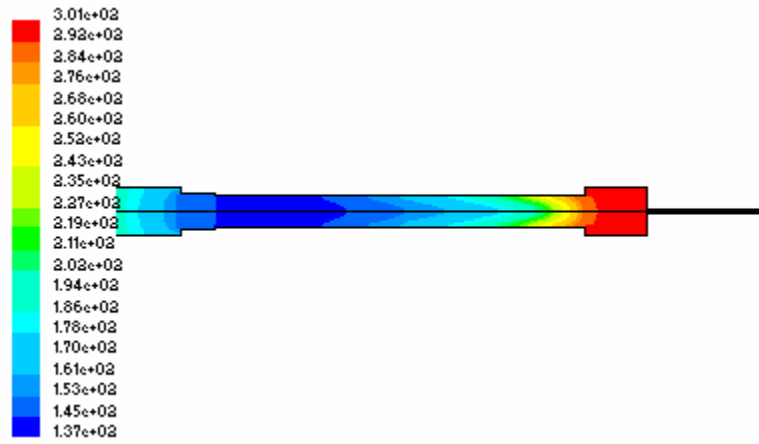


Fig. 5.26 Temperature contour for case3.

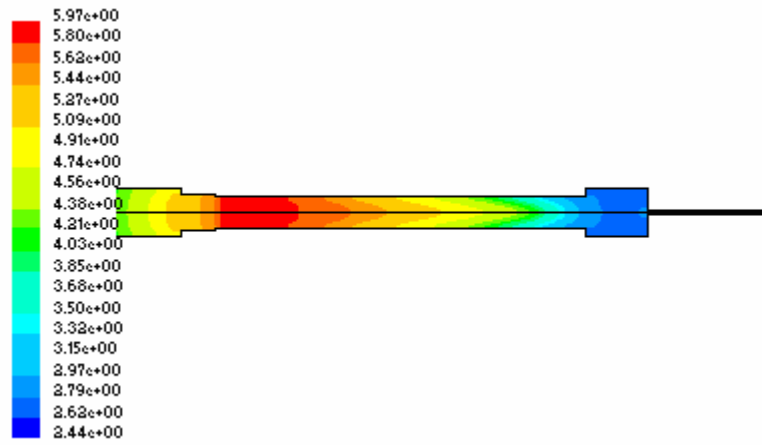


Fig. 5.27 Density contour for case3

## 5.7 Results of CFD Simulations of OPTR

The OPTR is simulated with the same boundary condition as the ITPTR. For OPTR the dimension of component and its different boundary conditions are given in Table 5.3 and 5.4 respectively. For orifice pulse tube refrigerator steady periodic CFD simulation results will be discussed in this section for different boundary conditions at cold end heat exchanger.

### 5.7.1 Case 1: Adiabatic Boundary Condition

This case corresponds to adiabatic boundary condition at cold end heat exchanger. The cooling behavior of the cold end exchanger for case1 and case2 are shown in the Fig.5.28. The figure shows that the cold end temperature decreases with simulation time till cyclic steady state condition is reached.

The system reaches a steady periodic condition and the cold end heat exchanger reaches a minimum temperature of 109.6K for case1 as shown in Fig. 5.29. Figures 5.30 and 5.31 shows the temperature and density distribution respectively along the axial position after the system reaches a steady periodic condition. Fig.5.32 and Fig.5.33 show the snapshot of temperature and density contours respectively. Fig.5.34 shows the velocity vector in the pulse tube. These graphs are having similar trends as discussed earlier for ITPTR.

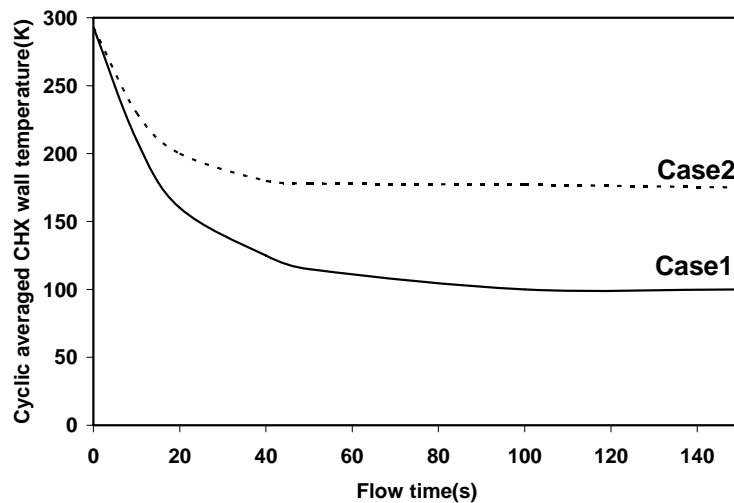


Fig.5.28 Cooling behavior for orifice pulse tube refrigerator (Case1 and 2)



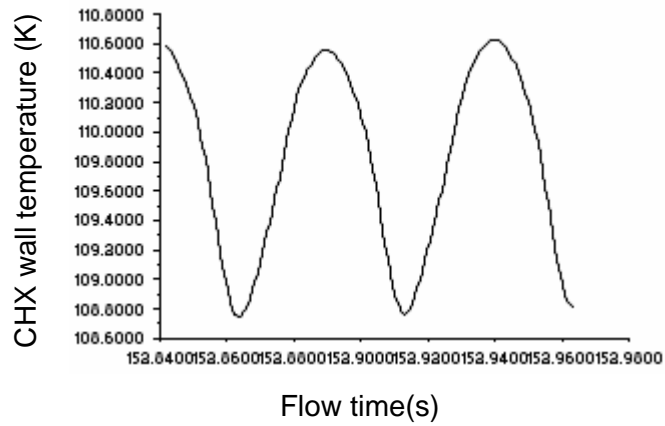


Fig.5.29 CHX wall temperature variation at cyclic steady state condition (case1).

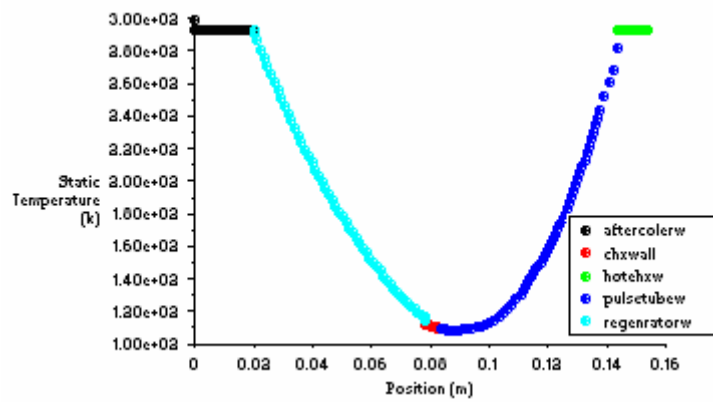


Fig.5.30 Temperature distributions along axial direction (case1).

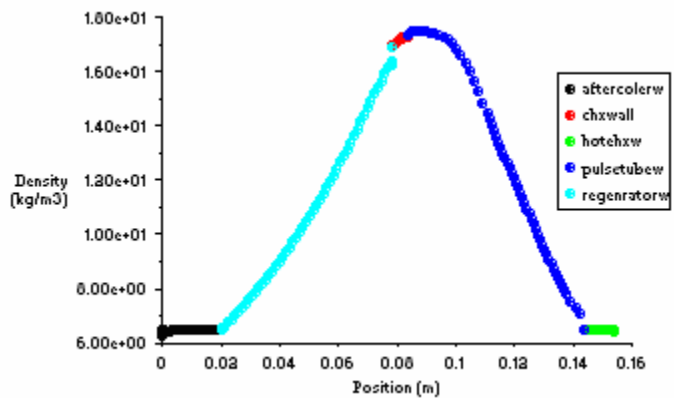


Fig.5.31 Density distributions along axial direction (case1).

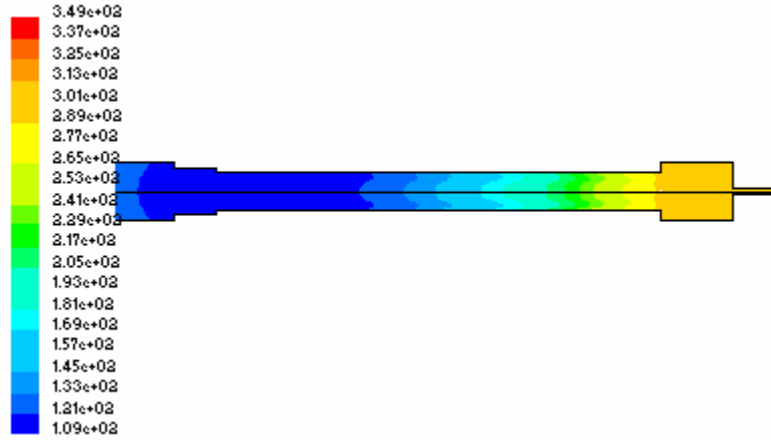


Fig.5.32 Temperature contour along axial direction (case1).

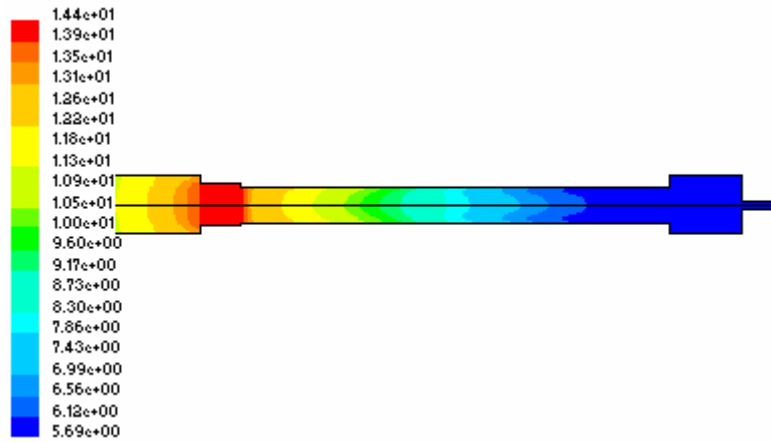


Fig.5.33 Density contour along axial direction (case1).

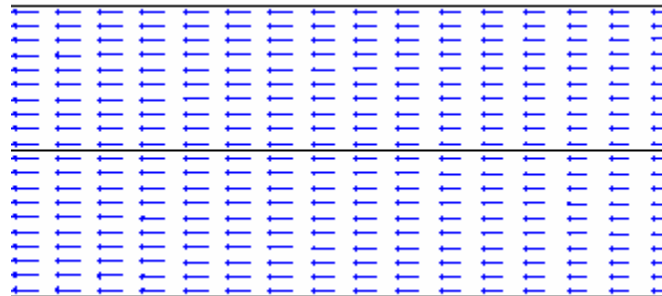


Fig. 5.34 Velocity vector in the pulse tube for OPTR.

### 5.7.2 Case 2: Known Heat Load Boundary Condition

In this case a 5W constant heat load is applied at the cold heat exchanger side wall and the hot end heat exchanger side wall is held isothermal at 293K. A quasi-steady state has been reached with the cold end heat exchanger approaching a cycle average temperature of 181K as shown in Fig.5.35. Fig. 5.36 and Fig.5.37 show the variation of temperature and density respectively along the length of entire simulated system. Fig.5.38 and 5.39 depict the contour of temperature and density respectively. These graphs are having similar trends as discussed earlier for ITPTR.

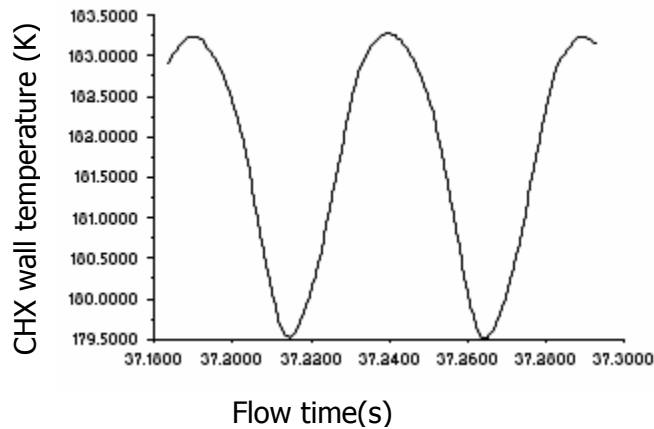


Fig.5.35 CHX wall temperature variation at cyclic steady state condition (case2).

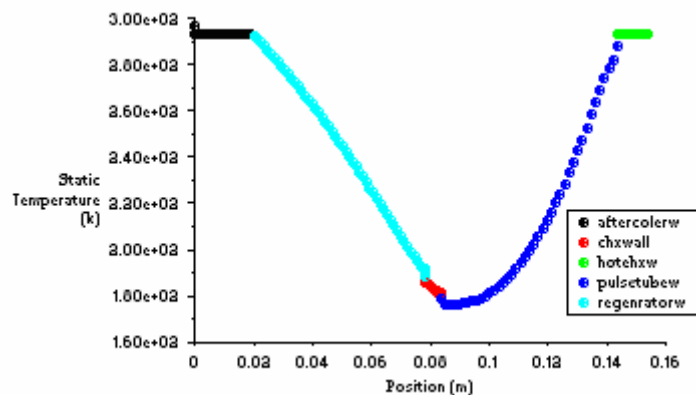


Fig. 5.36 Temperature distribution along axial direction for case2.

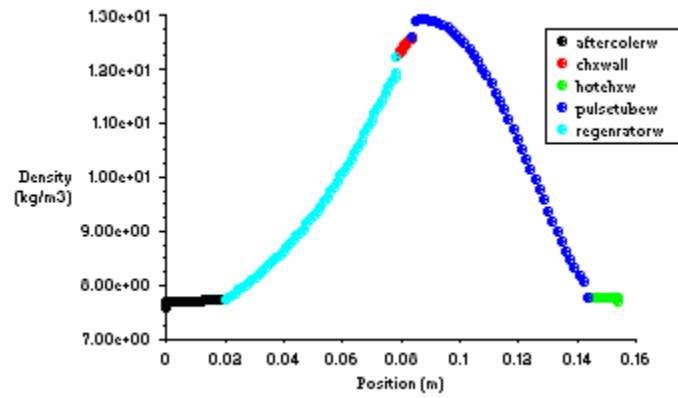


Fig. 5.37 Density distribution along axial direction (case2).

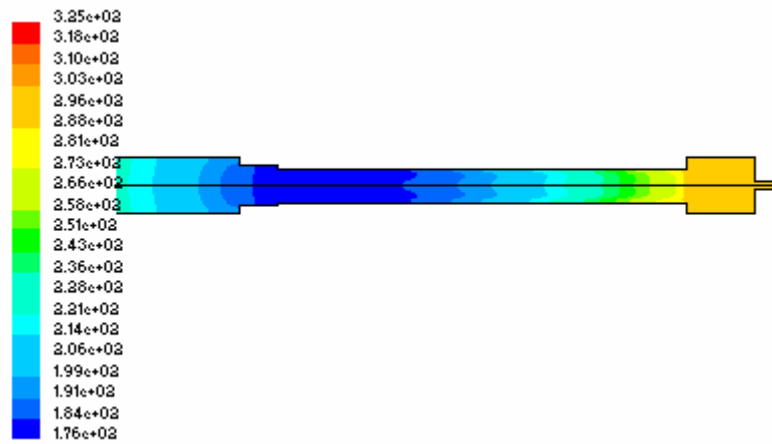


Fig. 5.38 Temperature contour along axial direction (case2).

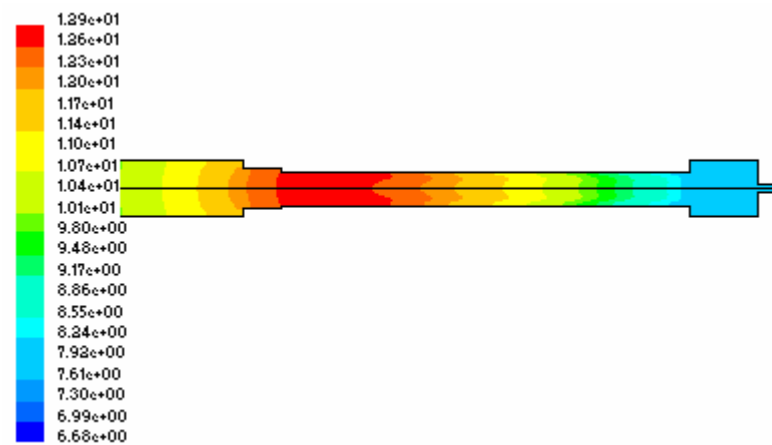


Fig.5.39 Density contour along axial direction (case2)

### 5.7.3 Case 3: Isothermal Boundary Condition

In this case, a constant surface temperature of 150K is imposed and the heat rate coming into the cold end is calculated. The steady- periodic condition should in principle be assumed when the cold end wall heat flux is identically repeated from one cycle to the next. According to the simulation results, steady periodic state has been reached with a cooling load of 3.72W. This means that the system is disposing 3.72W of refrigeration load at an operating cold temperature of 150K. Figures 5.40 and 5.41 depict the temperature and density distributions respectively along the length of the tube. Figures 5.42 and 5.43 depict the temperature and density contours for the system respectively.

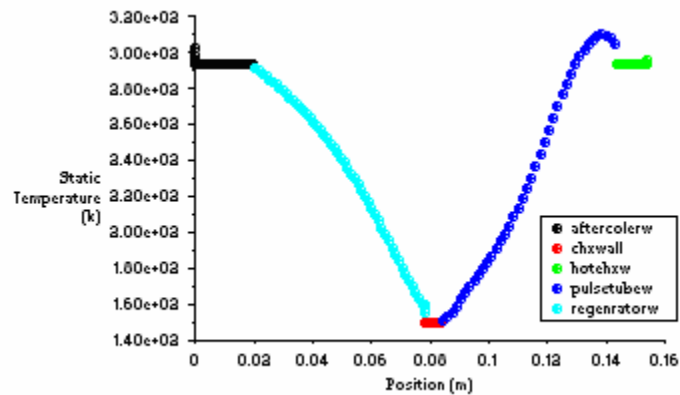


Fig.5.40 Temperature distribution along axial direction (case3).

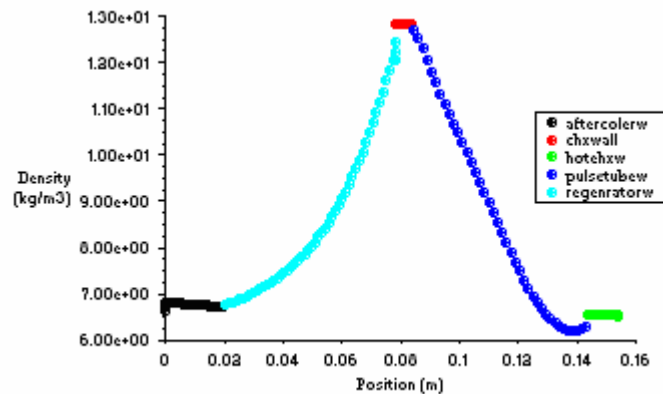


Fig.5.41 Density distribution along axial direction

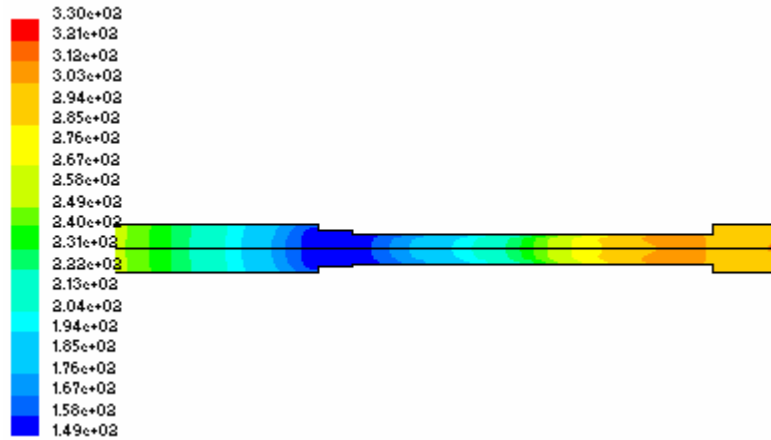


Fig.5.42 Temperature contour along axial direction (case3).

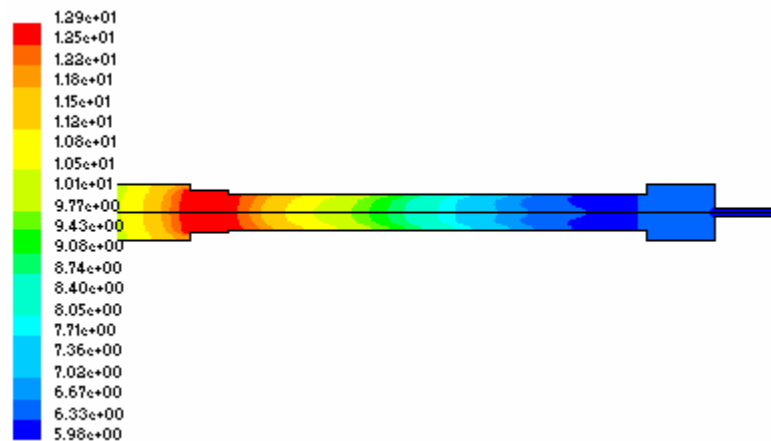


Fig. 5.43 Density contour along axial direction (case3).

### 5.8 Performance Comparisons between ITPTR and OPTR

In order to study the refrigeration performance, some of the important results of steady periodic CFD simulation with adiabatic boundary condition are presented for ITPTR and OPTR. The Table5.5 gives the results obtained for different boundary conditions. First of all frequency optimization for ITPTR has been performed. From the simulation, ITPTR provides minimum cold end temperature at 20 Hz. The optimum valve opening in order to achieve minimum temperature at a frequency shows that minimum temperature is achieved at 20Hz frequency. For performance comparisons, 20Hz is taken as optimum frequency for both the PTR systems. Fig. 5.44 shows the variation of cold heat exchanger temperature with frequency for ITPTR and OPTR. It depicts that at 20Hz the minimum temperature is achieved for both the models.

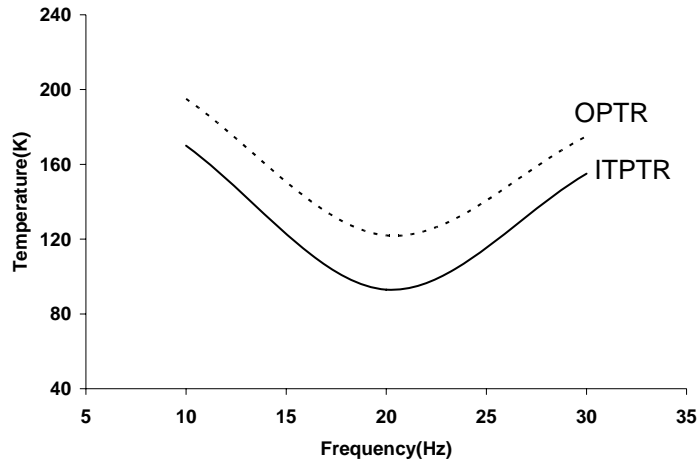


Fig. 5.44 Variation of cold wall temperature with frequency for ITPTR and OPTR.

Figures 5.45 and 5.46 show the phase relation between mass flow rate and pressure at cold end section of the pulse tube for ITPTR and OPTR respectively. Comparing the Figures 5.45 and 5.46, it can be seen that the phase lag for ITPTR is  $40^\circ$  and for OPTR, it is  $56^\circ$ . Hence ITPTR provides better phase relations between oscillating pressure and oscillating mass flow rate at the cold end. Thus, ITPTR provides more cooling effect as compared with OPTR for the same regenerator and pulse tube parameters.

For the given specific dimensions of ITPTR and OPTR, Figure 5.47 shows mass flow rates inside the pulse tube section for both the models. It is obvious from the graph that the oscillating mass flow rate amplitude is more in case of ITPTR in comparison to OPTR. So more refrigerating effect is produced in case of ITPTR, which is shown in Fig. 5.48. However if one increases the diameter of orifice valve to increase the mass flow rate, it will lead to poor phase relation between mass flow rate and pressure. An orifice that is wide open to the reservoir will cause very small pressure oscillations in the pulse tube. Such small oscillations cannot carry the heat away from the cold heat exchanger.

From the above discussions it is clear that the performance of the ITPTR is found superior to that of OPTR. It is due to two reasons. First reason is that there is proper phase relation between mass flow rate and pressure and second reason is that the amplitude of mass flow rate in the pulse tube section of ITPTR is large.

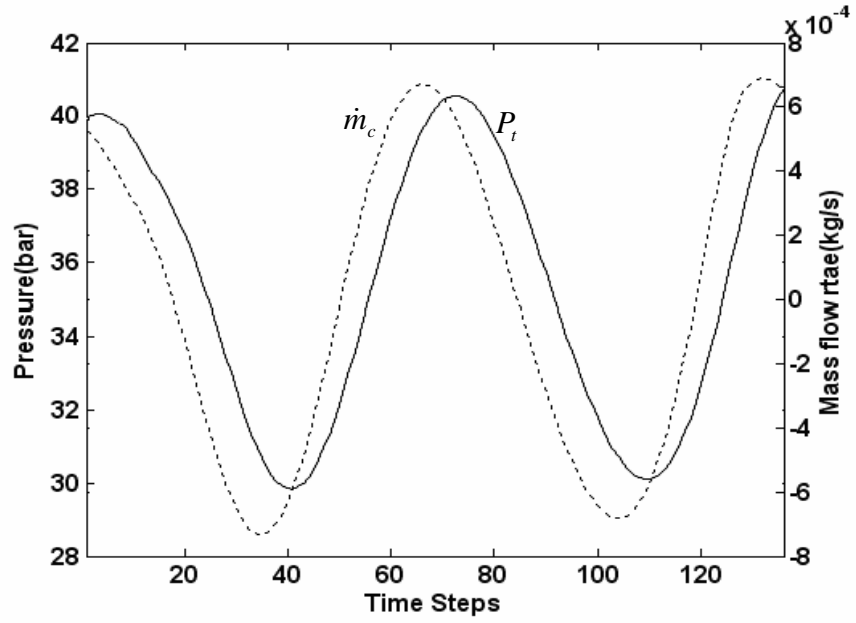


Fig.5.45 Phase relation between mass flow and pressure at CHX for ITPTR.

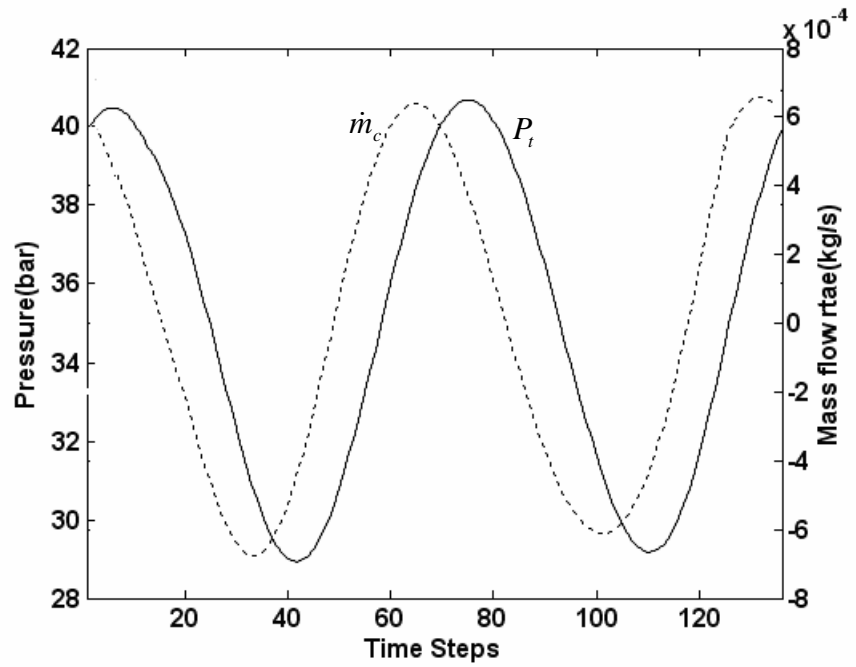


Fig.5.46 Phase relation between mass flow and pressure at CHX for OPTR.



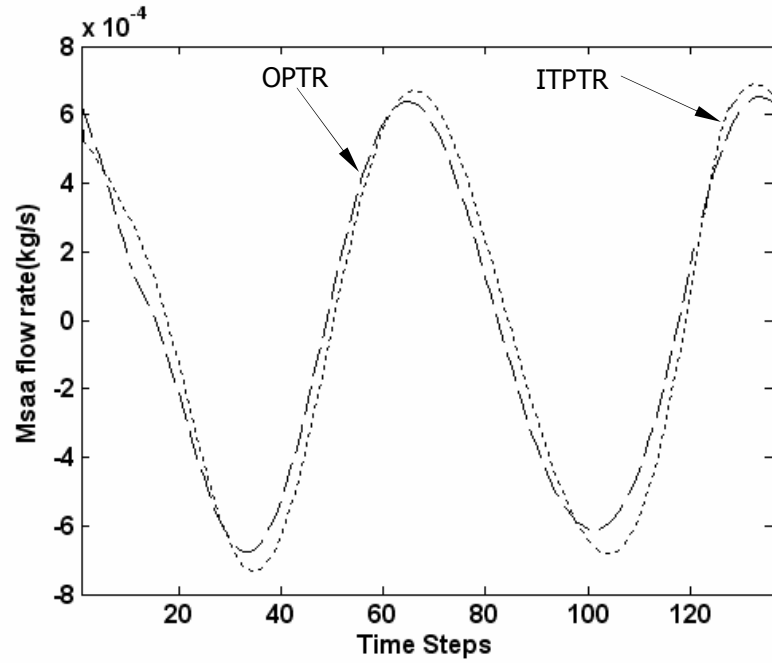


Fig. 5.47 Mass flow rates at cold end section for ITPTR and OPTR.

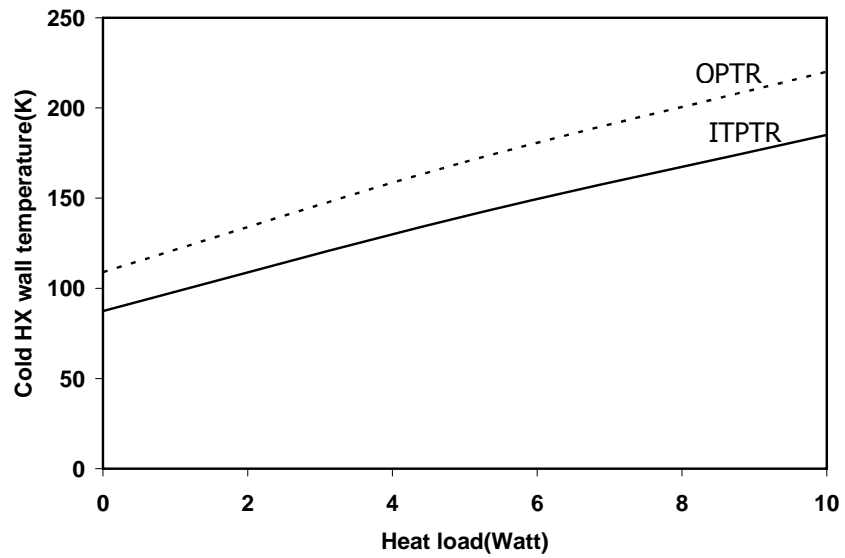


Fig.5.48 Heat load comparisons for ITPTR and OPTR.

## 5.9 Discussions

The simulation results show that in case of adiabatic (case1) cold-end heat exchanger (CHX) the temperature achieved at cold end is 87.4K in case of ITPTR and 109.6K in case of OPTR. When a constant heat load of 5W is imposed at CHX, the temperature achieved at cold end is 147K in case of ITPTR and 181K in case of OPTR. The refrigerating load obtained at CHX is 5.35W in case of ITPTR and 3.72W in case of OPTR when CHX ends for both the systems are maintained at 150K. The following table shows the result obtained in different case.

Table 5.5 Simulation Result of ITPTR and OPTR

	Adiabatic Case (Achieved Temp.)	Constant Heat Flux(5W) (Achieved Temp.)	Constant Temp(150K) (Achieved load)
ITPTR	87.4K	147.5K	5.35W
OPTR	109.6K	181K	3.72W

From the above table it is clear that the performance of the ITPTR is found superior to that of OPTR. The reasons are phase difference and amplitude. Thus due to better phase difference and larger amplitude enthalpy flow from cold end towards hot end, ITPTR is better than OPTR.

## *Chapter VI*

# **CFD Analysis of G-M Type Pulse Tube Refrigerators**

## *6.1 Introduction*

The working principle of Gifford–McMahon (G–M) type pulse tube refrigerator (PTR) is different from Stirling type PTR model in view of pressure distribution. In G–M type PTR pressure distribution system limits its working frequency. Generally rotary valve is used as pressure distribution system. Therefore, a G–M-type pulse tube refrigerator usually works at low frequencies (1Hz-5Hz) with large oscillating amplitudes to yield lower temperature compared to Stirling model. Because of this the heat transfer characteristics are different than Stirling type PTR.

This chapter presents the details of geometry and boundary conditions for the CFD simulation of GM type DIPTR by using commercial software, Fluent6.1. The dimensions of each component of pulse tube refrigerator, its geometry created in gambit software and complete meshing of the geometry and also the boundary conditions for each model are presented in this chapter. In the first part of study, analysis has been performed considering 2-dimensional geometry of DIPTR. In the second part of study, 3-dimensional geometry is considered for the CFD simulations and its results are compared with available experimental data.

## *6.2 2-D Geometry of Double inlet Pulse Tube Refrigerator*

A two-dimensional, schematic of the DIPTR system is shown in Fig.6.1. Fig.6.2 shows the complete meshing of the 2-D geometry of the simulated system. The system consists of a compressor, a rotary valve, a transfer line, an after cooler, a regenerator, cold end heat exchanger, pulse tube, hot end heat exchanger, connecting tube, an orifice valve, a double

inlet bypass valve and a reservoir. The configuration parameter is identical to the experimental apparatus given in [128]. The dimensions and boundary conditions of the DIPTR are tabulated in Tables 6.1 and 6.2 respectively.

In order to supply gas pressurization and depressurization in the closed chamber, a user defined function (UDF) is developed in C programming language[177]. A harmonic pressure wave described in Eq. (6.1) is used for the user defined function (UDF) in Fluent.

$$P = P_1 + P_a \sin(\omega t) \quad (6.1)$$

In Eq. (6.1),  $P_a = 0.5MPa$  is the oscillating pressure amplitude,  $\omega = 2 * \pi * f$  is the angular velocity and the operating frequency is  $f = 2Hz$ . The mean pressure of oscillation ( $P_1=1.6MPa$ ) is used as the operating pressure in Fluent. Detailed nodalization of all components is performed, whereby regions deemed more sensitive, such as the vicinity of component-to-component junctions, are represented by finer mesh than others. Once the model is created in Gambit software (pre-processor) and exported to Fluent (solver), the model boundaries have to be defined. In porous regions the momentum transport equation includes a source term which is used to specify inertial and viscous resistance factors as input for these zones. After the boundaries are defined, the solver and flow characteristics are activated in Fluent. A segregated solver is used for all models. This solver solves the flow and energy equations separately and implicitly. Since the flow inside of a pulse tube is a turbulent flow, the " $k - \varepsilon$ " turbulent model is applied for the simulation. In order to observe the difference of refrigeration performance among different cases, same pressure UDF is applied for the simulation. The phase relation between pressure and mass flow rate at pulse tube section for different values of valve opening conditions are compared to find out the best performance of the system. In this simulation a cycle is divided into 50 time steps. For the above cases the after cooler wall and hot end heat exchanger are maintained at 293K (Isothermal condition).The regenerator and pulse tube of the system are insulated and rest of the components are at atmospheric temperature of 300K.

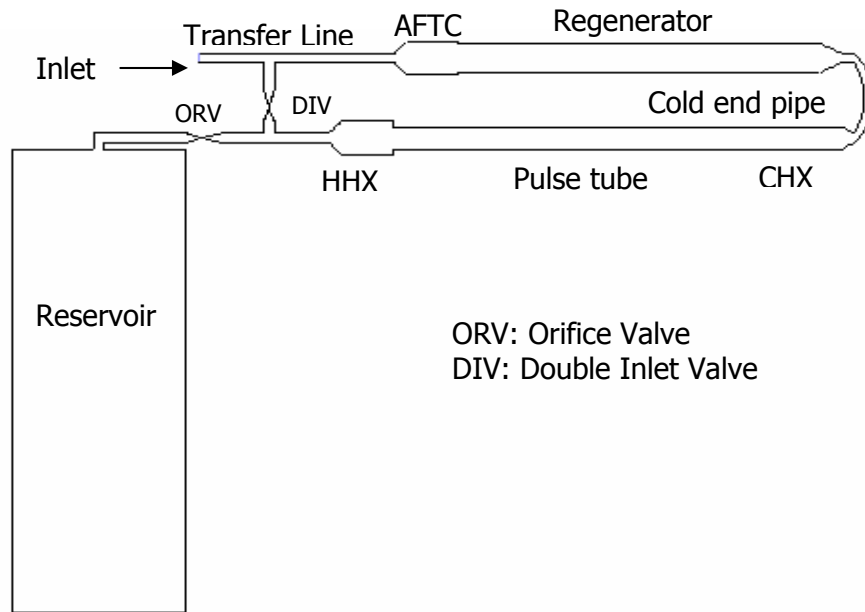


Fig.6.1 Schematics of the physical model of GM type DIPTR.

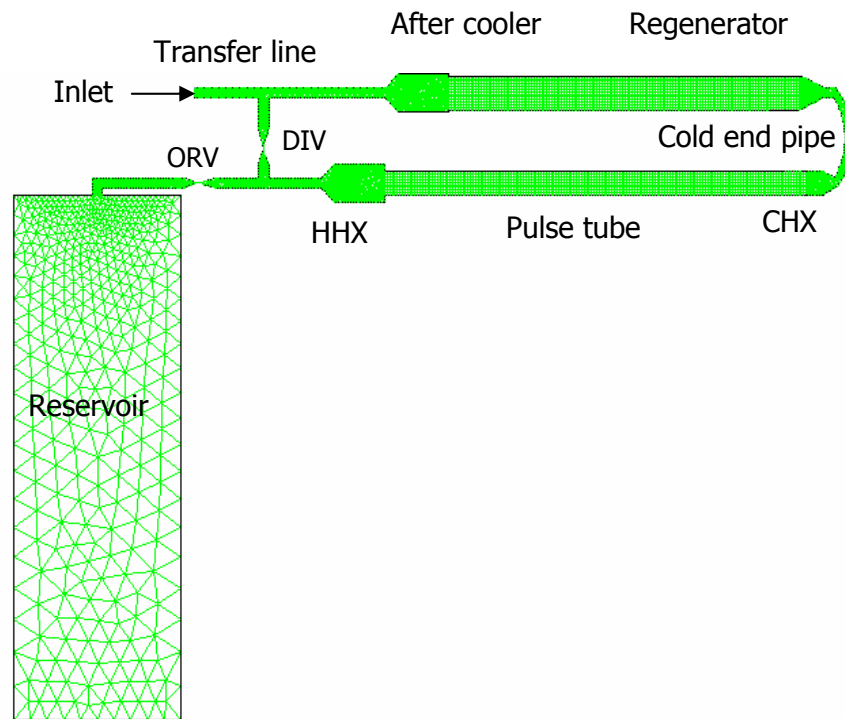


Fig.6.2 Two-dimensional geometry with complete mesh for DIPTR.

Table 6.1 Dimensions of DIPTR for 2-D simulations

Components	Diameter (m)	Length (m)
Transfer line	5.30E-03	11.50E-02
After cooler	22.00E-03	20.00E-03
Regenerator	20.00E-03	21.00E-02
Cold end exchanger	15.0E-03	20.0E-03
Pulse tube	15.00E-03	25.0E-02
Hot end exchanger	22.00E-03	20.0E-03
Surge volume	10.00E-02	30.00E-02

Table 6.2 Boundary and initial conditions of DIPTR for 2D simulations

Study Case	Case 1			Case 2	Case3
	(a)	(b)	(c)		
Inlet	UDF	UDF	UDF	UDF	UDF
Transfer line wall	300K	300K	300K	300K	300K
After cooler wall	293K	293K	293K	293K	293K
Regenerator wall	Adiabatic	Adiabatic	Adiabatic	Adiabatic	Adiabatic
Cold end wall	Adiabatic	Adiabatic	Adiabatic	Heat flux 1W	150K
Pulse tube wall	Adiabatic	Adiabatic	Adiabatic	Adiabatic	Adiabatic
Hot end wall	293K	293K	293K	293K	293K
Orifice tube wall	300K	300K	300K	300K	300K
Reservoir wall	300K	300K	300K	300K	300K
Viscous -resistance (m <sup>-2</sup> )	4.15e+09	4.15e+09	4.15e+09	4.15e+09	4.15e+09
Inertial – resistance (m <sup>-1</sup> )	12140	12140	12140	12140	12140
Initial conditions	300K	300K	300K	300K	300K
Cold end load	0	0	0	1W	3.68W*
Cold end temp	123K*	140K*	163K*	130K*	150K

\*Results obtained by simulation

Table 6.3 Percentage of valve opening

	Case1(a)	Case1(b)	Case1(c)	Case2	Case3
Double inlet valve opening	20%	30%	40%	20%	20%
Orifice valve opening	40%	40%	40%	40%	40%
Cold end load	0W	0W	0W	1W	150K

- *Pressure UDF*

Similar to velocity user defined functions for Stirling type PTR as discussed earlier, the pressure UDF could also be written for G-M type pulse tube refrigerator using Fluent UDF manual. This UDF is saved by giving suitable name like "press.c". In Fluent this source code will be given as input to the G-M type DIPTR system. This ensures the sinusoidal pressure inlet in the G-M type DIPTR system. Using Fluents user defined function manual [177] the pressure UDF as an input to G-M type double inlet pulse tube system is as follows.

```
#include "udf.h"
DEFINE_PROFILE (unsteady_pressure, thread, position)
{
Face_t f;
real t = CURRENT_TIME;
begin_f_loop (f, thread)
{
F_PROFILE (f, thread, position) = 101325.0*(16.0 + 5.0 * sin(12.56 * t));
}
end_f_loop (f, thread)
}
```

- *Compiling pressure UDF*

For compiling UDF in fluent the first step is to click Define → User-Defined → Functions → Interpreted... By this command the interpreted UDFs panel will open. In this window one select proper path and select the source code "press.c", then click interprets then close the interpreted UDFs panel. By this command the UDF is ready to be used by

solver. The second step is to set unsteady boundary condition at inlet. For this one clicks define boundary conditions and then select inlet boundary condition as **udf\_unsteady\_pressure**. This command will provide oscillating pressure input to one end of the system.

### ***6.3 Results of 2-D Simulations***

The single stage GM type double inlet pulse tube (DIPTR) system model is simulated with various boundary conditions to optimize the openings of orifice valve and double inlet valve to achieve the lowest temperature at the cold end. The 2D simulation means that the geometry is created by giving unit thickness in the z-coordinate. Steady periodic CFD simulation results are discussed in this section. Case configuration is summarized in Table 6.1 and results are given in Table 6.4. There are 5 simulation cases out of which cases 1(a), (b) and (c) corresponds to adiabatic boundary conditions for different valve openings of DIPTR. Out of these three simulations, the optimum valve opening for the best refrigeration performance is selected. With this optimum valve opening, the known heat load and isothermal boundary conditions are applied as describe in case2 and case3 respectively. In order to observe the difference of refrigeration performance among different cases, same pressure UDF (user defined function) has been applied at inlet to regenerator in lieu of a compressor. The phase relation between pressure and mass flow rate at pulse tube section for different cases is compared to find out the refrigeration performance. The results of CFD simulation are compared with available experimental data.

#### ***6.3.1 Case1: Adiabatic Boundary Condition***

Three simulations are analyzed under this adiabatic boundary condition. The orifice valve opening of 40% corresponding to 20%, 30% and 40% of double inlet valve opening are analysed in this section. The optimum pair of valve opening is utilized in the subsequent analysis for known heat load and isothermal boundary conditions.

##### ***(a) Double inlet valve opening of 20% and orifice valve opening of 40%***

This utilizes an adiabatic wall boundary condition at the cold end which is equivalent to no refrigeration load applied to the overall system. The simulation started with an initial



temperature of 300K. Figure6.3 shows the variation of the cold tip temperature as a function of time for case 1(a), (b) and(c) with different valve opening. For case1(a) the ultimate cold end temperature of 123K is obtained after a simulation for 160 seconds. For case1(b) and case1(c) the minimum cold end temperatures achieved are 140K and 163K respectively. From the Figure6.3, it is clear that case1(a) provides minimum cold end temperature. However, it should be emphasized that in the actual systems the cooling time will be higher than what is predicted in the result since the thermal mass has not been implemented in the system.

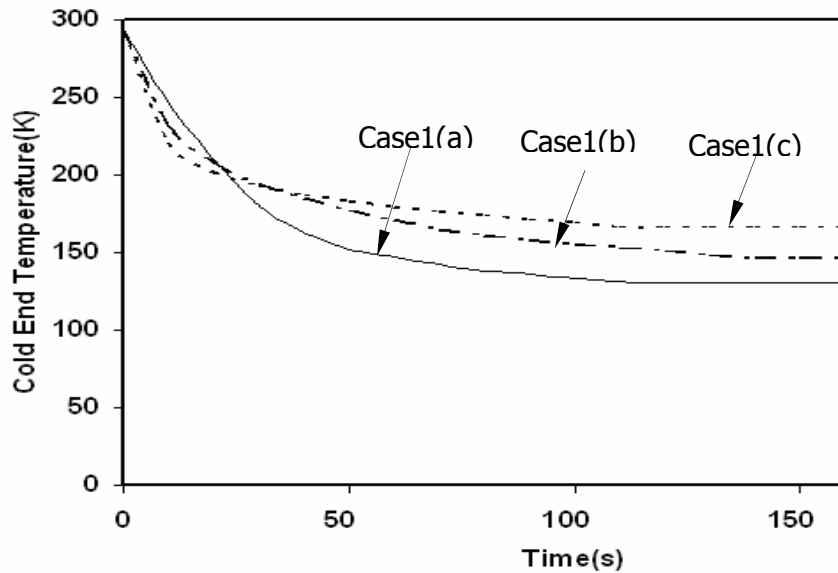


Fig.6.3 Cooling behavior of cold end temperature for DIPTR.

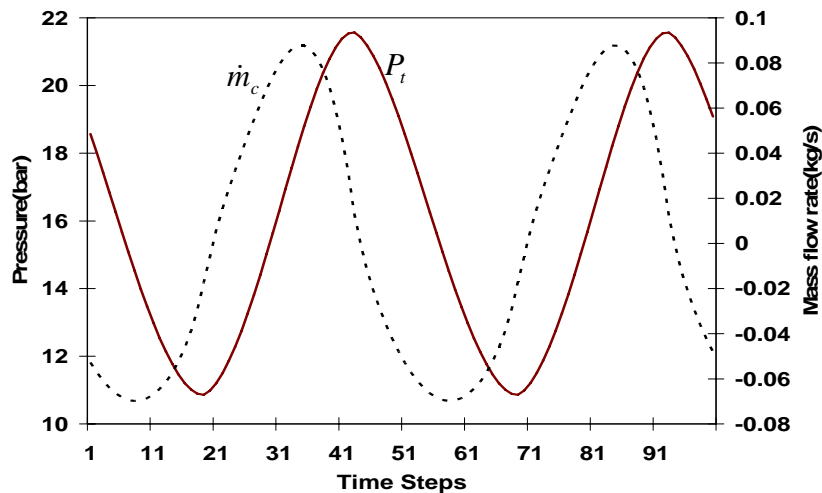


Fig.6.4 Phase relation between pressure and mass flow rate for case1 (a).

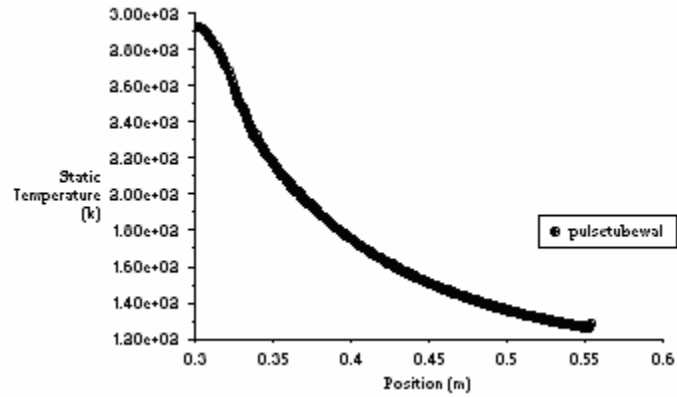


Fig.6.5 Temperature distribution along axial direction of pulse tube for case1(a).

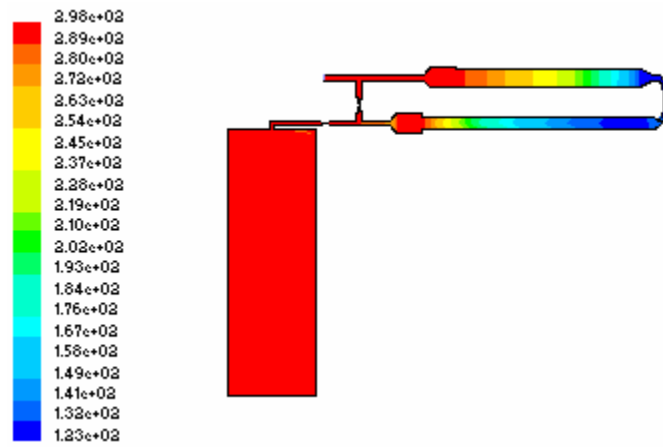


Fig.6.6 Temperature contour for case1(a).

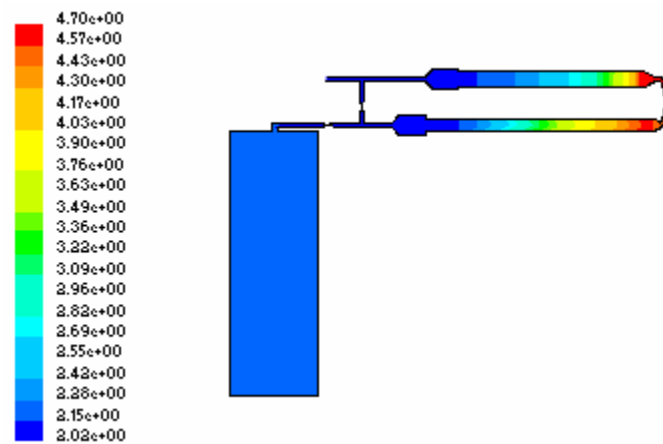


Fig.6.7 Density contour for case1(a).

Figure 6.4 shows the phase difference between mass flow rate and pressure at cold end section of the pulse tube. It depicts that phase difference is small compared to other cases, and hence providing better cooling effect. Fig.6.5 depicts the temperature variation along the length of pulse tube for case1 (a). This shows that minimum temperature is reached near the cold end of pulse tube. The temperature and density contours are presented in Fig.6.6 and Fig.6.7 respectively. In this simulation, the entire system is initially at 300K. Once steady periodic state is achieved, the cold end is stabilized at 123K. In the depicted simulation, to verify that the system has reached steady periodic simulation, Fluent examines the cold end to see if the temperature of the cold end is identically repeated from one cycle to the next. However, the temperature and density profile depicts a local instantaneous snapshot of the system.

***(b) Double inlet valve opening of 30% and orifice valve opening of 40%***

This case represents the simulation of 30-40 models (30% opening of DI valve and 40% opening of orifice valve) with adiabatic cold end heat exchanger. The simulation is started from an assumed temperature of 300K and continued until steady periodic conditions are reached. As noted from the graph shown in Fig.6.3, the simulation predicts a cold end temperature of 140K. Fig.6.8 shows the phase relation between pressure and mass flow rate where as Fig.6.9 and Fig.6.10 show the temperature and density contours for this case.

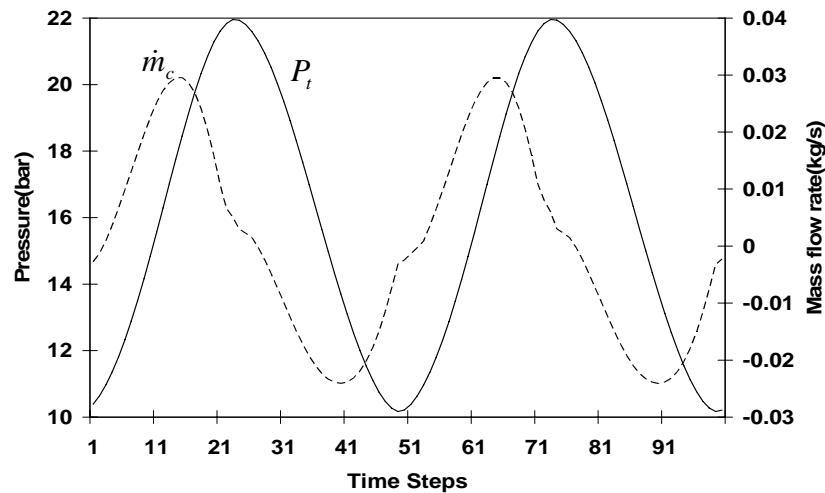


Fig.6.8 Phase relation between  $P_t$  pressure and mass flow case1(b).

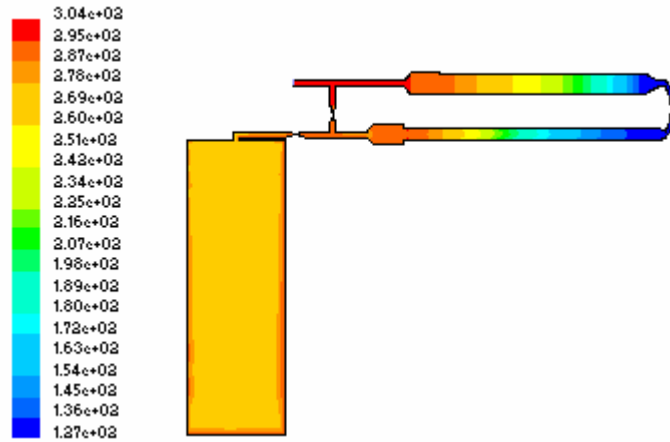


Fig.6.9 Temperature contour for case1(b).

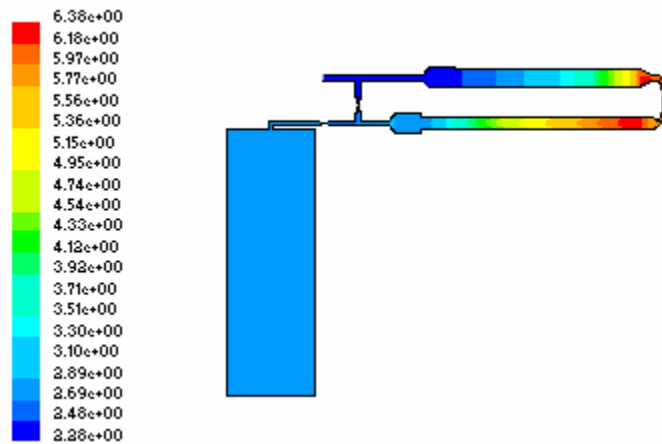


Fig.6.10 Density contour for case1(b).

*(c) Double inlet valve opening of 40% and orifice valve opening of 40%*

In this case also the physical system and boundary conditions are same as case 1(a) and case 1(b), with exception of valve openings. In this case, 40% DI valve opening and 40% orifice valve opening are imposed. The simulation is started from an assumed temperature of 293K and continued until steady periodic conditions are reached. As discussed earlier, Fig.6.3 displays the variation of temperature of the cold end. As noted from the graph, the simulation predicts a cold end temperature of 163K. Fig.6.11 shows the phase relation between pressure and mass flow rate at pulse tube section. Fig.6.12 and Fig.6.13 shows the temperature and density contours respectively for this case.

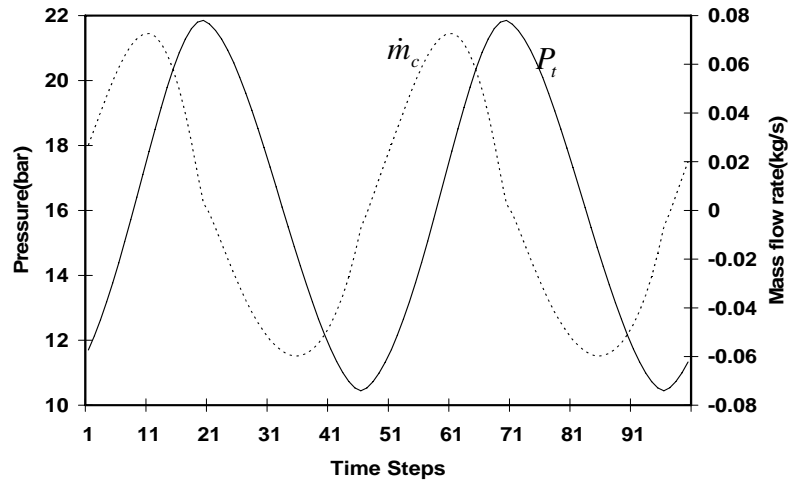


Fig.6.11 Phase relation between pressure and mass flow rate case1(c).

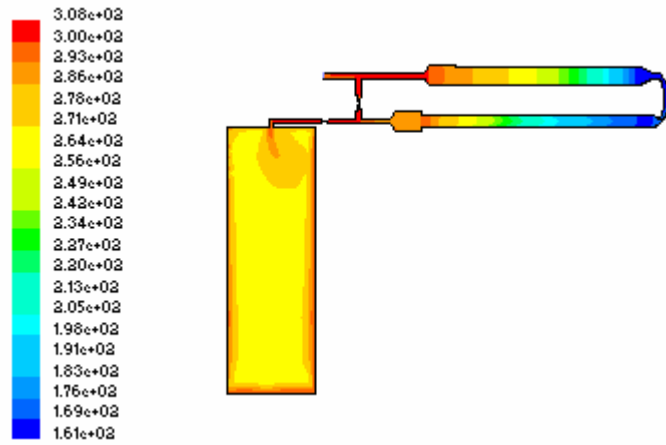


Fig.6.12 Temperature contour for case1(c).

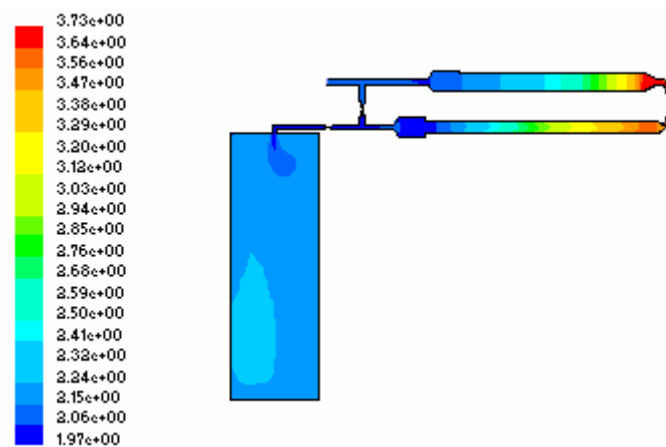


Fig.6.13 Density contour for case1(c).

- *Comparisons among case1 (a), case1 (b) and case1(c):*

Figure 6.14 depicts the cyclic mass flow rate variations with time for case1 (a), case1 (b) and case1 (c). From the figure it is clear that in case1 (a) the amplitude of mass flow rate is more as compared with case1 (b) and case1 (c). This high mass flow rate amplitude causes more enthalpy flow from cold end to hot end in case1 (a) and thus provides minimum cold end temperature in case1 (a) as shown in Fig6.3. From phase relation graphs in case1 (a) the phase lag between pressure and mass flow rate is minimum compared with case1 (b) and case1 (c). Because of above two reasons case1 (a) provides better performance.

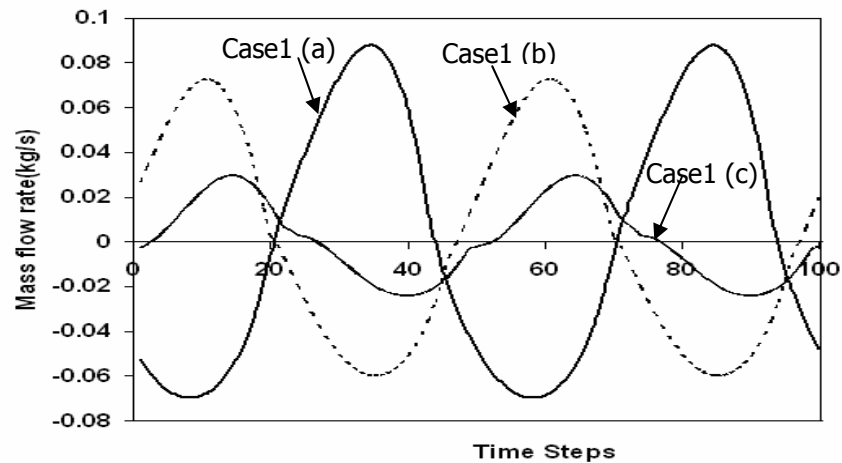


Fig.6.14 Mass flow rates through pulse tube cross section.

### 6.3.2 Case2: *Known Heat Load Boundary Condition*

This case represents the optimized valve opening of case1 (a) pulse tube model with constant heat load of 1W at cold end heat exchanger. This is equivalent to the system undergoing a refrigeration load of 1W. The simulation is started from an assumed temperature of 300K and continued until steady periodic conditions are reached. Fig.6.15 displays the variation of temperature of the cold end. As noted from the graph, the simulation predicts a cold end temperature of 130K. Figure 6.16 shows the phase relation between mass flow rate and pressure at the cold end. Figures 6.17 and 6.18 show the temperature contour and density contour respectively. The trends of graphs are similar as depicted earlier.

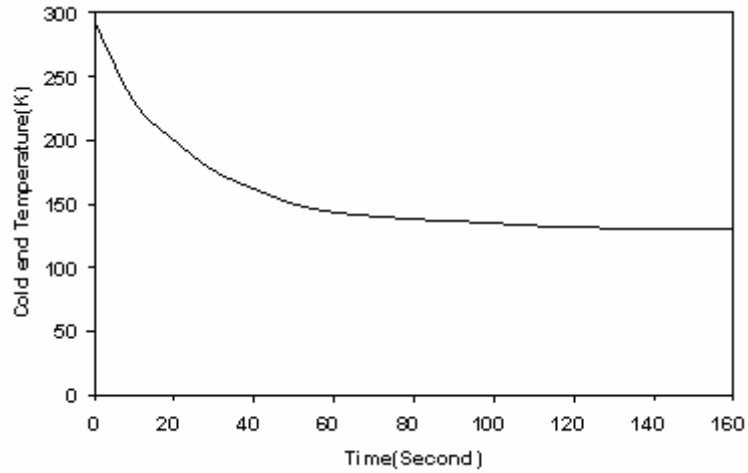


Fig. 6.15 Cooling behavior of cold end temperature for case2

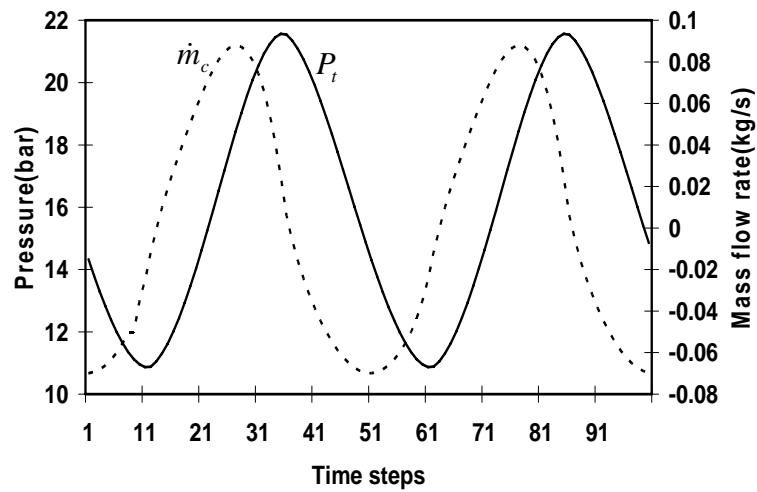


Fig. 6.16 Phase relation between mass flow rate and pressure (case2).

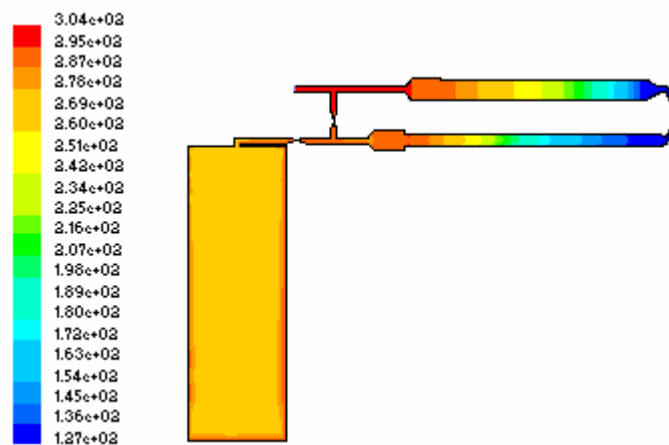


Fig. 6.17 Temperature contour for case2.

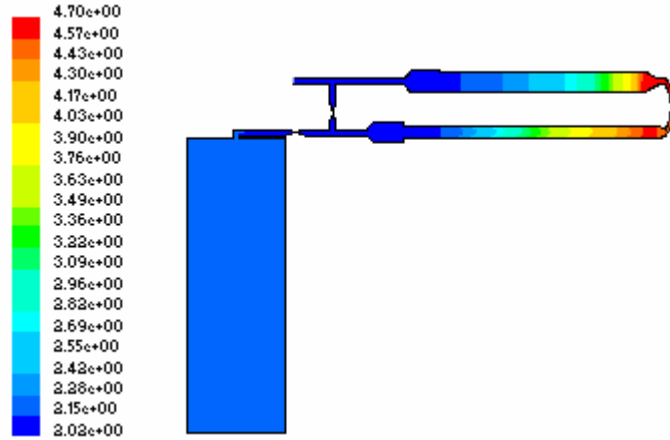


Fig. 6.18 Density contour for case2.

### 6.3.3 Case3: Isothermal Boundary Condition

In this case, a constant surface temperature of 150K is imposed at the cold heat exchanger in the optimized model of case1 (a). In this case, because of the imposed cold end isothermal wall boundary condition, the heat rate coming into the cold end is calculated. Accordingly, steady- periodic condition should in principle be assumed when the cold end wall heat flux is identically repeated from one cycle to the next. The simulation results reach the steady periodic state with a cooling load of 3.68W. Fig.6.19 shows the total heat transfer rate over a cycle. It depicts that the cycle averaged heat transfer is a positive value. Figures 6.20 and 6.21 show the temperature contour and density contour respectively for isothermal boundary conditions.

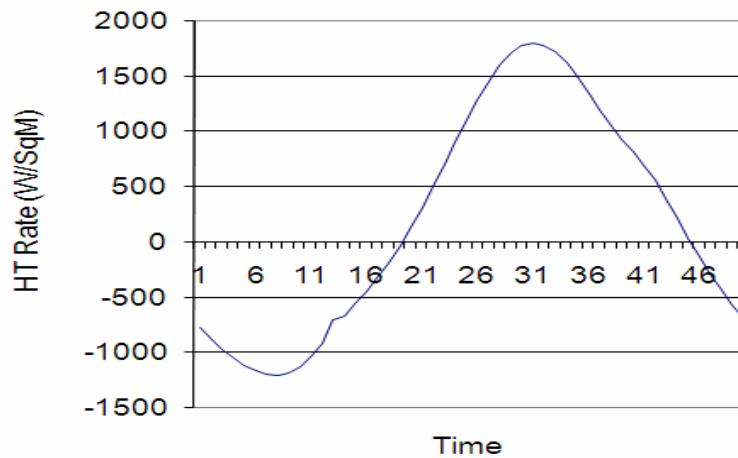


Fig. 6.19 Heat transfer rate over a cycle at CHX for case3.



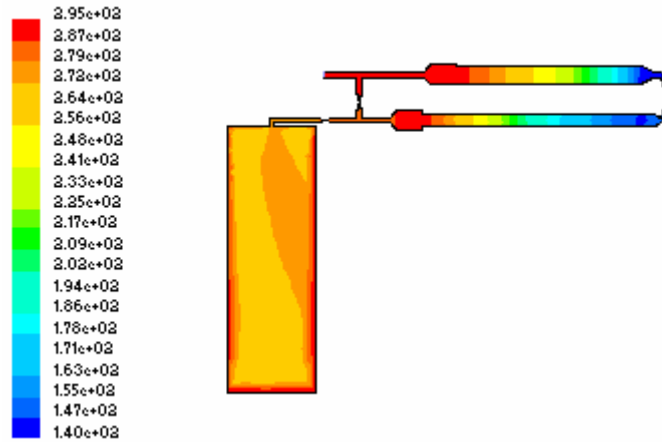


Fig. 6.20 Temperature contour for case3.

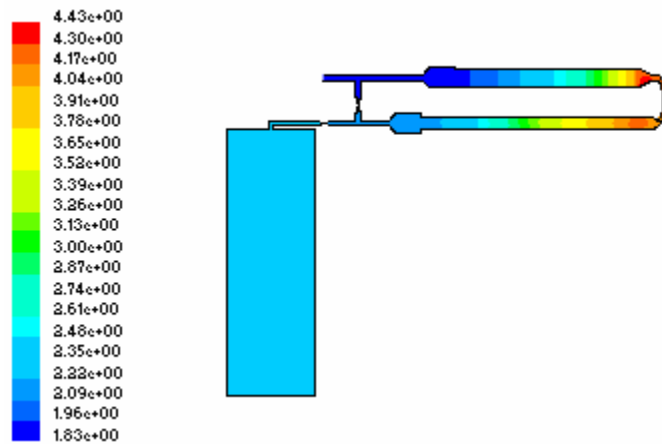


Fig. 6.21 Density contour for case3.

### 6.3.4 Comparison with Experimental Data

The 2D simulation is an approximate geometrical model having unit thickness in the z-direction. For the validation of the CFD simulation results, the experimental data given in [128] is chosen. Some of the important parameters like pressure wave at inlet to regenerator cool down behaviour and refrigeration load are compared and presented in this section. Fig.6.22 depicts the comparison of experimental and CFD simulation for pressure wave form at the inlet of regenerator of the GM type DIPTR. It can be seen that the experimental wave form is in between the rectangular and sinusoidal shapes with the same amplitude. But the CFD simulation pressure wave form is sinusoidal. The Figure6.23 depicts the comparisons of cool down behaviour of CFD simulation results and experimental cool down behaviour for DIPTR model. The figure shows that there is a good agreement between CFD results and

experimental results. The comparison of cooling power between the experimental results and CFD simulation results are presented in Fig.6.24. This figure depicts a good agreement between experimental and numerical results. Figure 6.25 depicts the comparisons of experimental and CFD simulation temperature distribution along the pulse tube length. There is a quite similarity between experimental and CFD simulation results.

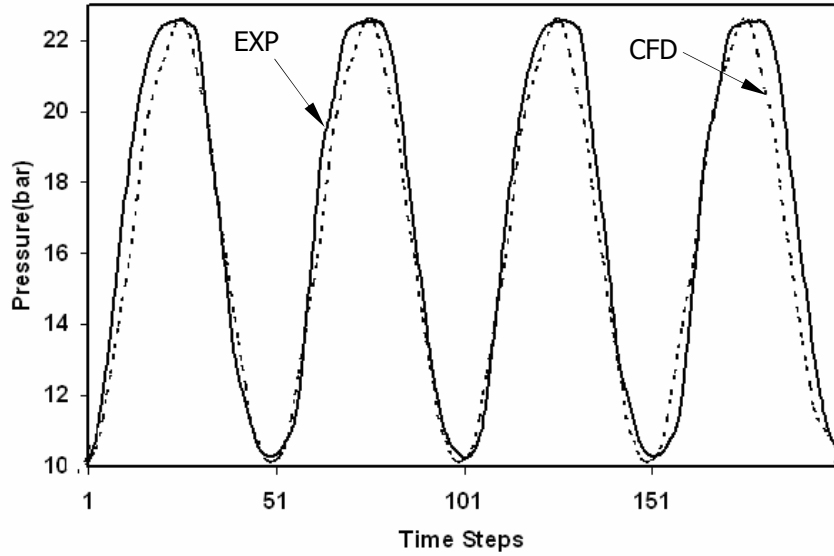


Fig. 6.22 Comparison of pressure wave at the inlet of regenerator.

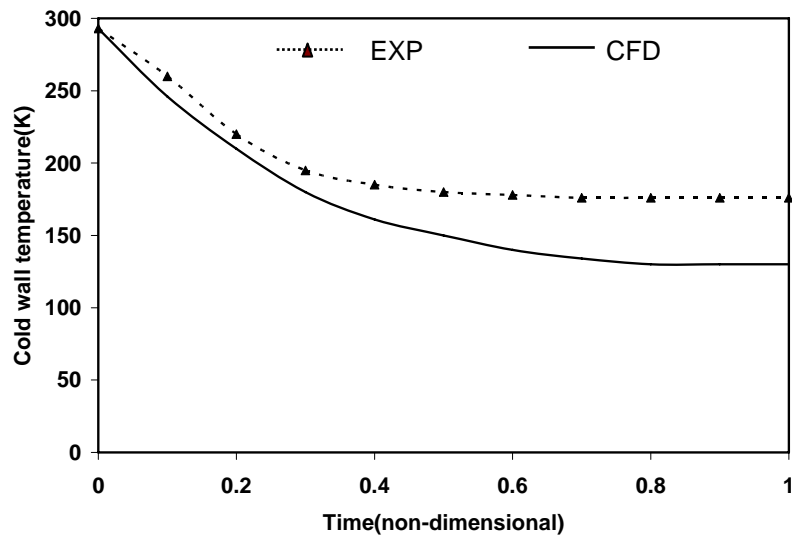


FIG. 6.23 Comparison of cool down behaviour.

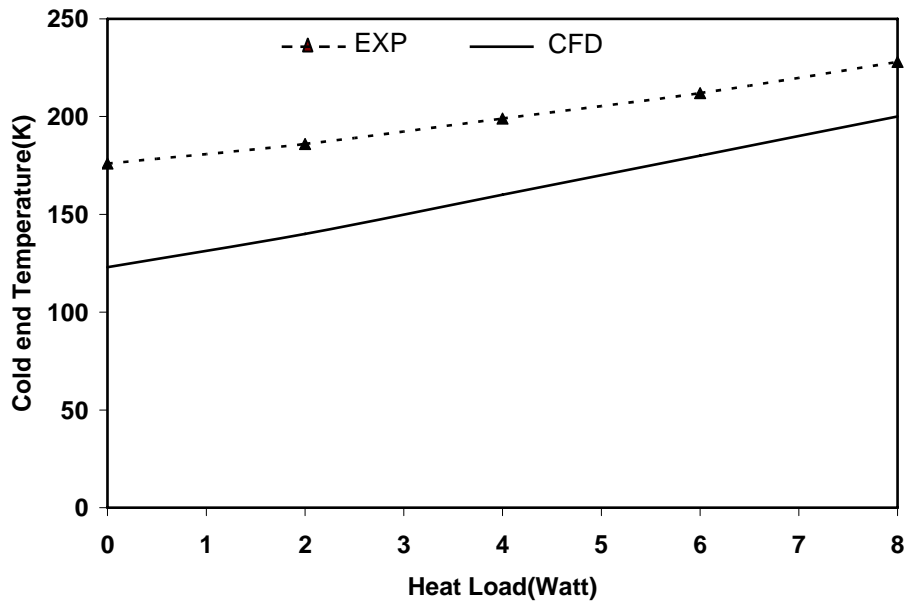


FIG. 6.24 Comparison of heat load.

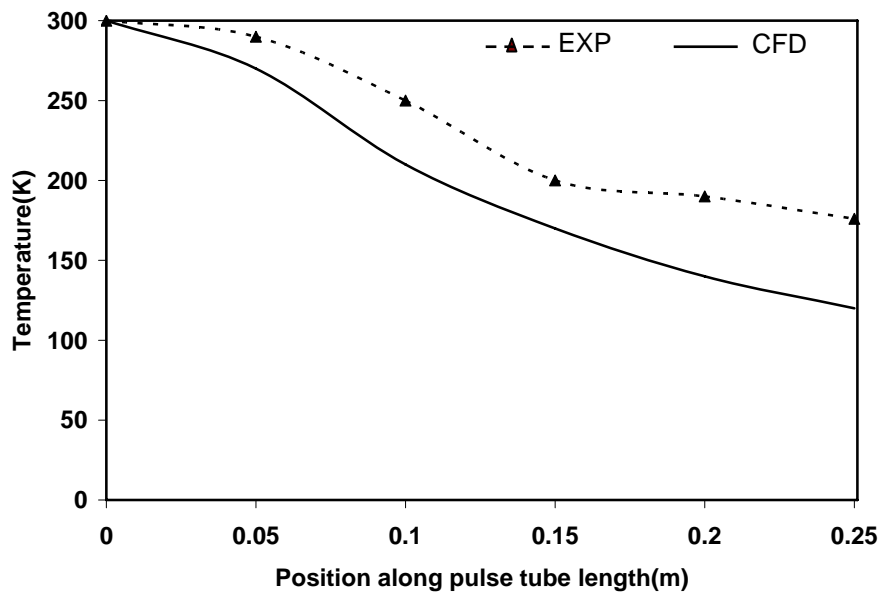


Fig. 6.25 Comparison of temperature variation along the pulse tube length.

### 6.3.5 Discussions

The simulation results show that in case of adiabatic cold-end heat exchanger (CHX) for case1 (a), (b) and (c) the temperature achieved at cold end is 123 K, 140K, and 163K respectively. It seems that the minimum optimum cold end temperature is 123K. Thus case1 (a) provide the optimum valve opening which corresponds to 20% DIV and 40% ORV. This optimum valve opening is used for known heat load (case2) and isothermal (case3) boundary conditions. For this valve opening when a constant heat of 1W is imposed at CHX (case2), the temperature achieved at cold end is 130K. Similarly for this valve opening, the refrigeration load obtained at CHX is 3.68W, when isothermal boundary condition (case3) of 150K is maintained. Table6.4 shows the summery of results obtained for different boundary conditions.

Table 6.4 Summery of result of 2-D simulation of DIPTR

	Adiabatic (Achieved Temp.)	Constant Heat Flux(1W) (Achieved Temp.)	Constant Temp.(150K) (Achieved load)
DIPTR	123K	130K	3.68W

From the above results it is clear that the performance in case1 (a) with adiabatic boundary condition for the optimum valve opening is superior to other two cases. the discrepancy between the experimental and CFD simulation may be attributed due to unaccounted inefficiency losses in the system and use of a 2-D simulation for analysis.

### 6.4 3-D Geometry of Double Inlet Pulse Tube Refrigerator

The geometry of single stage G-M type DIPTR is taken from [125]. Figure 6.26 shows different components of a single stage GM type DIPTR for the 3-D simulations. Fig.6.27 shows the 3-D Gambit geometry of the system. The system consists of a compressor, a rotary valve, a transfer line, an after cooler, a regenerator, cold end heat exchanger, pulse tube, hot end heat exchanger, connecting tube, an orifice valve, a DI valve and a reservoir. The complete meshing of the system is shown in Fig.6.28. The initial and boundary conditions are similar to 2-D simulations as discussed earlier. The same pressure user defined function (UDF)

as described earlier for 2-D simulation is given as input which provides sinusoidal oscillating pressure input to the system. The Tables 6.5, 6.6 and 6.7 give the detailed dimensions, valve opening positions and boundary conditions of the DIPTR system respectively for the 3-D simulation.

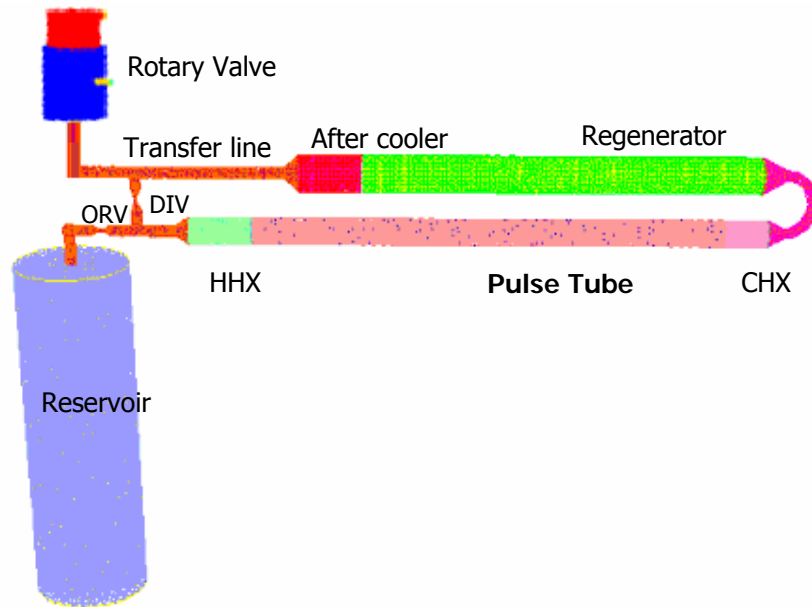


Fig.6.26 Schematic diagram of single stage GM type double inlet pulse tube refrigerator (DIPTR)

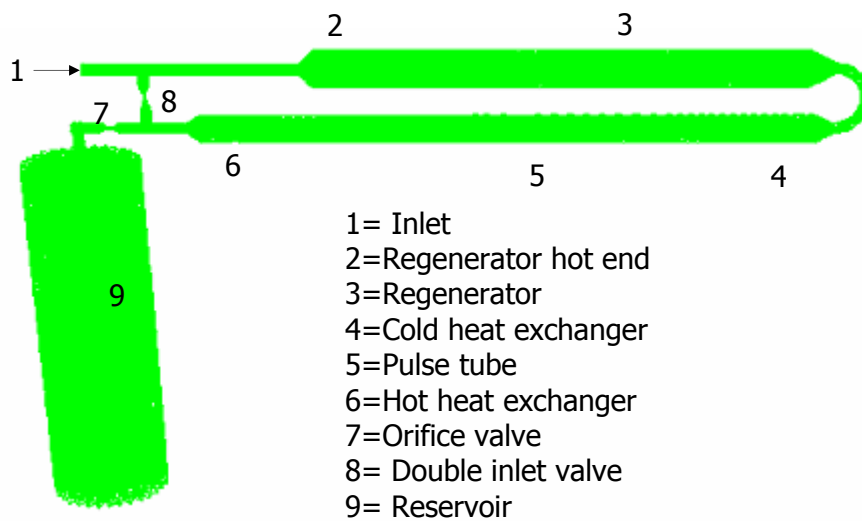


Fig.6.27 Three-dimensional mesh for GM type DIPTR.

Table 6.5 Dimensions of DIPTR for 3-D simulations [125]

Components	Inner Diameter (m)	Outer Diameter (m)	Length (m)
Transfer line	5.30E-03	6.0E-03	115.0E-03
After cooler	18.35E-03	19.0E-03	30.0E-03
Regenerator	18.35E-03	19.05E-03	210.0E-03
Cold end exchanger	14.0E-03	20.0E-03	22.0E-03
Pulse tube	13.3E-03	14.0E-03	250.0E-03
Hot end exchanger	18.35E-03	20.00E-03	30.0E-03
Surge volume	60.00E-03	64.00E-03	180.0E-03

Table 6.6 Percentage of valve opening

	Case1(a)	Case1(b)	Case1(c)	Case2	Case3
Double inlet valve opening	40%	60%	80%	40%	40%
Orifice valve opening	60%	60%	60%	60%	60%
Cold end load	0W	0W	0W	5W	100K

Table 6.7 Boundary and initial conditions of DIPTR for 3D simulations

Study Case	Case 1			Case 2	Case3
	(a)	(b)	(c)		
Inlet	UDF	UDF	UDF	UDF	UDF
Transfer line wall	300K	300K	300K	300K	300K
After cooler wall	293K	293K	293K	293K	293K
Regenerator wall	Adiabatic	Adiabatic	Adiabatic	Adiabatic	Adiabatic
Cold end wall	Adiabatic	Adiabatic	Adiabatic	Heat flux 5W	100K
Pulse tube wall	Adiabatic	Adiabatic	Adiabatic	Adiabatic	Adiabatic
Hot end wall	293K	293K	293K	293K	293K
Orifice tube wall	300K	300K	300K	300K	300K

Reservoir wall	300K	300K	300K	300K	300K
Viscous -resistance (m <sup>-2</sup> )	4.15e+09	4.15e+09	4.15e+09	4.15e+09	4.15e+09
Inertial – resistance (m <sup>-1</sup> )	12140	12140	12140	12140	12140
Initial conditions	300K	300K	300K	300K	300K
Cold end load	0	0	0	5W	8.3W*
Cold end temp	33K*	84K*	233K*	61K*	100K

\*Results obtained by simulation

## 6.5 Results of 3-D Simulations

The 3-D simulation refers to actual geometry where geometry can not be treated as an axis-symmetric one. For the DIPTR with actual geometry, the simulation becomes 3-D simulation rather than 2-D axis-symmetric simulation as in the case of ITPTR. The single stage GM type double inlet pulse tube refrigerator (DIPTR) is simulated with various boundary conditions considering 3-D geometry of the system. The openings of orifice valve and double inlet valves are optimized for its best performance. Some of the important results of steady periodic CFD simulation are discussed in this section. Case configurations are summarized in Tables 6.5 and results are summarized in Tables 6.8. There are 5 simulation cases out of which cases 1(a), (b) and (c) corresponds to adiabatic boundary conditions for different valve openings of DIPTR. Out of these three simulations, the optimum valve opening for the best refrigeration performance is selected. With this optimum valve opening, the known heat load and isothermal boundary conditions are applied as described in case2 and case3 respectively. In order to observe the difference of refrigeration performance among different cases, a same pressure UDF (user defined function) is applied for the simulation at inlet to regenerator instead of a compressor. The general results such as cool down behaviour, phase difference between mass flow rate and pressure at cold end, the temperature profiles along the wall as well as the temperature oscillations at cold end for different boundary conditions are presented in this section. The phase relation between pressure and mass flow rate at pulse tube section for different cases is compared to find out the refrigeration performance. The simulation results are compared with available experimental results [125]. There is an

excellent agreement of simulation result with the experimental data. This conclusion leads that numerical simulation by Fluent is capable of predicting the performance and optimum design of PTR.

### ***6.5.1 Case1: Adiabatic Boundary Condition***

Three simulations are analyzed under this adiabatic boundary condition. The orifice valve opening of 60% corresponding to 40% , 60% and 80% of double inlet valve opening are taken into consideration. The optimum pair of valve opening is utilized in the subsequent analysis for known heat load and isothermal boundary conditions.

#### ***(a) Double inlet valve opening of 40% and orifice valve opening of 60%***

This utilizes an adiabatic wall boundary condition at the cold end which is equivalent to no refrigeration load applied to the overall system. The simulation started with an initial temperature of 300K. Figure 6.28 shows the wall temperature variation of the cold end heat exchanger just after the simulation has started. This shows that the wall temperature decreases with simulation time. Figure 6.29 shows the cyclic average cold tip temperature variation as a function of time for case 1(a) till cyclic steady state is reached. The ultimate cold end temperature of 33K is obtained after a simulation of 500 seconds. However, it should be emphasized that in the actual systems the cooling time will be higher than what is predicted in the result since the thermal mass has not been implemented in the system.

Figure 6.30 shows the cold end wall temperature cyclic variation for case1(a) and depicts that the cyclic steady state condition has reached. For case1(a) the minimum cold end temperature achieved is 33K. Figure 6.31 shows the temperature variations along the axial direction of pulse tube. This figure depicts that the minimum temperature is achieved near the cold end of pulse tube. Figure 6.32 shows the phase relation between mass flow rate and pressure at the cold end section of the DIPTR for case1(a). It depicts that both are in phase and hence providing cooling effect. The phase difference between cold end mass flow rate and pressure is 52°. Figures 6.33 and 6.34 show the snapshots of the temperature and density contours respectively for the system for case1(a). The trends of the figures are similar as reported in various published literatures. The Figure 6.35 depicts the velocity vector for the system. Similarly Figure 6.36 shows the enlarged view of velocity vector near cold end. Smooth flow without swirl is observed from this figure.



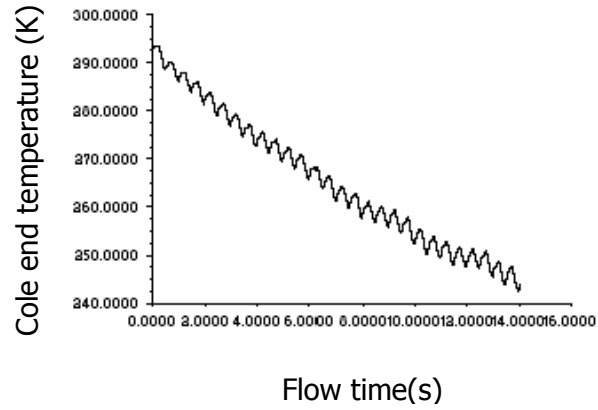


Fig.6.28 Cool down behaviour at the beginning of simulation.

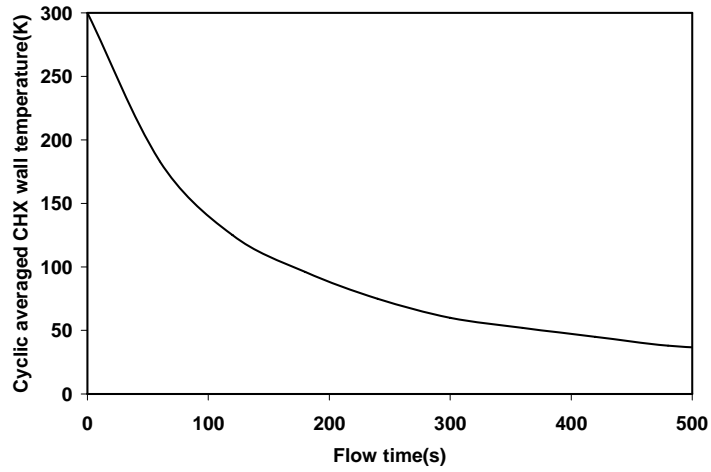


Fig.6.29 Cool down behaviour till cyclic steady state condition for case1(a).

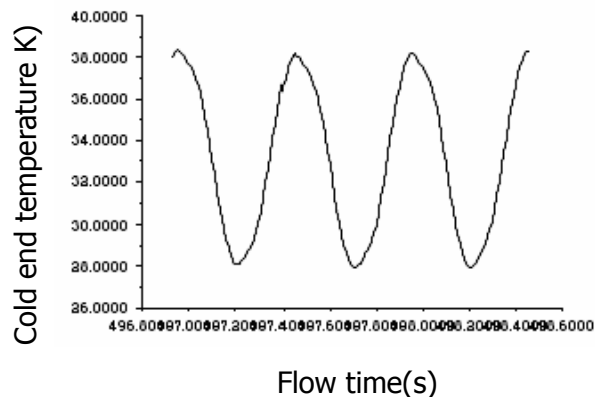


Fig.6.30 CHX Wall temperature variation at cyclic steady condition case1(a)

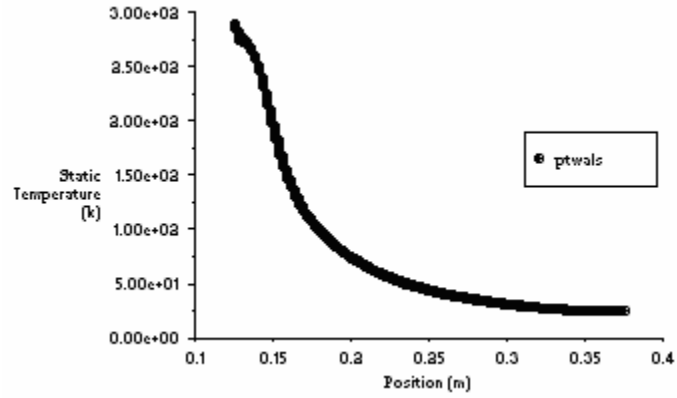


Fig.6.31 Temperature variation along pulse tube length for case1(a).

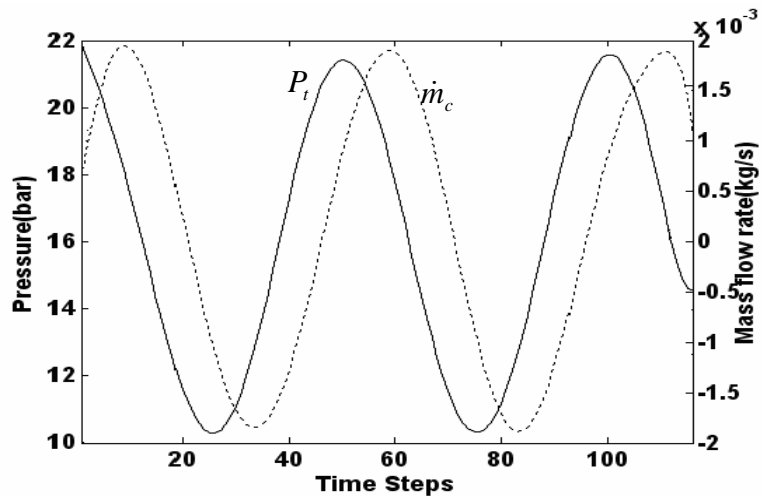


Fig.6.32 Phase relation between mass flow and pressure.

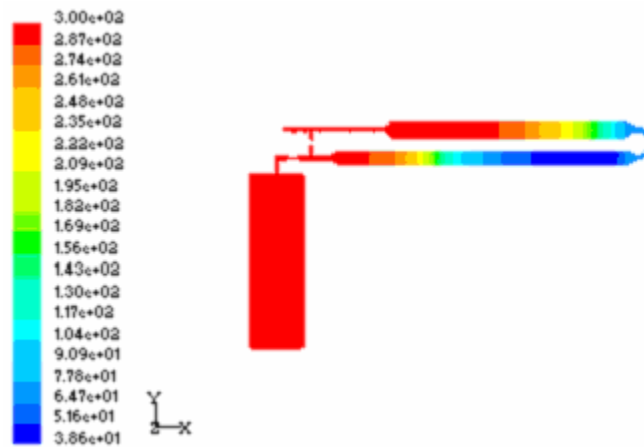


Fig.6.33 Temperature contour for case1(a).

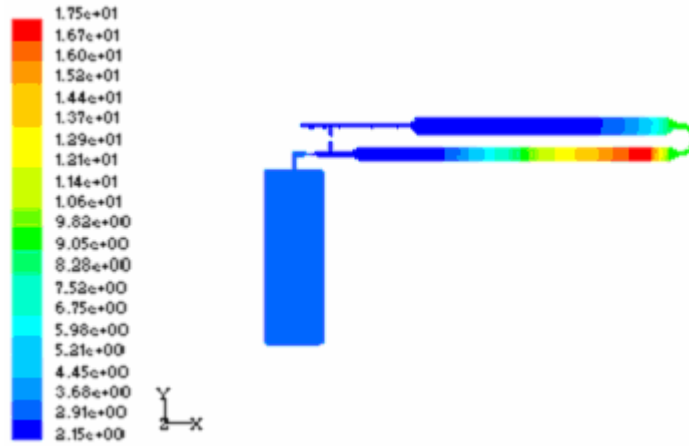


Fig.6.34 Density contour for case1 .

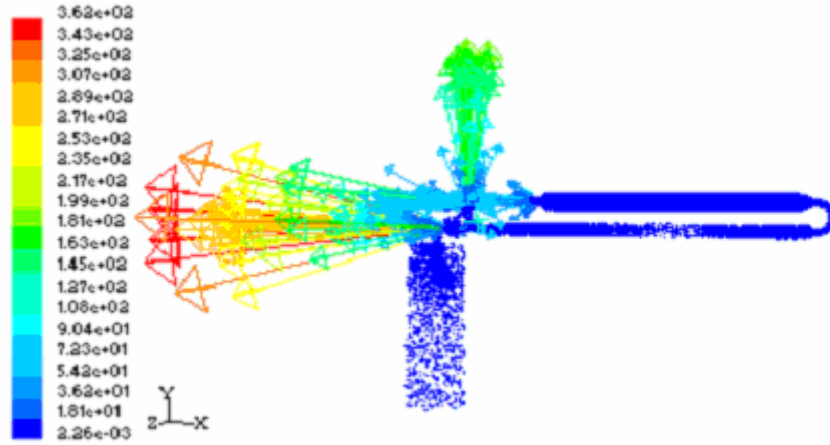


Fig.6.35 Velocity vector for the entire system.

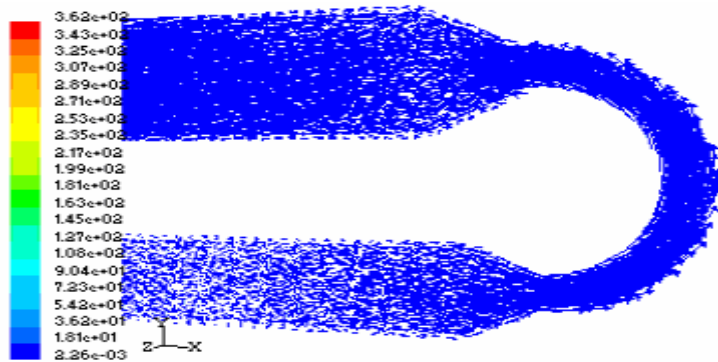


Fig.6.36 Velocity vector near the cold end.

***(b) Double inlet valve opening of 60% and orifice valve opening of 60%***

This case represents the simulation of 60-60 models (60% opening of DI valve and 60% opening of ORV) with adiabatic cold end heat exchanger. The simulation is started from an assumed temperature of 300K and continued until steady periodic conditions are reached. As noted from the graph shown in Fig 6.37, the simulation predicts a cyclic steady state cold end temperature of 84K. Fig.6.38 shows the phase relation between pressure and mass flow rate for this case1 (b). Fig.6.39 and Fig.6.40 show the temperature and density contours respectively for this case. The trends are similar as discussed for case1 (a).

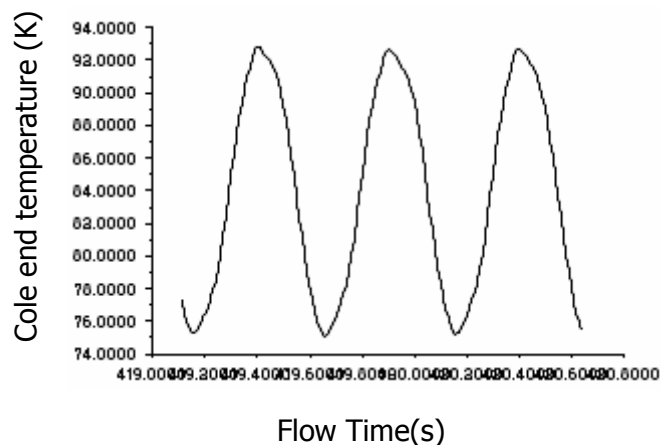


Fig.6.37 Wall temperature variation of the cold heat exchanger case1(b).

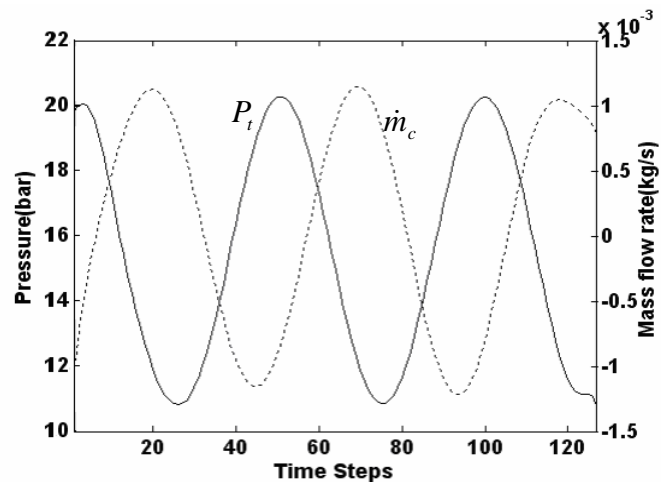


Fig.6.38 Phase relation between mass flow and pressure.

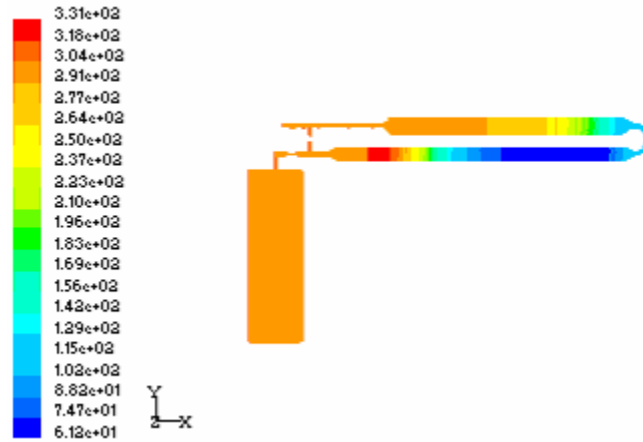


Fig.6.39 Temperature contour for case1(b).

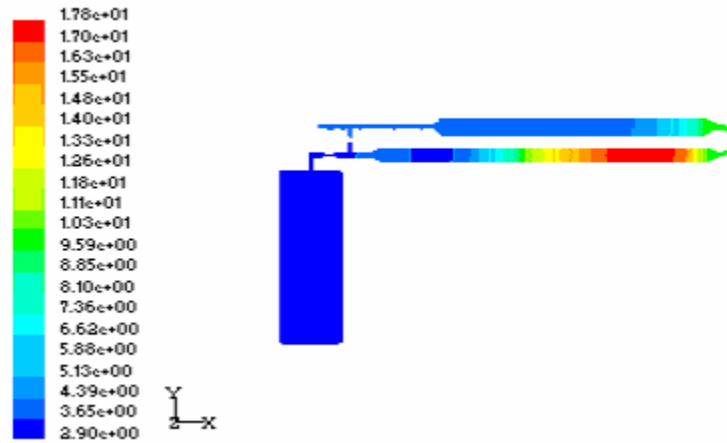


Fig.6.40 Density contour for case1(b).

*(c) Double inlet valve opening of 80% and orifice valve opening of 40%*

In this case also the physical system and boundary conditions are same as case 1(a) and case 1(b), with exception of the percentage of valve openings. The simulation is initiated from an assumed temperature of 300K and continued until steady periodic conditions are reached. Fig.6.41 displays the variation of temperature of the cold end. As noted from the graph, the simulation predicts a cold end temperature of 235K. Fig.6.42 shows the phase relation between pressure and mass flow rate at pulse tube section. Fig 6.43 and Fig.6.44 show the temperature and density contours for this case.

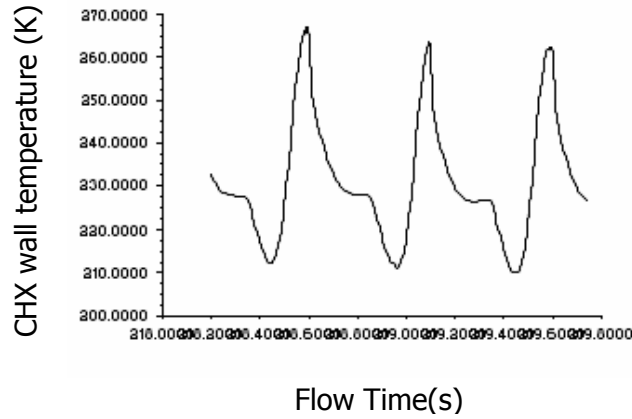


Fig.6.41 Wall temperature variation of the cold heat exchanger case1 (c).

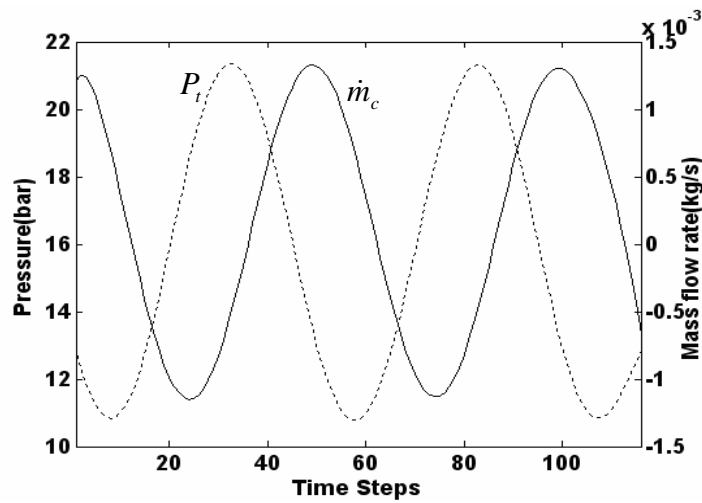


Fig.6.42 Phase relation between mass flow and pressure for case1(c).

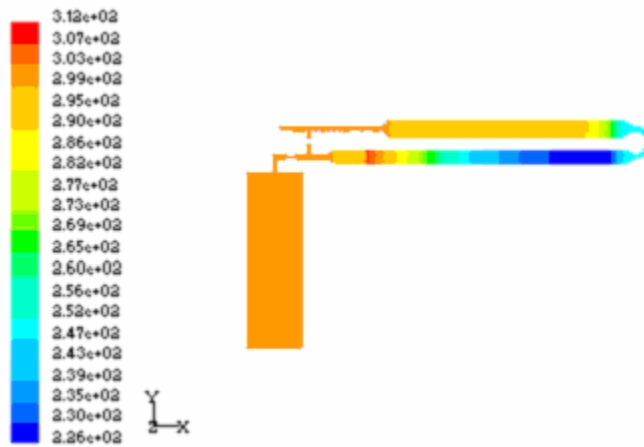


Fig.6.43 Temperature contour for case1(c).

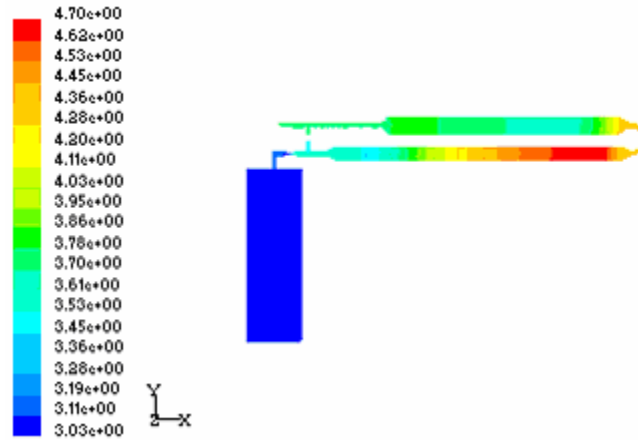


Fig.6.44 Density contour for case1(c).

### 6.5.2 Case2: Known Heat Load Boundary Condition

This case represents the simulation of pulse tube model with constant heat load of 5W at cold end heat exchanger with the optimized valve opening. This is equivalent to the system undergoing a refrigeration load of 5W. The simulation is started from an assumed temperature of 300K and continued until steady periodic conditions are reached. Fig.6.45 displays the variation of temperature of the cold end. As noted from the graph, the simulation predicts a cold end temperature of 61K. Fig.6.46 and Fig.6.47 show the temperature contour and density contour respectively. The trends are similar as discussed earlier.

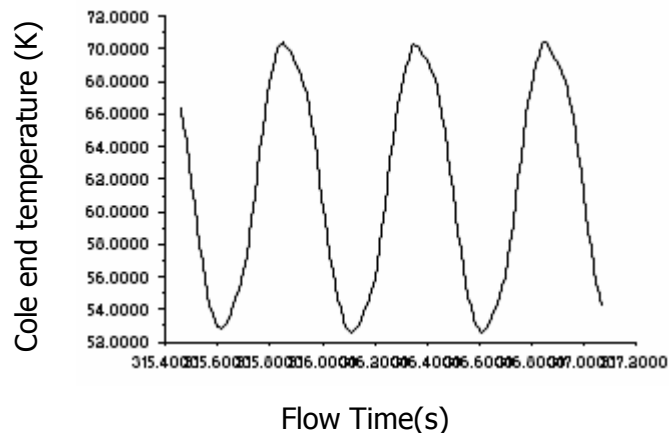


Fig.6.45 Wall temperature variation of cold heat exchanger for case2.

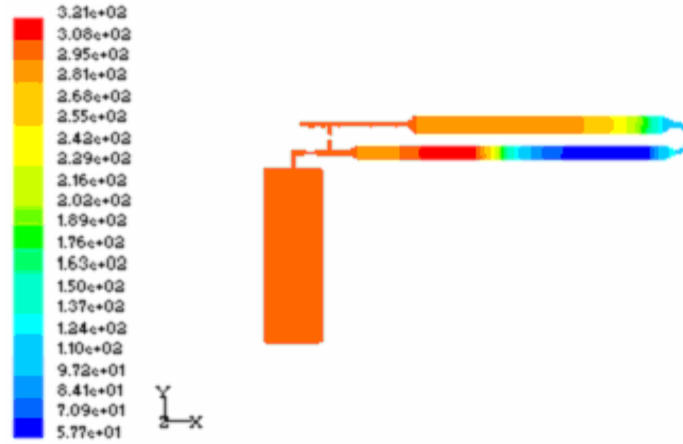


Fig.6.46 Temperature contour for case2

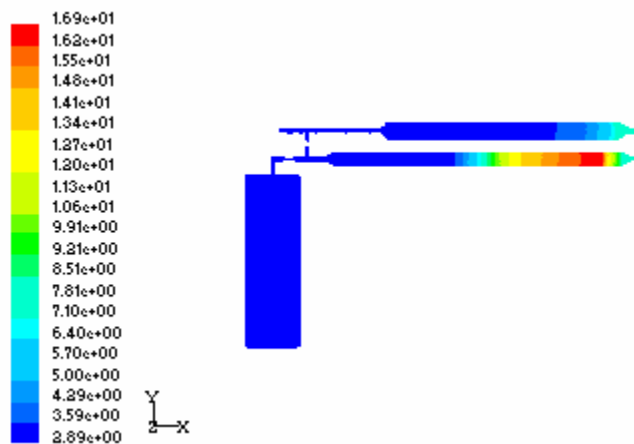


Fig.6.47 Density contour for case2

### 6.5.3 Case3: Isothermal Boundary Condition

In this case, a constant surface temperature of 100K is imposed at the cold heat exchanger for the optimized valve opening as described earlier. Because of the imposed cold end isothermal wall boundary condition, the heat rate coming into the cold end is calculated. Accordingly steady- periodic condition should in principle be assumed when the cold end wall heat flux is identically repeated from one cycle to the next. The simulation results reach periodic state with a cooling load of 8.2W. Fig.6.48 shows the total heat transfer rate over a cycle. It depicts that the cyclic averaged heat transfer is positive value. Figure 6.49 shows the wall temperature variation for this case. Figures 6.50 and 6.51 show the temperature and density contour respectively for isothermal boundary condition model.



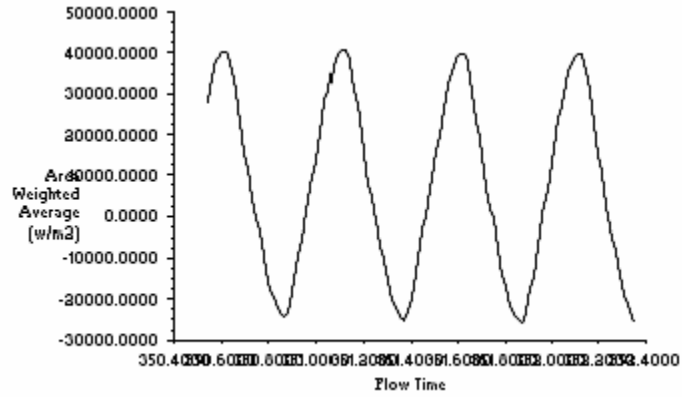


Fig.6.48 Heat transfer rate over a cycle at CHX for case3

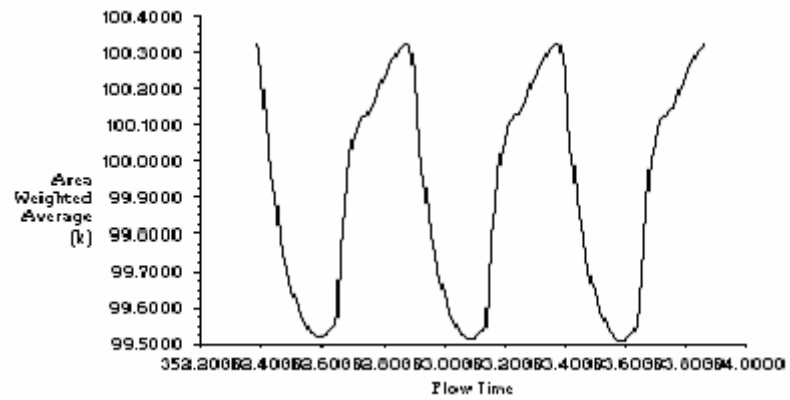


Fig.6.49 Wall temperature variation with time for case3

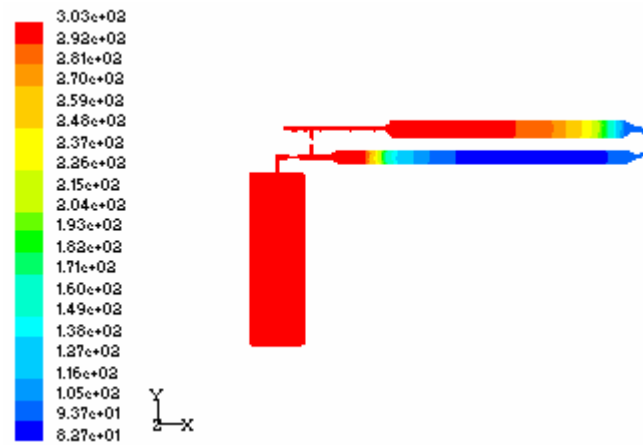


Fig.6.50 Temperature contour for case3.

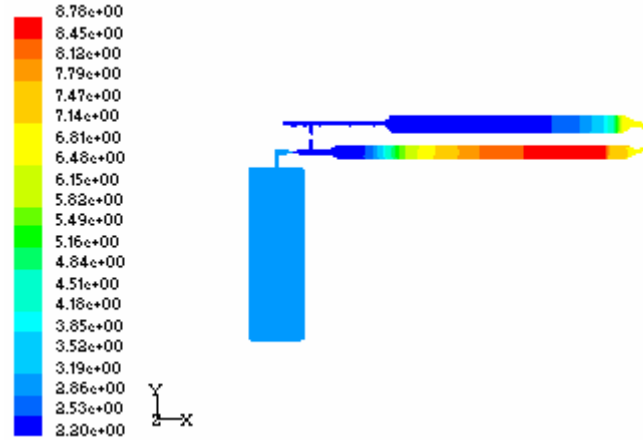


Fig.6.51 Density contours for case3.

- *Comparisons among case1 (a), case1 (b) and case1(c):*

Figure 6.52 depicts the mass flow rate variations with time over a cycle for case1 (a), case1 (b) and case1(c). From the figure it is clear that in case1 (a) the amplitude of mass flow rate is more as compared with case1 (b) and case1(c). This high mass flow rate amplitude causes more enthalpy flow from cold end to hot end in case1 (a). This provides minimum cold end temperature in case1 (a). From phase relation graphs in case1 (a) the phase lag between pressure and mass flow rate is minimum compared with case1 (b) and case1(c). Because of above two reasons case1 (a) provides better performance.

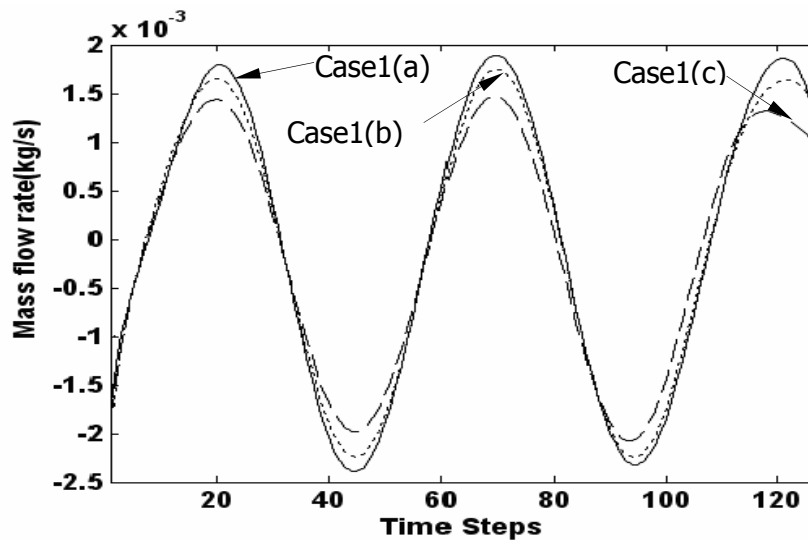


Fig.6.52 Mass flow rates through pulse tube cross section.

#### *6.5.4 Comparison with Experimental Data*

This part of the investigation is devoted to comparison of CFD simulation results with available experimental results. The DIPTR system consists of a rotary valve , an inlet pipe, an after cooler, regenerator, cold end heat exchanger , pulse tube , hot end heat exchanger , orifice valve, double inlet valve and reservoir. The dimensions of the DIPTR system are taken from [124]. The 3-dimensional geometry of the entire DIPTR is created in Gambit software (preprocessor of Fluent software). After meshing the geometry and defining various zones and continuum the gambit geometry is imported in Fluent (the solver). In Fluent the material properties and boundary conditions are specified as given in Table6.5.

The regenerator, after cooler, cold and hot heat exchangers are modeled as porous media. For modeling porous media in Fluent the important input parameters are porosity, viscous resistance and inertial resistance of the porous matrix. These parameters are calculated by using the Equ.(4.29) as discussed in chapter4. The Operational parameters of the porous media are given in Table4.1. For 200 mesh 304SS woven wire mesh the wire diameter is  $52\text{e-}6\text{m}$  , porosity is 0.679, pitch is  $127\text{e-}6\text{m}$ , mesh distance is  $75\text{e-}6\text{m}$  , opening area ratio is 0.349[155] . With these data using Equ. (4.29) the viscous resistance and inertial resistance factor are calculated and its values are  $4.15\text{e+}9(\text{m}^{-1})$  and  $1.214\text{e+}4(\text{m}^2)$  respectively. Similarly for after cooler, CHX and HHX copper wire of 100 mesh size is assumed in place of copper blocks with multiple holes, for which the wire diameter is  $10\text{e-}3\text{m}$ , pitch is  $63.5\text{e-}6\text{m}$ , porosity is 0.697 and the viscous and inertial resistance are  $1.085\text{e+}9(\text{m}^{-1})$  and  $5.75\text{e+}3(\text{m}^2)$  respectively. The procedure for numerical experimentation in Fluent is similar like real experimental procedure. First of all the orifice valve is optimized keeping double inlet valve closed. Now keeping orifice valve opening constant, the double inlet valve is adjusted for the best performance of the system. This is done by creating the geometry in Gambit and using boundary conditions. The particular combination of both valve opening provides minimum cold end temperature.

Some of the important results like pressure wave at inlet to regenerator, cool down behaviour, axial temperature distribution along pulse tube length and refrigeration load are compared and presented. Figure 6.53 depicts the comparison of experimental [123] and CFD simulation pressure wave at the inlet of regenerator of the GM type DIPTR. It can be seen that the experimental wave is in between the rectangular and sinusoidal shapes. However the

CFD simulation pressure wave is sinusoidal and the amplitude of both the pressure waves are same. The Figure 6.54 depicts the comparisons of cool down behaviour of CFD simulation and experimental results. The figure shows that there is a good agreement between CFD results and experimental result. The comparison of cooling power between the experimental and CFD simulation results are presented in Figure 6.55. This figure depicts that CFD results are in agreement with the experimental results. Figure 6.56 depicts comparisons of experimental and CFD simulation temperature distribution along the pulse tube length. The nature of both the curves is almost same. The discrepancy between the theoretical and experimental results is due to the unaccounted inefficiency losses in the system such as thermal mass effect, heat conduction through the wall, etc.

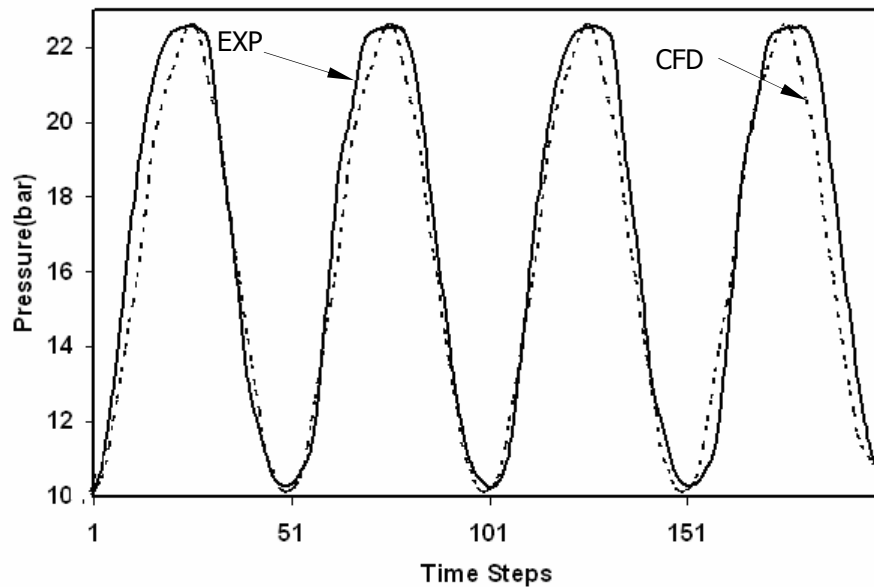


Fig.6.53 Comparison of pressure wave at the inlet of regenerator.

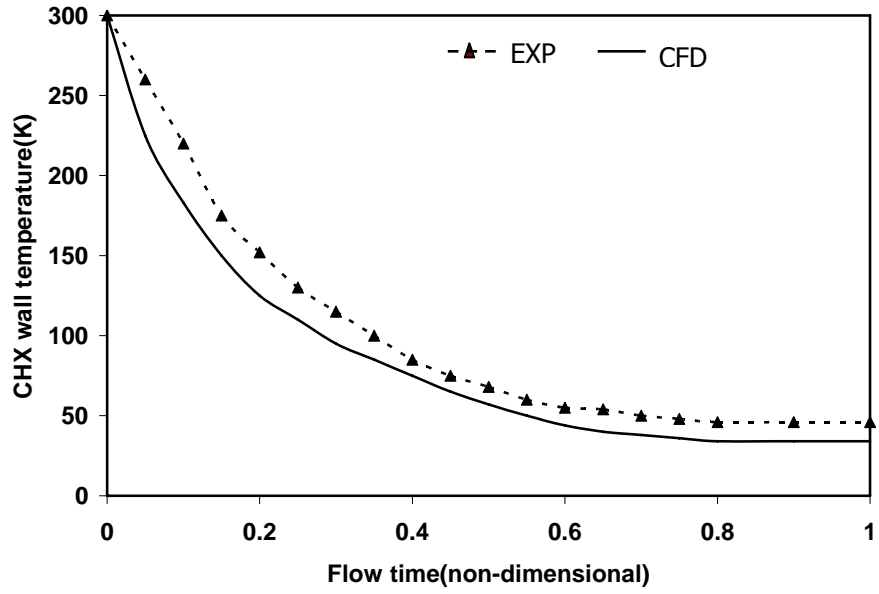


Fig.6.54 Comparison of cool down behaviour.

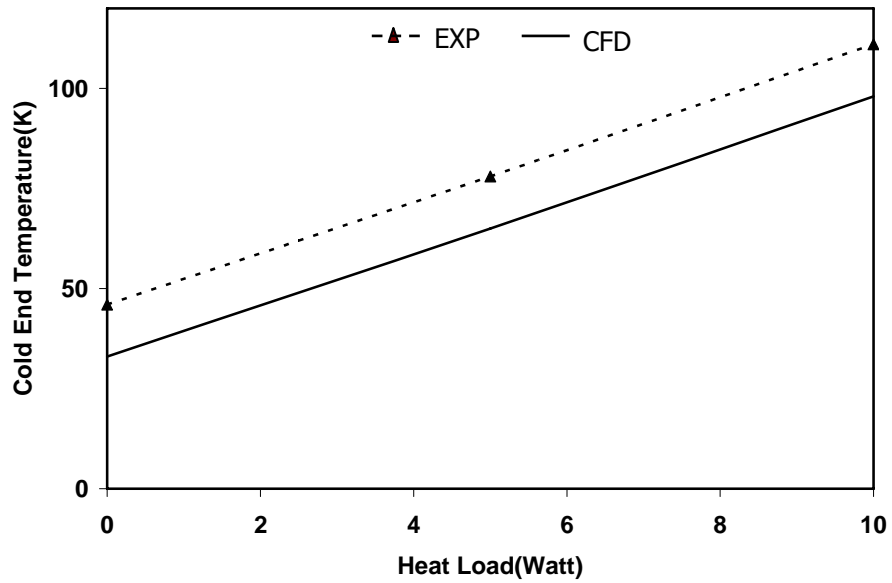


Fig.6.55 Comparison of heat load.

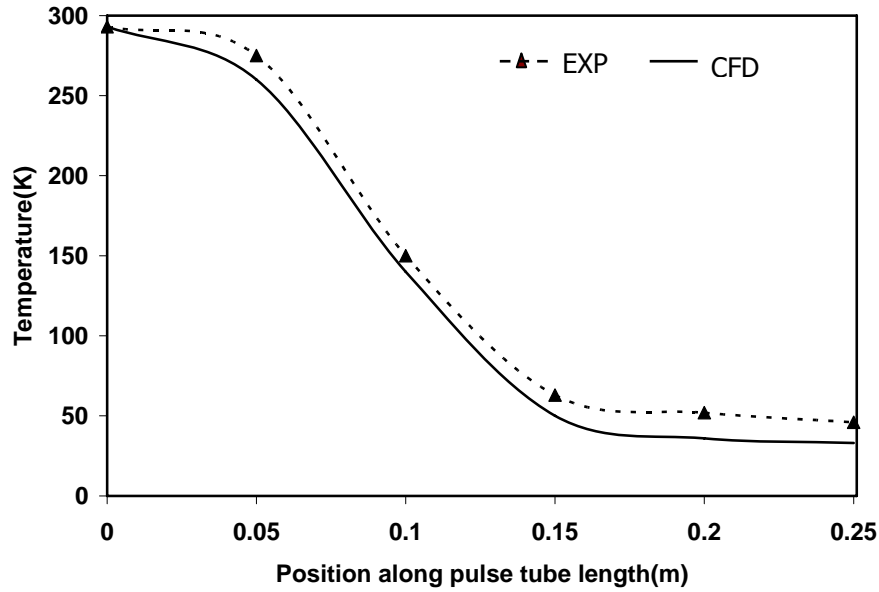


Fig.6.56 Comparison of temperature variation along the pulse tube length.

### 6.5.5 Discussion

The simulation results show that in case of adiabatic cold-end heat exchanger (CHX) for case1 the temperature achieved at cold end is 33 K for 40% DI valve and 60% orifice valve opening. When a constant heat load of 5W is imposed at CHX, the temperature achieved at cold end is 61K. The refrigerating load obtained at CHX is 8.2W, when it is maintained at 100K. Table 6.8 shows the summery of results obtained for different boundary conditions.

Table 6.8 Summery of result of 3-D simulation of DIPTR

	Adiabatic (Achieved Temp)	Const Heat Flux (Achieved Temp)	Const Temp (Achieved load)
DIPTR	33K	61K	8.2W

The comparison of CFD results with experimental data reveals that both the results are in excellent agreement. The little discrepancy between these two may be due to the finite wall thickness of the pulse tube components, unaccounted inefficiency of the system and experimental uncertainty.

## *Chapter VII*

# Conclusions

### *7.1 Highlights of Stirling type PTR Models*

In this study, the commercial computational fluid dynamic (CFD) package, Fluent is utilized for modeling the pulse tube system. In the first part of study, single stage Stirling type ITPTR and OPTR systems that includes a compressor, an after cooler, a regenerator, a pulse tube, cold and warm heat exchangers, an inertance tube/orifice valve and a reservoir are taken. The simulations represent a fully-coupled system operating in steady periodic mode, without any arbitrary assumptions other than ideal gas and no gravity effect. The sole external boundary conditions imposed on the model are a sinusoidal oscillating piston face velocity along with one of the thermal boundary conditions, adiabatic, isothermal or known heat flux at the cold end heat exchanger. The objective is to compare the performance of ITPTR and OPTR. In order to observe the difference of refrigeration performance between inertance type pulse tube and orifice type pulse tube refrigerators, pressure wave of same amplitude and frequency are applied. The physical dimensions of other components are kept same except that inertance tube is replaced by an orifice valve.

For each system three separate simulations are analyzed. One simulation assumes an adiabatic cold-end heat exchanger (CHX); another assumes a known cooling heat load, and the last assumes a pre-specified CHX temperature. Each simulation started with an assumed uniform system temperature, and continued until steady periodic conditions are achieved. The transient CFD model successfully predicts pulse tube refrigerator performance through solving the Navier–Stokes Equations for fluid momentum and heat transfer, along with an ideal gas equation. The result shows that the performance of the ITPTR is superior to that of OPTR.

The use of the ITPTR configuration offers a better potential for higher performance and efficiency. The improvement can be explained in terms of mass flow rate inside the pulse tube and the favourable phase relation between the mass flow rate and pressure at the cold end section of the pulse tube.

## *7.2 Highlights of G-M type Double Inlet Pulse Tube Refrigerators*

### *7.2.1 Highlights of DIPTR 2D Simulations*

This is the second part of the study where G-M type double inlet PTR is considered. Similar to Stirling type model, in this study, the commercial computational fluid dynamic (CFD) package, Fluent is utilized for modeling the G-M type DIPTR system. The simulation represents an integrated system operating in steady periodic mode, without any arbitrary assumptions. Initially the valve openings (orifice and double inlet valve) are optimized to achieve minimum temperature at the adiabatic condition of cold end heat exchanger. This optimized valve openings are used for other boundary conditions i.e., known heat load and isothermal conditions. In this simulation the physical dimensions of all the components are kept constant and pressure input is generated from the same UDF (User Defined Function).

In the DIPTR system, five separate simulations are analyzed. For adiabatic cold end boundary conditions three cases are simulated to optimize the valve openings. Based on this optimized valve opening, simulations are performed on other boundary conditions. Each simulation started with an assumed uniform system temperature, and continued until steady periodic conditions are achieved.

The results showed that CFD simulations are capable of elucidating the complex periodic processes in DIPTR very well. This simulation is compared with the available experimental data. The result shows that the comparison is satisfactory under the limitation of 2D numerical model.

### *7.2.2 Highlights of DIPTR 3D Simulations*

The CFD simulation is extended to 3D simulations of DIPTR. For 3D simulations of DIPTR system three separate simulations are analyzed. First simulation assumed an adiabatic cold heat exchanger, second assumed a known heat load, and the third simulation assumed a



pre-specified cold heat exchanger temperature. In the first simulation with adiabatic boundary condition, the optimized valve openings are evaluated in order to achieve the lowest temperature. This optimized valve openings are retained for the other boundary conditions.

The simulation results are compared with the available experimental results. There is an excellent agreement of simulation result with the experimental data. These conclusions lead that numerical simulation by Fluent is capable of designing and optimizing the pulse tube refrigerator.

### *7.3 Scope of Future Work*

The Fluent simulation results presented and discussed in this dissertation provide reasonable predictions that have expected trends everywhere. Such CFD simulations provide very valuable details about local and instantaneous thermo-fluid process. However some of the important suggestions for the extensive CFD simulations for future work are as follows:

- (i) In the Fluent simulation the wall thickness of the components are neglected. However there is always some conductance loss. Extensive studies are needed to account these effects.
- (ii) The Fluent simulation of rotary valve to generate pressure wave in a GM type PTR is complex. It becomes more complex when this rotary valve is integrated with the pulse tube system. An extensive study is needed to simulate the entire GM type pulse tube system.
- (iii) At present, multistage pulse tube are commonly used for different application. So numerical simulations need its extension for analysis of these equipment.

## *References*

1. Gifford, W.E. and Longworth, R.C. Pulse tube refrigeration, *Trans ASME B J Eng Industry* 86(1964), pp.264-267.
2. Gifford, W.E. and Longworth, R.C. Pulse tube refrigeration progress, *Advances in cryogenic engineering* 3B (1964), pp.69-79.
3. Gifford, W.E. and Longworth, R.C. Surface heat pumping, *Advances in cryogenic engineering* 11(1966), pp.171-179.
4. Gifford, W.E. and Kyanka, G.H. Reversible pulse tube refrigerator, *Advances in cryogenic engineering* 12(1967), pp.619-630.
5. de Boer, P. C. T., Thermodynamic analysis of the basic pulse-tube refrigerator, *Cryogenics*34(1994) ,pp. 699-711 .
6. de Boer, P. C. T., Analysis of basic pulse-tube refrigerator with regenerator, *Cryogenics*, 36(1996) ,pp. 547-553.
7. Soo J. E., Secondary flow in basic pulse tube refrigerators, *Cryogenics*36 (1996), pp.317-323.
8. Storch, P.J. and Radebaugh, R Development and experimental test of an analytical model of the orifice pulse tube refrigerator, *Advances in cryogenic engineering* 33(1988), pp.851-859.
9. Wu, P. and Zhu, S. Mechanism and numerical analysis of orifice pulse tube refrigerator with a valve less compressor, *Proc. Int. Conf., Cryogenica and Refrigeration* (1989), pp. 85-90.
10. Richardson, R. N., Valved pulse tube refrigerator development, *Cryogenics*30 (1989), pp. 850-853.
11. Tward, E. Chan, C.K. and Burt, W.W. Pulse tube performance, *Advances in cryogenic engineering* 35(1990), pp.1207-1220.
12. Lee, J.M. and Dill, H.R. The influences of gas velocity on surface heat pumping for the orifice pulse tube refrigerator, *Advances in cryogenic engineering* 35(1990), pp.1223-1229.
13. Kasuya M, Yuyama J, Geng Q, Goto E. Optimum phase angle between pressure and gas displacement oscillations in a pulse tube refrigerator *Cryogenics*32 (1992), pp. 303-8.
14. Wang, Chao, Wu, Peiyi and Chen, Zhongqi, Numerical modeling of an orifice pulse tube refrigerator, *Cryogenics*32 (1992), pp. 785-790.
15. Kittel, P., Ideal orifice pulse tube refrigerator performance, *Cryogenics*32 (1992), pp. 843-844.

16. David, M., Marechal, J. -C., Simon, Y. and Guilpin, C., Theory of ideal orifice pulse tube refrigerator, *Cryogenics*33 (1993), pp. 154-161.
17. Storch, P.J. and Radebaugh, R. Development and experimental test of an analytical model of the orifice pulse tube refrigerator, *Advances in cryogenic engineering* 33(1988), pp.851-859.
18. Zhu, S. W. and Chen, Z. Q., Isothermal model of pulse tube refrigerator, *Cryogenics*34 (1994), pp. 591-595.
19. Wu, P.Y., Zhang, Li. Qian, L.L. and Zhang, L. Numerical modeling of orifice pulse tube refrigerator by using the method of characteristics, *Advances in cryogenic engineering* 39(1994), pp.1417-1431.
20. Kittel, P., Lee, J.M., and Timmerhaus, K. D. Steady Secondary Momentum and Enthalpy Streaming in the Pulse Tube refrigerator. *Cryocooler* 8(1994), June 28-30.
21. Roach, P.R. and Kashani, A. A simple modeling program for orifice pulse tube coolers, *Advances in cryogenic engineering*, (1995).
22. Rawlins, W., Radebaugh, R. and Bradley, P.E., Energy flows in an orifice pulse tube refrigerator" *Advances in cryogenic engineering* 39(1994), pp.1425-1431.
23. Kittel P., Kashani, A. Lee, J. M. and Roach, P. R., General pulse tube theory, *Cryogenics*, 36(1996), pp.849-857.
24. Huang, B. J. and Chuang, M. D., System design of orifice pulse-tube refrigerator using linear flow network analysis *Cryogenics*,36(1996) , pp.889-902.
25. Xu, M. Y., He, Y. L. and Chen, Z. Q., Analysis of an orifice pulse tube refrigerator using the method of characteristics, *Cryogenics*, 39(1999), pp. 751-757.
26. Kuriyama and Radebaugh R., Analysis of mass and energy flow rates in an orifice pulse-tube refrigerator .*Cryogenics*, 39(1999), pp. 85-92.
27. de Waele ,A. T. A. M., Steijaert P. P. and Koning, J. J., Thermodynamical aspects of pulse tubes II . *Cryogenics*, 38(1998), pp.329-335.
28. de Waele A. T. A. M., Optimization of pulse tubes .*Cryogenics*,39(1999) pp. 13-15.
29. Gerster J., Thürk M., Reißig L. and Seidel P., Hot end loss at pulse tube refrigerators, *Cryogenics*, 38(1998), pp. 679-682.
30. Hagiwara, Nara, Y., K., Ito S. and Saito T., Temperature measurement in pulse tube with Rayleigh scattering and computation of enthalpy flow. *Cryogenics*, 39(1999), pp. 425-434.
31. de Boer ,P. C. T., Optimization of the orifice pulse tube ,*Cryogenics* 40(2000) ,pp.701-711
32. Roach R., A Simple Modeling Program for Orifice Pulse Tube Coolers NASA Ames Research Center (2004).

33. Deshai K.P. , H.B. Naik, Narayankhedkar K.G. , Phasor analysis of Orifice Pulse Tube Refrigerator, Proceedings of ICEC18, Mumbai, India 2000.
34. Smith W. R., One-dimensional models for heat and mass transfer in pulse-tube refrigerators. *Cryogenics*, 41(2001), pp.573-582.
35. Zhu Shaowei, Wu Peiyi and Chen Zhongqi, Double inlet pulse tube refrigerators: an important improvement, *Cryogenics*30 (1990), pp. 514-520.
36. Ju Y. L., Wang C. and Zhou Y. , Numerical simulation and experimental verification of the oscillating flow in pulse tube refrigerator, *Cryogenics*, 38(1998), pp.169-176.
37. Wang, C., Wu, P. and Chen, Z., Numerical analysis of double-inlet pulse tube refrigerator, *Cryogenics*33 (1993), pp.526-530.
38. Harold Mirels Double inlet pulse tube cryocooler with steeped piston compressor, *Advances in cryogenic engineering* 39(1994), pp.1425-1431.
39. Zhu Shaowei, Kawano Shin, Nogawa Masahumi and Inoue Tatsuo, Work loss in double-inlet pulse tube refrigerators .*Cryogenics*, 38(1998) ,pp. 803-807.
40. Kirkconnell, C. S. 1995. Numerical analysis of the mass flow and thermal behavior in high-frequency pulse tubes. Ph.D. Thesis, Georgia Institute of Technology, Atlanta, Ga.
41. Zhu Shaowei and Chen Zhongqi, Enthalpy flow rate of a pulse tube in pulse tube refrigerator .*Cryogenics*, 38(1998), pp.1213-1216.
42. Thummes G. and Heiden C. Control of DC gas flow in a single-stage double-inlet pulse tube cooler *Cryogenics* 38 (1998) 843–847C. Institute of Applied Physics, University of Giessen,
43. Liang, J., Ravex, A. and Rolland, P., Study on pulse tube refrigeration Part 1: Thermodynamic nonsymmetry effect .*Cryogenics*, 36(1996), pp. 87-93.
44. Liang, J., Ravex, A. and Rolland, P., Study on pulse tube refrigeration Part 2: Theoretical modeling, *Cryogenics*, 36(1996), pp. 95-99.
45. Hoffmann A. and Pan H., Phase shifting in pulse tube refrigerators, *Cryogenics*, 39(1999), pp. 529-537.
46. Yuan, J. and Pfothenhauer, J. M., Thermodynamic analysis of active valve pulse tube refrigerators .*Cryogenics*, 39(1999), pp. 283-292
47. Xu, M. Y., de Waele, A. T. A. M. and Ju Y. L., A pulse tube refrigerator below 2 K. *Cryogenics*, 39(1999), pp. 865-869.
48. de Boer P.C.T. "Characteristics of the double inlet pulse tube" *Cryogenics* 43 (2003) 379–391.

49. Chokhawala M.D., Deshai K.P. , H.B. Naik, Narayankhedkar K.G. , Phasor analysis for Double Inlet Pulse Tube Cryocooler, *Advances in cryogenic Engineering*, Vol 45, PP159-165.
50. Banjare Y.P. , Sahoo R.K., Sarangi S.K. Sarangi "Numerical analysis of double inlet pulse tube refrigerator" National conference on RECT, GGDU Bilaspur(C.G.) Chhattisgarh, India ,2007
51. Atrey, M.D. Bapat, S.L., Narayankhedkar K.G., Cyclic simulation of Stirling cryocoolers, *Cryogenics*(1990),Vol30, PP 341-347.
52. CEP Short term course"Cryocoolers –Theory, Design and Practice" 19-22 February 2008, Dept. of Mech. Engg. IIT, Bombay
53. Radebaugh, Ray. Development of the pulse tube refrigerator as an efficient and reliable cryocooler, *Proc. Institution of Refrigeration (London)* 1999-2000.
54. Popescu, G. Radcenco, V. Gargalian, E. and Ramany, Bala P. A critical review of pulse tube cryogenerator research, *International Journal of Refrigeration* 24(2001), pp. 230-237.
55. Zhang X.B., L.M. Qiu, Z.H. Gan, Y.L. He, Effects of reservoir volume on performance of pulse tube cooler, *International Journal of Refrigeration* 30 (2007) 11-18
56. Razani A., Dodson C., B. Flake and T. Roberts, The effect of phase-shifting mechanisms on the energy and exergy flow in pulse tube refrigerators, *Advances in Cryogenic Engineering* 2006, Vol 51, pp1572-1579, AIP Proceedings.
57. Ju, Y. L., Thermodynamic analysis of GM-type pulse tube coolers, *Cryogenics*, 41(2001), pp. 513-520.
58. Gardner D.L., Swift G.W., Use of inertance in orifice pulse tube refrigerators, *Cryogenics*, 37(1997), pp. 117-121.
59. Roach, P.R. and Kashani, A., Pulse tube coolers with an intertance tube: theory, modeling, and practice. In: *Advances in cryogenic engineering* 43, plenum press, New York (1998), pp.1895-1902.
60. de Boer, P. C. T., Performance of the inertance pulse tube , *Cryogenics* 42(2002),pp. 209-221.
61. Zhu, Shaowei and Matsubara, Yoichi. Numerical method of inertance tube pulse tube refrigerator, *Cryogenics*, 44(2004), pp. 649-660.
62. Wei Dai, Jianying Hu and Ercang Luo, Comparison of two different ways of using inertance tube in a pulse tube cooler, *Cryogenics* 46(2006), Pages 273-277.
63. Tward, E., Chan, Jaco, C. K., C., Godden, J., Chapsky, J. and Clancy, P. Miniature space pulse tube cryocoolers. *Cryogenics*, 39(1999), pp. 717-720.

64. de Waele, A.T.A.M., Xu, M.Y., Ju, Y. L. Non Ideal Gas Behavior in the Regenerator, *Cryogenics* 39(1999), pp. 847-851.
65. Von A. Schneidmesser, Thummes G. and Heiden C., Generation of liquid helium temperatures using a lead regenerator in a GM precooled pulse tube stage. *Cryogenics*, 40(2000), pp. 67-70.
66. Neveu Pierre and Babo Coret, A simplified model for pulse tube refrigeration, *Cryogenics*, 40(2000), pp. 191-201.
67. Chen, Guobang, Gan Zhihua, Thummes G. and Heiden C., Thermodynamic performance prediction of pulse tube refrigeration with mixture fluids. *Cryogenics*, 40(2000), pp. 261-267.
68. Baek, Sang Ho, Jeong, Eun Soo and Jeon, Sangkwon, Two-dimensional model for tapered pulse tubes. Part 1: theoretical modeling and net enthalpy flow, *Cryogenics*, 40(2000), pp. 379-385.
69. Baek, Sang Ho, Jeong, Eun Soo and Jeon, Sangkwon, Two-dimensional model for tapered pulse tubes. Part 2: mass streaming and streaming-driven enthalpy flow loss, *Cryogenics*, 40(2000) Pages 387-392.
70. de Waele ,A. T. A. M., Tanaeva ,I. A. and Ju ,Y. L., Multistage pulse tubes , *Cryogenics*,40(2000) ,pp. 459-464.
71. Gao, C. M., He, Y. L. and Chen, Z. Q., Study on a pulse tube cryocooler using gas mixture as its working fluid. *Cryogenics*, 40(2000), pp. 475-480.
72. Lu, Guoqiang and Cheng, Ping, Flow characteristics of a metering valve in a pulse tube refrigerator. *Cryogenics*, 40(2000), pp. 721-727
73. de Waele, A.T.A.M., Xu,M. Y. and Ju, Y. L. pulse –tube performance at very low temperature ,*Physica B: Condensed Matter* 284-2288(2000),pp.2018-2019.
74. Pan, H., Hoffmann, A. and Oellrich, L., Single-stage 4-valve and active buffer pulse tube refrigerators, *Cryogenics*, 41(2001), pp.281-284.
75. Brito, M. C. and Peskett, G. D., Numerical model of free warm expander pulse tube cooler. *Cryogenics*, 41(2001), pp. 751-755.
76. Park Hee Chan, Jeong Eun Soo and Jeong Sangkwon. Two-dimensional model for tapered pulse tubes: Part 3: unsteady components of second-order mass flux and temperature, *Cryogenics*, 42(2002), pp. 485-493.
77. Graziani A. Dall'Oglio G., L. Martinis, L. Pizzo and L. Sabbatini "A new generation of 3He refrigerators " *Cryogenics* 43 (2003) 659–662.
78. Waldauf, A., Thürk, M. and Seidel, P. Observation and control of temperature instabilities in a four-valve pulse tube refrigerator *Cryogenics*, 44(2004), pp. 75-79.

79. Masao Shiraishi, Koichi Takamatsu, Masahide Murakami and Akihiro Nakano. Dependence of convective secondary flow on inclination angle in an inclined pulse tube refrigerator revealed by visualization. *Cryogenics*, 44(2004), pp. 101-107.
80. Ronald, G. Jr. and Johnson, Dean L. Effect of gravity orientation on the thermal performance of Stirling-type pulse tube cryocoolers *Cryogenics*, 44(2004), pp. 403-408.
81. Will, M. E., Tanaeva, I. A., Li, R. and de Waele, A. T. A. M. New rotary valves for pulse-tube refrigerators, *Cryogenics*, 44(2004), pp.793-800.
82. Jiang, N., Lindemann, U., Giebeler, F. and Thumme, G. A <sup>3</sup>He pulse tube cooler operating down to 1.3 K *Cryogenics*, 44(2004), pp.809-816.
83. Devlin, M. J., Dicker, S. R., Klein, J. and Supanich, M. P. A high capacity completely closed-cycle 250 mK <sup>3</sup>He refrigeration system based on a pulse tube cooler, *Cryogenics*, 44(2004), pp. 611-616.
84. He, Ya Ling, Wu, Ming, Tao, Wen-Quan, Chen Zhong-Qi Improvement of the thermal performance of pulse tube refrigerator by using a general principle for enhancing energy transport and conversion process, *Applied Thermal Engg.*24 (2004), pp.79-93.
85. Yang, L.W. and Thummes, G. High frequency two-stage pulse tube cryocooler with base temperature below 20 K, *Cryogenics*, 45(2005), pp. 155-159.
86. Dang, H.Z., Ju, Y.L., Liang, J.T., Cai, J.H., Zhao, M.G. and Zhou, Y. Performance of Stirling-type non-magnetic and non-metallic co-axial pulse tube cryocoolers for high-T<sub>c</sub> SQUIDs operation, *Cryogenics*, 45(2005), pp. 213-223.
87. Jung, Jeheon and Jeong, Sangkwon. Expansion efficiency of pulse tube in pulse tube refrigerator including shuttle heat transfer effect. *Cryogenics*, 45(2005), pp. 386-396.
88. Yong, Xiaoqin, Chung, J.N. Size effect on Miniature Stirling Cycle Cryocooler, *Cryogenics*, 45 (2005), pp.537-545.
89. Tanaeva, I.A. and de Waele, A.T.A.M. A small helium-3 pulse-tube refrigerator. *Cryogenics*, 45(2005), pp. 578-584.
90. Qiu, Limin, He Yonglin, Gan Zhihua, Wan Laihong & Chen Guobang A separate two-stage pulse tube cooler working at liquid helium temperature *Chinese Science Bulletin* 2005 Vol. 50 No. 1 January 2005,pp1-4.
91. Will M.E. and A.T.A.M. de Waele, Analytical treatment of counter flow pulse-tube refrigerators, *Cryogenics* 46(2006), Pages 421-431.
92. Koettig T., S. Moldenhauer, R. Nawrodt, M. Thürk, P. Seidel, Two-stage pulse tube refrigerator in an entire coaxial configuration, *Cryogenics* 46(2006),pp888-891.

93. Ling H. Y , Jing Huang, Zhao Chun-Feng, Liu Ying-Wen First and second law analysis of pulse tube refrigerator Applied Thermal Engineering 26 (2006) 2301–2307
94. Razani A.i, T. Roberts, B. Flake, A thermodynamic model based on exergy flow for analysis and optimization of pulse tube refrigerators, Cryogenics47,2007,166–173.
95. Richardson, R. N. Development of a practical pulse tube refrigerator: co-axial designs and the influence of viscosity. Cryogenics28 (1988), pp.516-520.
96. Longsworth, R.C. An experimental investigation of pulse tube refrigeration heat pumping rates, Advances in cryogenic engineering 12(1967), pp.608-618.
97. Mikulin, E.I., Tarasow, A.A. and Shkrebyonock, M.P. Low temperature expansion pulse tube, Advances in cryogenic engineering 29(1984), pp.629-637.
98. Radebaugh, R., Zimmermann, J.D., Smith, R. and Louie, B.A. Comparison of three types of pulse tube refrigerators: new methods for reaching 60K, Advances in cryogenic engineering 31(1986), pp.779-789.
99. Narayankhedkar,K. G. and Mane, V.D. Investigation of pulse tube refrigerator ,Journal of Engineering for Industry, (1973) pp. 373-378.
100. Richardson R.N., Pulse tube refrigerator- an alternative cryocooler, Cryogenics26 (1986), pp. 331-340.
101. Zhou, Y. Zhu, W. and Sun, Y. Pulse tube with axial curvature, Advances in cryogenic engineering 33(1988), pp.860-868.
102. Liang, J. Zhou. and Zhu, W. Development of a single stage pulse tube refrigerator capable of reaching 49K. Cryogenics 30(1990), pp. 49-51.
103. Baks, M. J. A., Hirsch berg, Ceelen, A., B. J. van der and Gijsman, H. M. Experimental verification of an analytical model for orifice pulse tube refrigeration, Cryogenics30 (1990), pp. 947-951.
104. Kasuya, M., Nakatsu, M., Geng, Q., Yuyama, J. and Goto, E., Work and heat flows in a pulse-tube refrigerator .Cryogenics31 (1991), pp.786-790.
105. Cai, J. H., Zhou, Y., Wang, J. J. and Zhu, W. X., Experimental analysis of double-inlet principle in pulse tube refrigerators, Cryogenics 33(1993), pp.522-525.
106. Wang, C., Wu, P. and Chen, Z. Q., Theoretical and experimental studies of a double-inlet reversible pulse tube refrigerator. Cryogenics33 (1993), pp.648-652.
107. Yuyama, J. and Kasuya, M., Experimental study on refrigeration losses in pulse tube refrigerator, Cryogenics33 (1993), pp. 1132-1136.
108. Huang, B. J. and Tzeng, T. M., Performance characteristics of pulse tube refrigerators, Cryogenics33 (1993), pp. 1132-1136.



109. Wang, C., Wu, P. and Chen,Z., Modified orifice pulse tube refrigerator without reservoir. *Cryogenics*34 (1994), pp. 25-30.
110. Gao, J. L. and Matsubara, Y. Experimental investigation of 4 K pulse tube refrigerator, *Cryogenics*34 (1994), pp.25-30.
111. Cai, J. H., Wang, J. J., Zhu, W. X. and Zhou, Y., Experimental analysis of the multi-bypass principle in pulse tube refrigerators. *Cryogenics*34 (1994), pp. 713-715.
112. Wang, C., S. Wang, Q., Cai, J. H. and Yuan, Z., Experimental study of multi-bypass pulse-tube refrigerator, *Cryogenics*, 36(1996), pp. 555-558.
113. Liang, J., Ravex, A. and Rolland, P, Study on pulse tube refrigeration Part 3: Experimental verification, *Cryogenics*, 36(1996), pp.101-106.
114. Xu, M., He, Y., Wu, P. and Chen, Z., Experimental research of a miniature coaxial pulse tube refrigerator using nylon tube .*Cryogenics*,36(1996) ,pp.131-133.
115. Kirkconnell, C. S., Soloski, S.C., and Price, K. D., 1997. Experiments on the effects of pulse tube geometry on PTR performance. *Cryocoolers 9*, Plenum Press, New York and London, 285.
116. Zhu Shaowei, Kakimi, Yasuhiro and Matsubara, Yoichi, Waiting time effect of a GM type orifice pulse tube refrigerator. *Cryogenics*, 38(1998), pp.619-624.
117. Yang Luwei, Zhou Yuan and Liang Jingta, DC flow analysis and second orifice version pulse tube refrigerator .*Cryogenics*, 39(1999) ,pp. 187-192.
118. Yang Luwei, Zhou Yuan and Liang Jingtao, Research of pulse tube refrigerator with high and low temperature double-inlet .*Cryogenics*, 39(1999) pp. 417-423
119. Luwei,Y., Zhou Yuan, Liang Jingtao and Zhu Wenxiu, Analytical study of the performance of pulse tube refrigerator with symmetry-nozzle, *Cryogenics*, 39(1999), pp.723-727.
120. Charles, I., Duband, L. and Ravex, A., Permanent flow in low and high frequency pulse tube coolers – experimental results ,*Cryogenics*, 39(1999), pp. 777-782.
121. Von A. Schneidmesser, Thummes, G. and Heiden, C., Performance of a single-stage 4 K pulse tube cooler with neodymium regenerator precooled with a single-stage GM refrigerator .*Cryogenics*, 39(1999),pp.783-789.
122. Gan Z. H., Chen G. B., Thummes G. and Heiden C., Experimental study on pulse tube refrigeration with helium and nitrogen mixtures, *Cryogenics* 40(2000), pp. 333-339.
123. Kasthuriengan S., Jacob S., Karunanithi R., Nadig D.S. and Behera Upendra. "Indigenous Development of Rotary valve for Cryocooler Applications", *Journal of Instrument Society of India*,2001

124. Kasthuriengan S., Jacob S., Karunanithi R., Nadig D.S. and Behera Upendra. "A six watt single stage pulse tube refrigerator operating at 77K", Journal of Instrument Society of India,2001
125. Kasthuriengan S., Jacob S., Karunanithi R., Development and studies on convection free single stage pulse tube cooler operating at 77K, Final Technical Report, April 2000, Centre for cryogenic Technology IISC, Bangalore.
126. Karunanithi R., Kasthuriengan S. and Jacob S. "Design and Development of a single stage double inlet pulse tube refrigerator" Proceedings of ICEC 18, Mumbai, India 2000.
127. Huang, B.J. and Yu ,G. L., Experimental study on the design of orifice pulse tube refrigerator, International Journal of Refrigeration,24(2001),400-408.
128. Roy P. C., Sarangi S.K., Das P.K. Some theoretical and Experimental Studies on Pulse tube refrigeration, MS Thesis, Dept. of Mech. Engg. IIT Kharagpur, 2003.
129. Ju, Y.L., He G.Q., Hou, Y.K. Experimental measurement of the flow resistance and inductance of inertance tube of high acoustic amplitudes, Cryogenics43, 2003, pp. 1-7.
130. Lu, G.Q., Cheng P., Numerical and experimental study of a Gifford-McMahon–Type Pulse Tube Refrigerator, Journal of Thermophyscs and Heat transfer Vol.17, No.4, (2003) pp. 457-463.
131. Shinji Masuyama, Yang-Hun Kim, Seong-Je Park, Yong-Ju Hong, Hyo-Bong Kim and Sung-Hong Lee, Experimental research of Stirling type pulse tube refrigerator with an active phase control, Cryogenics 46(2006), Pages 385-390.
132. Wang K., Q.R. Zheng, C. Zhang, W.S. Lin, X.S. Lu and A.Z. Gu, The experimental investigation of a pulse tube refrigerator with a 'L' type pulse tube and two orifice valves, Cryogenics 46(2006), Pages 643-647.
133. Koettig T., S. Moldenhauer, M. Patze, M. Thurk, P. Seidel, Investigation on the internal thermal link of pulse tube refrigerators, Cryogenics 47(2007),pp 137-142.
134. Barrett Flake and Arsalan Razani .Modeling Pulse Tube Cryocooler with CFD, Adv in Cry Engg 49 (2004) AIP Proceedings pp 1493-1499.
135. Yarbrough A., Flake B.A , Razani A. Computational fluid dynamic modeling of pressure drop through wire mesh (AIP Proceeding) (Adv in Cry Engg.49(2004)pp1338-45
136. Jiao, Anjun, Jeong, Sangkwon and Ma, H. B. Heat transfer characteristics of cryogenic helium gas through a miniature tube with a large temperature difference , Cryogenics,44(2004), pp. 859-866
137. Cha, J.S. Ghiaasiaan S.M, Desai P.V. Harvey J.P and Kirkconnell C.S. "Multi-dimensional flow effects in pulse tube refrigerators" Cryogenics 46 (2006) 658–665.

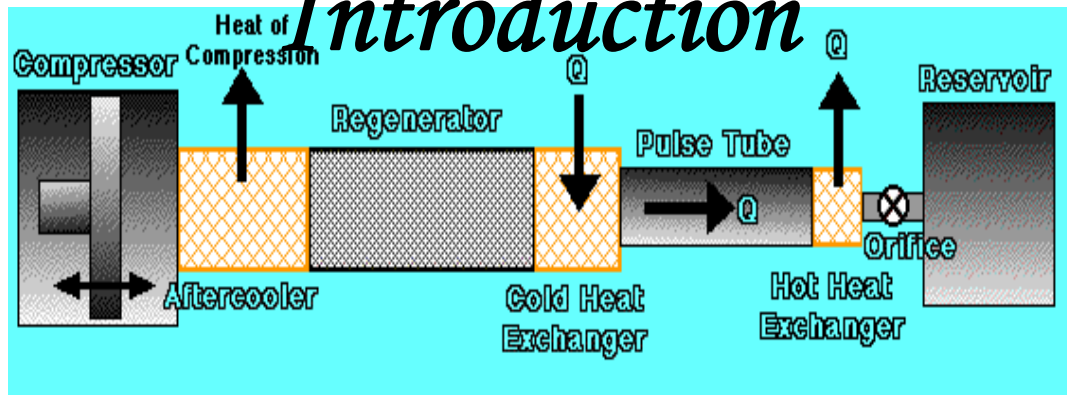
138. Gustafson S., B. Flake, A. Razani, CFD Simulation of Oscillating Flow in an Inertance tube and its Comparison to other Models, *Advances in Cryogenic Engineering* 2006, Vol 51, pp1497-1507, AIP Proceedings.
139. Zhang X. B., Qui L. M., Gan Z. H., He Y.L., CFD study of a simple orifice pulse tube cooler, *Cryogenics* 47 (2007) 315–321.
140. Xiao-bin Zhang, Zhi-hua Gan, Li-Min Qui, Computational fluid dynamics simulation of an inter-phasing pulse tube cooler. *Journal of Zhejiang University Science A* 2008 9(1) 93-38.
141. Banjare Y.P., Sahoo R.K., Sarangi S. K. "CFD Simulation of Inertance tube Pulse Tube Refrigerator. 19<sup>th</sup> National and 8<sup>th</sup> ISHMT-ASME Heat and Mass Transfer Conference JNTU College of Engineering Hyderabad, India January 3-5, 2008 .Paper No. EXM-7, PP34.
142. Banjare Y.P., Sahoo R.K., Sarangi S. K.,"CFD Simulation of Orifice Pulse Tube Refrigerators" International Conference on "Recent trends in Mechanical Engineering IRCTME 2007, Dept. of Mech. Engg. Ujjain Engg College Ujjain October 4-6, 2007, Paper no. HT1, pp235-45.
143. Roach, P. R. and Kashani, A. Theoretical analysis of a pulse tube regenerator, *Advances in cryogenic engineering*, (1995), Vol. 41 pp.1357.
144. de Waele ,A. T. A. M. Hooijkass, H. W. G. Steijaert P. P. and Benschop A.A.J. Regenerator dynamics in the harmonic approximation, *Cryogenics*, 38(1998), pp.995-1006.
145. Liang, J., Zhou, Y., Zhu, W., Sun, W., Yang, J. and Li, S., Study on miniature pulse tube cryocooler for space application, *Cryogenics*, 40(2000), pp. 229-233.
146. Yonglin J U "On the oscillating flow behavior of pulse tube Refrigerators" International Congress of Refrigeration 2003. Page 1-8.
147. Nam, Kwanwoo and Jeong, Sangkwon. Measurement of cryogenic regenerator characteristics under oscillating flow and pulsating pressure, *Cryogenics*, 43(2003), pp. 575-581.
148. Zhu, Shaowei and Matsubara, Yoichi, A numerical method of regenerator, *Cryogenics*, 44(2004), pp. 131-140.
149. Choi, Sungryel, Nam, Kwanwoo and Jeong, Sangkwon. Investigation on the pressure drop characteristics of cryocooler regenerators under oscillating flow and pulsating pressure conditions *Cryogenics*, 44(2004), pp. 203-210.
150. Chen, G.B. Tang, K., Huang, Y.H., Gan, Z.H. and Bao,R.Refrigeration performance enhancement of pulse tube refrigerators with He-H<sub>2</sub> mixture and Er<sub>3</sub>NiHx regenerative material, *Cryogenics*44(2004), pp. 833-837.
151. Razani, C. Dodson, B. Flake and T. Roberts The effect of phase-shifting mechanisms on the energy and exergy flow in pulse tube refrigerators. *Adv Cry Engg* 49 (2004) pp1572-1579.

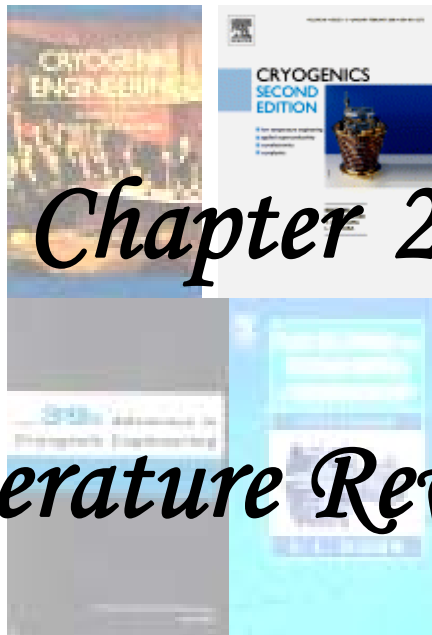
152. Nam, Kwanwoo and Jeong, Sangkwon. Novel flow analysis of regenerator under oscillating flow with pulsating pressure. *Cryogenics*, 45(2005), pp. 368-379.
153. Qiu, L.M., He, Y.L., Gan, Z.H. and Chen, G.B. A single-stage pulse tube cooler reached 12.6 K. *Cryogenics*, 45(2005), pp. 641-643.
154. Kwanwoo Nam, Sangknow Jeong Investigation of oscillating flow friction factor for Cryocooler regenerator considering cryogenic temperature effect, *Cryogenic* 45(2006) Page 733-738.
155. Kwanwoo Nam and Sangkwon Jeong, Development of parallel wire regenerator for cryocoolers, *Cryogenics* 46(2006), Pages 278-287.
156. Cha J. S., Ghiaasiaan S. M. and Desai P.V., Measurement of Anisotropic Hydrodynamic Parameters of Pulse Tube or Stirling Cryocooler Regenerators, Georgia Institute of Technology Atlanta, Ga, 30332, USA, *Advances in Cryogenic Engineering* 2006, Vol 51, pp1911-18, AIP Proceedings.
157. Wang K., Y.L. Ju, X.S. Lu, A.Z. Gu, On the performance of copper foaming metal in the heat exchangers of pulse tube refrigerator, *Cryogenics* 47(2007), pp 19-24.
158. Qiu L.M., Y.L. He, Z.H. Gan, X.B. Zhang, G.B. Chen, Regenerator performance improvement of a single-stage pulse tube cooler reached 11.1 K, *Cryogenics* 47 (2007) 49–55.
159. Yanyan Chen , Ercang Luo , Wei Dai, Heat transfer characteristics of oscillating flow regenerator filled with circular tubes or parallel plates, *Cryogenics* 47(2007)40–48.
160. Bernd Thomas, Deborah Pittman, Update on the evaluation of the different correlations for the flow friction factor and heat transfer of Stirling type engine regenerators. *American institute of Aeronautics* 2000. pp 76-83.
161. Robbert AA. *Cryogenic regenerative heat exchangers*. New York; Plenum Press; 1997.
162. Wheatly, J. C., Hofler, T., Swift G.W., and Migliori, A. Understanding some simple phenomenon in thermo acoustics with application to acoustical heat engines, *Am. J. Phy.* 53(1985) pp. 147-162.
163. Jin, T., Chen G. B. and Shen Y., A thermo acoustically driven pulse tube refrigerator capable of working below 120 K, *Cryogenics*, 41(2001), pp. 595-601.
164. Qiu Tu a, Qing Li , Fangzhong Guo , Jihao Wu , Junxia Liu , Temperature difference generated in thermo-driven thermo acoustic refrigerator *Cryogenics*, 43(2003), pp. 515-522
165. Tang, K., Chen, G. B. and Kong, B. A 115K thermo acoustically driven pulse tube refrigerator with low onset temperature, *Cryogenics*, 44(2004), pp.287-291.
166. Sugita, H., Matsubara, Y., Kushino, A., Ohnishi, T., Kobayashi, H. and Dai, W. Experimental study on thermally actuated pressure wave generator for space cryocooler, *Cryogenics*, 44(2004), pp. 431-437.

167. Tang K., Chen, G.B., Jin, Bao, T., R., Kong, B. and Qiu, L.M. Influence of resonance tube length on performance of thermo acoustically driven pulse tube refrigerator. *Cryogenics*, 45(2005), pp. 185-191.
168. Qiu, L.M. Sun, D.M. Yan, W.L. Chen, P. Gan, Z.H. . Zhang, X.J. Chen G.B. "Investigation on a thermo acoustically driven pulse tubecooler working at 80 K" *Cryogenics* 45 (2005) 380–385.
169. Hu, J.Y., Luo, E.C. and Dai, W. An innovative configuration for thermo acoustically driven pulse tube coolers. *Cryogenics*, 45(2005), pp. 523-527.
170. Siegel, R. 1983. Effect of flow oscillations on axial energy transport in a porous media. *Transactions of the ASME, JHT*, Vol. 109, 242-244.
171. Siegel, R. 1987. Influence of oscillation-induced diffusion on heat transfer in a uniformly heated channel. *Transactions of the ASME, JHT*, Vol. 109, 244-247.
172. Whitaker's., *Flow in Porous Media. A theoretical derivation of Darcy's law, Transport in Porous Media*, 1, 3-25.
173. Watson, E. J. 1983. Diffusion in oscillatory pipe flow". *Journal of Fluid Mechanics*, Vol. 133, 233-244.
174. Walker, G.1983.*Cryocoolers*.Plenum Press, New York and London.
175. Fluent INC.2003.*Fluent 6.1 User Manual*
176. Fluent INC.2003. *Gambit 6.1 User Manual*
177. Fluent INC.2003. *Fluent 6.1 User Defined Functions manual*
178. Patankar S.V., *Numerical Heat Transfer and Fluid Flow*. Hemisphere Publishing Corporation, New York,1980.
179. Willems, Daniel W.J., *High Power Cryocooling*, PhD Thesis 2007, Technische Universiteit Eindhoven, The Neatherland.(Figure at Chapter7 is taken from this Thesis)
180. [www.cfd-online.com](http://www.cfd-online.com)

# Chapter 1

## Introduction

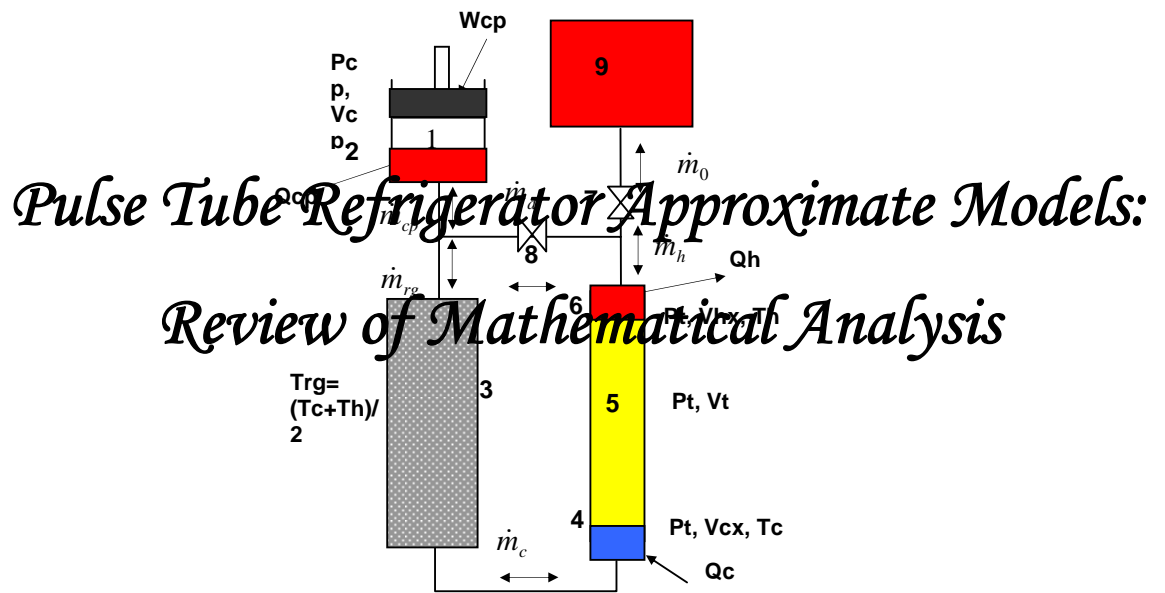




# *Chapter 2*

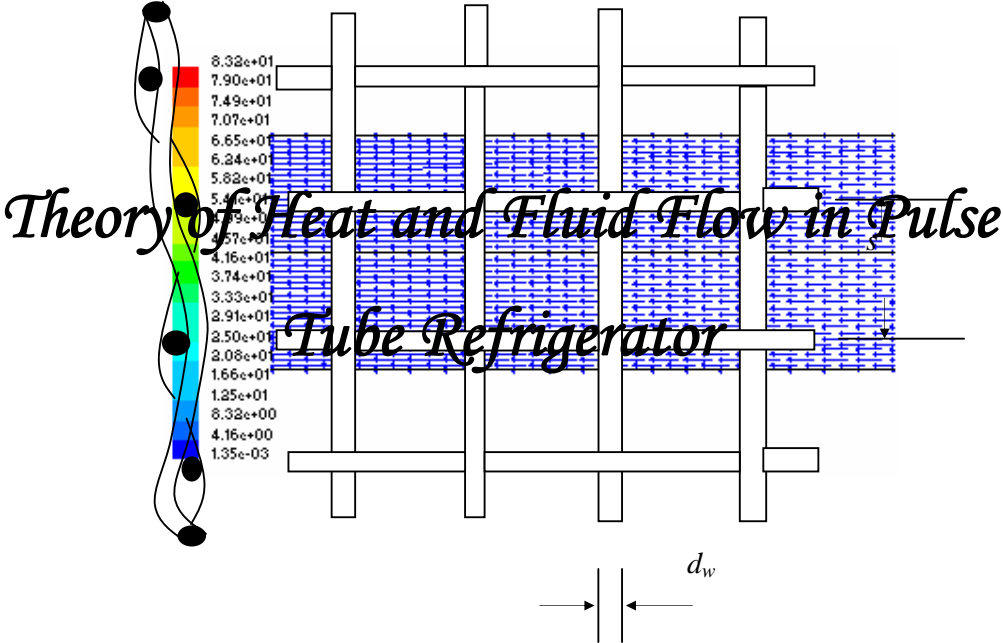
# *Literature Review*

# Chapter 3





# Chapter 4

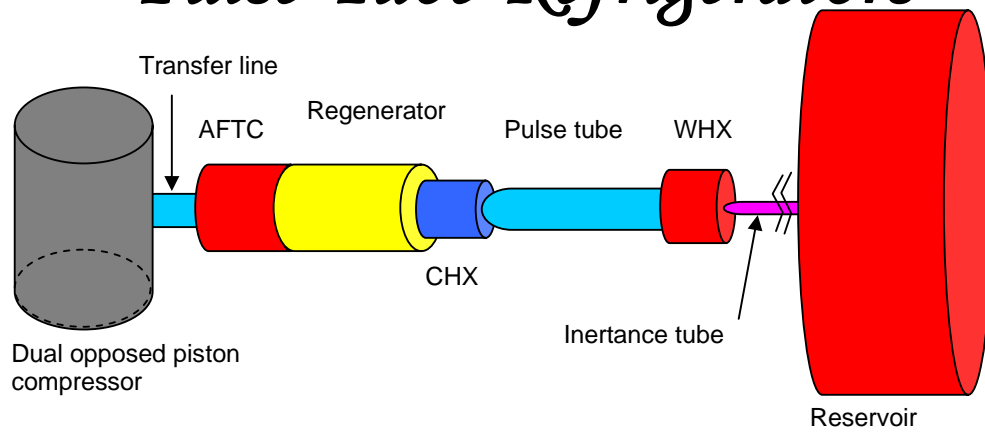


*Theory of Heat and Fluid Flow in Pulse*

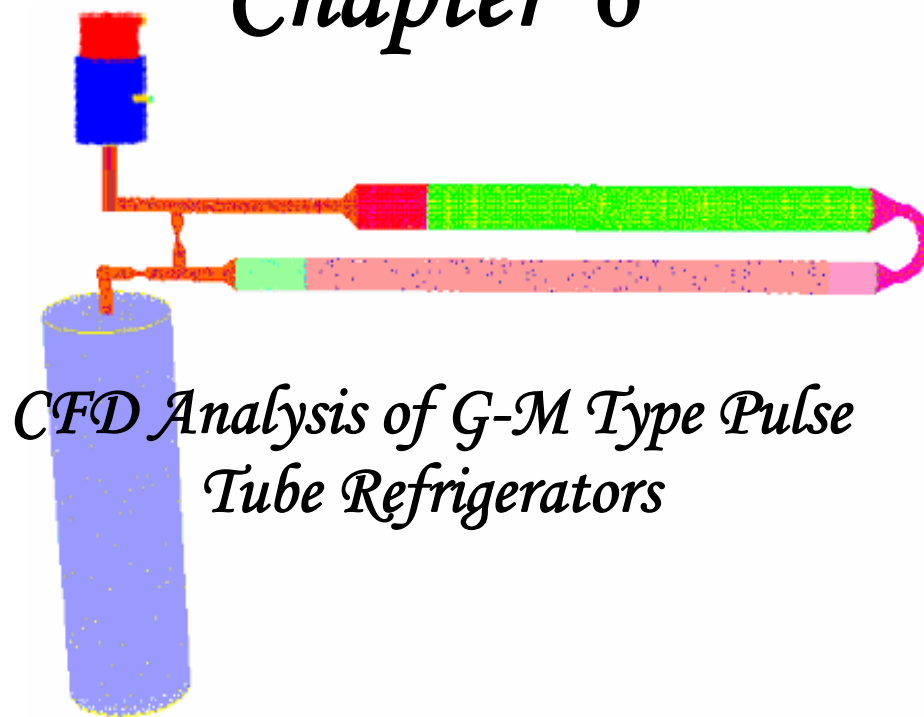
*Tube Refrigerator*

# Chapter 5

## *CFD Analysis of Stirling Type Pulse Tube Refrigerators*

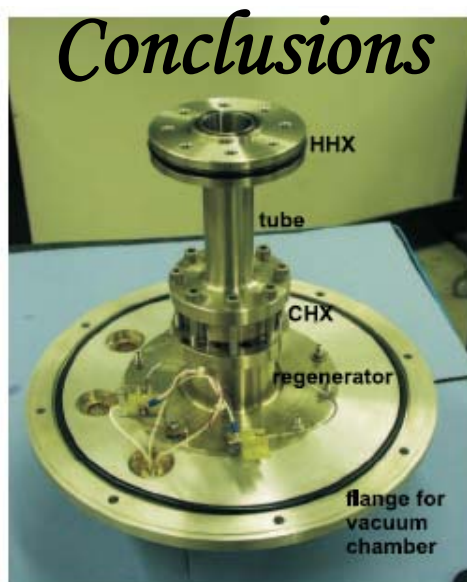


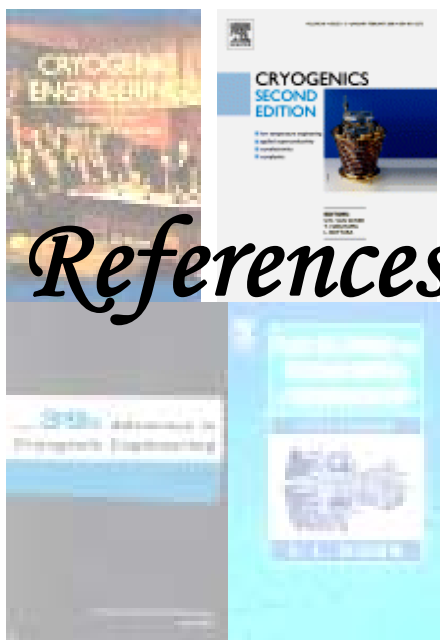
# *Chapter 6*



*CFD Analysis of G-M Type Pulse  
Tube Refrigerators*

# *Chapter 7*





# *References*